

# **BIOMECHANICAL RISK FACTORS AND REDUCED BONE HEALTH IN LOWER LIMB AMPUTEES**

**Olivia Helen Brown**

**a thesis submitted in partial fulfilment of the requirements of Nottingham Trent  
University for the degree of Doctor of Philosophy**

**September 2019**

## **STATEMENT OF COPYRIGHT**

This work is the intellectual property of Olivia Brown. You may copy up to 5% of this work for private study, or personal, non-commercial research. Any re-use of the information contained within this document should be fully referenced, quoting the author, title, university, degree level and pagination. Queries or requests for any other use, or if a more substantial copy is required, should be directed in the owner(s) of the Intellectual Property Rights.

## **ABSTRACT**

Bone constantly adapts to its surroundings through the formation and resorption of material, controlled by bone modelling and remodelling. Strains produced by mechanical loading are one factor that drive these processes and thus determine bone health. Lower limb amputees (LLA) adopt an asymmetrical movement pattern to compensate for the loss of a limb, resulting in a change in mechanical loading and subsequently a degradation in bone health. The aetiology of the majority of amputations is vascular diseases, which affect bone health. Therefore, it is not clear whether the asymmetrical loading, or comorbidities cause the degradation in bone health in LLA. Finite element models (FEM) are used to generate strain plots and predict the bone's response to mechanical loading. To understand the relationship between the degradation in bone health and asymmetrical loads in LLAs the asymmetrical loads can be applied to a healthy bone using FEMs, or simulated within a healthy population using restrictive devices. Therefore, the overall aim was to investigate the relationship between asymmetrical loading, as observed in LLA's, and bone health, through the use of semi-subject specific FEMs and restrictive lower limb devices.

Study one established a novel image processing method to convert peripheral quantitative computed tomography (pQCT) scan images into binary and segment the tibia. The outer perimeter of the tibia was identified and sectioned to produce landmarks. The outer geometry landmarks were used to morph a base FEM, constructed from open source scan images to create semi-subject tibia FEM. Study two applied subject-specific joint reaction and muscle forces to the semi-subject tibia FEM. The strain plots output from Study two were validated against longitudinal geometrical changes from Study three. Study three, used 3D motion capture, pQCT

and dual energy x-ray absorptiometry (DXA) to investigate gait and tibial geometry within a lower limb amputee and able-bodied population across twelve months. The coefficient of variation (CV) for able bodied subjects was less than 10% for ground reaction force (GRF) in level walking and less than 4% for bone total area. Study four, used a rigid foot orthosis and a trans-femoral prosthesis, to restrict able-bodied gait. Results showed participants walked significantly slower ( $p<0.01$ ) in the restricted conditions, with a longer non-restricted step length ( $p<0.001$ ). The loading rate and maximum GRF were higher in the non-restricted limb ( $p<0.05$ ). Larger knee adductor moments were shown in the un-restricted leg in the trans-tibial condition ( $p<0.05$ ).

This thesis presents a novel method of constructing semi-subject specific FEMs from pQCT scans. This can be used to further investigate the link between asymmetrical loading and bone health in LLA's and other populations with asymmetrical gait. The use of restrictive devices allow investigation into LLA's specifically, without the interference of prosthetic variability, or comorbidities.

**Keywords: Bone, Tibia, Strain, Bone health, Lower limb amputation, Finite element analysis, pQCT, Gait.**

# **DISSEMINATION OF RESEARCH**

## **Conference Presentations**

Brown, O., Sale, C., Dobson, C. A., Watson, P. J., Barnett, C. T., (2017) Lower limb amputee gait biomechanics and reduced bone health: A measurement and simulation study, Science and Technology Annual Research (STAR) Conference, 11, Nottingham Trent University

Brown, O., Sale, C., Barnett, C. T., (2017) Does the method used to locate force platform centre of pressure affect biomechanical measures obtained during stair walking on an instrumented staircase? Biomechanics Interest Group (BIG) meeting, Portsmouth, UK

Brown, O., Sale, C., Barnett, C. T., (2018) Investigating the effects of joint restriction to simulate prosthetic gait on loading and movement asymmetries in able-bodied individuals. World Congress of Biomechanics Dublin Ireland

Brown, O., Sale, C., Lewis M.G.C., Barnett C. T.,(2019) An image processing method to assess changes in tibial geometry from peripheral quantitative computerised tomography scans, International Society of Biomechanics (ISB) Conference, Calgary, Canada

## **ACKNOWLEDGEMENTS**

This academic journey has been one of great difficulties and great achievements.

There are no words to express my gratitude to all those who have helped me on this journey but let the following be a start.

Firstly to my supervisory team. Thank you to Dr Catherine Dobson for opening my eyes to an academic career and leading me to the start of this journey. Thank you to Dr Peter Watson for your guidance and tutoring. Thank you to Professor Craig Sale and Dr Cleveland Barnett for your endless patience and wisdom during the many, many problem solving sessions. Thank you also to Dr Martin Lewis and Dr Ian Varley for sharing your expertise and providing assistance throughout.

To my friends. Thank you to my fellow Ph.D colleagues, for the tea runs, actual runs (Rebecca Jones) and support both at the desk (Rachel Malcolm) and in the lab.

Thank you to my other friends, for not always understanding but always caring.

To my new colleagues. Thank you to (soon to be) Dr Franky Mulloy, Professor David Mullineaux and all those at Plum, your patience, understanding and endless support has been invaluable.

To my family. Without your support and encouragement I would not have been able to do this. Thank you for everything.

Finally, to my partner, Farrell Ray. You are there every day with your unwavering support and patience. This is for you, for us.

# CONTENTS

STATEMENT OF COPYRIGHT .....	II
ABSTRACT .....	III
DISSEMINATION OF RESEARCH .....	V
Conference Presentations .....	V
ACKNOWLEDGEMENTS .....	VI
LIST OF FIGURES .....	XII
LIST OF TABLES .....	XIX
GLOSSARY OF TERMS .....	XXI
THESIS STRUCTURE.....	1
1.    GENERAL INTRODUCTION .....	4
1.1    Aims and objectives .....	8
2.    LITERATURE REVIEW.....	10
2.1    Introduction .....	10
2.2    The Human Skeleton .....	10
2.2.1    Long bones of the lower limb .....	10
2.2.3    Internal Tibia Structure.....	15
2.2.4    Bone Formation.....	18
2.2.5    The bone modelling and remodelling processes .....	18
2.2.6    Bone Material Properties .....	20
2.3    Musculoskeletal Modelling of Level Walking Gait .....	23
2.4    Biomechanics of Able- Bodied Locomotion.....	30
2.4.1    Level walking biomechanics .....	30
2.4.2    Stair walking biomechanics .....	35
2.4.3    Biomechanical loading on the tibia .....	39
2.5    Lower limb amputee statistics .....	41
2.5.1    Geometrical and structural adaptations in bone in amputees .....	43
2.5.2    Biomechanical adaptations in lower limb amputees .....	44
2.6    Restrictive devices to simulate amputee gait.....	51
2.7    Finite element analysis.....	53
2.7.1    Generation of finite element model geometry .....	54
2.7.2    Material Behaviours and Properties of Finite element models .....	57

2.7.3	Application of constrains to finite element models.....	59
2.7.4	Application of physiological loading to finite element models .....	61
2.7.5	Finite element models of lower limb amputees.....	62
2.8	Summary of literature review .....	63
<b>3.</b>	<b>GENERAL METHODS .....</b>	<b>65</b>
3.1	Participants .....	65
3.1.1	Ethical Approval .....	65
3.1.2	Inclusion and Exclusion Criteria .....	65
3.1.3	Sample size .....	67
3.2	Method for collection of bone images.....	68
3.2.1	Peripheral Quantative Computed Tomography .....	68
3.2.2	Dual Energy X-ray Absorptiometry .....	69
3.3	Method for collection of biomechanics.....	71
3.3.1	3D motion capture.....	71
3.3.2	Calibration of a 3D volume .....	73
3.3.3	Movement data preparation and collection method .....	73
3.3.4	Segment Definition .....	77
3.3.5	Method of processing 3D motion capture data.....	84
3.3.6	Statistical analyses.....	88
<b>4</b>	<b>STUDY ONE: THE DEVELOPMENT OF A SEMI-SUBJECT SPECIFIC FINITE ELEMENT MODEL OF THE TIBIA.....</b>	<b>89</b>
4.1	Introduction .....	90
4.2	Processing of tibia scan images.....	92
4.3	Base Model Images .....	100
4.4	Base Model Development.....	102
4.4.1	Processing of base model images .....	105
4.4.2	Validity of the bone imaging acquisition and processing through assessments of accuracy and reliability.....	106
4.4.3	Morphing of the base finite element model of the tibia.....	121
4.4.4	Subject-specific model generation .....	123
4.4.5	Model material properties .....	123
4.5	Discussion.....	124
4.6	Limitations and Future directions.....	128
4.7	Conclusion.....	129
<b>5</b>	<b>STUDY TWO: VALIDATION AND EVALUATION OF A SEMI-SUBJECT SPECIFIC FINITE ELEMENT MODEL OF THE TIBIA.....</b>	<b>130</b>

5.1	Introduction .....	130
5.2	Methods.....	133
5.2.1	Musculoskeletal modelling .....	133
5.2.2	Muscle force output.....	138
5.2.3	Finite element model .....	144
5.2.4	Subject-specific physiological data application to semi-subject specific finite element model.....	148
5.2.5	Effect of subject-specific physiological data application to the semi-subject specific finite element model.....	150
5.2.6	Validation and evaluation of the semi-subject finite element model using subject specific longitudinal physiological data .....	155
5.3	Limitation and Future directions .....	165
5.4	Conclusion.....	166
<b>6</b>	<b>STUDY THREE: THE VARIATION IN TIBIAL BONE HEALTH AND LOWER LIMB BIOMECHANICS ACROSS A 12-MONTH PERIOD.....</b>	<b>168</b>
6.1	Introduction .....	169
6.2	Methods.....	174
6.2.1	Participants .....	174
6.2.2	Experimental design.....	176
6.2.3	Bone Imaging .....	177
6.2.4	Questionnaires.....	178
6.2.5	Movement Analysis .....	179
6.2.6	Processing of data.....	182
6.2.7	Dependant variables.....	182
6.2.8	Statistical analysis .....	183
6.3	Results .....	183
6.3.1	Variation in bone structure and geometry .....	183
6.3.2	Variation in biomechanics .....	188
6.4	Discussion.....	192
6.5	Limitations and Future directions.....	194
6.6	Conclusion.....	195
<b>7</b>	<b>STUDY FOUR: THE USE OF JOINT RESTRICTION IN ABLE BODIED INDIVIDUALS TO SIMULATE THE TEMPORAL- SPATIAL, GROUND REACTION FORCES AND KNEE ADDUCTION MOMENT ADAPTATIONS SEEN IN LOWER LIMB AMPUTEES. ....</b>	<b>197</b>
7.1	Introduction .....	198
7.2	Study Methods .....	201

7.2.1	Ethical approval .....	201
7.2.2	Participants .....	201
7.2.3	Experimental Set-up .....	203
7.2.4	Experimental Protocol .....	204
7.2.5	Data Collection .....	209
7.2.6	Data processing .....	216
7.2.7	Statistical Analyses .....	218
7.3	Results .....	218
7.4	Limitations .....	230
7.5	Conclusion.....	230
8	GENERAL DISCUSSION.....	232
8.1	Introduction .....	232
8.2	Summation and critical analysis of research objectives.....	233
9.	LIMITATIONS AND FUTURE DIRECTIONS .....	242
10.	CONCLUSION.....	243
11.	REFERENCES .....	245
	Appendix A- Staircase Validation Study .....	284
1.1	Introduction .....	284
1.2	Methods.....	285
1.3	Results of variation in force plate location as identified by differing methods.....	287
1.4	Discussion.....	297
1.5	Conclusion.....	298
	Appendix B- Participant Information Sheet Study Three .....	299
	Appendix C- Bone Scan Form, Study Three .....	307
	Appendix D- Participant Consent Form Study Three .....	309
	Appendix E- SF 36 Questionnaire-Study Three.....	311
	Appendix F- Bone-specific Physical Activity Questionnaire-Study Three .....	315
	Appendix G- International Physical Activity Questionnaire .....	317
	Appendix H- Participant Information Sheet-Study four .....	320
	Appendix I- Informed Consent form-Study four .....	323



# LIST OF FIGURES

Figure 1: The thesis workflow for each of the four experimental studies. ....	3
Figure 2: Anatomy of the ankle joint, posterior cross-sectional view. Adapted from Webscape, WebMD (1994-2018).....	11
Figure 3: Anatomy of the Knee joint. A; Cross sectional view. B; Posterior view .....	11
Figure 4: The Tibia bone with bony landmarks identified in colour.....	12
Figure 5 : Schematic of long bone loading and response. Loading can be applied in combinations of bending moment (M), torsional moment (T) and compressive load (F). The compressive (+) and tensile (-) strains about the neutral axis (NA) are as a result of this compressive load. Adapted from (Levenston et al. 1998; Lieberman et al. 2004).....	13
Figure 6: The cross section of a tibia bone with the neutral axis represented as a dashed line. The second moment of area is defined by equation 1. ....	14
Figure 7: Structure of whole bones as adapted from (Bartholomew et al., 2012).....	15
Figure 8: Schematic representation of hierarchical structure of bone. Adapted from (Rho et al. 1998) and (Caeiro et al. 2013). ....	17
Figure 9: The strain values relating to the different of regions of bone remodelling, modelling and absorption. Adapted from Forward and Turner (1995).....	19
Figure 10: The stress strain relationship of bone to define Young's Modulus developed from (Turner 1998).....	20
Figure 11: Hill type muscle model diagram (developed from Caldwell, 2014). The active element is the contractile component (cc), the elastic element; the series elastic component (SEC) and the passive element; parallel elastic component (PEC).....	23
Figure 12: Muscle composition definitions, A: pennation angle and B: physiological cross-sectional area. ....	25
Figure 13: The outline of the inverse dynamics and forward dynamics used in musculoskeletal modelling. Adapted from (Robertson et al. 2014). ....	29
Figure 14: The level walking gait cycle broken down into its phases. Adapted from Uustal et al. (2004). ....	34
Figure 15: Stair ascent and stair descent gait cycle. Adapted from Novak et al. (2010).....	38
Figure 16: The loading across the tibia during walking. Tension is expressed as a solid red line, compression as a dashed red line and shear loading as a dotted blue line. Adapted from Bankoff (2012).....	39
Figure 17: Amputee level definition, adapted from (Stewart 2008) .....	41

Figure 18: Work flow for determining the mechanical behaviour of a finite element system, in this case a bone. Developed from (Brekelmans et al. 1972).....	53
Figure 19: The Stratec pQCT XCT 2000 with leg fixation and foot holder for scanning of the tibia. ....	56
Figure 20: Line drawing of the set-up which was used in study 3 and study 4. Gantry mounted cameras are labelled 1-8 and FP1 is the ground embedded force plate, AMTI OR6-7-2000. Portable cameras were labelled 9-12 and the high-speed camera labelled as 13. FP4, Kistler 9260AA3 and FP5, Kistler 9286B are the portable force plate in the stair case (Study 3 only). These are connected to the computer through A, B and C. A; Kistler DAQ board. B; 64 channel AD board. C; AMTI MSA-6 six channel strain gage amplifiers. ....	72
Figure 21: Calibration frame dimension A; 550mm, B;200mm, C; 750mm and Calibration wand length; 751mm.....	73
Figure 22: Locations of the 37-marker model set. ....	74
Figure 23: The head segment definition using markers and landmarks. ....	78
Figure 24: The thorax markers and landmarks which define the cylindrical segment. ....	79
Figure 25: The pelvis markers and landmarks used to define the segment. ....	80
Figure 26: The thigh markers and landmarks used to define the segment.....	81
Figure 27: The markers and landmarks that define the shank segment.....	82
Figure 28: The markers and landmarks which define the foot segment. The bold coordinate system which originate at the calcaneus defines the virtual foot segment. ....	83
Figure 29: Four reference frame options for 3D modelling. A) Resolve to the shank segment, B) Resolve to the thigh segment, C) Project the flexion axis from the proximal frame and internal rotation axis from the distal segment and a perpendicular adduction axis, D) The Plane of Progression fixes the flexion axis perpendicular and the adduction and internal rotation axis, taken from the distal axis, are projected. Adapted from (Selbie et al. 2004; Brandon and Deluzio 2011) .....	86
Figure 30: Locations of the pQCT scans along the length of the tibia.....	92
Figure 31: The pQCT image processing sequence commences at the top left and moves clockwise. The image is rotated by 23 degrees and then flipped horizontally. A threshold is applied to the bone and the image converted to binary. An area filter is applied to select the tibia only. Area segmentation is used to identify the two area masses; cortical and trabecular. The outer perimeter is calculated and is seen applied to the binary image and the RGB image. ....	94
Figure 32: Graph of mass identification when a range of thresholds to image generated at the 14% site of the tibia. At the point of each step down of the curve the associated pixel threshold identifies another material. E.g. at ~100 only cortical bone is identified. ....	96

Figure 33: Outer perimeter of bone with both the smoothed (blue) and original (red) parameter displayed. As well as the centre point displayed as a black ‘\*’ and as a green ‘\*’. The orientation is also labelled at each axis, the origin is generated from the original image hence not 0, 0 in this Figure. .... 99

Figure 34: The maximum axial cross-sectional diameter in the X (red line) and Y (blue line) diameter. .... 99

Figure 35: Generation of landmarks through visual dissection of the tibia. The red line is the outer perimeter of the tibia and each circle represents identification of a landmark. .... 100

Figure 36: A; Visible Human Female three-dimensional image reconstruction. Taken from Waldby (2000) (image courtesy of Lorensen and G.E. Imaging and Visualisation Laboratory) B; The musculoskeletal reconstruction of the visible human female taken from Yanamadala (2014). .... 101

Figure 37: The view of the tibia slices in the X direction (red boundary) and the Z direction (blue boundary). The checked blue area identifies trabecular bone and the checked yellow area is the cortical bone. .... 103

Figure 38: Diagram to define aspect ratio of a triangular element. .... 105

Figure 39: Image of tibia from the proximal end to explain the rotation factor applied to the participant images. .... 106

Figure 40: Labelled diagram of cylinder model (Left) and tibia model (right) (Sawbones, Sweden). .... 107

Figure 41: Positioning of the cylinder model within the pQCT prior to scanning. .... 108

Figure 42: Positioning of the tibia within the pQCT machine, with the reference laser (red line) at the distal end of the tibia. The proximal tibia is secured with a push fit within the blue foam cylinder (a simulated thigh) on the right of the image. .... 109

Figure 43: Scout scan laser and the resulting reference point for starting the scan ..... 110

Figure 44: Manual identification of the region of interest using the polygon tool (green line). .... 110

Figure 45: Percentage error of the diameter, generated from varying the threshold within the image processing method. A is at the 4% site, B the 14% site, C the 38% site and D the 66% site. At 0% error the diameter is equal to the manufacturers provided measurement of 160mm. .... 112

Figure 46: Centre points generated through the image processing method. The centre point, based on manufactured diameter is represented by black \* Each site is represented 4% (red), 14% (yellow), 38% (green), 66% (blue). The repeated scans are represented by symbols, scan 1 (\*), scan 2 (o) and scan 3 (+). The perimeter of the cylinder is represented by the black circle. .... 113

Figure 47: The coefficient of variation in the x (red line) and y (blue line) coordinates of each landmark around the perimeter of the tibia. A is 4%, B is 14%, C is 38% and D is 66%... 118

Figure 48: The outer perimeter of the model tibia at the 4% (A), 14%(B); 38%(C) and 66% (D) sites. Red lines correspond to the first scan, yellow, scan2, green scan 3 and blue scan 4. .... 119

Figure 49: The coefficient of variation of in the x (red) and y(blue) of the landmark coordinates around the perimeter of the tibia for each scan site 4% (A), 14%(B), 38%(C) and 66%(D). .... 120

Figure 50: Landmarks on the base tibia model. Yellow represents the landmarks generated from the base model and blue are those generated from participant data..... 121

Figure 51: Morphed model in the medial lateral and anterior posterior positions. Base surface model is presented in yellow and the semi-subject specific morphed model is presented in blue..... 122

Figure 52: The seven segment, lower extremity model developed by Delp et al (1990) taken from OpenSim documentation. .... 135

Figure 53: The gait2392 model taken directly from OpenSim ..... 136

Figure 54: Semi-subject specific participant model with muscle attachment sites represented as landmarks. The semitendinosus, gracillis and Sartorius and tibialis anterior can be seen on the anterior view. The flexor digitorum longus, soleus, tibialis anterior and semimembranosus can be identified on the posterior view. The joint reaction force application landmarks (Medial and lateral contact) can also be seen on the medial and lateral condyles. .... 137

Figure 55: A schematic of the feedback loop that is used to compute muscle control based on (Thelen and Anderson 2006) The first half details the PD control law with inputs being joint accelerations;  $\ddot{q}^{exp}$ , joint velocities;  $\dot{q}^{exp}$ , and joint positions;  $q^{exp}$  with tracking errors  $e_q$  and  $e_{\dot{q}}$ .  $K_v$  and  $K_p$  are the feedback gains. Muscle excitations, represented by  $u$  are calculated through the input of expected muscle forces  $f^{exp}$  into the static optimisation. .... 141

Figure 56: Locations of the point loading on the condyles at the type of the tibia. The size of the arrow shows the larger distribution of load 60% on the medial c-ondyle compared to 40% on lateral condyle. .... 146

Figure 57: The triangular formation of the constraints at the distal end of the tibia to simulate the ankle. .... 146

Figure 58: The breakdown of the inverse dynamic's procedure used by Visual 3d. A; The definition of vectors for distance between centre of mass of the distal joint to proximal joint (red and blue arrows). B; The joint torques (green arrows) and forces at the proximal joint (blue arrows). C; the external forces (blue arrow), their location in relation the segment mass (red arrow) and external couples (green arrow). .... 149

Figure 59: Resultant strain plot from the application of loads to finite elements models generated from different bone image scan data. From top; full length tibia, from distal end of tibia, proximal end of tibia. ....	153
Figure 60: The same FEM geometry with application of loads generated from different biomechanics .....	154
Figure 61: All Participant strain ( $\mu\epsilon$ ) plots across the tibia alongside 4, 14,38 and 66% cross sections. ....	158
Figure 62: The minimum strain ( $\mu\epsilon$ ) across the tibia for all participant models. ....	159
Figure 63: The maximum strain ( $\mu\epsilon$ ) at the 14% site of the tibia for each semi-subject specific model. ....	159
Figure 64: Cross section of the finite element model at 14% tibia length and the pQCT external geometry plots for baseline (red), visit 2 (green) and visit 3 (blue). Yellow represents higher strain and blue, areas of lower strain. Landmarks at the highest and lowest strain points are identified by a circle in the corresponding colour. ....	160
Figure 65: Participant recruitment progress. A; recruitment of controls and their progression through the study. B; progression of recruitment of LLA into the study, culminating in no LLA .....	175
Figure 66: The experimental protocol for each visit across the 12-month period. The two-minute walk test and movement analysis are carried out at every time point. The bone imaging is carried out at visits 1, 3 and 5. ....	176
Figure 67: Engineering drawings for the staircase. A; the side view of the staircase with ..... sections detailing the recesses. B; the plan view and C; the isometric view of the staircase with the two force plates placed in the recesses. ....	181
Figure 68: The coefficient of variation across for the total bone density across all three time points for each participant. At the 66% the muscle mass is the main measurement and therefore no bone density was processed. ....	184
Figure 69: The coefficient of variation of total bone area, calculated from the mean and standard deviation across the three time points. The solid black bar denotes 4% and the white bar denotes 66% and the shades of grey in between show the 14 and 38% sites respectively. ....	184
Figure 70: The outer perimeter of P01 tibia at the 66%, generated from the pQCT and image processing method as developed in study one and two. The Red line represents scan 1, green line scan 3 and blue line scan 5. The black line is a circle and us used as a reference shape. ....	185
Figure 71: The outer perimeter of the P02, at the 4% site. The red line represents scan 1, green line is scan 3 and the blue line is scan 5. ....	186

Figure 72: Max vertical GRF across the gait cycle for each visit. The overall average across all participants is also presented. ....	189
Figure 73: The average maximum ground reaction force across all force plates (ground force plate, first step force plate and second step force plate) for both ascending and descending the staircase. ....	190
Figure 74: The Air step walker boot used as the rigid ankle-foot orthoses, side and front view. ....	204
Figure 75: The components on the trans-femoral simulator; A; the carbon fibre shell, B; spring-leaf prosthetic foot, C; four bar linkage knee and pylon. ....	205
Figure 76: Rigid ankle-foot orthosis worn in the TT condition, view from the side and from the front .....	207
Figure 77: Participant wearing the harness attached to the ceiling and fitted to the transfemoral prosthesis. The pelvis is level (red dashed line) and prosthetic foot orientation mirroring the orientation of un-restricted foot. ....	208
Figure 78: The marker definitions for the transtibial condition. ....	210
Figure 79: The marker set up for the transfemoral simulator .....	211
Figure 80: The visual 3D model, where the prosthetic simulator is represented by an anatomical shank and anatomical foot in the correct physiological orientation for standing. The ‘real’ shank and foot are represented by those at 90-degree flexion from the anatomical knee. ....	213
Figure 81: Anatomical thigh segment. Markers in black and landmarks in blue. ....	214
Figure 82: Anatomical shank segment. Markers in black and landmarks in blue. ....	214
Figure 83: Anatomical foot segment. Markers in black and landmarks in blue. ....	215
Figure 84: Prosthetic shank segment. Markers are in black and landmarks in blue. ....	215
Figure 85: Prosthetic foot segment. Markers are in black and landmarks are in blue. ....	216
Figure 86: Percentage change in distance walked between consecutive two-minute walk tests in meters in the transtibial condition (grey) For the TT condition (A) and TF condition (B) participants were familiarised to 5% for both lab visits for the TT condition and to 10% at lab visit one and to 5% at lab visit for the TF condition (5% and 10% familiarisation denoted by the red lines). ....	220
Figure 87: The vertical ground reaction force normalised for body weight across the stance phase. A; the unrestricted leg and B; the restricted leg, .....	224
Figure 88: Knee adduction moment normalised for body weight and walking speed for the unrestricted limb across stance phase. The first peak was KAM1 and the second peak as	

KAM2. For the TF condition, the first peak was KAM1 and the second peak (at ~40%) was KAM2. ....	225
Figure 89: Schematic of Portable staircase with portable force plates (SFP1,SFP2) next to the floor embedded force plate (FFP) FFP- Floor force plate (Model OR6-7-200, AMTI, Advanced Mechanical Technology Inc. USA), SFP1- Stair force plate 1(Model 9286B, Kistler, Winterhur, Switzerland), SFP2 - Stair force Plate 2 (Model 9260AA3 Kistler, Winterhur, Switzerland). ....	286
Figure 90: 3D scatter plot of centre of pressure (COP) when ascending the staircase across three force plates; the AMTI embedded floor force plate (FFP) and the two portable Kistler force plates, stair force plate one (SFP1) and stair force plate 2 (SFP2). ....	289
Figure 91: 3D scatter plot of centre of pressure (COP) when descending the staircase across three force plates; the AMTI embedded floor force plate (FFP) and the two portable Kistler force plates, stair force plate one (SFP1) and stair force plate 2 (SFP2). ....	290
Figure 92: Root mean square of dynamic COP across three force plates. A; when ascending the staircase and B; when descending the staircase. FFP; Floor force plate, SFP1; Stair force plate 1, SFP2; Stair Force plate 2. ....	291
Figure 93: Joint moments during stance phase for Ankle, Knee and Hip during stair ascent (A, B, C) and stair descent (D, E, F). ....	293
Figure 94: Root mean square of the joint moments when Ascending the staircase (A) and descending the staircase (B) across the three force plates; Floor force plate (FFP), Stair force plate (SFP1) and stair force plate (SFP2). ....	294
Figure 95: Joint Powers for the Ankle, Knee and hip across the stance phase for both ascending (A, B, C) and descending (D, E, F) the staircase. ....	295
Figure 96: Joint Powers for the Ankle, Knee and hip when ascending (A) and descending (B) the staircase, across three force plates; Floor force plate (FFP), Stair force plate 1 (SFP1) and stair force plate 2 (SFP2). ....	296
Figure 97: DXA scanner. ....	302
Figure 98: pQCT scanner. ....	303

# LIST OF TABLES

Table 1: Definitions of the level of bone health based on average bone density values, adapted from (NIH 2015) ..... 21

Table 2: Details of the development of musculoskeletal models including their source and their implementation into software. Adapted from (Rajagopal et al. 2015). ..... 26

Table 3: The K-level classification (Medicare, 1995)..... 45

Table 4: Abbreviation expansion of the markers detailed above and the process of identification of said landmark. (Van Sint Jan, 2007)..... 75

Table 5: Landmark definitions for head segment ..... 79

Table 6: Hip Joint centre definitions based on the regression equations developed by Bell et al (1989, 1990)..... 81

Table 7: Landmark definitions for pelvis segment ..... 81

Table 8: The definition of the landmarks at the shank. .... 82

Table 9: The definition of the landmarks at the foot. .... 84

Table 10: Accuracy and reliability of the pQCT; the percentage error when comparing the diameter of the cylinder as derived from the pQCT to the 160mm diameter specified by the manufacturer ..... 115

Table 11: Reliability of the pQCT Coefficient of variation of all scan sites (4, 14, 38 and 66%) at each scan time point (scan 1, scan 2 and scan 3). .... 116

Table 12: Reliability of the pQCT. Coefficient of variation between scan time points (scan 1, scan2 and scan 3) for each scan site (4, 14, 38 and 66%)..... 116

Table 13: Material properties for trabecular and cortical bone based on literature (Lai et al. 2015) ..... 123

Table 14: Definitions of the location of the reference frame for each segment of the model. Adapted from the OpenSim documentation ..... 135

Table 15: To investigate the effect of variation of geometry, three FEM generated from bone imaging data from scan time point 1 (FEM1), scan time point 2 (FEM2) and scan time point 3 (FEM3) were loaded with a reference set of loads (column 4). To investigate the effect of varying loads, each FEM was loaded with the corresponding time specific loads and a set of reference loads. .... 151

Table 16: The coordinates of the landmarks which correspond to the location where the FEM has identified highest strain levels and lowest strain levels. The X, Y coordinates are presented for each of the three time points. The positive X is Medial and positive Y is Posterior. .... 161

Table 17: Variables values used to determine required sample size ..... 174

Table 18: Technical information of the Stratec 2000L Peripheral Quantitative Computed Tomography Scanner .....	69
Table 19: The total bone area across all scan time points for participant one, P01 at the 66% site. ....	186
Table 20: The Total Bone area for each scan time point, for participant P02, scan site 4%. ....	187
Table 21: Coefficient of Variation (%) for distance covered and strides taken by each participant across the five visits. ....	188
Table 22: The coefficient of variation across all visits for right leg contact on each force plate when ascending the staircase. ....	191
Table 23: The coefficient of variation across all visits for right leg contact on each force plate when descending the staircase. ....	191
Table 24: Variables values used to determine required sample size. ....	202
Table 25: The additional definitions of the marker set included in the prosthetic simulator. ....	212
Table 26: Landmark definitions used to define the anatomical shank and foot. ....	215
Table 27: Landmark definitions for the prosthetic segments. ....	216
Table 28: Group mean (SD) temporal/ spatial parameters for each condition and leg .....	222
Table 29 : Statistical properties of the temporal-spatial parameters and ground reaction force across both limbs and knee moment in the unrestricted limb. Results are presented as F and p value with *denoting significance. ....	226
Table 30: An overview of the objects addressed throughout the Ph.D and the key outcomes from the respective objectives. ....	241
Table 31: Difference in force plate centre coordinate (mm) when compared to the reference method across the three force plates. ....	288
Table 32: Study Outline for controls.....	301

## **GLOSSARY OF TERMS**

ADL	Activities of Daily Living
BMD	Bone Mineral Density
CON	Control condition
CV	Coefficient of Variation
CT	Computed Tomography
DXA	Dual Energy X-ray absorptiometry
FEA	Finite Element Analysis
FEM	Finite Element Model
FP	Force Plate
GRF	Ground Reaction Force
LLA	Lower Limb Amputee
MRI	Magnetic Resonance Imaging
pQCT	Peripheral Quantitative Computed Tomography
RMS	Root Mean Square
TF	Trans-femoral
TT	Trans-tibial
VHP	Visible Human Project
3D	Three-Dimensional

# THESIS STRUCTURE

The thesis starts with a general introduction (Chapter One) providing an overview of current research and justification for the current research. This chapter concludes with the overall aim and individual objectives of the thesis.

Chapter Two, the literature review, which includes information detailing bone tissue, its formation, subsequent geometry and structure before detailing how this changes within an amputee population. Able-bodied gait biomechanics for both level ground and stair walking are then presented, followed by how amputees biomechanically adapt to the loss of a limb. The literature review concludes with the topic of finite element modelling as a link between bone health and mechanical loading from gait.

Chapter Three informs the reader of the general methods, which have been used specifically in the collection and processing of the biomechanical data collected within Study Three (Chapter Six) and Study Four (Chapter Seven).

Chapter Four (Study One) details the novel method by which a base tibia model was morphed using pQCT bone scan data from Chapter Six (Study Three) to construct a semi-subject specific finite element model. Validity of the method of image acquisition and processing was assessed using a uniform cylinder model and a non-uniform tibia model. Accuracy was assessed through comparison of the cylinders known diameter to the processed diameter using coefficient of variation. Repeatability of the pQCT scanner was assessed using test re-test of the tibia model and was analysed using coefficient of variation.

Chapter Five (Study Two) gave the semi-subject specific tibia model developed in Chapter Four (Study One) physiological validation. Subject specific muscle forces and joint contact forces calculated from each participants movement data collected as part of Chapter Six (Study

Three) were applied to the same participants semi-subject specific finite element model. The strain outputs from the finite element models were compared to the outer geometry plots developed from the novel image processing method to analyse physiological validity.

Chapter Six (Study Three) investigated the longitudinal changes in gait and tibial bone geometry and structure in an able-bodied population. Six able-bodied participants (mean  $\pm$  1 S.D., height  $1.82 \pm 0.05\text{m}$ , weight  $90 \pm 12\text{kg}$ ) volunteered for this study. The study employed a longitudinal repeated measures design with a laboratory visit every three months for a period of 12 months. Level walking and stair gait was assessed using three-dimensional motion capture at every visit. Body composition and tibial geometry and structure was assessed using dual energy x-ray (DXA) and a peripheral quantitative computed tomography (pQCT) scans at every six months. The results were used to assess normative variation values within an able-bodied population and provided input data for the physiological validation conducted in Chapter Five. Kinetic data and bone health parameters were then further analysed using the coefficient of variation to determine an individual participant's variation across the twelve months.

Chapter Seven (Study Four) compare the use of a restrictive rigid foot-ankle orthotic (TT condition) and a trans-femoral prosthetic (TF condition) to a control condition to simulate amputee gait without the interference of comorbidities associated with amputee gait. Twelve healthy able-bodied (mean  $\pm$  1 S.D.,  $21.8 \pm 2.5$  years, height  $1.81 \pm 0.09\text{m}$ , weight  $75.4 \pm 9\text{kg}$ ) volunteered for the study. Three-dimensional motion capture was used to assess temporal-spatial, kinetic and kinematic variables. Upon satisfaction of normality, data was analysed using an analysis of variance (ANOVA) with post hoc analyses performed using a Bonferroni correction, statistical significance was set at a p value of  $\leq 0.05$ . A comparison of main effect of conditions (CON, TT, and TF), legs (restricted and unrestricted) and an interaction effect between condition and leg were analysed.

Finally, Chapter Eight summaries the findings from all chapters and evaluates the finite element analyses as a predictive tool for changes in bone as a result of biomechanics. The application of this tool in clinical populations, such as those with lower limb amputations, is discussed with potential developments in other populations who have asymmetrical gait patterns. This chapter also identifies limitations within the thesis. The entire thesis is then summarised in a concluding statement.

Figure 1 presents the structure of the four experimental studies (Chapter Four, Five, Six and Seven) and how they link to each other through the thesis.

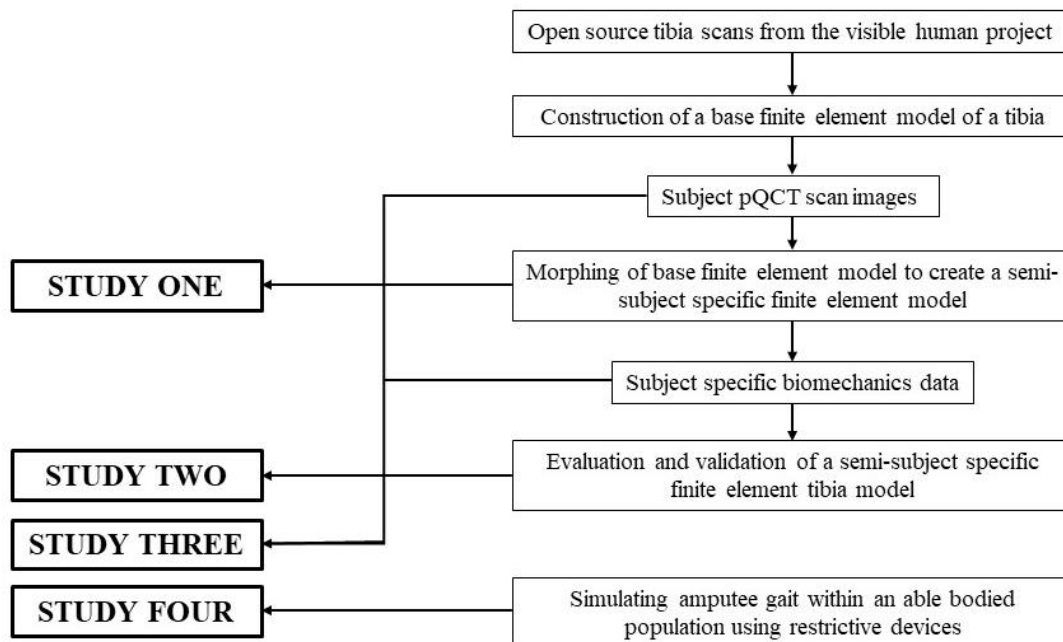


**Figure 1: The thesis workflow for each of the four experimental studies.**

# 1. GENERAL INTRODUCTION

Bone is constantly adapting to its surroundings, forming and resorbing material as a result of the modelling and remodelling processes. These processes are driven by cytokines, hormones (including oestrogen/testosterone) and strains generated by mechanical loads (Boyce et al. 2009). Environmental factors, such as strains produced in mechanical usage of the skeleton for movement have been reported to account for up to fifty percent of bone mass, geometry and structure (US Department of Health and Human Services 2004). Julius Wolf first defined the feedback system associated with bone's response to strains, in Wolff's law. *"Each change in the form and function of a bone or only its function is followed by certain definitive changes in its internal architecture, and secondary changes equally definitive in its external compliance, in accordance to the mathematics law"*. (Wolff, 1986). This work was further developed to determine that bones respond to strains, induced by the mechanical loading as a result of movement (Boyce et al. 2009). A simple explanation was that higher strains lead to bone deposition and lower strains, to bone resorption (Lanyon 1982). This feedback system was further investigated to determine that increased levels of strain encourage bone formation, whilst decreased strain encourages bone remodelling, which results in the removal of material (Currey 2006). This system is now referred to as the Mechanostat Theorem (Frost 1994). A change in mechanical loading causes an imbalance in the modelling/remodelling processes, subsequently affecting bone health. It is often assumed that in an able-bodied population that gait is symmetrical and not subjected to changes across time (Horst et al. 2017, Sadeghi et al. 2000). Therefore, it can be assumed that without changes in loading, bone health also does not change. However, there are no studies which longitudinally investigate bone health and gait in able-bodied subjects. Without this knowledge, changes in gait and bone health in clinical populations who have asymmetrical gait are harder to quantify.

One population where bone health degradation is thought to be as a result of the adoption of asymmetrical loading, is those who experience lower limb amputations. In 2008 it was estimated that approximately 185,000 Americans underwent amputations (including upper and lower limbs) in a year. In the UK there are an estimated 6000 amputations every year, a number that will rise, potentially double by 2050 (Ziegler-Graham et al. 2008). Therefore, the need to address the health issues associated with lower limb amputation is imperative. The rehabilitation process for lower limb amputees (LLA) involves a prolonged period of reduced activity before prescription of a definitive prosthesis (Bemben et al. 2017). At this point, LLAs can start to increase load bearing with the aim to restore both mobility and stability (Schaarschmidt et al. 2012). In adapting to the loss of biological structures, however, patients will alter their walking pattern through a variety of temporal, spatial, kinetic and kinematic characteristics resulting in asymmetrical gait (Nolan et al. 2003; Sadeghi et al. 2000; Sagawa et al. 2011). Explanations as to why lower limb amputees use these compensatory mechanisms are in loading their intact limb more, the residual limb is protected (Nolan et al. 2003; Sanderson and Martin 1997; Hurley et al. 1990). Also in distributing more of their body weight over the intact limb, the centre of gravity is closer to the intact limb, improving the sense of stability and balance (Nolan et al. 2003). The prolonged period of reduced use and then altered loading pattern associated with an asymmetrical movement pattern means that the mechanical loading changes. Thus, the remodelling and modelling processes established prior to amputation may change. This has been postulated to be why lower limb amputees suffer with poor bone health. Specifically, research has reported poor bone health as a measure of reduced bone mineral density (BMD) and a therefore increased risk of osteoporosis (porous bones) (Yazicioglu et al. 2008; Gailey et al. 2008; Kulkarni et al. 1998; Sherk et al. 2008), as well as an increased risk of osteoarthritis (degeneration of the joint).

The majority of amputations are the result of dysvascular disease, including diabetes related complications (90% annually) and atherosclerosis, specifically peripheral arterial disease (PAD) (Ahmad et al. 2016; Stewart 2008; Glaser et al. 2013). The risk factors for these diseases include advanced age, smoking and a poor diet (NCSCT 2012; Nosova, et al. 2015). Both diabetes and smoking has been shown to impair the formation of bone (Jiao et al., 2015), increasing the risk of osteoporosis. The rate of degradation of bone health, and the risk of developing conditions such as osteoporosis also increases with advanced age. Vascular amputation occurs most commonly in those between the ages of 50 and 84 years, with the average age of an amputee in the UK being 68-70 years old (Davie-Smith et al. 2015; Stewart 2008; Ahmad et al. 2014). Therefore, vascular amputees are already at an increased risk of degrading bone health. Being able to identify the cause of the degradation of bone health becomes imperative in order to determine if it is the change in mechanical loading, further complications relating to the aetiology of the amputation, or a combination of the two.

To investigate the effect of an asymmetrical movement pattern on bone whilst isolating the complications relating to the aetiology, healthy bone can be used. Research has simulated asymmetrical gait within a healthy able-bodied population through the use of restrictive orthotics and prosthetics (Vanicek et al. 2007; Lemaire et al. 2000; Ota et al. 2014; Stefanyshyn et al. 1994; Nepomuceno et al. 2017; Ohm and Osl 2010). These publications used casts and rigid foot orthosis to restrict the ankle and simulate transtibial amputee gait (Nepomuceno et al. 2017; Böhm and Hösl 2010; Ota et al. 2014; Stefanyshyn et al. 1994) and transfemoral prosthesis to restrict both the knee and ankle to simulate trans-femoral gait (Lemaire et al., 2000; Vanicek et al. 2007). These publications concluded that the kinetic, kinematic and temporal-spatial adaptations within the restricted limb are comparable to LLA. However, restricted devices have not been used to investigate the effect of asymmetrical gait on the intact

limb. There was also no research that used both type of simulators within the same able-bodied cohort.

The other option to investigate the causation of poor bone health as a result of asymmetrical movement is to simulate the biological system, using the engineering concept of finite element analysis (FEA). This involves the modelling of an object through a set of tetrahedral elements, which when subjected to loading, deform and produce strain plots, predicting the original objects response (Rao 2011). This has been used to evaluate the mechanics of the musculoskeletal system since 1972 (Huiskes and Chao 1983b; Brekelmans et al. 1972). The success of these models relies on the accuracy of the input, *i.e.* the more anatomically accurate the FEM, the more physiologically accurate the output. Recent developments have used subject-specific models generated from bone imaging scans, to increase precision of the modelling outputs; such as computed tomography (CT) or magnetic resonance imaging (MRI) (Carey et al. 2014; Schileo et al. 2007a; Taddei et al. 2006; Viceconti et al. 2004). The disadvantages of this is that the former exposes participants to high levels of radiation and both methods incur high cost. Peripheral Quantitative Computed Tomography (pQCT) offers an attractive alternative with comparably reduced radiation exposure and cost. The clinical use of this system typically scans the tibia at four points, (4, 14, 38 and 66% of tibia length) to capture areas of trabecular and cortical bone (Evans et al. 2012).

The relationship between gait and bone is well established. However, it is assumed that healthy able-bodied populations have a symmetrical gait which is unchanged over a 12 month period. Thus, changes in clinical populations who present with an asymmetrical gait are comparably more significant. This gap in research in longitudinal studies in able-bodied populations needs to be investigated to establish a base line level of mobility and bone health. In populations such as LLA it is postulated that asymmetrical gait results in bone degradation. However, there are

also comorbidities within this population that could affect bone health or cause the adoption of gait patterns irrespective of the removal of a limb. Using FEM healthy bone can be used to investigate the effect of an asymmetrical loading pattern whilst removing the interference of comorbidities. However, subject specific FEM are created using bone imaging techniques, which expose participants to high levels of radiation. There is no established method to produce a validated semi-subject specific FEM from non-invasive bone imaging techniques such as pQCT. A semi-subject specific FEM could then be used both within the research environment and be bought into a clinical environment. Further investigation into the relationship between asymmetrical gait and bone health can be done using restricted devices. Research has found this to be accurate in the simulation of amputee gait in the restricted limb however there has been no research investigating the intact limb. This is important as the intact limb is also shown to also have bone degradation.

Therefore, the overall aim of the Ph.D was to investigate the relationship between bone health and asymmetrical loading, as seen in LLA. Firstly, a novel method was established to develop a semi-subject specific finite element model of the tibia from pQCT scans. A longitudinal study was carried out to establish a base line level of gait and bone health variation in able-bodied subjects. Then restrictive devices were used to investigate if gait characteristics in lower limb amputates could be simulated in able-bodied population.

### **1.1 Aims and objectives**

The overall aim of this Ph.D was to investigate the relationship between asymmetrical gait, as seen in lower limb amputees and bone health through semi-subject specific finite element models, and restrictive lower limb devices.

The objectives were

1. To construct a base tibia finite element model from a set of open-source bone scans.
2. To establish a process of extracting anthropometric data from subject specific tibia peripheral quantitative computed tomography scans, to create a semi-subject specific finite element model.
3. To optimise and validate the semi-subject specific finite element model by applying muscle and joint reaction forces outputs from subject-specific biomechanics and comparing results to longitudinal bone geometry changes.
4. To analyse the variation in tibial bone geometry and walking gait in able-bodied subjects and lower limb amputees over a 12-month period. This subject-specific data was then used to optimise and validate the semi-subject specific model.
5. To use a rigid ankle-foot orthosis and a trans-femoral prosthesis to restrict the ankle and both ankle and knee concurrently in able-bodied participants to simulate the gait characteristics of lower limb amputees.

## **2 LITERATURE REVIEW**

### **2.1 Introduction**

The literature review first uses fundamental literature to explain bone as a material and its structural and geometrical properties as determinates of bone health. Further explanations into the theorems behind a bone's ability to adapt to its surroundings are also provided. Following this, a summary of key literature on biomechanical loading is presented. The literature review then introduces the clinical population addressed within this thesis; lower limb amputees (LLA). Critical analyses are then undertaken on current literature investigating LLA's bone and biomechanical adaptations. Finally this chapter addresses finite element modelling, providing a summary of the literature before concluding on the use of FEM within the LLA population.

### **2.2 The Human Skeleton**

The skeleton is a system made up of bone and connective tissues. The skeleton provides support, protection of internal organs and facilitates movement through the transmission of forces. The bones within the skeleton are classified as axial and appendicular. The former refers to the bones that make up the skull, vertebrae and trunk, responsible for protection of internal organs. The latter refers to bones that make up the limbs, pelvis and shoulder and are primarily responsible for movement, these are the bones of interest within the Ph.D, specifically the lower limb bones.

#### **2.2.1 Long bones of the lower limb**

The long bones in the legs are the bones that support body weight and provide functionality to move. The tibia is the larger of the two bones in the lower leg, the other bone in the lower leg is the fibula. Studies have shown that the body weight is supported mainly by the tibia, with up the fibula supporting up to 17% of the body weight load (Segal et al. 1984; Funk, 2006). As

such the fibula does not aid in the transfer of weight to the ankle (Martini, et al 2012). Therefore, the tibia will be studied independently within this thesis.

At the distal end of the tibia the medial malleolus identifies the inside of the ankle. At the lateral side, the tibia is in contact with the distal end of the fibula. Distally to the tibia is the talus bone, which makes up the ankle joint (Figure 2). At the proximal end of the tibia, the patella bone along with the distal end of the femur combine to make up the knee joint (Figure 3).

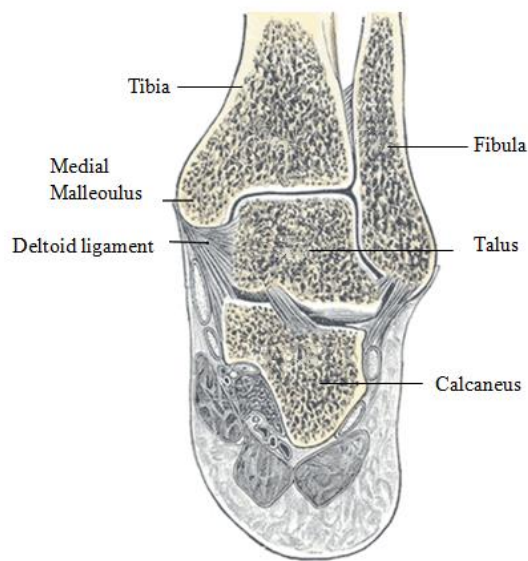


**Figure 2: Anatomy of the ankle joint, posterior cross-sectional view. Adapted from Webscape, WebMD (1994-2018)**

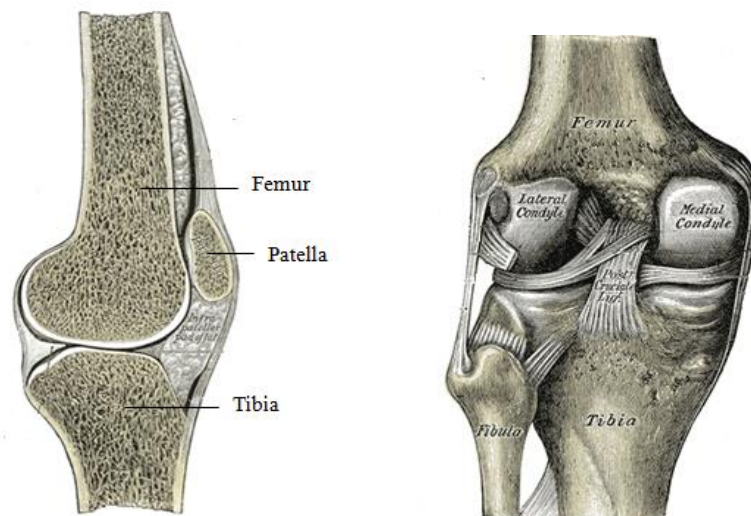


**Figure 3: Anatomy of the Knee joint. A; Cross sectional view. B; Posterior view**

## 2.2.2 Tibial Geometry

At the proximal end of the tibia is the widest part of the bone, the tibial plateau. Body mass is distributed across the medial and lateral condyle, situated either side of the intercondylar eminence. The most notable bony landmarks on the tibia is the tibial tuberosity, the site on the anterior side of the bone, where the patella tendon connects.

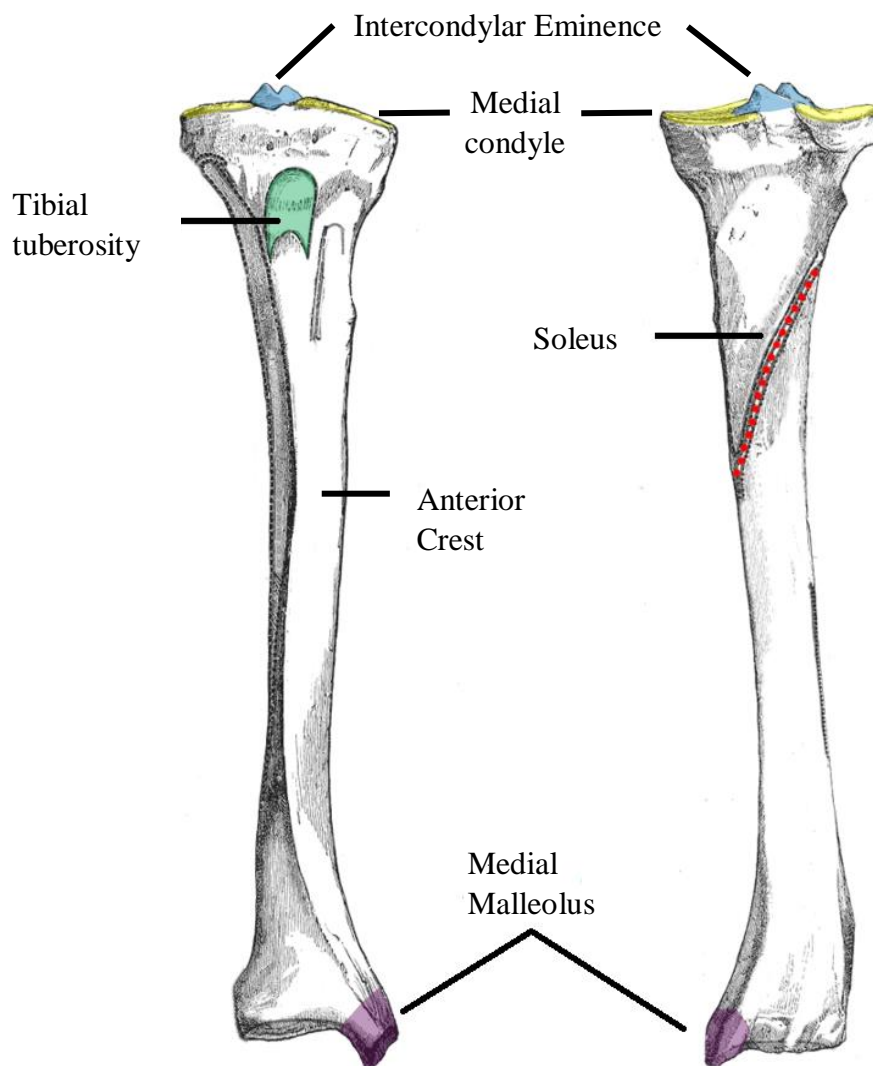


**Figure 4: The Tibia bone with bony landmarks identified in colour**

The tibia is a long bone, *i.e.* the bone is longer than it is wider, with a central shaft and two solid epiphyses at either end (see Figure 7) This structure is how bone have leant themselves to often be modeled simply as hollow beams with solid ends (Cowen 1990; Currey 2002; Lieberman, et al., 2004). This means its behavior is often modeled through beam theory (Koch, 1917; Salathe, Arangio and Salathe, 1989).

Beam theory, also known as Euler-Bernolli Beam theory, is the explanation of the deformation experienced by a beam in relation to the force applied to it. A bone is expected to support bending moments at either end, along its length, whilst the center of the bone deflects by a limited amount (Currey 2006; Lieberman, et al., 2004). Using the example of a bone which has been loaded in pure bending (Figure 5), the neutral axis will run through the middle of the bone. The magnitude of the moments applied, the length of the bone, the bone material properties (see 2.2.6) and bone geometry govern the maximum deflection.

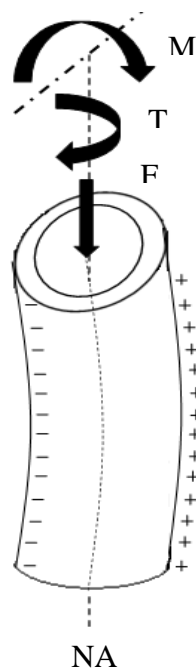
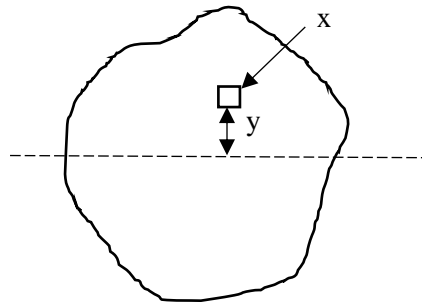


**Figure 5 : Schematic of long bone loading and response. Loading can be applied in combinations of bending moment (M), torsional moment (T) and compressive load (F). The compressive (+) and tensile (-) strains about the neutral axis (NA) are as a result of this compressive load. Adapted from (Levenston et al. 1998; Lieberman et al. 2004).**

The bone geometry in this scenario refers to the second moment of area, I. This is the distribution of material around the neutral axis and is defined with the following equation and Figure 6.

$$I = \Sigma x^2 * \Sigma y^2$$



y= distance from the neutral axis

x= one mm squared

**Figure 6: The cross section of a tibia bone with the neutral axis represented as a dashed line.**

**The second moment of area is defined by equation 1.**

To minimize mass and maximize the resistance to deflection, the distribution of mass should be as far from the neutral axis as possible, i.e. bones with higher second moments of area are more resistant to the strains produced as a result of mechanical loading (Currey 2006).

### 2.2.3 Internal Tibia Structure

On a macroscopic level, bone can be described as consisting of two parts; Cortical bone, synonymous with compact bone which makes up the solid outer layer of bone and trabecular bone, also known as cancellous or spongy bone which is found on the inside of bones. Figure 7 demonstrates the difference in structure in whole bones.

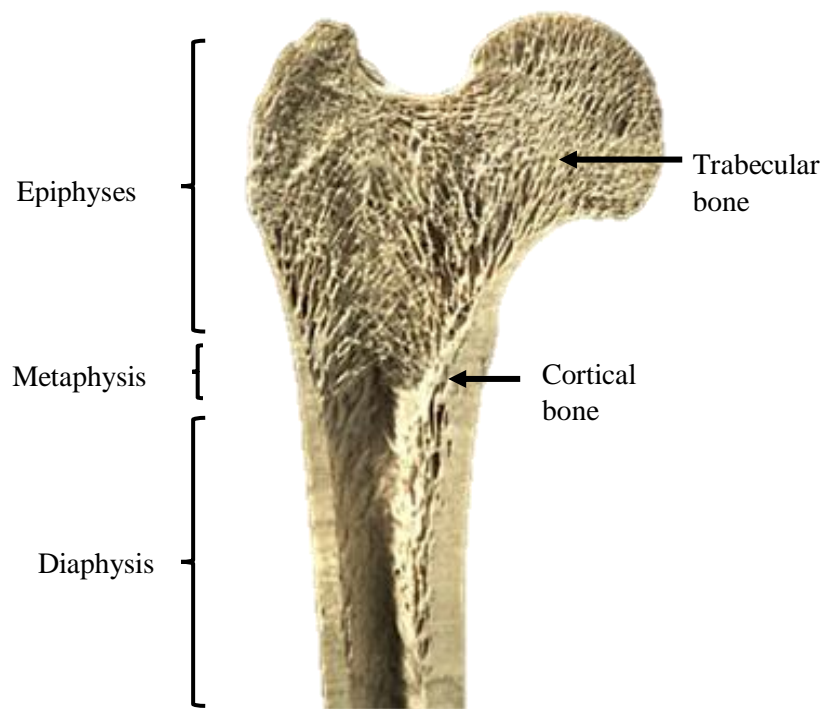


**Figure 7: Structure of whole bones as adapted from (Bartholomew et al., 2012)**

The distribution of cortical and trabecular bone varies across the skeleton. In long bones, as shown in Figure 7, the cortical bone is seen as a thick outer wall which covers the whole length, whereas trabecular bone is seen at the epiphyses, reducing and then absent in the diaphysis of the bone.

Although visibly identifiable by the difference in levels of porosity and density of the bone (Rho et al. 1998), the microscopic nature of these two types of bones is where true differentiation occurs (see Figure 8) and provides some justification for bone's biomechanical

properties. Osteons or Haversian systems run parallel to the long axis of the bone giving long bones their ability to resist the application of longitudinal and transverse loading (Caeiro, et al. 2013). Trabecular bone, on the other hand, consists of a framework of individual trabeculae. The orientation of which is dependent on the type of loading the bone is subjected to. Approximately 65-70% of the bones mass is made up of proteins and minerals (Bankoff 2012) this is reported as the bone mineral content (BMC), measured in grams. The amount of bone mineral (grams) in a given area of bone ( $\text{cm}^2$ ) is defined as bone mineral density (BMD) expressed as  $\text{g}/\text{cm}^2$  (Mooren 2012). The combination of fibrous protein and crystallized mineral provides bone with its ability to flex and ability to support high loads (Martini et al. 2012).

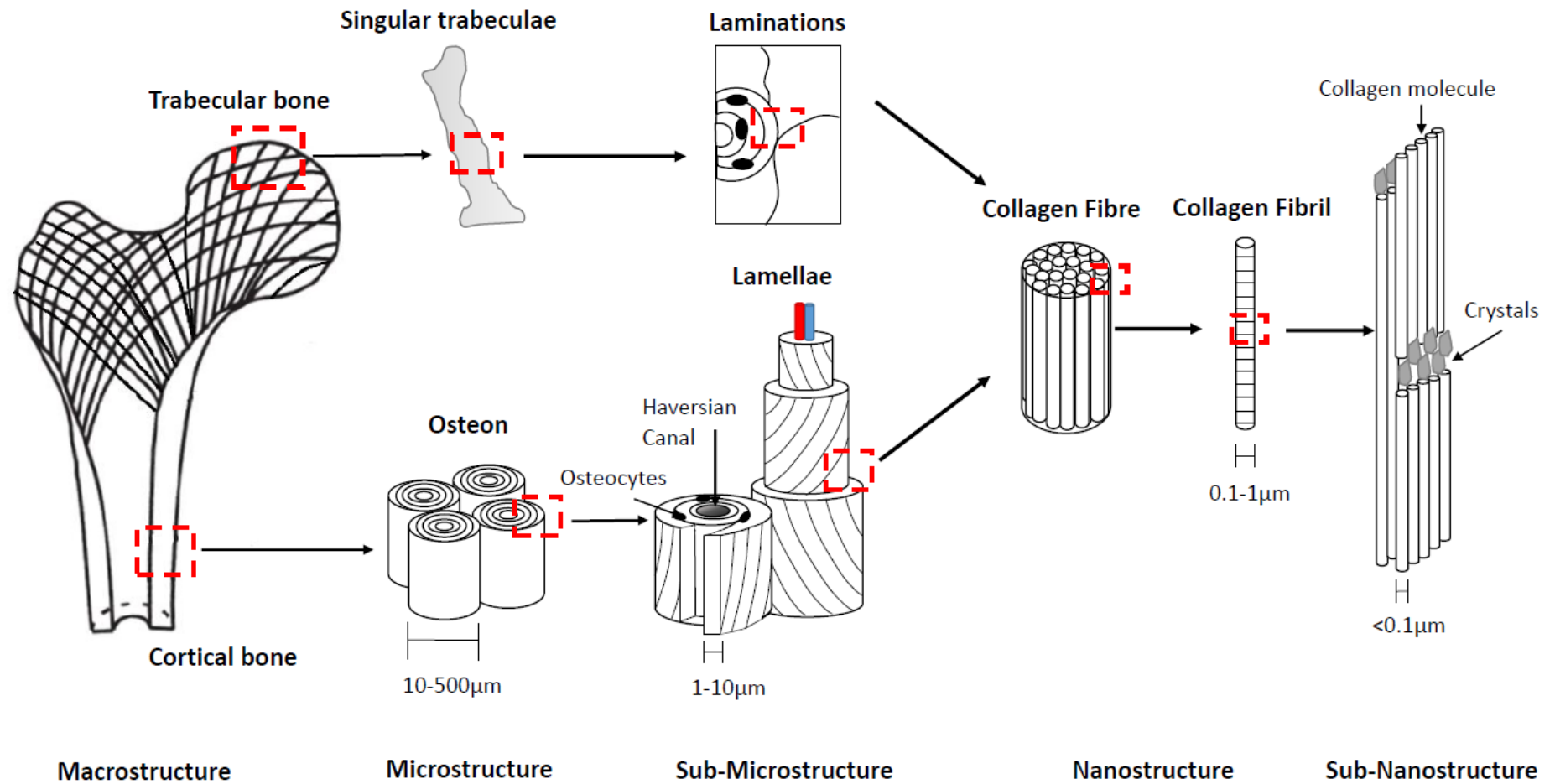


Figure 8: Schematic representation of hierarchical structure of bone. Adapted from (Rho et al. 1998) and (Caeiro et al. 2013).

#### **2.2.4 Bone Formation**

There are three types of cells which are significant in terms of bone structure and function; Osteoblasts, osteocytes and osteoclasts. Osteocytes are defined as osteoblastic cells, *i.e.* derived from osteoblasts and are found abundantly in bone, thought to outnumber osteoblasts and osteoclasts twenty fold (Robling and Turner 2009). Osteocytes have long dendrite processes which enable communication with other osteocytes as well as osteoblasts and osteoclasts. The osteocyte dendrites are embedded within channels surrounded with fluid known as lacuna and encased by a canalicular wall (Burra et al. 2010; Boyce et al. 2009). When the channel is subjected to mechanical loading, the fluid within the lacuna moves back and forth. It has been reported that the movement of the fluid instigates strain within the membrane of the cell. This strain instigates a signal sent to osteoblasts to enhance bone formation or to osteoclasts to inhibit bone resorption (Turner and Robling 2003). Osteoblasts are derived from bone lining cells and are responsible for the formation of bone. In brief, osteoblasts form bone through the synthetisation and secretion of un-mineralized bone matrix, known as the osteoid (Cowen, 1990; Currey, 2002; Martini,et al., 2012). Osteoclasts are large multi-nucleated cells responsible for the resorption of bone. This involves the secretion of enzymes, such as protease, along with hydrochloric acid to break down both the bone mineral and matrix (Currey, 2002; Boyce et al. 2009; Martini, et al. 2012).

#### **2.2.5 The bone modelling and remodelling processes**

The mechanical loading described in section 2.2.3 at the cellular level, originates from external loading. Although not the first researcher to acknowledge this, one of the most recognised feedback systems is that of the Bone Mechanostat theory developed by Harold Frost (Frost 1987). Simply, the Mechanostat theory explains the cell's processes in modelling and remodelling bone in response to strains caused by mechanical usage of the skeleton (Cointry et al. 2004). Bone modelling refers to the alteration of the bone as a whole, including structure,

size and subsequent geometry through the addition or subtraction from the periosteal or endosteal surfaces as a response to biomechanical factors (Currey 2002; Fogelman, et al., 2012; Cowen, 1990). This is the dominant process through adolescence into adulthood when peak bone mass is obtained, usually between the ages of 25-30 (AAOS 2012). Whereas in bone remodelling all the surfaces of the bone may be affected, on a smaller scale, involving a small collective of osteoblasts and osteoclast known as a basic multicellular unit (BMU) (Wheless 2011). The rate at which the bone is absorbed and formed is coordinated in younger skeletons with the average time span of a remodelling cycle being 2-8 months, with bone formation being the predominant process during this time (Fogelman, et al., 2012).

As part of the Mechanostat theory, it has been postulated that there is an optimum strain range at which bone remodelling and modelling is in balance and a positive bone health is maintained. *In vivo* studies have shown that bone strains in or above the 1500-3000 micro-strain range increase formation and therefore bone mass, while strains below the 100-300 micro-strain range encourage resorption (Frost 1987).

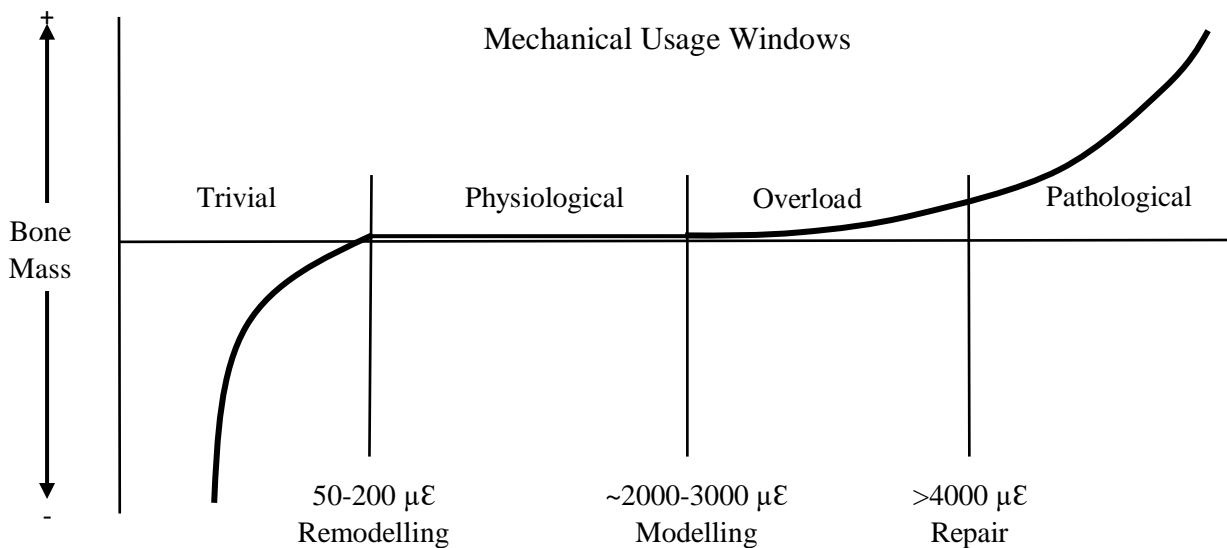


**Figure 9: The strain values relating to the different of regions of bone remodelling, modelling and absorption. Adapted from Forward and Turner (1995).**

### 2.2.6 Bone Material Properties

Another way to define bone health is using the material properties of bone. Bone is an anisotropic material, *i.e.* it changes how it responds dependant on the orientation of the load applied (Dalla and Bankoff 2012). Bone is heterogeneous, *i.e.* it has variance across its structure. In reference to Figure 8 this can be at the collagen fibril level up to the osteon level and involves the orientation and biomechanical properties of these levels. It is these properties that determine the overall mechanical function of the bone; including the stiffness and strength (Yao et al. 2010; Yassine et al. 2018). There has been investigation into if the heterogeneity of bone is advantageous or disadvantageous. For example, if a crack appears within the bone structure, the orientation of the surrounding cells can either cause this to propagate, or can act as a barrier, preventing any further damage (Currey 2005).

The stiffness of the bone is defined using Young's Modulus. By plotting stress and strain against each other the slope of the line can be calculated to determine the Young's Modulus. The linear relationship demonstrated by bone, *i.e.* that strain is proportional to stress up to the point of elastic deformation, prior to the point of breaking, determines bone to be a Hookean material (Pal 2014). Figure 10 depicts this relationship in graphical form.

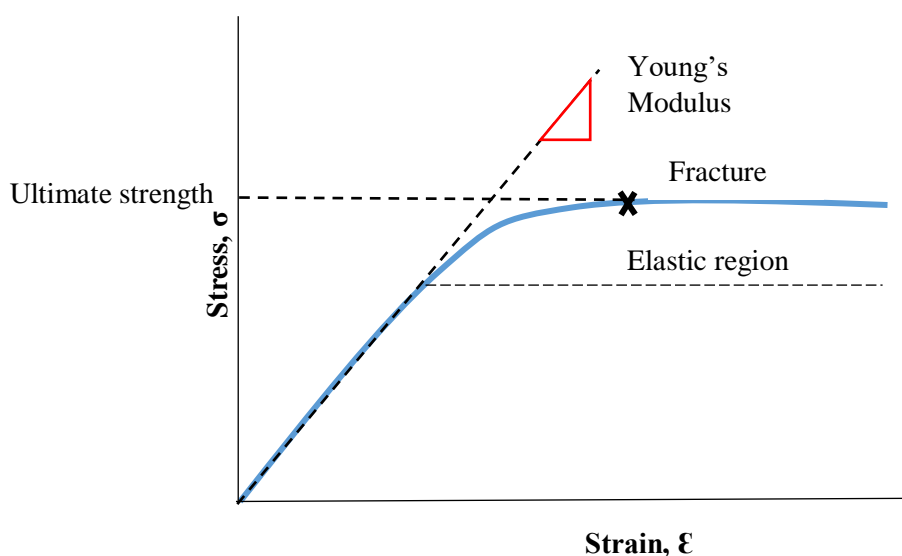


**Figure 10: The stress strain relationship of bone to define Young's Modulus developed from (Turner 1998).**

The area under this curve is the amount of energy needed to cause the bone to fail. The amount of stress the bone can sustain is referred to as its ultimate strength. This is not the same as bone strength, it is an intrinsic characteristic, *i.e.* it is independent of bone geometry (Turner 2006).

Bone mineral density is also used to infer strength. High mineralisation will mean that bone can absorb more of the energy and mean it is less likely to break. BMD is used within a clinical environment to categorise patients (NIH, 2015). When the BMD value falls below a certain number, the bone is considered osteopenic. Osteoporosis occurs when the re-modelling process becomes out of sync and osteoblasts lose their ability to reform bone, causing areas to lose their density, making bones more porous and therefore more susceptible to fracture (World Health Organisation, 2004).

**Table 1: Definitions of the level of bone health based on average bone density values, adapted from (NIH 2015)**

Level	Definition
Normal	Bone density is within 1 SD of the young adult mean
Low Bone Mass	Bone density is between 1 and 2.5 SD below the young adult mean
Osteoporosis	Bone density is 2.5 SD or more below the young adult mean
Severe (established) osteoporosis	Bone density is more than 2.5 SD below the young adult mean and there have been one or more osteoporotic fractures.

The categorisation of osteopenia is defined through the use of T and Z scores. A T score compares the BMD value of the person being measured to that of a normal young reference mean using the following calculation;

$$\frac{\textit{measured BMD} - \textit{Young normal mean BMD}}{\textit{Young normal Standard deviation BMD}}$$

A Z score is similar but compared to an age, sex and race matched ‘normal’ (Maghraoui 2012).

$$\frac{\textit{measured BMD} - \textit{age related mean BMD}}{\textit{Age related Standard deviation BMD}}$$

The database used to compare these values is based on the measurements taken at the Femur and can be found in the National Health and Nutrition Examination Survey database (NHANES III).

The current method for analysing BMD is through the use of bone imaging techniques, such as DXA (Cervinka et al. 2010). Dual Energy x-ray absorptiometry is a machines operate through the use of x-ray sources. ‘Dual’ refers to the two different energies emitted, one absorbed by the soft tissue and the other by the bone. The participant lies on a bed and the radiation is emitted from a source situated above the participant. This then passes through the body and the amount of radiation per pixel is detected. This is then converted to areal density and presented in  $\text{g/cm}^3$ . A bone with greater BMD will allow less radiation to pass through whereas a porous bone will allow more (Berger 2002).

The mechanostat theory states that bone formation and resorption is influenced by strains produced by mechanical loading. The term mechanical loading, specifically refers to muscle activity and external forces generated in movement. The following two sections detail methods of measuring muscle activity and external forces.

### 2.3 Musculoskeletal Modelling of Level Walking Gait

Muscle function was first modelled by Hill in 1938 and is referred to within literature as The Hill model. This model describes the basic mechanical function of a muscle using three components. The contractile component (CC), the active element converts the signals from the nervous system into force. This generated force is then expressed across the series elastic component (SEC). The third element, the parallel elastic component (PEC), is passive, yet when a force is applied to a muscle that results in stretching; the overall force can be added to that generated from the CC and PEC.

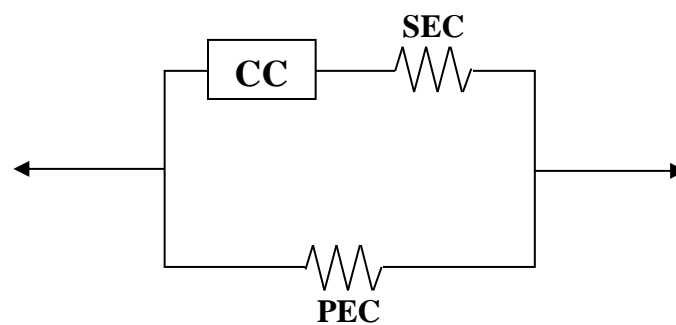


**Figure 11: Hill type muscle model diagram (developed from Caldwell, 2014). The active element is the contractile component (cc), the elastic element; the series elastic component (SEC) and the passive element; parallel elastic component (PEC).**

Muscles span joints within the human body and the overall force produced (as estimated by the hill type model) can be used through inverse dynamics to estimate the resultant joint moment (Robertson et al. 2014). However, the Hill model has limitations in that it can't be split to determine the individual muscle forces due to the inability to take into consideration all aspects that contribute to muscle force *e.g.* change in muscle length (Haeufle et al. 2014).

*In vivo* investigation of muscle force is very invasive, with surgical implantation and removal of transducers to measure force (Komi 1990). As such muscle force estimations have been studied *in vivo* within animal studies (Gregor et al. 1988). In analysis of human muscle forces, studies have investigated non-invasive measures of muscle forces, tracking vibrational behaviour (Martin et al. 2018). As an alternative to *in vivo* measurements, musculoskeletal modelling can take all the inputs of the system *e.g.* geometry and details of the movement to provide an estimate of joint contact and muscle forces. The Hill-type model has been shown to be a good estimation of the muscle properties (Lunn 2013). Thus, it has been implemented into many musculoskeletal models as a muscle actuator (Delp et al. 1990; Klein Horsman 1979; Carbone et al. 2015). The other inputs for the development of a muscle model include the musculoskeletal anatomy and the muscle architecture.

Muscle anatomy refers to the insertion sites, origin and any wrapping of the muscles. These can be identified via bone imaging techniques such as MRI (Fernandez and Pandy 2006), or using bony landmarks from cadavers. The easiest way to simulate a muscle is to model it as a line from its origin to its insertion site. Where the contact area is large, *i.e.* the gastrocnemius, it is often modelled as two muscles, the medial and lateral compartment (Robertson et al. 2014). This method is good at representing the length of a muscle but does not take into consideration any other contact points, for example, where a muscle may wrap around another bone, or overlies another muscle. Delp et al, (1990), solved this for musculoskeletal models by introducing a ‘via’ point. This via point acts as a frictionless constraint, which prevents the muscle from changing direction at a point at a where skeletal anatomy would encourage it to do so (Wagner et al. 2013; Robertson et al. 2014). Examples for where a via point is used is when modelling the tibialis anterior and the via point is on the distal part of the tibia.

Muscle architecture refers to the direction its fibres are aligned, pennation angle, its cross-sectional area and composition.

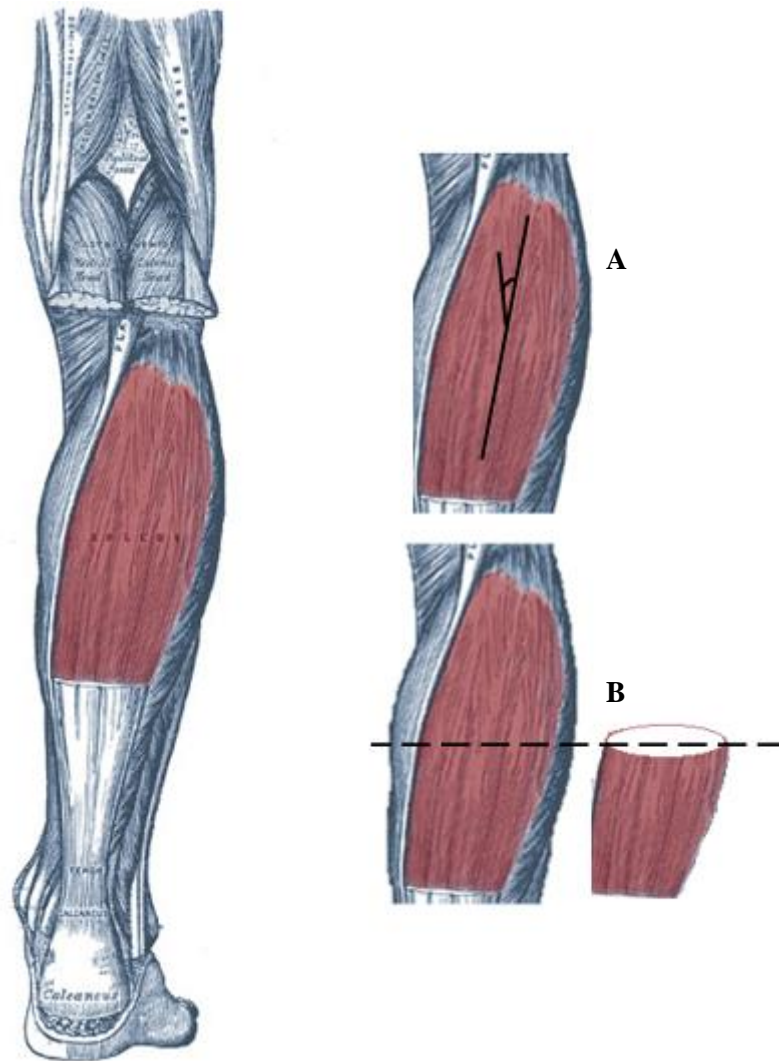


**Figure 12: Muscle composition definitions, A: pennation angle and B: physiological cross-sectional area.**

These data can be obtained from cadaveric dissection studies (Wickiewicz et al. 1983; Klein Horsman et al. 2007; Ward et al. 2009; Carbone et al. 2015). The model referenced extensively within literature is that developed by Delp et al, (1990), which was implemented into the musculoskeletal modelling software, OpenSim in their gait 2392 and 2354 models (see Study Two, Chapter Five, for further details on this). This used five cadaveric subjects taken from a

study conducted by Wickiewicz et al. (1983). Arguments have been made that only using 5 cadavers’ means that the model would not be representative the general population, hence the progression in models that have included larger cadaveric data sets, as seen in Table 2.

**Table 2: Details of the development of musculoskeletal models including their source and their implementation into software. Adapted from (Rajagopal et al. 2015).**

Model	Source of Muscle locations and architecture	Software implemented into
Delp et al. (1990)	5 cadaveric subjects (Wickiewicz et al. 1983)	OpenSim
Horsman et al. (2007)	Right lower limb cadaver (Horsman et al. 2007)	Anybody, OpenSim
Arnold et al. (2010)	22 cadaveric subjects (Ward et al. 2009)	OpenSim
Carbone et al. (2015)	Right lower limb cadaver (Carbone et al. 2015)	OpenSim, Anybody
Rajagopal et al. (2015)	22 cadaveric subjects (Ward et al. 2009) 24 MRI scans	OpenSim

Regardless of the number of cadaver studies used to develop a model, the base musculoskeletal model anatomy is scaled to the participant data. The most commonly used method is linear scaling (Lund et al. 2015; Nolte et al. 2016). This linear scaling method used the dynamic gait trial input, the location of the biomechanical markers on the subject are identified and the segments of the musculoskeletal models are scaled to agree with the subject segment lengths as identified by the marker locations. The newly scaled model was then re-applied to the

dynamic gait trial and the joint angles were calculated, these joint angles were carried through to inverse dynamic calculations. The inverse dynamic calculations were used to establish forces. The musculoskeletal modelling software, OpenSim used a scaling tool where the user chooses the relevant files to identify marker positions, which the program then adjusts the anatomical landmarks to agree with these. The musculoskeletal modelling software, AnyBody Modelling System<sup>TM</sup> uses an optimisation sequence developed by Anderson et al, (2010). In the investigation of the accuracy of these linearly scaled models when compared to non-linearly scaled models, it was found that the linearly scaled models were less accurate (Nolte et al. 2016). However, in order to improve accuracy, there is a need of medical images or cadaver data, which is not always available. Also, the problem of inter-subject variability still stands which could only be overcome by obtaining medical images for all participants.

Muscle force can be calculated in a number of ways including inverse dynamics, forward dynamics (see Figure 13) and EMG driven analysis for the improvement of muscle forces as estimated by musculoskeletal models (Schellenberg et al. 2015). Inverse dynamics takes the body segment dynamic movement and calculates the joint moments. The joint moments are then distributed to calculate individual muscle forces for each segment. Forward dynamics uses the muscle forces determined from muscle actuators to simulate the movement for an entire cycle. The benefit of using an inverse dynamics approach is that it takes less computational power, so is more time efficient (Schellenberg et al. 2015). The limitations are that any errors calculated in one segment are transferred up through the model and thus will be magnified. Forward dynamics, although requires higher computational power, does enable the incorporation of muscle properties within the calculations. Computed muscle control offers an alternative to these from the use of forward dynamics assisted by experimental data (Thelen and Anderson 2006). This generates movement from an initial set of actuators and compares

the gait to the experimental gait data. The actuators are then updated in order to produce movement which better represents the experimental data (Erdemir et al. 2007).

There are a number of different musculoskeletal modelling software packages. First developed in the 1990's, SIMM provided the first commercially available musculoskeletal modelling software package, (Delp et al. 1990). This was used widely within research, however, SIMM was unable to compute the muscle excitations and has limited capabilities in dynamic analysis (Delp et al. 2007). Since then, a number of musculoskeletal modelling software packages have become available, including AnyBody (Damsgaard et al. 2006), OpenSim (Delp et al. 2007) and BoB (Shippen et al., 2012). There are a number of differences between these software packages which have been reviewed extensively. The one advantage of the musculoskeletal modelling software, OpenSim, is that is an opensource software and its use among researchers has allowed the development of a large basis of musculoskeletal models and environments for other researchers to use.

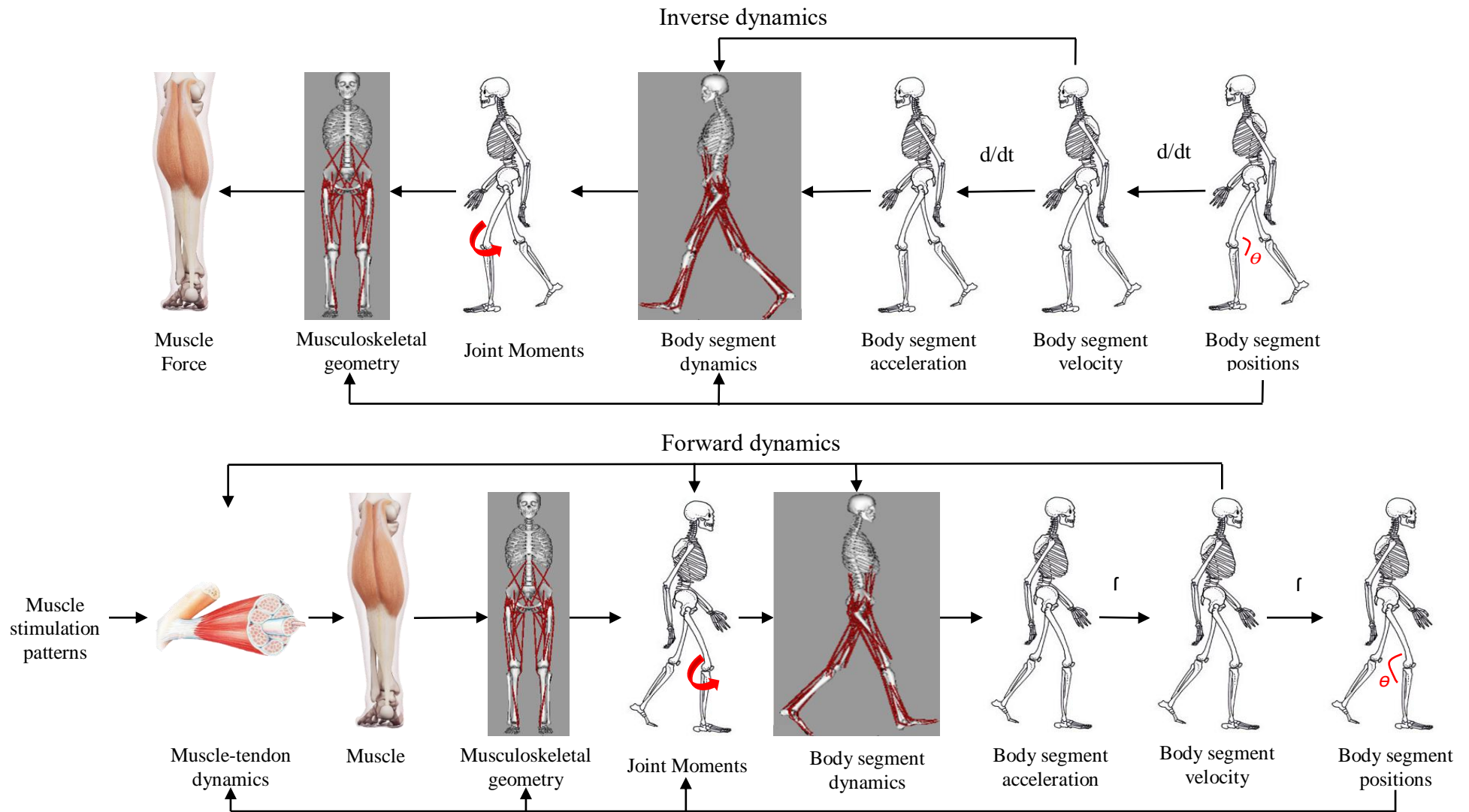


Figure 13: The outline of the inverse dynamics and forward dynamics used in musculoskeletal modelling. Adapted from (Robertson et al. 2014).

Despite the modelling limitations that are often identified in musculoskeletal modelling, it provides a non-invasive way to measure potential muscle forces within a gait model. There have also been recent developments in the extraction of these data to be input directly into other simulation programmes *e.g.* finite element analyses. For subject specific muscle forces, subject specific movement data must be collected and input. The following section details the basics of biomechanics of locomotion and their relevance within this thesis.

## **2.4 Biomechanics of Able- Bodied Locomotion**

### **2.4.1 Level walking biomechanics**

The gait cycle can be defined as the interval between two repeated events of walking (Levine et al.,2004). There are a number of characteristics used to determine a ‘normal’ walking pattern. The gait cycle is divided into two phases; stance and swing. The former describes when the foot is in contact with the ground and accounts for 60% of the gait and the latter when the foot is not (Kirtley, 2006). These two phases can be further broken down into seven events; initial contact, opposite toe off, heel rise, opposite initial contact, toe off, feet adjacent and tibia vertical (Whittle 1996). Figure 14 (page 27) is a graphical representation of this.

#### **Stance Phase**

Initial contact is considered the ‘start’ of the gait cycle. At the ankle, the foot is in a relatively neutral position in terms of dorsi/plantar-flexion with the tibia angled such that the heel first makes contact with the ground and absorbs energy as part of the braking mechanism. This heel contact creates a ground reaction force (GRF), which is high in magnitude and directed vertically and slightly posteriorly. The knee extends at the end of the swing phase and then it straightens for initial contact, the hamstrings then contract and the knee starts to flex in order to prepare for braking. At initial contact, the hip is at its maximum flexion, usually around 30°.

The contraction of the gluteus maximus and hamstrings produce an extensor moment as the hip begins to extend (Levine, et al., 2012) .

Still in the double support phase, which is approximately the first 10% of the gait cycle (Perry, 1992), the ankle begins to plantar-flex at the same time as the knee flexes. This ‘shortens’ the leg enabling the body to move over the leg and continue on a more horizontal path (Inman 1966). In able-bodied gait, the external plantar-flexion moment is matched with an internal dorsiflexor moment, which helps reduce the power through absorption and aids foot plantation. However, the limb is still loaded, so there is still a high vertical and posterior GRF. The hip continues to extend, this combined with the knee flexor moment, contribute to a power generation to assist later in gait (Levine, et al., 2012).

Mid-stance occurs at 10% to 30% of the gait cycle and is identified by the contralateral leg passing the stance leg, whilst the anterior/posterior component of the GRF is equal to zero. (Levine, et al., 2012). At the ankle, the foot stays flat on the floor, whilst the tibia rotates about the joint in a movement, which is labelled as the ‘mid-stance rocker’. The knee during mid-stance reaches maximal flexion of between 10° and 20°, (dependant on the individual) before contraction of the quadriceps instigate extension. At the hip, there is continued extension with the joint angles moving from hip flexion through to hip extension. Throughout mid-stance, body weight is supported by one limb only with the hip muscles providing the majority of activity to help with balance. (Levine, et al., 2012).

Terminal stance begins when the heel on the supporting limb starts to rise (Perry, 1992). As the heel rises, the ankle joint continues to dorsi-flex, which is maintained to reach a maximum post heel rise. Towards the end of terminal stance, the ankle starts to plantar-flex. Throughout

terminal stance, the forefoot remains in contact with the ground. At the knee the extension peaks around the same time as the heel rise, this combined with the commencing of plantar-flexion brings the ground reaction force in front of the knee (anterior peak). This coincides with a second vertical peak around opposite initial contact. The hip is still in extension, reaching a maximum of approximately  $20^\circ$  as the contralateral heel makes contact. (Levine, et al., 2012).

This is the second phase of double support and describes the stage between initial contact of the opposite leg and toe off of the supporting limb. As to be expected, the ankle is in plantar-flexion throughout this stage, with a relatively high plantar-flexor moment opposing the dorsiflexor moment, produced by the initial contact of the opposite limb. This results in a large power generation, which is needed to accelerate the limb through the swing phase; this is the peak at opposite initial contact, described in terminal stance (Levine, et al., 2012). The knee is in flexion throughout this stage, with the internal moment reversing to become an extensor moment and absorbing power. The hip, which was fully extended at terminal stance, starts to flex due to the contraction of the muscle, adductor longus (Perry, 1992). For the rest of the phase the GRF decreases in magnitude to be negligible at the start of the initial swing period.

### **Swing Phase**

This signifies the end of the stance phase and beginning of swing. Peak ankle plantar-flexion happens just after toe off and measures around  $25^\circ$ , after which the muscle contraction brings the ankle up into a more neutral, if not slightly dorsi-flexed position. At the beginning of this period the knee is flexed to about half its potential, with the contraction of the rectus femoris preventing excessive knee flexion (Nene, et al., 1999). It is during this initial swing period that the knee reaches its maximum flexion angle, of around  $60-70^\circ$ . The knee and hip work together

in a 'double pendulum', where the hip flexion cause the shank to be left behind and the knee to flex (Levine, et al., 2012).

During this phase, the ankle moves from plantar-flexion to dorsi-flexion. This allows for foot clearance through swing. To also aid with clearance, the knee is in flexion, which, as in initial swing, is as a result of flexion at the hip.

The tibia becoming vertical marks the end of the swing phase. The ankle position is in a relatively neutral position, varying by a few degrees in plantar-flexion and dorsi-flexion. The knee, which reached peak flexion in initial swing, has already started to extend, but goes through rapid extension in this phase, preparing the limb for initial contact. The hip reaches maximum flexion during mid swing, during terminal swing the hip stays fully extended with very little power crossing the joint.

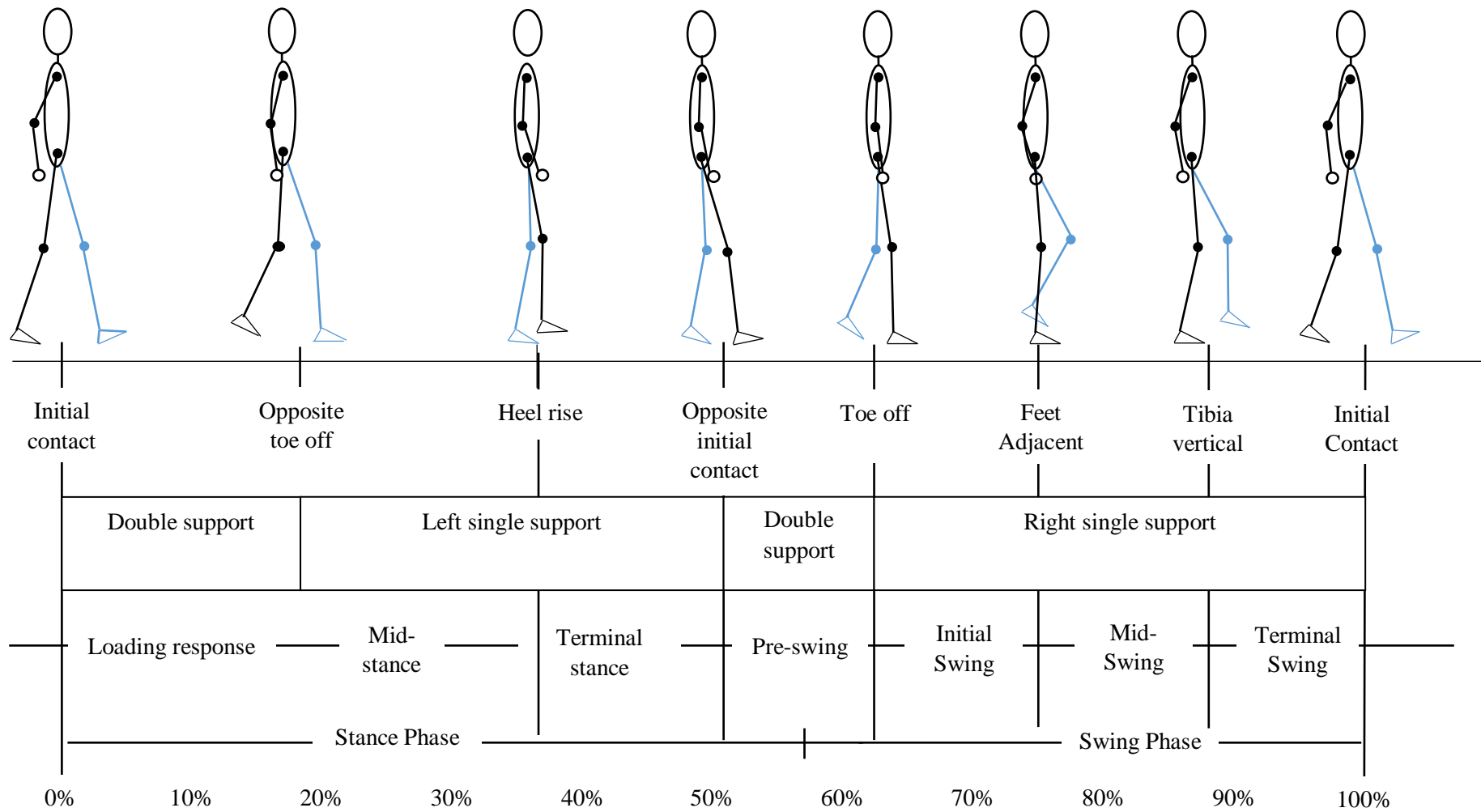


**Figure 14: The level walking gait cycle broken down into its phases. Adapted from Uustal et al. (2004).**

### **2.4.2 Stair walking biomechanics**

Classified as an activity of daily living, stair walking is part of community ambulation and is important for maintaining a good quality of life. However, this task is considerably more biomechanically demanding than level walking, with increased range of motion required at each joint, as well as increased joint power (Riener et al., 2002; Alcock et al., 2015; Protopapadaki et al. 2007; Reid et al. 2007). Research has been conducted with continual staircase walking as well as the difference in floor to step and from step to step within a staircase. Alike the level gait walking cycle, stair walking can be broken down into a stance phase approximately 65% and a swing phase (Zachazewski, Riley, and Krebs 1993). Figure 15 details the exact events within each of these phases.

#### **Stair ascent**

The stance phase begins with weight acceptance and accounts for approximately the first 17% of the gait cycle (Zachazewski et al. 1993). During this phase the knee and hip joints are in flexion and the ankle in dorsi-flexion (Andriacchi et al. 1980; Protopapadaki et al. 2007; Whatling et al. 2010; Riener et al. 2002). The largest moments occur during stance phase for both stair climbing and level walking. At the very start of weight acceptance, there is a knee extensor moment, which increases rapidly to become a flexor moment. This knee extensor moment has been reported to be as high as 1.0Nm/Kg (Costigan et al. 2002). In level walking this is when the knee is flexed to approximately 20°, whereas, in stair ascent the largest moments occur when the knee is flexed to 60°. Based on previous instrumented knee replacement literature the contact area at this point of flexion is small and could lead to higher stress within this region (Costigan et al. 2002).

The single support phase starts with the pull-up of the contra-lateral leg, the majority of energy needed for the pull-up is generated as a result of the extensor moment at the knee joint (Mcfadyen and Winter 1988). At the ankle joint there is a dorsiflexor moment, counter-acted by the plantar flexor muscles. As the contra lateral leg goes through forward continuation and the stance phase ends, the knee and hip continue to extend with the hip flexion moment decreasing (Protopapadaki et al. 2007). During swing the limb is in clearance where it goes over the lip of the next step before being placed on the next step of the stair case. The ankle moves through from plantar flexion to dorsiflexor and the knee and hip are in flexion before reaching maximum flexion prior to foot contact.

### **Stair descent**

At weight acceptance in stair descent the hip joint is slightly flexed, the knee is near full extension and the ankle is in plantar flexion (Andriacchi et al. 1980; Protopapadaki et al. 2007). In the stance phase during stair descent the hip and knee move into flexion and the ankle moves from plantar-flexion to dorsi-flexion within the first 20% of the cycle (Protopapadaki et al. 2007). The hip flexion angle during stair descent is smaller than during ascent. During stair descent there was an external knee extension moment from foot contact through the forward continuance and then an external knee flexion moment through the controlled lowering until the point of toe off (Protopapadaki et al. 2007). The ankle showed a dorsiflexor moment during swing of similar profile to that seen in ascent, but of smaller magnitude.

When comparing between walking down steps on a staircase to walking down onto the ground level, there was a higher peak hip extension angle in late stance phase in the latter with the hip not reaching full extension when walking down steps within a staircase (Alcock et al. 2015).

Vertical GRF were higher at the beginning of stance in stair descent compared to stair ascent (Riener et al. 2002; Protopapadaki et al. 2007). Protopapadaki, (2007) suggested this was due to the increased walking velocity when descending the staircase. At the end of stance phase the vertical ground reaction force was less during stair descent than ascent (Protopapadaki et al. 2007). Alcock et al. (2015) found that the vertical ground reaction force was increased when the participant was descending from step 2 to the level ground over descending from the top step to step one. The anterior/posterior ground reaction force is found to be posterior moving through to anterior at approximately 50% of the stance phase (Riener et al. 2002; Alcock et al. 2015; Mcfadyen and Winter 1988; Zachazewski et al. 1993). It was suggested that the fore-foot contact was the reason for why the A/P force was reduced (Riener et al. 2002).

Differences in magnitude of ground reaction force has also been presented when the inclination of staircase changes, the steeper the incline the larger the vertical ground reaction force, however it still follows the same profile as presented previously (Riener et al. 2002). In comparison to level walking, the A/P forces were reduced in stair walking, with a variation in inclination of the staircase having little effect on the magnitude of the force.

Ground reaction forces are only one source of the external loading on bone, with muscle loading also being a large contributor. It has recently been shown that tibial loading is not strongly correlated to GRF values (Matijevich et al. 2019). Therefore it is important to understand the loading on bones as an independent measure.

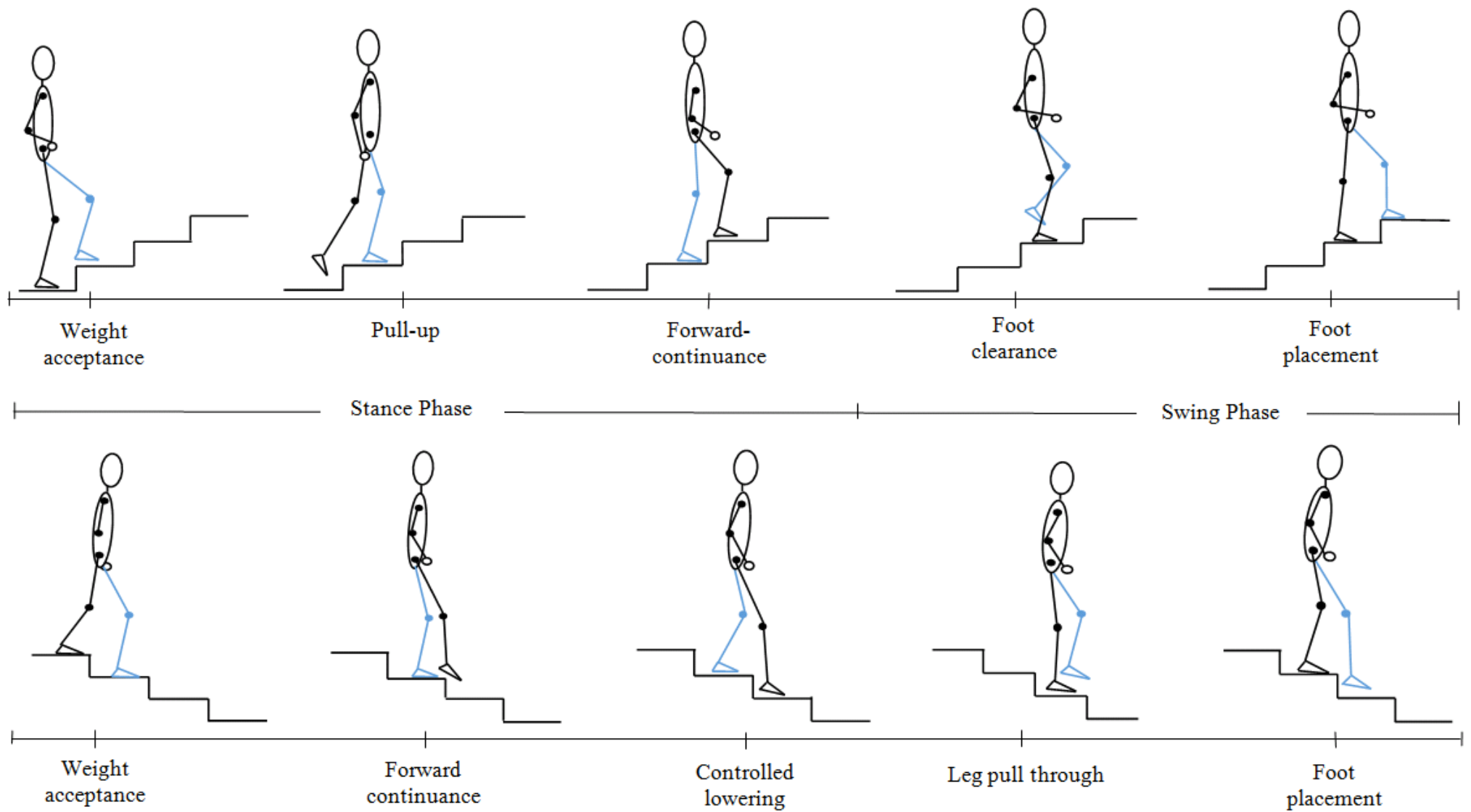
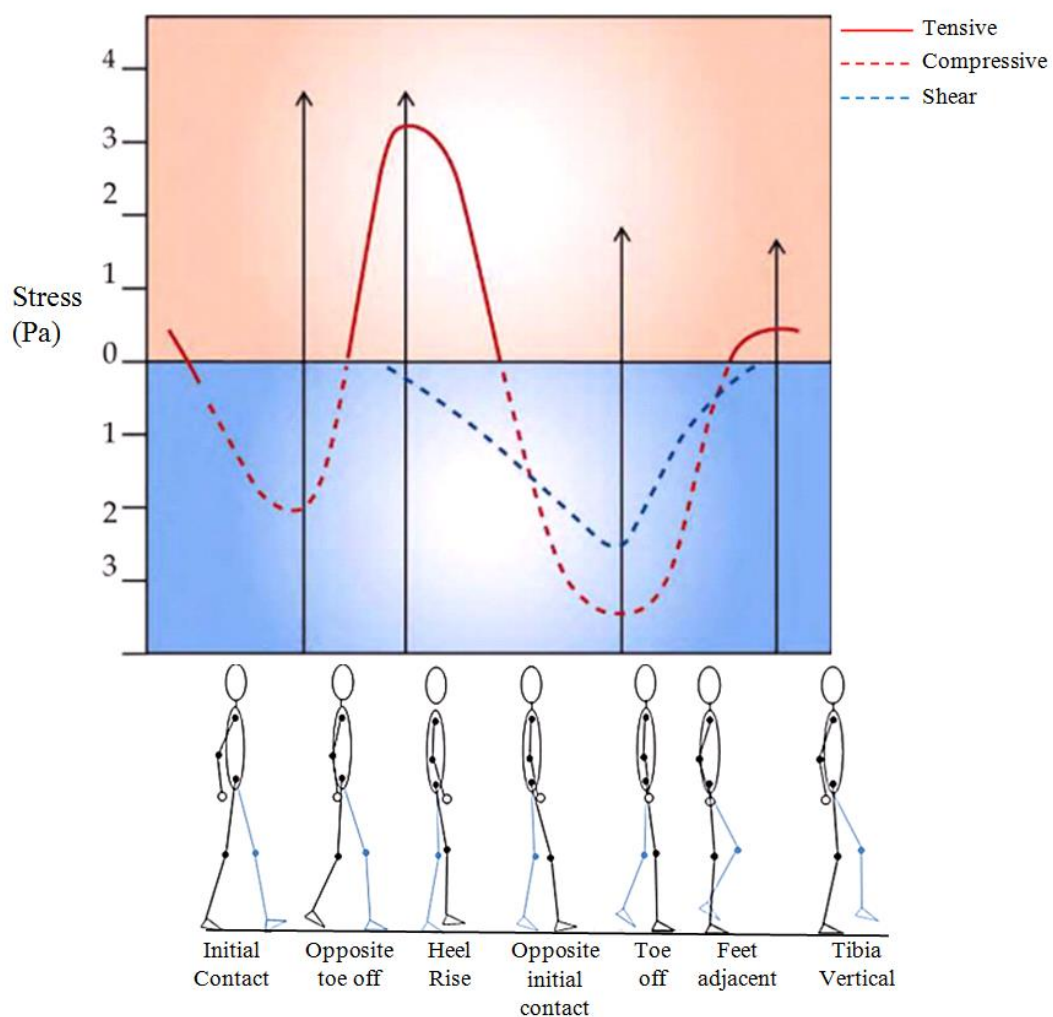


Figure 15: Stair ascent and stair descent gait cycle. Adapted from Novak et al. (2010)

### 2.4.3 Biomechanical loading on the tibia

The tibia is strongest when it is loaded under compression, i.e. when loads are applied which are intended to reduce the structure, as opposed to tensile loads that elongate a structure (Bankoff 2012). Figure 16 below shows the loading across the tibia in a normal gait cycle (Bankoff 2012). At heel contact, *i.e.* when the tibia is primarily loaded it is under compression. As the weight is transferred toward the proximal end of the foot and muscle contraction commences, the tibia is under tension.



**Figure 16: The loading across the tibia during walking. Tension is expressed as a solid red line, compression as a dashed red line and shear loading as a dotted blue line. Adapted from Bankoff (2012).**

This then reverts back to a compressive force as the foot begins to push off before entering the swing phase. The shear stress represents the twist that is experienced by the tibia throughout this motion. As can be seen by Figure 16 there is also a shear force present in stance. This is thought to be due to the external rotation of the tibia as the body prepares for the propulsive phase. (Holick 1998; Bankoff 2012; Nordin and Frankel 2001).

Nazer et al. (2012) collated literature from a number of *in vivo* studies which investigated strains within the tibia. The majority of these measures were taken at the medial tibial shaft, due to the ease of location for the surgical attachment of strain gauges (Nazer et al. 2012). Medial tibia strains for walking were within a range of 237–1250  $\mu\epsilon$ . A further review categorized these strains to tensile and compressive with values quoted at 30-580  $\mu\epsilon$ , 30-850  $\mu\epsilon$  in walking only studies. Higher values are associated with more vigorous exercises (Yang et al. 2011).

The limitations of these *in vivo* studies is that they only use only one strain gauge, often placed on the shaft of the tibia, meaning data is not representative of the entire bone (Cristofolini et al. 2013). Cadaveric studies that have placed strain gauges along the entirety of the bone have concluded that the strain distribution is very dependent upon the type of loading the bone is subjected to and that the diaphysis of the tibia is optimal for cantilever loading in both the sagittal and frontal plane.

As mentioned previously, tibia are often modeled simply as hollow beams with solid ends (Cowen 1990; Currey 2002; Lieberman, Polk, and Demes 2004). This means its behavior is often modeled through beam theory (Salathe et al., 1989; Brassey et al. 2012). Through the use of static equilibrium equations and calculations of cross-sectional area and moments of inertia

beam theory is applied to bones to address the relationship between the beam's ability to deform as a result of an application of load, *i.e.* the strain response (Salathe et al., 1989). Using knowledge of the Mechanostat theory, this beam can be related back to a bone by implying the bone response.

In understanding the magnitude, rate orientation of the load application to the bone and the strain produced as a result of this the link between physical activities and changes in bone can be investigated further. This becomes important in those clinical populations where a degradation in bone health is thought to be as a result of changes in gait *e.g.* in lower limb amputees.

## 2.5 Lower limb amputee statistics

Amputation refers to the removal of a biological structure. The level of amputation is defined in accordance with British Standard BS 7313 Part 3: 1993 and ISO 8548-2: 1993. This thesis concentrates on lower limb amputations, the classifications of which are depicted in Figure 17.

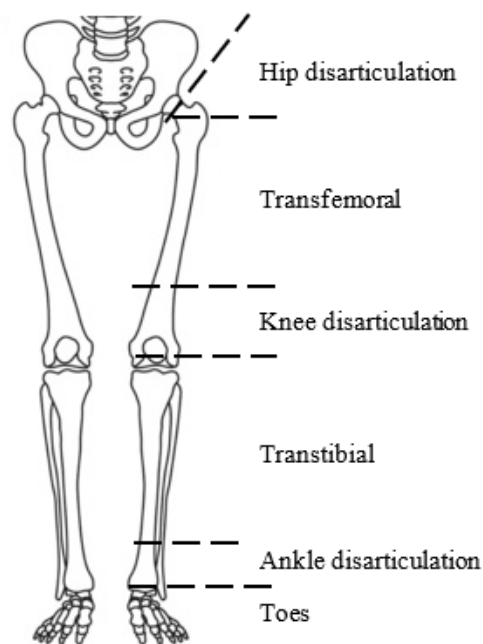


**Figure 17: Amputee level definition, adapted from (Stewart 2008)**

Amputations are often categorized as either traumatic, resulting from a road traffic collision or war and vascular (Stewart 2008). Approximately 90% of all UK and USA amputations are as a result of a dysvascular disease, specifically diabetes (Stewart 2008; Moxey et al. 2011). Dysvascular diseases also include conditions such as atherosclerosis, specifically peripheral arterial disease; the build-up of fatty material on the inner walls of arteries in the arms and legs (Ahmad et al. 2016; Stewart 2008; Glaser et al. 2013).

As of 2008 there was an estimated 6000 amputations in the UK per year (Diabetes UK, 2008). There has been some discrepancy in these numbers in subsequent publications, with the rate of amputations being expressed as little as 5.8 up to as much as 176 per 100,000 (Moxey et al. 2011; Ahmad et al. 2016; Canavan et al. 2008). The smaller rates reported by Moxey et al. (2011) take into account population demographics that are not at risk of amputation, for example children, thus underestimating the potential rate. In the last year Diabetes UK has published data that estimated an average of 7,000 people with diabetes undergo amputations each year (Kerr 2017). Even after amputation almost a third of amputees living with diabetes, risking further amputations (Schofield et al. 2006).

Whilst attempting to reduce further amputations, it must be considered the current cost to the NHS. There was an estimated expenditure £44 million for inpatient care on amputees within the NHS in 2014/15, breaking this down, in 2003 on average on amputation incurred in-patient costs of £8459 (Clarke et al. 2003). Post amputation, costs are reported to be as high as £21 million a year (Kerr 2017). The reported amputee statistics refer to the population and government bodies surrounding amputees, however, there are risks and complications that occur on an individual level that also need to be addressed.

### 2.5.1 Geometrical and structural adaptations in bone in amputees

Research has shown that a period of disuse or unloading, such as that associated with amputation recovery causes an acceleration in the turnover of bone, so that bone resorption occurs at a rate greater than bone formation, resulting in a loss of bone mass, affecting both the bone geometry and structure (Robling and Turner 2009). Studies investigating changes in bone geometry in an amputee population have included both humans and animal cohorts. The early animal studies found an increased density at the end of the residual limbs, although it was unclear to whether the rabbits, were ambulating on the stump (Sevastikoglou et al. 1969). Studies in humans have concluded that the end of the residual limbs of amputees lost significant amounts of both total bone area and cortical area, combined with reduced volumetric BMD (Sherk et al. 2008). Investigation into geometric changes within the intact limb are limited. Of data published, the geometry of the intact limb was reported to not significantly change over a 12 month period (Bemben et al. 2017). The data reported were close to significance but this could be due to the small sample size of eight traumatic amputees within this study and a larger cohort could result in significant changes (Bemben et al. 2017).

Amputees have lower BMD than able-bodied populations (Leclercq et al. 2003; Bemben et al. 2017; Sherk et al. 2008; Royer and Koenig 2005). There is some disagreement within literature to the influence of level of amputation, (*i.e.* above or below knee) on BMD across all sites. Smith et al. (2011) concluded that level of amputation had no effect on the BMD value at any site (Smith et al. 2011). On the other hand there are a number of studies which reported a significantly greater percentage difference in BMD, compared to control, in above knee amputees against below the knee amputees. Sherk et al (2008) reported 1.044 g/cm<sup>2</sup> for transtibial and 0.680g/cm<sup>2</sup> for transfemoral compared to controls whose values ranged from 1.093g/cm<sup>2</sup> to 1.143g/cm<sup>2</sup> (Kulkarni et al. 1998; Sherk et al. 2008; Leclercq et al. 2003).

The demographics of the amputee population show that the average age of an amputee in the UK is 68-70 years old (Davie-Smith et al. 2015; Stewart 2008). Bone has been reported to reach peak mass from late teens up to late twenties after which a natural decrease in BMD occurs (Berger et al. 2016). As mentioned in section 2.5, the most common cause of amputation is diabetes. Within a diabetic population, research has shown increased values of BMD as well as increased risk of fracture, suggesting that diabetic patients have a biomechanically altered bone (Lecka-Czernik 2010). Contrarily however, BMD has been reported to be an average of 10.4% to 12% lower on the intact limb, with variations depending on where in the body the measurement is taken (Smith et al. 2011).

The other, within group, research has shown an increase of the occurrence of osteoarthritis in the intact limb of LLA. It is thought that asymmetrical loading across the knee, specifically increased knee adduction moments are contributing factor to the progression of this disease (Gailey et al. 2008; Morgenroth et al. 2012; Burke et al. 1978). Along with the increased risk of osteoarthritis, the biomechanical adaptations found in amputees have been thought to be a contributor to other conditions which are associated with poor bone health.

## **2.5.2 Biomechanical adaptations in lower limb amputees**

### **Activities of daily living**

Activities of daily living (ADL) refer to basic tasks that are required to care for oneself, examples of which include eating, grooming and mobility (Wiener et al. 1990). Mobility is the category in reference where the term ADL's are used in this thesis. In an amputee population the ability to carry out ADL's is an important assessment criteria in the measurement of mobility and prosthesis function and has become of increasing importance (Frossard et al.

2011). One measure of gait functionality is the ‘K-level’, a 0-4 point scale of function descriptive developed by Medicare to determine level of ambulation and therefore prosthesis requirement (Orendurff et al. 2015).

**Table 3: The K-level classification (Medicare, 1995).**

Level	Description
K-0	Does not have the ability or potential to ambulate or transfer safely with or without assistance and a prosthesis does not enhance quality of life or mobility.
K-1	Has the ability or potential to use a prosthesis for transfers or ambulation on level surfaces at fixed cadence. Typical of the limited and unlimited household ambulatory.
K-2	Has the ability or potential for ambulation with the ability to traverse low-level environmental barriers such as curbs, stairs, or uneven surfaces. Typical of the limited community ambulatory.
K-3	Has the ability or potential for ambulation with variable cadence. Typical of the community ambulator who has the ability to traverse most environmental barriers and may have vocational, therapeutic, or exercise activity that demands prosthetic utilization beyond simple locomotion.
K-4	Has the ability or potential for prosthetic ambulation that exceeds the basic ambulation skills, exhibiting high impact, stress, or energy levels, typical of the prosthetic demands of the child, active adult, or athlete.

The K-level of an amputee is determined through self-assessment questionnaires and physical tasks (Parker et al. 2010; Frossard et al. 2011).

In terms of temporal-spatial adaptations LLA walk slower, have a longer step length compared to able-bodied subjects with proportionally more time spent on the intact limb in stance than

on the prosthetic (Cheung et al. 1983; Hurley et al. 1990; Sadeghi et al. 2000; Schulz et al. 2010; Kovac et al. 2010; Schaarschmidt et al. 2012; Roerdink et al. 2012). The average level walking speeds for amputees range from 1 to 1.3m.s<sup>-1</sup> (Levine et al. 2012). It has been shown that the asymmetries associated with amputee gait could be reduced by increasing the walking speed (Nolan et al. 2003; Detrembleur et al. 2005; Isakov et al. 1996). However it is thought that by slowing the walking speed amputees are acting to decrease the forces acting upon the contra-lateral limb (Hurley et al. 1990). Comparing level of amputation, transfemoral amputees have been shown to adopt shorter, wider steps, that are longer in duration compared to transtibial amputees (Schulz et al. 2010) concluding that transfemoral amputees walk with greater temporal, but not spatial, asymmetry.

In TT amputee gait, the lack of biological system at the ankle means that they rely on the prosthetic ankle to provide planter flexion. Dependant on the level of functionality of the prosthesis depends on the amount of support within gait it provides. The simplest prosthetic ankle removes range of motion at the ankle but maintains power, as the material used for prosthesis are designed to absorb the energy and return it for forward propulsion (Stevens et al. 2018; Mitchell et al. 2013). However, more of this energy is absorbed by the material rather than returned which could be another explanation for why the power generation moment is so small (Bateni and Olney 2002). Winter and Sienko (1998) reported that at its peak an amputee's plantar-flexor moment would still only reach 60-70% of able-bodied individuals. The resulting lack of plantar flexion at the ankle on the prosthetic limb is compensated for by increased knee power and sagittal planar moment in the intact limb (Royer and Koenig, 2005; Sanderson and Martin, 1997). Other compensatory mechanisms used by amputees include the use of hip extensors to reduce hip flexion during early to mid-stance and to produce power for forward propulsion (Winter and Sienko 1988; Seroussi et al. 1996; Soares et al. 2009). It is also well

documented that transtibial amputees have a smaller knee flexion in their residual limb during stance (Bateni and Olney 2002; Powers et al. 1998; Sanderson and Martin, 1997; Breakey 1976). These adaptations allow for the thigh to remain more vertical and knee more extended reducing the requirements of the muscles to prevent knee buckling and providing greater stability for the amputee (Sanderson and Martin 1997).

Transfemoral amputees lack biological systems at both the knee and ankle therefore have two prosthetic joints for support. In a non-computerised prosthetic this would lead to minimal knee flexion in stance phase, locking it in extension in order to provide stability (Segal et al. 2006; Detrembleur et al. 2005; Johansson et al. 2005; Petit et al. 2005; Farahmand et al. 2006). At the hip, the compensatory mechanisms depend on the type of the knee. In a mechanical knee the lack of flexion means the extensors in the hip have to be used for power generation, the same as in transtibial amputation, but in transfemoral a hip flexor moment at the end of stance has also been seen (Levine et al. 2012; Seroussi et al. 1996). The type of prosthetic knee does have some effect on the kinematics of amputee and gait and it is for this reason most literature which uses transfemoral amputees as subjects investigate the effect of different types of prosthesis (Segal et al. 2006; Kaufman et al. 2007; Kaufman et al. 2012; Johansson et al. 2005). The lack of ankle plantar flexors and in transfemoral amputees, the absence of a biological system at the knee means that the hip is the only method of generating power for forward progression of the residual limb. The first increase in hip moment is seen at initial contact, McNealy and Gard, (2008) reported a moment in LLA that was twice that seen in able-bodied participants. Bateni & Olney (2002) explain that this increase in hip moment was used not only as power generation, but as a support moment, which is usually contributed to by knee flexor moment and an ankle dorsiflexor moment. The second recorded increase in hip moments and corresponding powers is in late stance through pre swing and is used to ensure foot clearance

and provides power through swing, which, in normal gait, would be provided by the ankle plantar flexors (Levine, et al. 2012; Winter and Sienko 1988; Sagawa et al. 2011; Silverman et al. 2008).

Comparing GRF in amputees and able bodied subject it has been found that people with unilateral amputation have up to 23% GRF asymmetry compared to less than 10% asymmetry in able bodied gait (Gailey et al. 2008). The magnitude of GRF for the affected limb are reduced in both vertical and A/P direction for propulsive and breaking, but for the intact limb both are greater (Nolan et al. 2003; Silverman et al. 2008; Lloyd et al. 2010; Sanderson and Martin 1997; Royer and Koenig 2005; Silverman and Neptune 2014; Levine, et al. 2012). Lower limb amputees have also been shown to have an increased rate of loading on their intact limb (Hobara et al. 2014, Gabrowski and D'Andrea 2013). One theory for the adoption of this is that by loading their intact limb more, amputees are protecting their residual limb (Nolan et al. 2003; Sanderson and Martin 1997; Hurley et al. 1990). Another theory discussed, is that amputees distribute more of their body weight over the intact limb to have a centre of gravity closer to their intact limb, to assist with balance (Nolan et al. 2003). When comparing GRF in transfemoral and transtibial amputees, transfemoral amputees have been reported as having a larger vertical GRF (Silverman et al. 2008). Nolan et al. (2003) explains that the reason for this could be due to the lack of ankle plantar-flexor and knee flexion means that the limb is more vertical in orientation meaning the projection of their centre of mass also remains more vertical.

These asymmetries in ground reaction force have been reported to be susceptible to change with changing temporal/spatial variables. An increase in walking speed has been correlated with an increase in ground reaction force (Nolan et al. 2003; Fey and Neptune 2012). Although research showed that an increase in walking speed did not affect GRF asymmetry, concluding

that the residual leg was able to compensate for lack of plantar flexors (Silverman et al. 2008). Another explanation for an increased GRF could be time since amputation, as it can increase confidence and therefore ability to increase walking speed (Fey and Neptune 2012).

### **Stair adaptations adopted by lower limb amputees**

It is well reported within literature that amputees find stair ambulation difficult (Hobara et al. 2011; Jones et al. 2006). This is due to the loss of musculature and absence of joints resulting in a loss of balance and increased need for proprioception to carry out this kinematically and kinetically demanding task (Alimusaj et al. 2009). Alongside this, at times amputees rely on their prosthetic limb completely and some prosthetic components do not provide the joint mobility to allow for easy stair ambulation (Hobara et al. 2011; Schmalz, et l. 2007a).

With prosthesis type affecting gait adaptations, it is unsurprising then that literature has published studies on the effect of differing prosthesis (Sinitski et al. 2012; Alimusaj et al. 2009). An adaptive ankle, which increases the dorsiflexion, has been shown to decrease the plantarflexion moment at the contralateral limb (Alimusaj et al. 2009). Also, microprocessor knees have been shown to enable knee flexion similar to that of able bodied subjects (Jones et al. 2006). During rehabilitation, however, amputees are often provided with the basic prosthetic components which do not allow for an increased range of motion. As a result of this patients are advised to lead with their prosthetic limb, when traversing stairs, and to do so one step at a time (Jones et al. 2006). Therefore, research often investigates amputees 'stepping up' or 'stepping down' using a two-step staircase. In research staircases are often used when investigating transtibial amputees only as trans-femoral amputees find stair ambulation without hand rails or walking aid difficult (Hobara et al. 2011).

The ankle is extremely important in stair ambulation as plantarflexions raises the centre of gravity to allow placement of the contralateral limb and dorsiflexion in order for foot clearance

when ascending the staircase (Schmalz et al. 2007a). In stair descent the increased plantarflexion in able-bodied subjects allows the ball of the foot to first make contact with the stair and allowing a more controlled descent (Schmalz et al. 2007a). In order to generate the power to move the centre of mass over the current step and ascend to the next amputees will instead display an increased ankle plantarflexion in the contralateral limb during late stance phase (Sinitski et al. 2012; Alimusaj et al. 2009). This has also been concluded by the evidence of a posteriorly placed centre of pressure seen in the intact limb (Jones et al. 2006). In stair descent amputees roll their prosthetic foot over the step, and display low ankle range of motion across stair ambulation (Jones et al. 2006). In the contralateral joint, both amputee groups start the support phase with excessive plantar flexion but follow an able-bodied ankle moment profile for the remainder (Schmalz et al. 2007b). This excessive ankle planar flexion in the intact limb is used for power absorption when descending the staircase (Alimusaj et al. 2009).

For stair ascent, in stance phase, the prosthetic limb has been found to reach extension early on and maintain this until toe off (Hobara et al. 2011). When supported by the contralateral limb, in stance phase, the knee flexion moment is increased when compared to able-bodied participants, the change then to extension occurs at a quicker rate. (Schmalz et al. 2007b). This has also been shown in a study in transfemoral amputees who used step over step gait (i.e. one foot on each step) to ascend staircase (Hobara et al. 2011). Hobara et al., (2011) suggested that this rapid flexion was for power generation, utilising the energy from quadriceps of the intact limb. In stair descent with the prosthetic limb the range of motion at the knee of the prosthetic limb is reduced with a smaller knee angle produced and delayed knee flexion moment that is activated at approximately 80% through stance and then exceeds that seen in able-bodied subjects. This is so that the prosthetic leg is more vertical (Schmalz et al. 2007b). When descending with their contralateral limb, a knee flexion moment is displayed in early stance,

resulting in a local maximum, this is larger in transfemoral amputees (Schmalz et al. 2007b). Hip extension was increased in the prosthetic limb when ascending the stairs, this suggests that the hamstrings are being used as a method of increasing power generation (Schmalz et al. 2007a).

During stair ascent, when TT amputees are supported by their intact limb the vertical ground reaction force is increased, specifically in the second peak (Schmalz et al. 2007b; Torburn et al. 1994). It is thought that this is as a result of the trunk being further forward, moving the centre of the mass further over the stairs and assisting with propulsion (Pickle et al. 2014). During stair descent the vertical ground reaction force is reduced when amputees are being supported by their prosthetic limb. This further decreases during the latter half of stance. However, when amputees are on their non-amputated limb the vertical ground reaction force is increased, up to 45% in the first peak (Schmalz et al. 2007b; Torburn et al. 1994).

## **2.6 Restrictive devices to simulate amputee gait**

The aetiology of amputation is more often as a result of dysvascular disease. The associated risk factors in conjunction with the disease itself are known to cause a degradation in bone health. This bone degradation, along with the knowledge that amputees develop comorbidities as a result of their amputation (Fey and Neptune 2012), including lower back pain (Gailey et al. 2008; Gulgin et al. 2017) and joint pain could explain some of the movement asymmetries adopted by LLA. Restrictive orthotics, such as rigid ankle-foot orthosis (Ota et al. 2014; Gulgin et al. 2017), a cast (Nepomuceno et al. 2017) and a rigid boot (Böhm and Hösl 2010) have been used to restrict the ankle and simulate transtibial gait. Simulators that fix the knee at approximately 90 degrees of flexion have been used to simulate transfemoral amputees (Vanicek et al. 2007). These devices can be used to simulate asymmetrical movement, as seen in LLA, whilst controlling for the presence of comorbidities or disease progression.

Of the ankle restriction studies, only one study has aimed to investigate the effect of ankle immobilisation on gait as a method of increasing understanding of LLA gait (Nepomuceno et al. 2017). Other studies, have used differing levels of restriction to manipulate the dorsiflexion angle at the ankle and investigate the effects on the knee joint (Böhm and Hösl 2010; Ota et al. 2014). In using a stiff boot over a soft boot Ohm et al. 2010 showed a significant reduction in ankle dorsiflexion from  $18.1^{\circ}$  to  $16.7^{\circ}$ . Whereas Ota et al. (2014) allowed for controlled ankle movement at four levels; ranging from  $10^{\circ}$  of ankle dorsiflexion up to  $10^{\circ}$  of plantar flexion. Both studies concluded that a decrease in ankle range of motion resulted in increased knee loading as demonstrated by an increased knee varus moment (Ota et al. 2014) and greater knee eccentric energy absorption (Böhm and Hösl 2010). An orthotic boot, which restricts the ankle, was used by Gulgin et al. (2017) to investigate leg length discrepancy. They found that there was increased GRF and knee adductor moments on the longer limb (non-restricted limb). The restriction in the Nepomuceno et al. (2017) study fixed the ankle allowing for  $6.5^{\circ}$  of ankle plantar/dorsi flexion, which was within the same range as the Ota et al. (2014) study. The knee joint moment was not reported within the, however the results did find increased braking and propulsive forces in the non-restricted (no cast) leg, which is in agreement with the Gulgin et al. (2017) study. The temporal-spatial adaptations reported showed the restricted condition to result in a shorter step length and a slower walking speed (Nepomuceno et al. 2017; Böhm and Hösl 2010). Similar temporal-spatial adaptations have been seen in transfemoral restriction studies, with the walking speed and step length shorter in the restricted condition (Vanicek et al. 2007). Comparing these results to studies which have simulated transtibial gait, the walking speed and step length are slower than simulated transtibial gait, which is also a feature of lower limb amputee gait (Schulz et al. 2010).

Although the aim of these studies was not solely to investigate if restrictive devices could simulate amputee gait, *e.g.* effect of a leg length discrepancy or boot stiffness of joint power. The results show promise in the ability to use restrictive devices to simulate amputee gait. Further investigation is needed to simulate both transtibial and trans-femoral gait within the same healthy participant group.

## 2.7 Finite element analysis

Finite element analysis refers to the engineering concept that uses numerical methods to model an object and subject it to loading to predict its responses (Rao 2011). Originally developed for aircraft analysis, it has since been utilised in a number of areas, with its introduction to orthopaedic biomechanics in 1972 (Huiskes and Chao 1983a). The model is constructed of a number of ‘element’s, interconnected by points or ‘nodes. When an external load is applied to these nodes they will displace, the sum of this displacement can be used to determine the stress and strain operating within the structure (Prendergast 1997). It is this strain response that enables finite element models to be directly comparable to biological structures, simulating the responses of materials, such as bone.

In order to predict this response a number of factors have to be known; a work flow seen in Figure 18 developed by Brekelmans (1972), demonstrates this. In order determine the mechanical behaviour of a system, such as a bone; you need to know the characteristics of the model and the environment of loading. The following section details each aspect of the system.

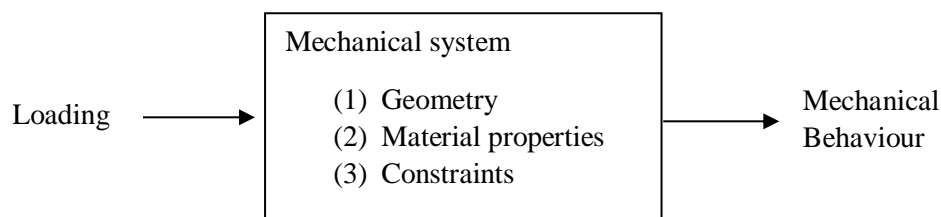


**Figure 18: Work flow for determining the mechanical behaviour of a finite element system, in this case a bone. Developed from (Brekelmans et al. 1972)**

### 2.7.1 Generation of finite element model geometry

One of the first finite element models of the tibia was an axisymmetric model of the lateral tibial plateau developed by Hayes et al. (1977). The model geometry, tibio-femoral forces and joint contact areas were estimated from the literature and a resultant force of 445N, derived from mathematical computation, was applied to an assumed area on the condyles. In order to generate realistic mechanical behaviour, the geometry of the model has to also be realistic. Little et al (1986) constructed a 3D model of the upper tibia through digitisation of a cadaveric specimen. Since then, Computerized Tomography (CT) scans have been used to provide clinicians and researchers with highly detailed *in vivo* scans.

The process of model construction from CT scans has been automated (Viceconti et al. 2004; Couteau et al. 2000). The development of image processing programmes such as Mimics, enable those with less expertise in this area to develop scans into 3D models (Phate et al. 2014). These scans produce models in such high detail that they require intense computational power to process. As finite element models developed, it then became apparent that they could be used to also simulate musculoskeletal problems. By combining CT imaging with magnetic resonance imaging (MRI), muscle attachments and contact areas could be modelled (Lunn 2013; Périé and Hobatho 1998). Further expansion on this, is provided by the combination of the CT and MRI data with dynamic fluoroscopy (moving x-rays). Dynamic fluoroscopy avoids the need to for invasive *in vivo* research, by imaging the joint through movement to understand contact and joint mechanics accurately. This can be used to create FE models of joints, with knowledge of contact area and interaction throughout a movement, improving the subject specificity (Carey et al. 2014; Dennis et al. 2005). The field of view that is seen in dynamic fluoroscopy, however, is very limited, with reported areas of 160mm square (Li et al. 2008) and is usually used only at joint. It also requires extensive equipment that may not be available

to every clinic or research lab. Alongside this, both CT scans and x-rays expose the participant to high amounts of radiation; approx. 0.065 mSv for a chest x-ray (National Cancer Institute 2009) and between 8 and 10mSv for a abdomen CT, which is the most common CT in America (Smith-Bindman et al. 2009) . So, unless for already established medical conditions, exposing participants to this amount of radiation, would be unethical.

In an attempt to combat these issues, Shim et al. (2007) developed a method that used a sparse CT set, reducing the amount of radiation participants are exposed to. To supplement the finite element model, they used data from the open source set of CT scans obtained as part of the visible human project (further information can be found in Study 2). The results showed that the more slices the less the RMS error, with 10 slices used the root mean square value is 3mm. When this is later validated against cadaveric models, under simple mechanical loading, the sparsest data set yielded average RMSE of 24.6% (Poelert et al. 2013). Although, Shim et al. (2007) stated their confidence at this being relevant in clinical applications, there is a need to reduce these errors, whilst still maintaining a smaller radiation dose.

Another method for reduced radiation exposure, which has been used in patient groups, who have already been exposed to high radiation, is peripheral quantitative computed tomography (pQCT). A pQCT scanner is similar to a CT scanner in that it has an x-ray source. The patient puts their peripheral limb *e.g.* forearm or lower leg, through the bore hole of the scanner with adapters to fix the thigh or arm in place. The pQCT scanner first takes a scout scan to identify the distal end of the limb and traverses up, scanning at four sites, based on the overall bone length. For the tibia 4 %, 14%, 38% and 66% of total length are the sites typically used as these enable the analyses of both the cortical and trabecular bone (Evans et al. 2012). Most literature publishes data using the Stratec XCT 2000, seen in Figure 19 (Stratec Medizintechnik,

Pforzheim, Germany). Previously, when creating a finite element model from these scans, pQCT was used in conjunction with 2D biplane radiographs (Caouette et al. 2015). This was in a patient group who had regular radiographs as part of disease management, this is not viable for general research as it exposes participants to excessive radiation.

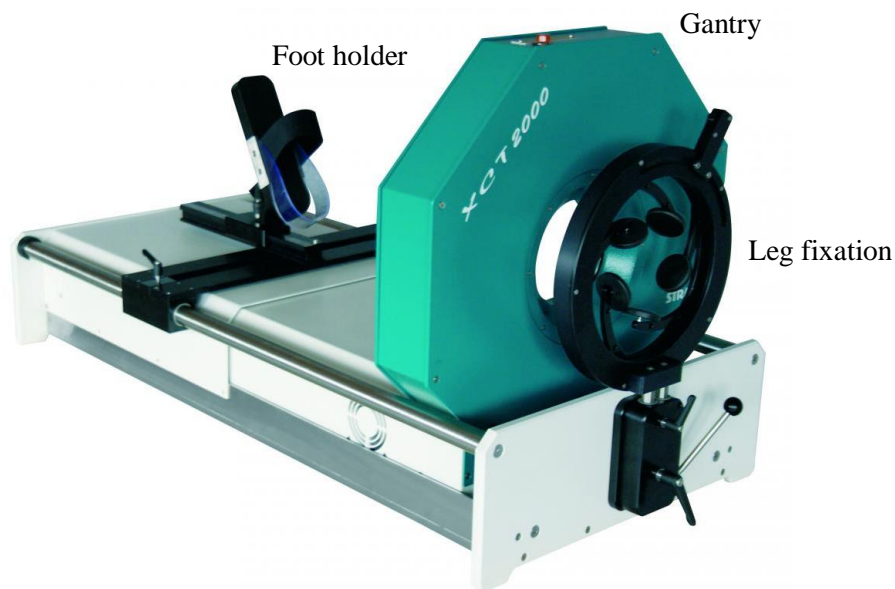


**Figure 19: The Stratec pQCT XCT 2000 with leg fixation and foot holder for scanning of the tibia.**

Although not used independently to generate FEM, pQCT has been used as an analyses tool for bone properties. The pQCT automatically analyses internal properties of bone *e.g.* BMD, bone area including cortical and trabecular. The external geometry of the bone, however is not processed.

Previous research has developed numerical computational code to process the images generated from the pQCT. The BAMpack – Bone alignment and measurement package developed by Evans et al (2008). This image processing code written in MATLAB (Statistics Toolbox Release 2017a/2017b, The MathWorks, Inc., Natick, Massachusetts, United States)

takes the images generated from the pQCT and first applies a rotation factor to align the images. The tibia is then isolated from the image and taken forward. Thresholds are then applied to distinguish the biological material based on their pixel density; based on its density value as being either trabecular (100-600 mg/cm<sup>3</sup>), transitional (600-800 mg/cm<sup>3</sup>), or cortical (800-1500 mg/cm<sup>3</sup>). The tibia image is then sectioned to provide analyses regions; Lateral Anterior, Anterior, Medial Anterior, Medial Posterior, Posterior, and Lateral Posterior (Evans et al. 2012). The information generated by the BAMpack software includes internal property measures e.g. bone mineral density and cortical and trabecular area which are automatically generated from the pQCT. Whilst the outer geometry plot of the bone, generated by BAMpack is not able to be extracted by the pQCT, thus adding informed values of bone strength, it is not quantifiable, i.e. not associated with a coordinate system. The processes are described in the publication by Evans et al. (2012) although they are not documented in enough detail as for other researchers to compare or replicate.

### **2.7.2 Material Behaviours and Properties of Finite element models**

The material behaviour refers to how the model responds as a result of its composition. As detailed previously bone is considered an anisotropic material (the material properties differ depending on the direction). In order to assign a finite element model, anisotropic material properties, nine different mechanical elastic components are needed to be known. This includes three young moduli, three shear moduli and three poisons ratio (Vignoli and Kenedi 2016). For isotropic materials, the relationship is deemed linear, so only one young's modulus and one poisons ratio are required.

Determining such a large number of elastic properties requires computational power and time to create a complicated model and has resulted in the publication of simplified models

(Prendergast 1997; Zysset, Dall'ara, et al. 2013; Kazakia et al. 2014; Sanders and Daly 1993). In isotropic, anisotropic comparison studies, it has been found that the distribution pattern for both is very similar (Vignoli and Kenedi 2016; Kazembakhshi and Luo 2014). The maximum principle stress and strain has been reported to be under-estimated within the linear models. This has a larger effect on the trabecular bone over the cortical bone (Kazembakhshi and Luo 2014). Although the trade-off between computational time and output can't be quantified, FEM's are designed to be a simulation. So, for ease of use and time efficiency, the statement of linearity can be used to inform readers of possible underestimation in the model output.

In order to assign heterogeneity, each element must be assigned an individual stiffness value. This is timely and takes large computation power, up to 1.5 more running time and twice the memory used (Yassine et al. 2018). Hence, many researchers have proceeded with homogenous models, where the properties are assumed to be uniform throughout. In the analyses stage the heterogeneity has been found to have impact on the stress and strain outputs. A homogenous model has found to underestimate the strain with error values of up to -13.25% reported (Yassine et al. 2018). Smaller values have also been reported with max stress values being 0.27MPa underestimated in homogenous models. In order to minimise computational power and maximise time efficiency, a homogenous model will be used in this thesis in agreement with previous literature (Haut Donahue et al. 2002).

Material properties of finite element models have previously, when using a cadaveric specimen, been done through indentation studies. This is done by pressing a hard tip into the bone with a known force, the resulting imprint is measured and the contact area calculated. The information gathered from the experiment can then be put into a pre-determined formula to obtain the material properties of bone. Using this method, research has reported the young's

modulus, for the tibia, to be from 13.1 GPa to 32.2 GPa (Turner 2009; Zysset, Dall'ara, et al. 2013). Such an invasive procedure cannot, however, be performed on healthy living participants.

A non-invasive determination of material properties is the conversion of Hounsfield unit (HU), the quantitative measure used to express radiation attenuation from CT scans. It is assumed that there is a linear relationship between the HU and bone ash density (Schileo et al. 2007a). Such that ratio between ash density and apparent density is expressed as the following

$$\frac{\rho_{ash}}{\rho_{app}} = 0.6$$

The resulting reported Poisson's ratio,  $\nu$ , usually allocated to finite element models of bone is 0.3 (Curtis et al. 2011; Schileo et al. 2007a; Dragomir-Daescu et al. 2015). Following this same process, the Young's Modulus can be deduced. There are a number of different equations, but researchers have justified the use of the following, on its number of citations (Carter et al., 1977)

$$E = 3.790\rho_{app}^3$$

The Young's Modulus and Poisson's ratio are well researched and documented in literature, so for this thesis, material properties were taken from literature.

### **2.7.3 Application of constraints to finite element models**

Another factor in the mechanical environment is the constraints placed upon the model. When modelling the tibia, constraints are usually applied to the distal end of the segment, *i.e.* at the ankle. This is to stop any movement that in a physiological sense would be prevented by the presence of the talus, ligaments and tendons. How you apply the constraints is important as it has been shown that strains can vary up to 150% when modifying the application of constraints (Razi et al. 2014).

Total ankle constraints have been applied to finite element models (Lesso-Arroyo et al. 2004; Phate et al. 2014) in previous literature. The model presented in Phate et al. (2014) was a very simple model and with half body weight applied to the proximal end of the tibia. The aim of this paper was to analyse the tibia in regards to safety when introducing implants. The model presented in Lesso-Arroyo et al. (2004) was again a simplified model but the purpose of this paper was the biomechanical behaviour of the knee and thus, the distal end of the model was less relevant to the model output. Physiological loading studies have used contact pressures to map out the stress contours between the talus and the distal end of the tibia (Anderson et al. 2008; Kim 2017; Sofia De Oliveira and Rodrigues 2013). The resulting pressure shows that there is increased stress in two areas along the tibia-talus contact. A comparison of these pressure distributions showed an agreement in the number of areas of larger stresses, although not always in correlating areas. When Kim (2017) compared their results with other literature the variation in area's of high stress was due to the varying use of ligaments/muscles/tendons as well as boundary conditions and the application of loads to the proximal end of the FEM. The size of this contact area changed throughout the gait cycle and therefore applying a distributed load to simulate the whole contact would result in over constraining (Sofia De Oliveira and Rodrigues 2013). In order to resolve this, researchers have used point loading based on the physiological loading investigated through contact pressures (Duda et al. 2001; Pérez et al. 2009b). Although the location of the point loads was not detailed accurately, they are reported to be based on joint cartilage contact imaged from MRI. Based on the physiological loading reported through contact stresses and the anatomy of the ankle (see Figure 3) it can be assumed that these three-point loads correspond to the talus and the ligament attachments.

#### **2.7.4 Application of physiological loading to finite element models**

Preliminary modelling work done by Morrison (1970) used generic mechanical principles to simulate knee joint contact forces. Since then, FEMs have been used to predict contact force, area and distribution (Beillas et al. 2004; Adouni, Shirazi-Adl, and Shirazi 2012; Périé and Hobatho 1998).

At the proximal end, the two condyles interact with the patella and the distal end of the femur to form the knee joint. It is across these two condyles that the loading is distributed. Instrumented knee joints, dynamic fluoroscopy and cadaveric studies have been used to investigate the contact pressure magnitude and distribution. During stance it has been reported that the contact location on each condyle is 25% of the width of the tibia away from the centre of the knee (Schipplein and Andriacchi 1991) and anterior to the mid-line of the tibia (Carey et al. 2014). The location and distribution of this contact then changes when physical activity is introduced.

Forces across the knee have been measured at up to 3 times body weight (Adouni et al. 2012; Kutzner et al. 2010; Taylor et al. 2004) Research has found that there is a higher magnitude of force across the medial condyle than the lateral condyle, with reports of a 60/40% distribution (Duda et al. 2001; Zhao et al. 2007). Through dynamic fluoroscopy it has been reported that within a dynamic movement, *e.g.* knee flexion the contact becomes more posterior across the lateral condyle whilst there is minimal change in the contact on the medial condyle (Dennis et al. 2005). MRI studies have shown some agreement with this in terms of the contact on the lateral condyle; though, Wretenberg et al (2002) reported some movement in the contact area across the medial contact. This movement was only a few millimetres so could easily be missed during dynamic imaging studies, such as in dynamic fluoroscopy. Cadaveric studies have

shown a decrease in contact areas as the knee flexion angle increased (Kazemi et al. 2013). Although throughout this flexion the contact area on the medial condyle remained to be larger than the contact area at the lateral condyle (Périeré and Hobatho 1998). It is known that the loading profile across the knee does not consist of just one point of contact (Hashemi et al. 2004; Carey et al. 2014). But with disagreements on how the contact moves and the need for CT, MRI or dynamic fluoroscopy to investigate this on an individual level, studies have used a resultant force applied through a point load (Kutzner et al. 2010). The data generated from FE is validated to that gathered from instrumented total knee arthroplasty as well as instrumented knee prosthesis (Kutzner et al. 2010). It was then found that the introduction of participant specificity through CT, MRI scans and dynamic fluoroscopy improved the prediction of contact forces considerably (Gerus et al. 2013).

### **2.7.5 Finite element models of lower limb amputees**

FEMs have been used to model the interaction between a prosthesis and the residual limb (Zachariah and Sanders 1996; Silver-Thorn and Childress 1997; Sanders and Daly 1993; Portnoy et al. 2008; Dickinson et al. 2017). The aim of these studies is to provide clinicians with the knowledge to improve the fitting of a prosthesis, thus reducing further complications and improving the quality of life of the amputees. Modelling of the intact limb, however, is limited, with no literature, to this researcher's knowledge, currently aiming to produce this. If FE modelling is going to be introduced to the medical environment to improve prosthesis fit, then the skills needed to model the intact limb are already present. Then, by applying loads from the current gait pattern the eventual bone health can be predicted. Further to this, loading the model with theoretical loading conditions from rehabilitating based physical activity it can be investigated which exercises provide the best loading condition for the rehabilitation of the

patient. This patient-specific treatment not only improves the quality of life of amputees but makes clinics more efficient, thus reducing the cost on the NHS.

## **2.8 Summary of literature review**

Bone is constantly adapting to its surroundings, with stimulus for modelling and remodelling coming from mechanical usage of the skeleton. An imbalance in these processes can have a detrimental effect on bone health. One patient group where asymmetrical loading is postulated to cause a degradation in bone health is lower limb amputees. Extensive research has been carried out into the change in gait pattern as a result of amputation as well as the change in bone health experienced by lower limb amputees. Research into bone health as a result of gait changes is limited. However, the aetiology of amputation along with the demographics of the population have been found to independently, cause a decrease in bone health. Researchers therefore have to use techniques which control for the health status due to prior conditions or comorbidities.

One approach is finite element analysis which has been used to investigate the bones response to mechanical loads for decades (Huiskes and Chao 1983a). A FEM consists of small tetrahedral shaped elements that deform when a load is applied to them. This deformation produces a strain plot, thus, predicting where the bone may experience formation and absorption. In recent years the use of CT, MRI and dynamic fluoroscopy has allowed FEMs to become subject-specific. These methods, however, are computationally expensive and require the use of specific equipment that delivers high doses of radiation. Some researchers have tried to solve this by using sparse CT data sets (Shim et al. 2007), low radiation equipment such as pQCT in conjunction with patient data but further investigation is needed for a solution.

Another approach is to simulate amputee gait using a population who have healthy bone. Simulation studies have used restrictive orthotic and prosthetic devices to investigate changes in gait, although not all aimed at an amputee population. Results have shown that temporal-spatial and some kinetic variables adapt in the same way that amputees adapt but further investigation is needed to provide conclusive evidence that both transtibial and transfemoral amputee gait can be simulated.

Therefore, the overall aim of this Ph.D was to establish a method to investigate the relationship between gait and bone health, in clinical populations such as lower limb amputees, through the use of semi-subject specific finite element models and restrictive devices.

## **3. GENERAL METHODS**

### **3.1 Introduction**

The following chapter details the methods used in the collection and analyses of the movement data within studies three (Chapter Six) and four (Chapter Seven). Particular information pertaining to each study is detailed in the relevant chapters.

### **3.1 Participants**

Both Study Three (Chapter Six) and Study Four (Chapter Seven) recruited able-bodied participants from the general population. Study Three also recruited lower limb amputees from The Mobility Centre, City Hospital, Nottingham, UK. Specific participant demographics are detailed in each study methodology section.

#### **3.1.1 Ethical Approval**

Due to this research recruiting participants identified from National Health Service (NHS), as well as the use of ionising radiation, NHS research ethics committee (REC 16/EM/0316) review was required. Approval was granted by the Nottingham 2, National Research Ethics Service Committee on the 14<sup>th</sup> of September 2016 with further approval granted by the Health Research Authority on the 12<sup>th</sup> of October 2016. Ethical approval for Study Three was also granted by Nottingham Trent human invasive ethics committee (reference 445). Study Four was granted approval by Nottingham Trent's ethical committee for human biological investigation in April 2015 (reference 427)

#### **3.1.2 Inclusion and Exclusion Criteria**

Inclusion criteria for Studies Three and Four were that participants were above the age of 25 years to account for age related increases in bone mass between the ages of 18 and 25 years

(Campbell 2012). All participants had to be able to walk un-aided for at least ten minutes and have no heart complaints or current neuromuscular or musculoskeletal injury in order to ensure they could complete the study.

Potential participants were excluded from the studies if they were currently smokers as smoking increases the risk of bone fracture and occurrence of osteoporosis by 40% (NCSCT 2012). Able-bodied participants were excluded if they had a current medical condition that would affect gait and/or balance *e.g.* Ménière's disease. In order to consent and safely participate in the study participants were excluded if they were unable to communicate, or understand written or verbal instruction in English.

For scanning health and safety, potential participants were excluded if they had any medical implants *e.g.* hip implant or pacemaker, as this could negatively interact with the scanner. Also, if they were pregnant or actively trying, as radiation would be harmful to a foetus. To keep within the Health Physics Society recommendation of no more than 50mSv of radiation in one year, participants were excluded if they had undergone an MRI or CT scan within a month prior to partaking in the trial (Health Physics Society, 2010).

All participants were asked to be able to travel to Nottingham Trent University of their own accord, with reimbursement available. Prior to the study participants were made aware of the participant information sheet and provided written informed consent (see appendix). For Study Three (Chapter Six) participants were additionally asked a series of questions to pre-approve them for ionising radiation, the request was then signed off by a registered health care professional.

### 3.1.3 Sample size

The total sample size for Study Three and Study Four were determined using a standard power model for repeated measures, within-between interaction study designs (Hedeker, 1999). The equation used to determine the sample was as follows:

$$N = \frac{2(z\alpha + z\beta)^2 (1 + (n-1) \rho)}{n[(\mu_1 - \mu_2)/\sigma]}$$

Where:

$z\alpha$  is the value of the standardized score cutting off  $\alpha/2$  proportion of each tail of a standard normal distribution (for a two tailed hypothesis test).

$z\beta$  is the value of the standardized score cutting off the upper  $\beta$  proportion.

$n$  is number of time points.

$\rho$  is the assumed correlation of repeated measures.

$\mu_1$  is the first group mean.

$\mu_2$  is the second group mean.

$\sigma$  is the assumed common variance in the two groups.

The term  $(\mu_1 - \mu_2)/\sigma$  represents the calculation of the effect size, therefore the equation can be simplified to read:

$$N = \frac{2(z\alpha + z\beta)^2 (1 + (n-1) \rho)}{n(ES)}$$

Where:

ES is the selected effect size.

Specific details pertaining to each study can be found in Chapter Six, section 2.1 and Chapter Seven, section 2.2.

## **3.2 Method for collection of bone images**

### **3.2.1 Peripheral Quantative Computed Tomography**

#### ***Quality Assurance of pQCT bone imaging***

All scans were performed by a trained operator using a Stratec XCT 2000 pQCT machine (STRATEC Medizintechnik, Germany), in conjunction with the company software, version 6.20. Prior to any testing a quality assurance scan was carried out; this was a calibration, detecting any system faults. This calibration used a phantom consisting of water and materials with equivalent properties to bone. The standard phantom scan was used to compare density values, with a less than 1% error considered successful. Whereas the cone phantom scan was used to check the linearity of results and through cross sectional area comparison, confirm repositioning precision.

#### ***Participant positioning within pQCT machine***

Before the participant was positioned the tibia was measured using a meter ruler from the medial epicondyle to the medial malleolus and the length was input into the scanner associated software. Participants were then sat adjacent to the scanner and placed their dominant limb through the gantry and placed their foot in the holder. The foot was secured when the ankle was approximately 1cm proximal to the laser position indicator, and the participant's leg was centred and straight as possible. Once completed the participant was then secured at the thigh, using the leg fixation device.

#### ***Data acquisition from pQCT tibial bone scanning***

The scanner first performed a scout scan in steps of 1mm to identify the distal end of the tibia. Once this was determined the pQCT scans at 4,14,38 and 66% length of the tibia, in order to obtain images of both cortical and trabecular bone. At each site the x-ray beam passes the arm

perpendicular to that of the axis of the tibia. After each transverse scan the gantry then rotated 12 degrees, this was then repeated 15 times to total 180 projections.

**Table 4: Technical information of the Stratec 2000L Peripheral Quantitative Computed Tomography Scanner**

Technical Measure	Value
Number of detectors	12
High Voltage	56-60 kV
Anode current	<550 $\mu$ A
Scan time	90 s
Radiation dose CT	<0.001mSV
Slice thickness	2.0mm
Voxel size	0.2-1.0mm

### 3.2.2 Dual Energy X-ray Absorptiometry

#### *Quality Assurance for DXA scans*

All scans were carried out by a trained operator on the Lunar iDXA (General Electric Healthcare, WI, USA). Prior to scanning a quality assurance scan was carried out to calibrate the scanner and test functionality. The calibration block, consisting of materials with properties of soft tissue and three chambers with properties of bone, was placed on the bed of the scanner, with the cross hair on the block in line with the laser projection from the gantry. Once complete the associated software awarded a pass to confirm calibration.

#### *Participant positioning in DXA*

In preparation for the scan the participant was asked to remove shoes and socks as well as all metal including jewellery and belts, ensuring that their remaining clothing had no metal zippers

or poppers. Height and weight as well as the individuals identifying information was input into the software, or selected from the database, if a repeated measure. For Study 1 the participants had a full body scan, for this the participant lay supine on the bed of the scanner with their body within the white outline drawn on the scanner bed and centred to the reference line. Their head was approximately 3cm below the outline with arms are by their side and their hands turned on the side, thumbs facing up, fingers closed, but not touching their thighs. Velcro straps were fastened around the participant's knees and ankles to maintain positioning throughout the scan. The participant was asked to lie as still as possible for the duration of the scan, approximately 10 minutes. The arm of the scanner passed across the body of the participant to incorporate a scan window of 198cm x 66cm. Once the participant was positioned the scanner was instructed to position itself, this involves the scan arm moving to be above the patient's head. Prior to the start of the scan the participant was told to keep their eyes closed until operator says otherwise (until the laser is past their chest) and remain still for the duration, approximately ten minutes.

The X-ray detector, in the scan arm of the DXA consists of four crystals of cadmium telluride (CdTe), arranged with a half cell offset. Each has sixteen cells lithographed onto them, increasing their density to create a high-density detector. The x-rays are omitted as a fan beam at both high energy (70keV) and low energy (38keV) at a current of 0.188 mA from a source under the table. The x-ray beam and detector arm move parallel to the table axis to scan the entire body.

Further details on analyses of Pqct and DXA scans can be found in 6.2.3.

### **3.3 Method for collection of biomechanics**

#### **3.3.1 3D motion capture**

Three-dimensional motion capture was carried out in the biomechanics lab at Nottingham Trent University, Nottingham, UK. A Qualisys motion capture system (Qualisys, Gothenburg, Sweden) was used along with associated hardware and the Qualisys provided software (version 2.17). The full set-up used for Study Three (Chapter Six) detailed in Figure 20 Study Four (Chapter 7) used the same set-up with the absence of the staircase, portable cameras and associated hardware. Studies Three and Four used eight wall mounted Oqus 400 cameras; an additional four Oqus 700+ cameras on portable mounts and one high speed Oqus 310+ camera was added for capture of the staircase for study 3 (Oqus; Qualisys AB, Gothenburg, Sweden). Kinematic data was captured at a rate of 100 Hz. Kinetic data were recorded through the use of force platforms, both studies used ground embedded AMTI OR6-7-2000 (dimensions: 464mm by 508mm) or AMTI optima, BP400600 (dimensions 400 by 600mm) strain gauge force platforms. The staircase used in Study 3 used portable force plates, namely Kistler 9286B (dimensions: 600mm by 400mm) and Kistler 9260AA3 (dimensions: 298.5mm by 500mm) force platforms. All force platforms measure the ground reaction force in three directional components,  $F_y$  (Anterior/posterior),  $F_x$  (medial/lateral) and  $F_z$  (vertical). Further details regarding to this set-up can be found in Chapter Six. The AMTI OR6-7-2000 force platforms were connected to the AMTI MSA-6, a six-channel strain gage amplifier with a fixed 1000Hz low pass filter. On the front panel of the amplifier there is a momentary switch which was used to automatically balance and zero the amplifier channels; this is executed prior to the participant stepping on the plate. The analogue output of this then went through a 64-channel analogue to digital (AD) board before entering the computer. The AMTI BP400600 was connected to the Optima signal conditioner, again the push button balancing and zeroing was present on the front plate of the device. This was connected via an USB port to the operating

computer. The portable force plates fed into a Kistler DAQ board, a 16-bit converter which digitised the analogue signals output from the force platforms and alike the AMTI BP400600 is connected to the computer via a USB port.

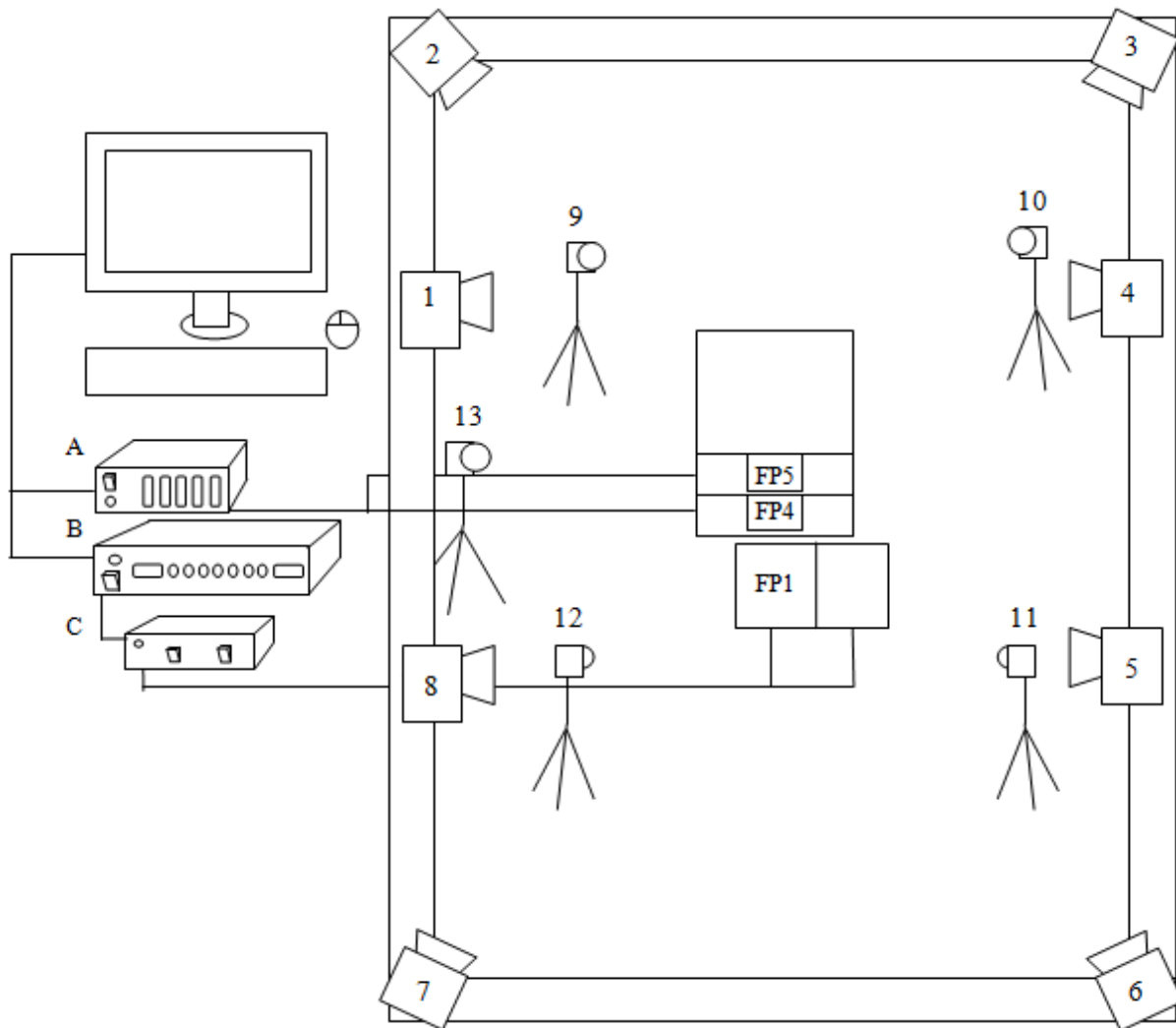


**Figure 20: Line drawing of the set-up which was used in study 3 and study 4. Gantry mounted cameras are labelled 1-8 and FP1 is the ground embedded force plate, AMTI OR6-7-2000. Portable cameras were labelled 9-12 and the high-speed camera labelled as 13. FP4, Kistler 9260AA3 and FP5, Kistler 9286B are the portable force plate in the stair case (Study 3 only). These are connected to the computer through A, B and C. A; Kistler DAQ board. B; 64 channel AD board. C; AMTI MSA-6 six channel strain gage amplifiers.**

### 3.3.2 Calibration of a 3D volume

Prior to testing the 3D motion capture system was calibrated. For all testing sessions an L-frame of known lengths (750mm by 250mm) was placed at the corner of the ground embedded force plates and used in conjunction with a carbon fibre T-wand of known lengths (751mm) was used to calibrate the volume. Calibration error for the cameras was required to be below 2mm for each camera as well as for wand length.

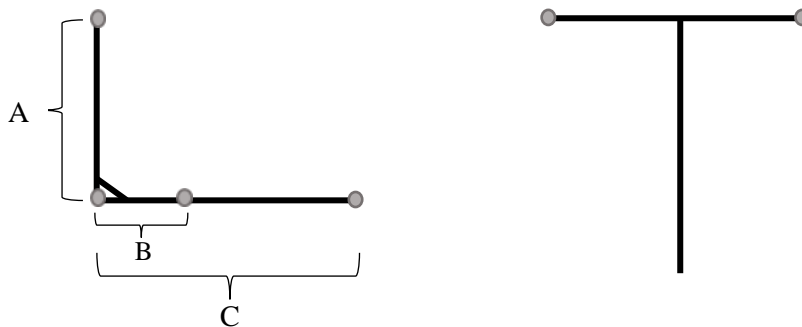


**Figure 21: Calibration frame dimension A; 550mm, B;200mm, C; 750mm and Calibration wand length; 751mm**

### 3.3.3 Movement data preparation and collection method

Prior to any movement analysis the participant's height and mass was recorded using a free-standing height measure and digital scales (Seca, Birmingham, UK). Participants completed all assessments wearing form fitting shorts and top and their normal everyday activity footwear.

#### 3.3.3.1 Biomechanical Model definition

Kinematic data was recorded through the tracking of 14 mm  $\varnothing$  spherical retro-reflective passive markers, placed at anatomical landmarks in accordance with the 6 degrees of freedom (DOF)

model defined in Figure 22. The anatomical landmarks were identified through palpation in accordance with the Colour Atlas of Skeletal Landmark Definitions (Van Sint Jan 2007). Table 4 shows the expansion of the abbreviations and details on how to identify them through palpation.

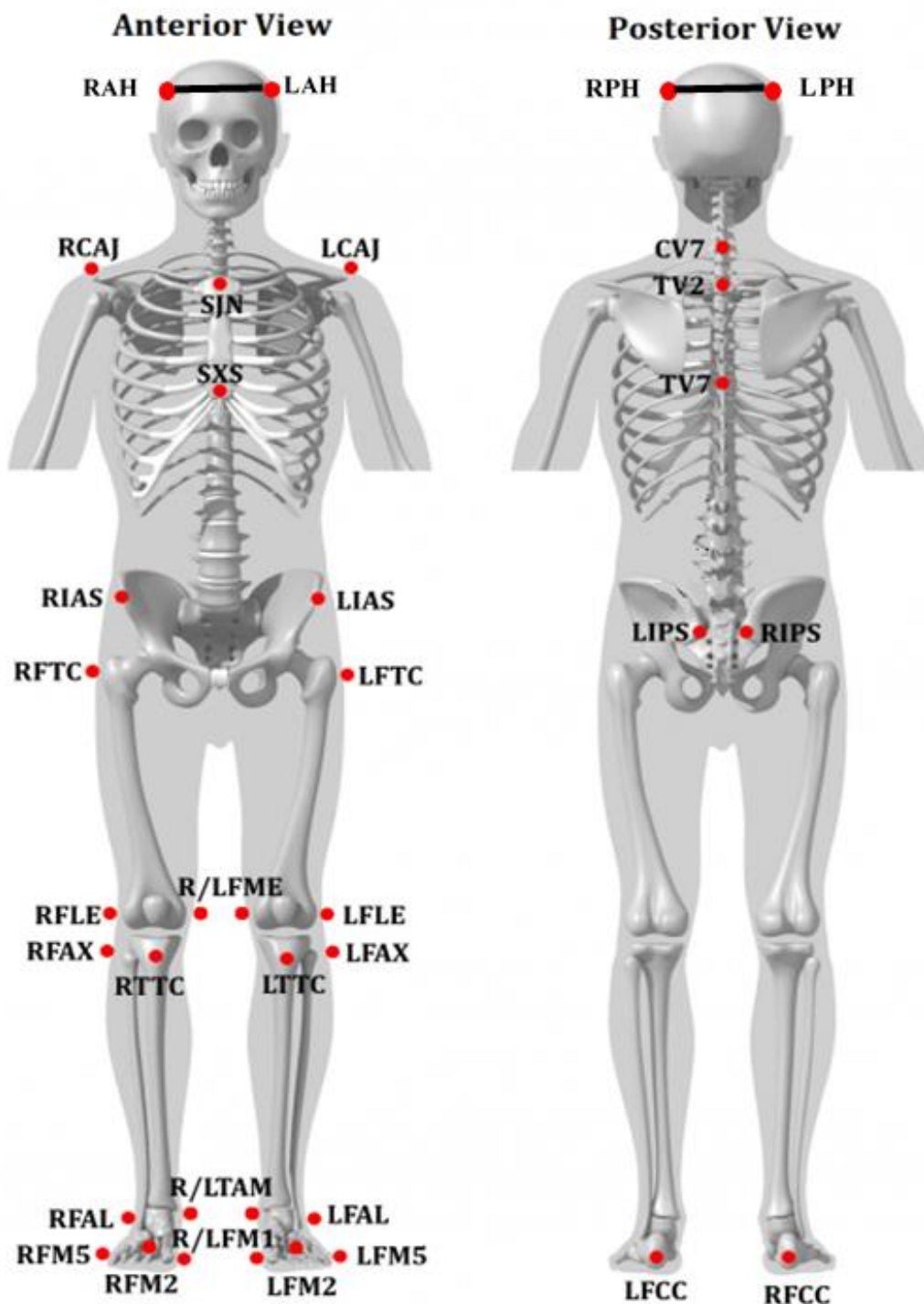


Figure 22: Locations of the 37-marker model set.

**Table 5: Abbreviation expansion of the markers detailed above and the process of identification of said landmark. (Van Sint Jan, 2007)**

Abbreviation	Marker name	Identification of landmark
L/RCAJ	Left/Right Clavicle Acromioclavicular Joint	Follow the clavicle until the depression of the acromioclavicular joint.
SJN	Sternum Jugular Notch	Depression between the two clavicles.
SXS	Sternum Xiphisterna joint	Four fingers will trace up the lower ridge of the of the ribs until the depression of the costoxiphoid angle.
CV7	Cervical Vertebrae 7	Palpate from the base of the skull down the spine, ask participant to flex/extend the spine to palpate the displacement of the spinous processes.
TV2,7	Thoracic Vertebrae 2,7	Repeat the above process to find the 2 <sup>nd</sup> and 7 <sup>th</sup> thoracic vertebrae.
LV1,3,5	Lumbar Vertebrae 1,3,5	Repeat process to find the 1 <sup>st</sup> , 3 <sup>rd</sup> and 5 <sup>th</sup> lumbar vertebrae.
L/RIPS	Left/Right Posterior Superior Iliac Spine	Found deep in the cutaneous hollows. Otherwise palpate the posterior iliac crest, moving down and backwards until you feel a prominent bony bump.
L/RIAS	Left/Right Anterior Superior Iliac Spine	Place hand on the participants flank, palpating for the iliac crest. Follow this forward until you find a bony bump which you can get around.

L/RFTC	Left/Right greater trochanter	The palpator places thumb on the iliac crest and little finger along the axis of the thigh to get approximate area. Ask participant to place heel on the floor and twist. The palpator should be able to feel the head of the greater trochanter moving.
L/RFME	Left/Right Medial femoral epicondyle	The palpator follows the front of the knee up and around the distal curves of the femur, following up to a small tubercle.
L/RFLE	Left/Right lateral femoral epicondyle	The palpator follows the front of the knee up and around the distal curve of the femur until a well-developed tubercle is identified.
L/RFAX	Left/Right fibula apex of the styloid process	Lateral side of the leg, the large bony landmark. Ask participant to flex and extend to ensure it is the most lateral/posterior part.
L/RTTC	Left/Right Tibial tuberosity	Follow the patella ligament distally until the bony attachment site.
L/RTAM	Left/Right Medial Malleolus	The distal aspect of the medial ankle
L/RFAL	Left/Right Apex of the lateral malleolus	The distal aspect of the lateral ankle
L/RFM1	Left/Right first metatarsal head	The base of the 'Big toe'
L/RFM2	Left/Right second metatarsal head	The base of the 'second toe'
L/RFM5	Left/Right fifth metatarsal head	The base of the 'little toe'
L/RFCC	Left/Right Calcaneus	The distal aspect of the foot

Participants stepped onto the force platform, then stood still, feet hip width apart, arms out at 45 degrees with palms facing out and head facing forward, for approximately 10 seconds. Once recorded, the visibility of markers was checked and participant then carried out motion capture as instructed.

From labelling one static trial an Automatic Identification of Markers (AIM) model was created to be applied to all further dynamic trials. An AIM model uses the local coordinate system of each marker to identify its location, distance and angle relative to other markers. Developed using the static trial, the AIM model was then trained using dynamic trials. Within each frame, the AIM model looks for the best solution. Trials were manually checked to ensure continuous identification of the visible markers. Trials were then cropped to include two steps prior to contact with the force plate and two steps post contact with the force plate in order to record at least one full gait cycle where the foot was in contact with the force plate (Study Three level walking and Study Four). For stair walking gait trials were cropped to show the participant either ascending or descending the staircase and one step prior and post, again, to ensure a full gait cycle was recorded with the foot in contact with the force plate. All trials were then exported as .c3d files to be taken into the biomechanics analysis software package, Visual 3D, for further analyses (C-Motion, Inc, Germantown, USA).

### **3.3.4 Segment Definition**

Prior to analysing the biomechanics data, a three dimensional model had to be created to identify the body segments. The markers presented in Figure 22 and Table 4 were placed and the distal/proximal and medial/lateral aspects of each joint, it is these which were used to define the body segments. The position of these markers is in relation to the lab coordinate

system. Using the assumption that throughout movement these markers stay attached to the body, a series of three markers was used to define the pose and orientation of a body segment. Between the distal end of one segment and the proximal of the adjacent segment, a joint was defined; this is not a constraint but merely an identification of the connection of two kinetic segments.

The individuals centre of gravity, moment of inertia, principle axis and moments were defined based on the anthropometric measurements from Hanavan (1964). The segmental mass was approximated using the regression equations developed by Dempster (1955). Sections 3.3.4.1 to 3.3.4.6 explain the general markers and landmarks (in blue) used to define each segment. Specific modelling pertaining to each study was found in the relevant chapters.

#### **3.3.4.1 Head**

Four markers were used to define the head segment, two at the forehead (LAH, RAH) and two placed distally in line with these (LPH, RPH). Four landmarks were created using these markers to identify the boundaries of the spherical segment. See Figure 23.

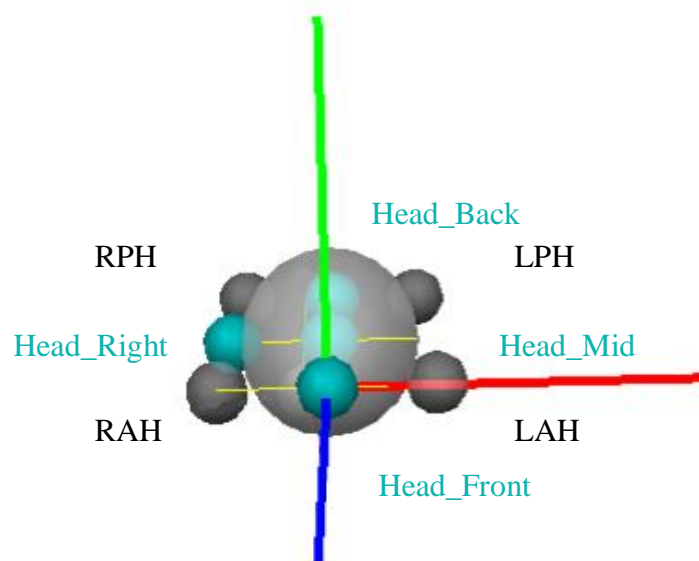


**Figure 23: The head segment definition using markers and landmarks.**

**Table 6: Landmark definitions for head segment**

Landmark	Starting point	End point
Head_Front	RAH	LAH
Head_Back	RPH	LPH
Head_Right	RAH	RPH
Head_Mid	Head_Front	Head_Back

### 3.3.4.2 Thorax

A cylinder was used to represent the thorax within the model. The medial and lateral points of the thorax were defined by the acromion joint. The proximal joint centre was defined by the notch in the jugularis; SJN, and the distal joint centre was defined by second thoracic vertebrae, T7. The radius of the segment was assigned the value of half the distance between the left and right acromion joints. A marker at the xiphoid process, SXN, was used as an additional identifier of the anterior of the segment. To track the segment TV3, TV7, SXN and SJN were used.

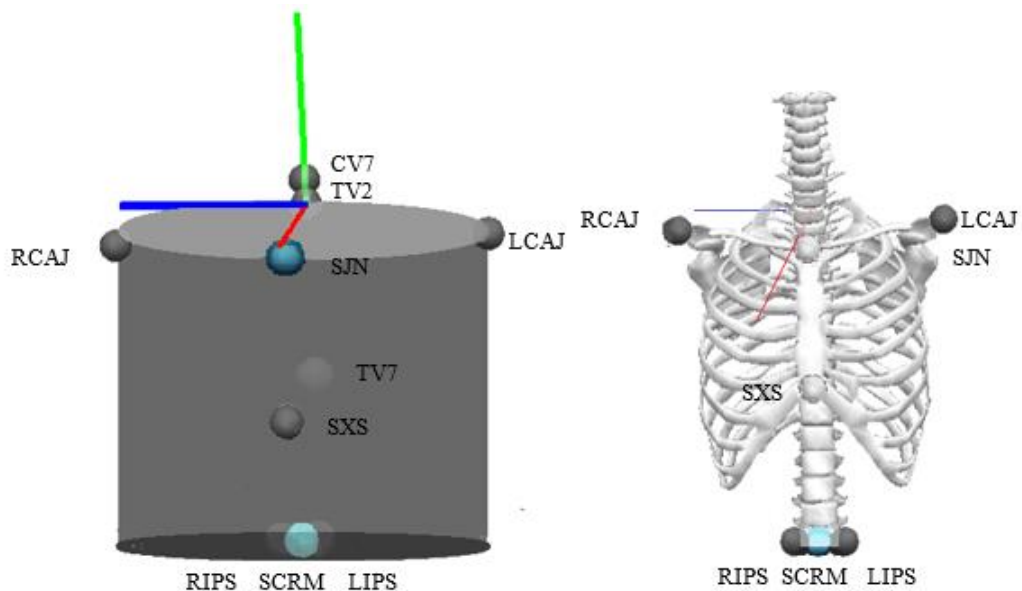


**Figure 24: The thorax markers and landmarks which define the cylindrical segment.**

### 3.3.4.3 Pelvis

A visual 3D composite pelvis was used in this model; this is based on the CODA pelvis. The CODA pelvis is defined using the ASIS (Anterior Superior Iliac Spine) and the PSIS (Posterior Superior Iliac Spine), two sets of bony protrusions found at the front and back of the pelvis. The origin of the pelvis was defined as the mid-point between the two ASIS markers, with the plane extended back to the mid-point of the PSIS, thus resulting in a centre of mass slightly further forward than is found anatomically. The composite pelvis has an origin defined as the mid-point between the mid-point of the PSIS (sacrum) and mid-point of the ASIS. To correct for the centre of mass position defined in the CODA pelvis, the composite pelvis defines the length of the segment as the distance between the origin and the mid-point between the hip joint centres.

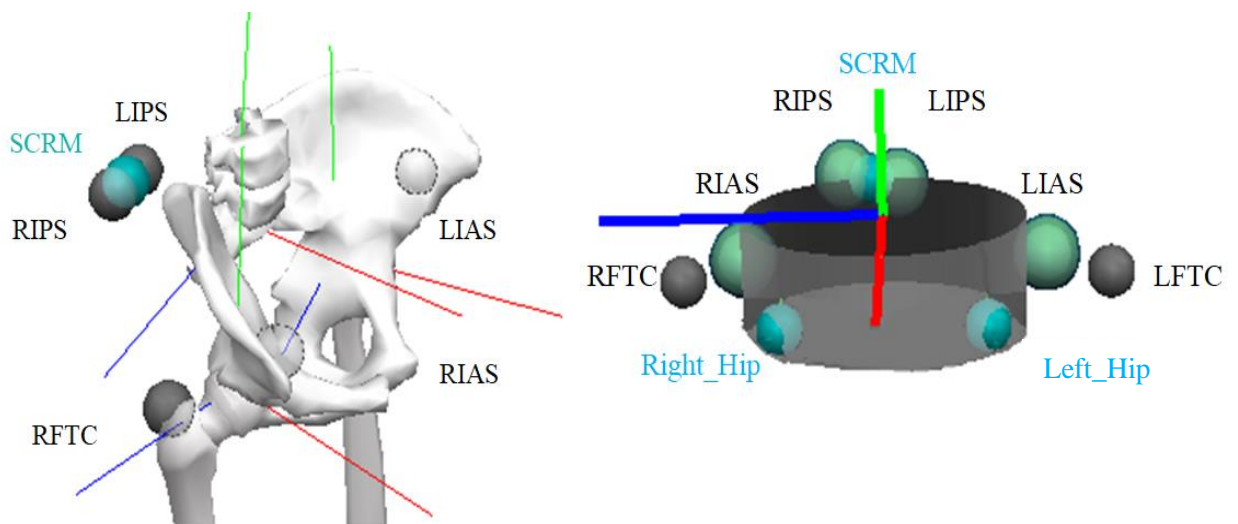


**Figure 25: The pelvis markers and landmarks used to define the segment.**

The hip joint landmarks were defined for both pelvis models using regression equations developed by Bell et al (Alexander L. Bell, Brand, and Pedersen 1989; A L Bell, Pedersen, and Brand 1990), the table below outlines the equations for both.

**Table 7: Hip Joint centre definitions based on the regression equations developed by Bell et al (1989, 1990).**

Hip Joint Centre	CODA pelvis	Visual 3D composite pelvis
Medial/Lateral	$0.36 * \text{ASIS\_Distance}$	$0.36 * \text{ASIS\_Distance}$
Anterior/Posterior	-	$-0.19 * \text{ASIS\_Distance} + (0.5 * \text{RPV\_Depth} - 0.19 * \text{ASIS\_Distance})$
Axial	$-0.3 * \text{ASIS\_Distance}$	$-0.3 * \text{ASIS\_Distance}$

**Table 8: Landmark definitions for pelvis segment**

Landmark	Starting point	End point
Sacrum (SCRM)	RIPS	LIPS

#### 3.3.4.4 Thigh

The distal end of the thigh segment was defined laterally and medially by the markers at the knee. The proximal end of the thigh was defined using the landmark at the hip, creating during modelling of the pelvis. The thigh was modelled using a truncated cone.

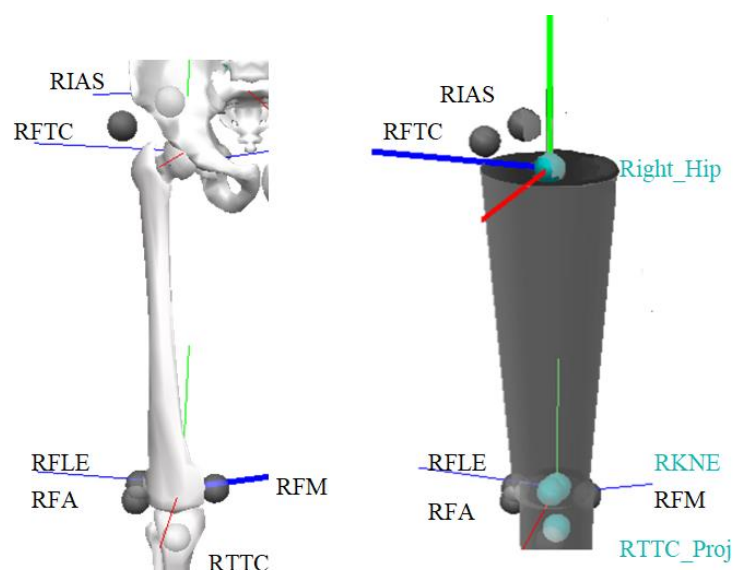


**Figure 26: The thigh markers and landmarks used to define the segment.**

### 3.3.4.5 Shank

The shank was also modelled as a truncated cone. The centre of the knee was defined using the LSK\_PROX landmark. The radius of the shank segment was half the distance of that between the lateral and medial knee markers. The lateral and medial ankle markers define the radius at the distal end of the segment.

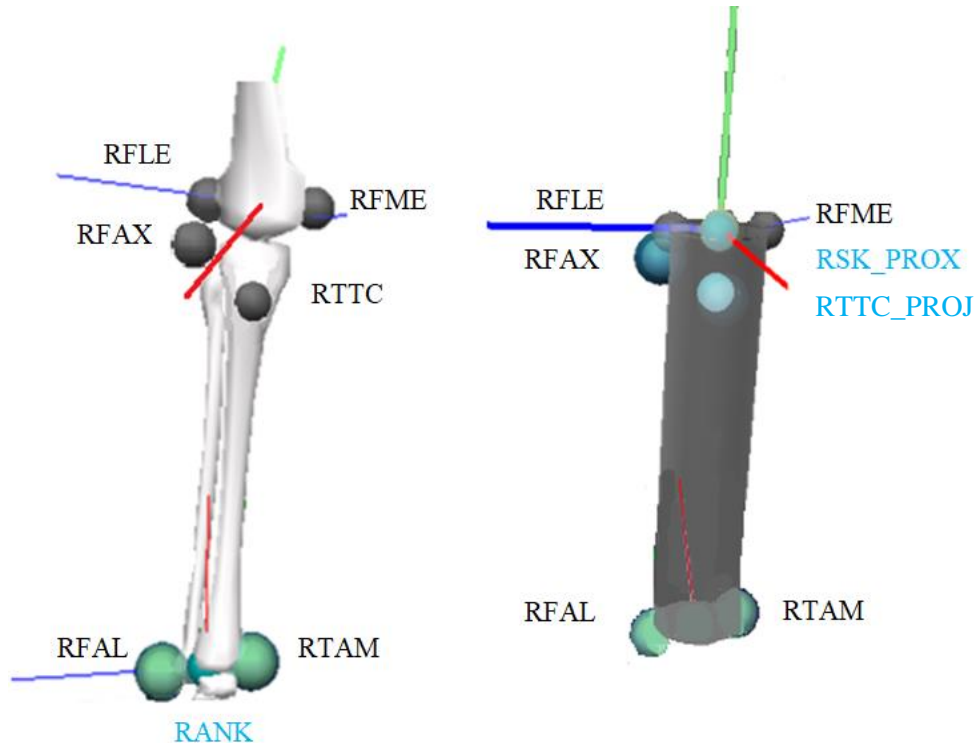


**Figure 27: The markers and landmarks that define the shank segment.**

**Table 9: The definition of the landmarks at the shank.**

Landmark	Starting point	End point	Lateral point	Projected from
Right Knee (RKNE)	RFLE	RFME		
Tibial Tuberosity projected (RTTC_Proj)	RFAX	RFAL	RTAM	RTTC
Right Shank_Proximal (RSK_PROX)	RANK	RTTC_PROJ		RKNE

### 3.3.4.6 Foot

The foot segment defined in the conventional gait method uses the 1<sup>st</sup> and 5<sup>th</sup> metatarsal to define the width of the foot. A landmark in between the medial and lateral ankle markers defined the joint centre of the ankle. However, when using this method, the orientation of the foot is so that it is in 30% plantarflexion (see Figure 28) which is not representative of true anatomy throughout movement. To correct this, a virtual foot was created and used for kinematic calculations, (note, it is not included in inverse dynamics calculations). The virtual foot is not another segment, but a segment coordinate system, which removes the plantarflexion offset. The neutral orientation the foot was modelled when it is flat on the floor and the shank segment is vertical. Due to the marker placement on the front of the foot not reflecting this ‘neutral axis’ the virtual foot uses landmarks at the distal foot as well as at the calcaneus to define the segment with its orientation +Y in the A/P direction and -X in the distal to proximal axis.

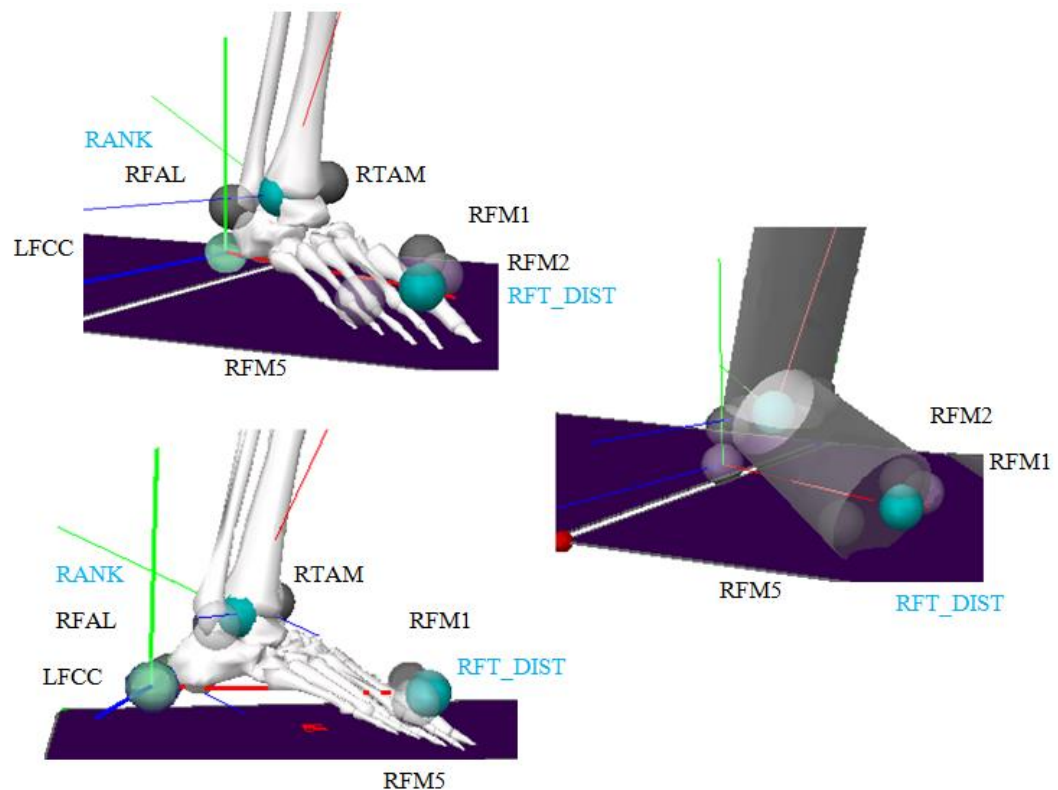


**Figure 28: The markers and landmarks which define the foot segment. The bold coordinate system which originate at the calcaneus defines the virtual foot segment.**

**Table 10: The definition of the landmarks at the foot.**

Landmark	Starting point	End point	Lateral Point	Projected from
Ankle (RANK)	RFAL	RTAM		
Foot_Distal (RFT_DIST)	RFCC	RFM5	RFM1	RFM2

### **3.3.5 Method of processing 3D motion capture data**

Once the model was created, the dynamic files were assigned to the participant's static file and were processed together and saved into one .cmz file. The signals from the dynamic file are stored in the data tree as TARGET signals, these are three degrees of freedom signals with five components; x,y,z, camera contribution and residual. The biomechanical analysis software package, Visual 3D, only displays four of these, the x, y, z coordinates of the marker in space and the residual associated with the camera during motion capture. To correct for any missing positional values, the signals were interpolated, using a third order polynomial fitted with a maximum frame gap of 10. A low pass Butterworth filter was then applied to both these processed target files (kinematic data) along with the force data. This filter attenuates the data to remove the higher frequency data. Kinetic data was processed to remove any noise, as errors have been found to be amplified when calculating segment inertia through inverse dynamics (Chiari et al., 2005). The force data was previously reported to be more accurate, so in less need of filtering (Roewer et al. 2014). Therefore for kinematic data the cut-off frequency is 6Hz and for the force data this is 25 Hz (Robertson and Dowling 2003).

For temporal-spatial analyses of trials, gait events had to be defined. First, the heel and toe markers were transformed into the pelvis co-ordinate system. The point of contact with the force plate was identified using an event threshold. The event was labelled ON when the vertical component of GRF exceeded 20 newtons and labelled as OFF when the vertical component descended below 20 newtons. This method used algorithms based on previously published literature (Zeni et al. 2008). In order to identify the leg which makes contact with the force plate, the events were manually edited to assign left or right on (LON, RON).

In computing joint reaction forces and net joint moments, there are four reference frames that can be used to resolve the signals (see Figure 29). The simplest approach is to resolve the signals within the global coordinate system, as the participants line of progression is usually aligned with the sagittal plane, making them one and the same. However, this 2D approach leaves the y and z (as the sagittal plane is usually in the x direction) difficult to interpret (Selbie et al. 2004). Although there is no recommendation for which reference frame reaction forces and net moments should be resolved to, each generates a signal with differing magnitude and shape (Brandon and Deluzio 2011). For studies within this Ph.D, the local segment coordinate system was defined as a Z-X-Y cardan sequence and joint moments were resolved in the proximal segments coordinate system.

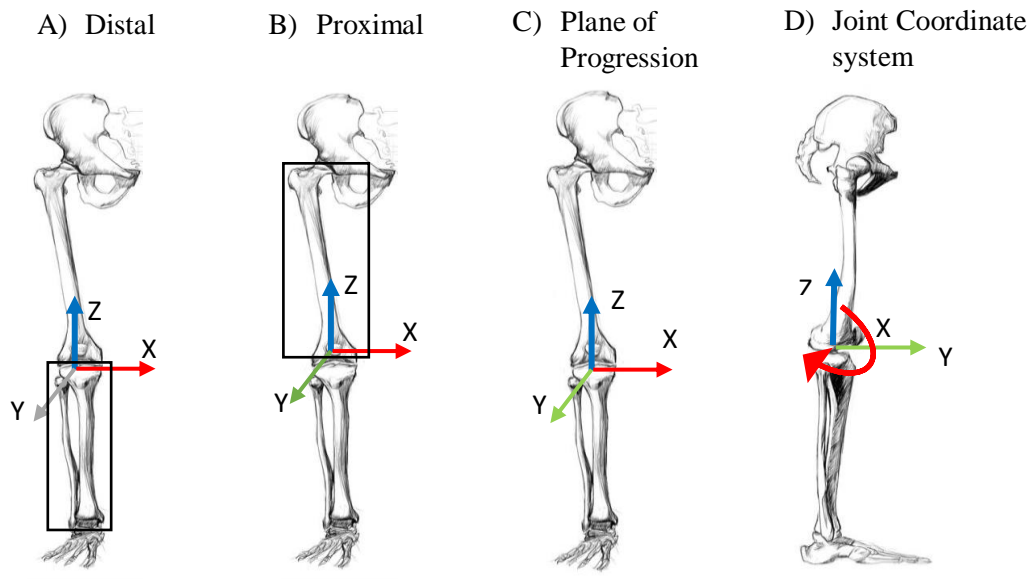


**Figure 29: Four reference frame options for 3D modelling. A) Resolve to the shank segment, B) Resolve to the thigh segment, C) Project the flexion axis from the proximal frame and internal rotation axis from the distal segment and a perpendicular adduction axis, D) The Plane of Progression fixes the flexion axis perpendicular and the adduction and internal rotation axis, taken from the distal axis, are projected. Adapted from (Selbie et al. 2004; Brandon and Deluzio 2011)**

Inverse dynamics within Visual 3D was used to process the joint moments normalised to body mass. The algorithm used for the calculation of proximal joint force, which takes into consideration any external forces applied on body segments is as follows:

$$F_{proximal} = \sum_{i=1}^n m_i(a_i + g) + \sum_{j=1}^q F_q$$

$m_i$  = mass of segment i

$a_i$  = acceleration of segment i

$n$  = the number of distal segments connected within the chain

$q$  = the number of external forces

$F_q$  = applied external forces

$g$  = gravity

The proximal moment computed at the proximal end of the segment using the local coordinate system using the following:

$$C'_i = I_i a'_i + \omega'_i * (I_i \omega'_i)$$

$I_i$  = Mass of segment i

$a_i$  = acceleration of segment i

$\omega_i$  = velocity of segment i

This torque is translated from the segment coordinate system into the global coordinate system that is computed from the 3D motion capture data.

The proximal moment due to the inertial forces and moments at the joint is defined as follows:

$$M_i = \sum_{i=1}^n (C_i + R_i * A_i) + \sum_{j=1}^q (P_j * F_q) + \sum_{k=1}^p \tau_k$$

$$A_i = m_i(a_i + g)$$

$$R_i = r_i + r'_i + r_{i-1}$$

$p$  = number of external couples

$P_j$  = vector from the application of the external force to the proximal joint

$R_i$  = distance from centre of gravity of each distal segment to proximal joint

$A_i$  = Acceleration

Specific segment moments that are measured are expanded on further in the relevant chapters.

### **3.3.6 Statistical analyses**

Statistical analyses were carried out in SPSS version 23 (SPSS Inc., Chicago, USA). Data were tested for normality using the Shapiro Wilks test. Upon the satisfaction that all data were distributed normally, a general repeated-measures analysis of variance (ANOVA) design was conducted. Another assumption for repeated-measures ANOVA is sphericity. This was tested for using Mauchly's test of sphericity. Where Mauchly's test of sphericity resulted in a violation, a greenhouse-geisser correction was applied. If statistical significance was shown then a Bonferroni post hoc test was carried out. Results were considered statistically significant at an alpha level of  $p \leq 0.05$ .

# **4 STUDY ONE: THE DEVELOPMENT OF A SEMI-SUBJECT SPECIFIC FINITE ELEMENT MODEL OF THE TIBIA**

## **Dissemination of research**

### **Conference presentation**

**Brown, Q.**, Sale, C., Lewis M.G.C., Barnett C. T.,(2019) An image processing method to assess changes in tibial geometry from peripheral quantitative computerised tomography scans, International Society of Biomechanics (ISB) Conference, Calgary, Canada.

## 4.1 Introduction

Finite element analysis has been used to study an individual's bone response to mechanical loading through the generation of strain plots (Schileo et al. 2008, 2007a; Phate et al. 2014; Pérez et al. 2009a). In the late 1990's early 2000's, the accuracy and the biological relevance of the strain output was increased through the introduction of subject specific FEM (Viceconti et al, 2004). Subject-specific FEM's were created from bone imaging scans *e.g.* CT scans. The segmentation of scans and 3D image reconstruction to create a subject specific FEM has since been automated by researchers using image processing software (Viceconti et al. 2004; Couteau et al. 2000). These models have then been improved further by combining CT imaging with magnetic resonance imaging (MRI), to model muscle attachments and contact areas (Lunn 2013; Périé and Hobatho 1998). Contact areas have been recorded through dynamic movement using radio-opaque markers implanted at the joint (Beillas et al. 2007). The joints are loaded concurrently to imaging through MRI (Yao, et al. 2008) and dynamic fluoroscopy (moving x-ray) (Carey et al. 2014; Dennis et al. 2005). These dynamic imaging techniques are either very invasive, expose the participants to excessive radiation, or not as accurate (Draper et al. 2017). However, CT, exposes patients to high doses of radiation, as such it is only ethically permissible to carry out these scans on cadavers or if the patient has an independent clinical need *e.g.* prior to surgery for amputation.

Research has attempted to reduce the radiation but still maintain subject-specific FEM by developing a model from sparse CT data sets (Poelert et al. 2013; Donlagic et al. 2008; Shim et al. 2007). Shim et al, (2007) instead of using MRI data, used slices from the visible human project (VHP), an open source set of bone scans, to provide geometrical data between the subject's CT scans. This removed the requirement of an MRI scanner, which is a costly

method of imaging, however, participants are still exposed to some radiation. Peripheral quantitative computed tomography (pQCT) offers a low dose alternative to CT. Peripheral quantitative computed tomography has a comparably reduced radiation exposure to CT. The post-scan processing provides information on volumetric bone mineral density as well as separating out the trabecular and cortical bone, proving advantageous against other low radiation scanning modalities such as dual-energy x-ray (DXA). The scan acquisition time for pQCT is approximately ninety seconds, which when using a single-slice machine, as is popular in research laboratories, does not allow the whole bone to be imaged in enough detail to produce a FEM (Mittag et al. 2017). Where research has used pQCT to influence finite element models previously it was limited to sections of bones rather than whole bones (Vilayphiou et al. 2011). Mittag et al. (2017) overcame this limitation by using an interpolation technique. This technique manually identified the centre point of the bone from two pQCT scans either side of the 'missing' section. Whilst this yielded an accurate model, the scanning was carried out ex-vivo to obtain as many slices as possible, so not in an environment easily replicable in a research or clinical environment. In a clinical environment, peripheral quantitative scanners image at four points along the tibial length; 4, 14, 38 and 66% to obtain information on both cortical and trabecular bone, without exposing participants to excessive radiation (Evans et al. 2012). Within literature there has not yet a method developed to analyse clinically produced pQCT scans which could be used to produce subject-specific FEM whilst maintaining low radiation exposure.

Therefore, the aim of this study is to establish a method that uses the four scans generated from a pQCT and a base model constructed from the VHP to construct a semi-subject specific model. The objectives of this study were to establish an image processing code which extracted tibia outer geometry coordinates. These coordinates were then used in the

second objective to morph the base model tibia to create a semi subject-specific model. The last objective was the validation and evaluation of this image processing method.

#### 4.2 Processing of tibia scan images

Peripheral quantitative computed tomography scans were performed by a trained operator using a Stratec XCT 2000 scanner (STRATEC Medizintechnik, Germany). Four images were collected on the right tibia (see Figure 30) of participants as part of Study Three (Chapter Six), please refer to methods (section 3.2.1) for further details.

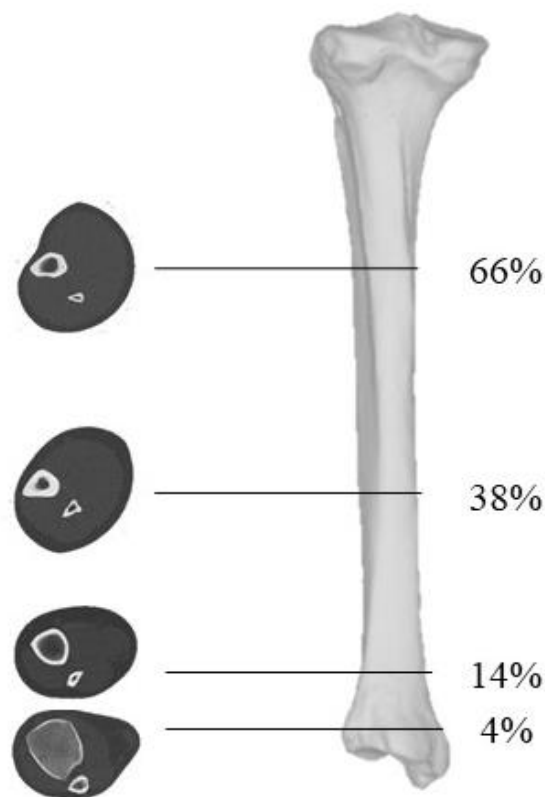


**Figure 30: Locations of the pQCT scans along the length of the tibia.**

Images were exported as text based image files (.mdl) and were converted into high quality image files (.tifs) using the commercially available image processing software Image J (Schneider et al. 2012). Further image processing was then carried out in MATLAB (The MathWorks, Inc., Natick, Massachusetts, United States), a multi-paradigm numerical

computing environment and proprietary programming language developed by MathWork (The Math Works Inc., Natick, MA, 2000). Figure 31 details the entire image processing sequence, specific details of each step can be found in the text following Figure 31.

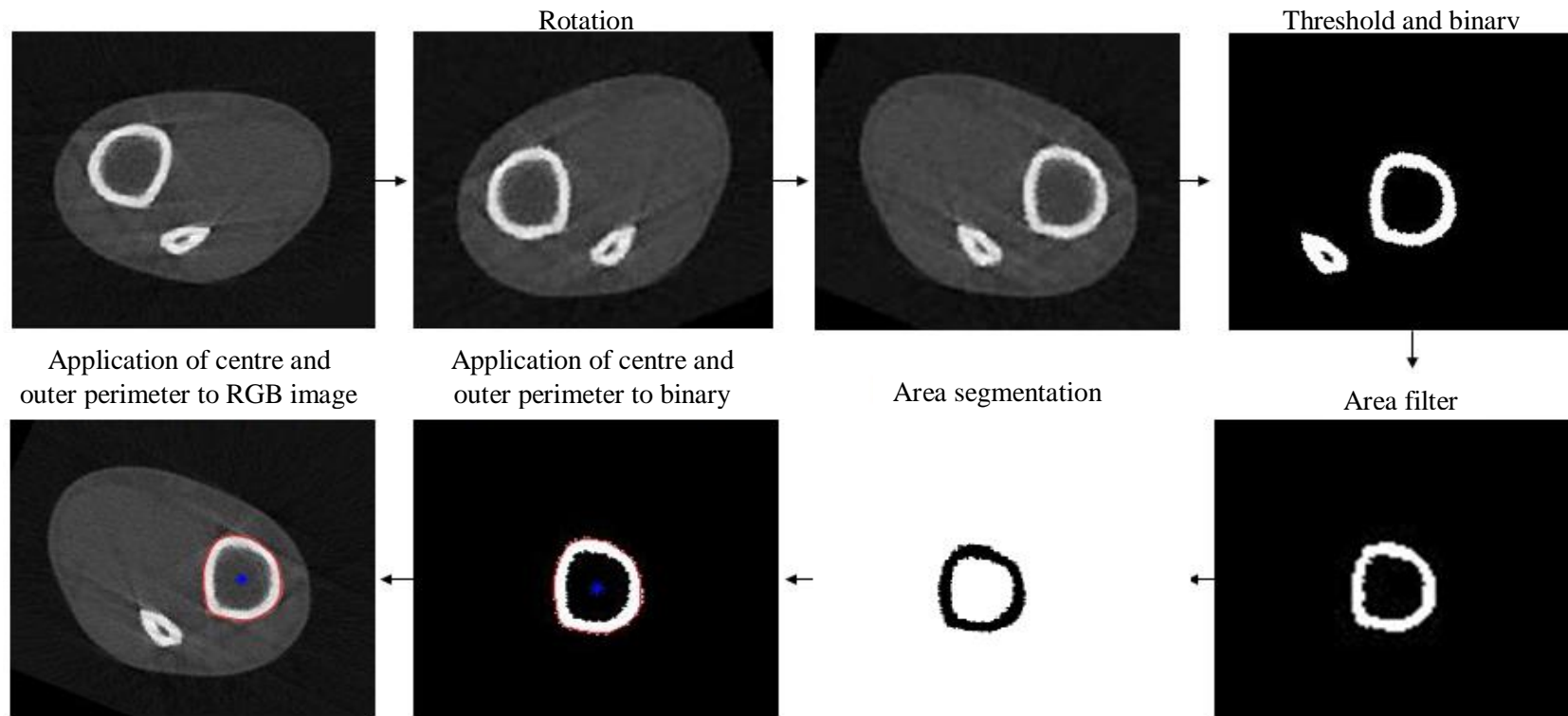


**Figure 31: The pQCT image processing sequence commences at the top left and moves clockwise. The image is rotated by 23 degrees and then flipped horizontally. A threshold is applied to the bone and the image converted to binary. An area filter is applied to select the tibia only. Area segmentation is used to identify the two area masses; cortical and trabecular. The outer perimeter is calculated and is seen applied to the binary image and the RGB image.**

The .tif files were imported into MATLAB (Statistics Toolbox Release 2017a/2017b, The MathWorks, Inc., Natick, Massachusetts, United States) in their in red, green, blue colour format. In order to identify the outer geometry of the bone, the outer shell of the tibia was classified as the area of interest. The outer shell is constructed of cortical bone, which, within this image was identified as the area of the image with the lightest pixels, *i.e.* white. The RGB code that corresponded to white pixels was when the red, green and blue components were equal to 255. Figure 32 shows how individual intensity values can be used to visually identify different types of bone/tissue. The graph was produced for every participant to aid in the decision of a threshold. When the line on the graph steps down, the corresponding threshold value identifies pixels at each level of tissue. The lowest threshold shows all fat and muscle mass, increasing the threshold decreases the number of different materials shown. The threshold graph in Figure 32 is an example of one participant at 14%, as you can see theoretically the cortical bone should be singularly identified at a threshold value of ~100. Through repeated investigation it was shown that the threshold identified using pixel mass on the graph (Figure 32) was not the necessary optimum threshold for identifying cortical bone only. Instead it was shown that, for cortical bone only, the threshold of 125 appropriate. Below which trabeculae bone was visible (this is not needed when identifying only outer geometry) and above which pixels on the outer boundary of the cortical bone may not have been included.

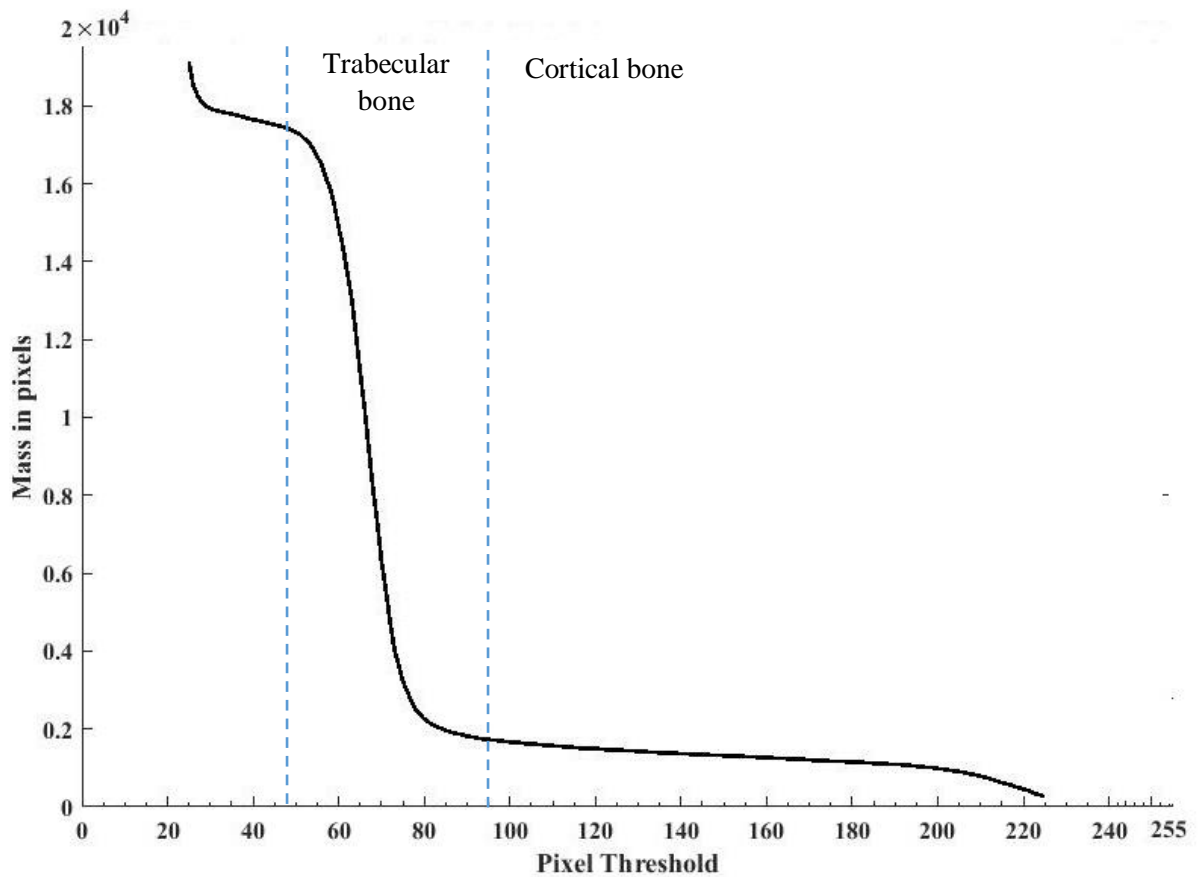


**Figure 32: Graph of mass identification when a range of thresholds to image generated at the 14% site of the tibia. At the point of each step down of the curve the associated pixel threshold identifies another material. E.g. at ~100 only cortical bone is identified.**

This information was used to determine a threshold range to segment the image and identify just the cortical bone. The threshold was then applied in conjunction with the binary mask to convert all pixels greater than the threshold value (e.g. 125) to equal 255, which in binary gives them a value of 1, *i.e.* white. The binary masking created two areas of white pixels, the larger area is the tibia and the smaller the fibula (see Figure 31). An area filter was then applied to find and display the largest area only, thus extracting and separating the tibia and fibula, allowing analyses to continue on the tibia only.

The coordinates of the outer edge of tibia were identified using the loop function. Only the outer most coordinates *i.e.* the largest and smallest x values and their corresponding y

coordinates were plotted (Figure 33). The centre point of the mass was also calculated. This was used as a reference point between the base model slices and the pQCT scans. A centroid function within region analyses calculated using the centre of mass of the region. The region, the perimeter of the tibia, was identified as an 8-connected component (object) within the binary image. In order to validate that the centre point was based on the mass of the entire structure, the binary image was also reversed, so that the cortical region was now given a value of 0 and thus displayed is black. The mass (the inner canal of the tibia) was given a value of 1, then undergoes the same region analyses as the cortical region (Figure 31, area filter and area segmentation).

The resolution of the pQCT scanner results in a pixelated perimeter, which may not accurately represent the outer topography of bone. To compensate for this a three-point moving average smoothing function was applied, the resulting shape uses the current data plots, taking an average over three data points in accordance with previous image processing research (Evans et al. 2012). Filtering over a small area means that any subtle changes in bone perimeter are maintained whilst also producing an anatomically representative shape. The process of identifying the outer perimeter and centre point, described above, was repeated after smoothing. The two outer perimeters generated can be seen in Figure 33. The smoothed outer perimeter was carried forward for further analyses.

One method of measuring bone health is through bone strength. Bone strength can be determined through both bone material properties and bone geometry. Peripheral quantitative computed tomography scans provide information specifically to bone geometry. The bones resistance to bending and torsion is quantified through the cross sectional and polar moment of inertia and sectional modulus (Sheu et al. 2011). All of these depend on the distribution

of material around the neutral axis of the bone. The further the deposition of material is from neutral axis, the bones ability to resist bending and torsion is increased. These measures are derived from distribution of bone about the neutral axis and the distance between the centroid and the outer most edge of the bone. Therefore, in calculating the cross-sectional diameter in both the x and y changes in strength can be inferred and input into calculations to quantify strength.

Finally, a set of coordinates around the outer geometry were derived. To improve computer processing time the entire perimeter was not included. Instead, the tibia perimeter was segmented. Sectional analyses has been used previously in the analyses of intervention studies within post-menopausal women (Cheng et al. 2002) as well as for comparison studies between different sexes within a military cohort (Evans et al. 2008). This lead to Evans et al., (2012) developing BAMpack- the Bone Alignment and Measurement package which dissected the bone every 60 degrees, unfortunately this is not available as open source software, so cannot be used for this research. To reduce computing whilst maintaining accurate shape representation in morphing, the bone was segmented at 30-degree intervals. The coordinates were then taken from each dissecting point, starting from the positive x axis, in an anti-clockwise motion for a 360 rotation around the tibia (see Figure 35).

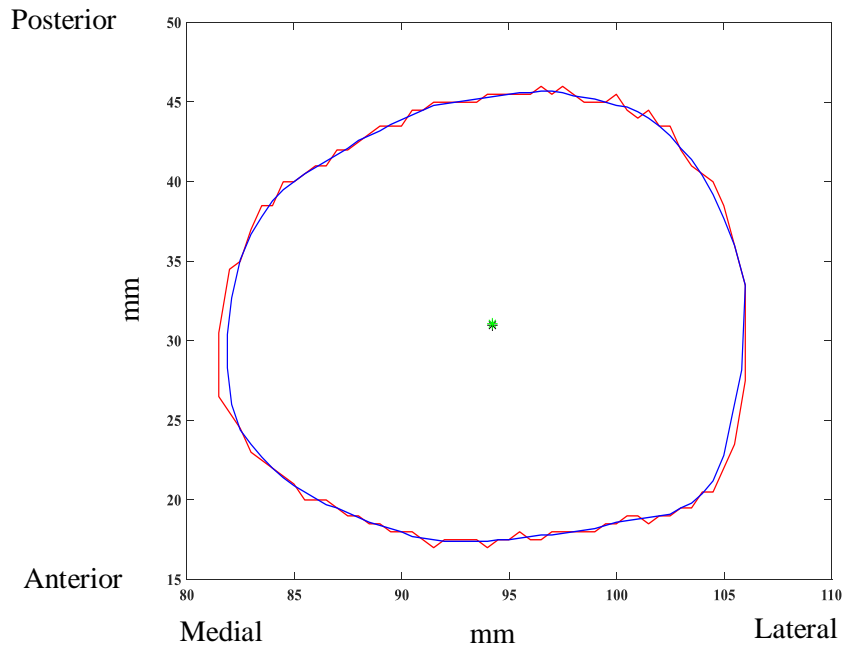


**Figure 33: Outer perimeter of bone with both the smoothed (blue) and original (red) parameter displayed. As well as the centre point displayed as a black '\*' and as a green '\*'. The orientation is also labelled at each axis, the origin is generated from the original image hence not 0, 0 in this Figure.**

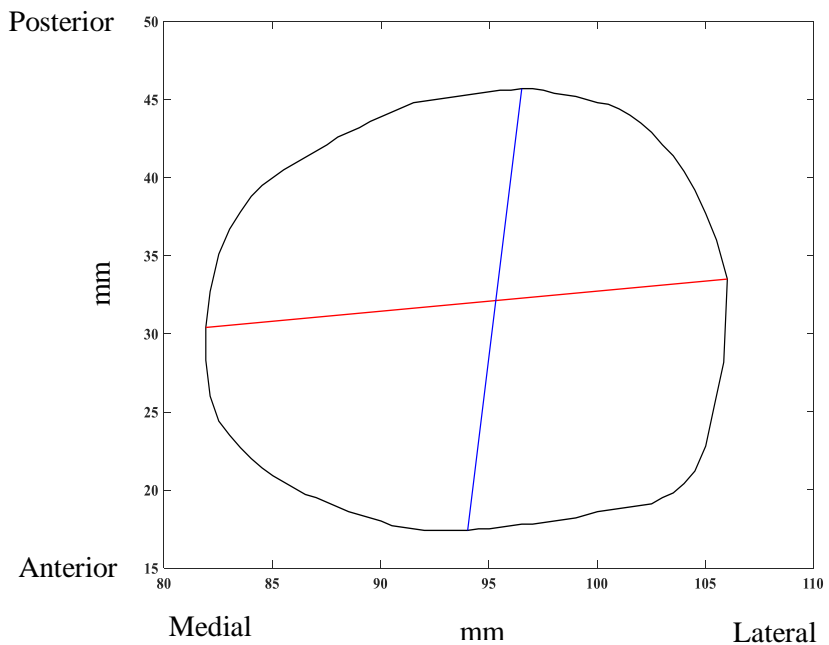


**Figure 34: The maximum axial cross-sectional diameter in the X (red line) and Y (blue line) diameter.**

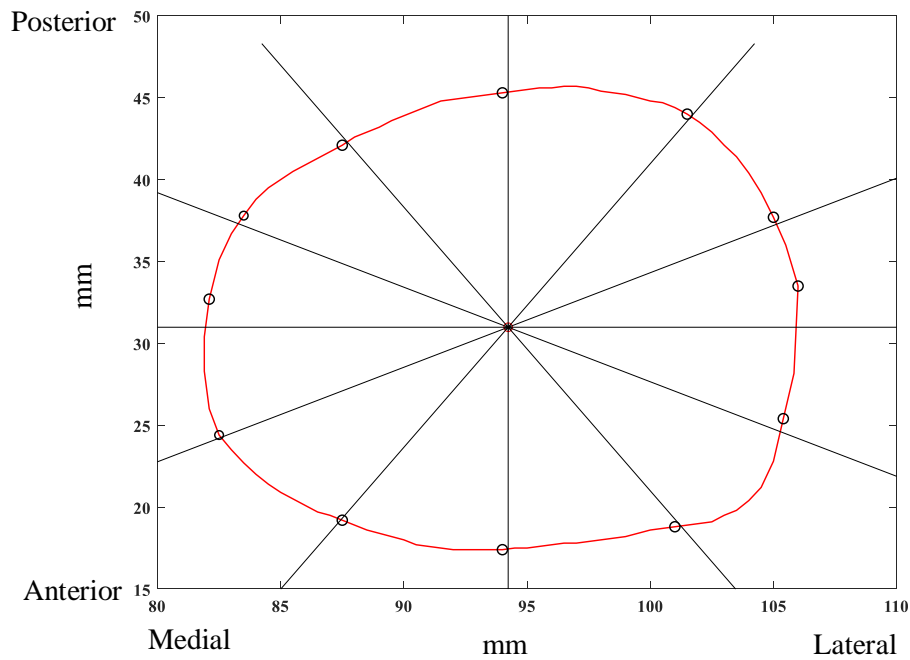


**Figure 35: Generation of landmarks through visual dissection of the tibia. The red line is the outer perimeter of the tibia and each circle represents identification of a landmark.**

A FEM cannot be constructed from only four scans; therefore a base model had to be created. Section 3.3 and 3.4 detail the process of sourcing and creating a base tibia FEM.

### 4.3 Base Model Images

The visible human project (VHP) was originally created to fulfil a gap in the educating material, providing two dimensional images to help students and health professionals understand the human physiology and the complex relationships found within the body (Ackerman 1999). The National Library of Medicine (NLM) gave approval given in the 1990 NLM long term plan report to pursue with the collection of such a data set (Spitzer et al. 1996).

The following year, two cadavers, a thirty eight year-old male and a fifty nine year old woman, were donated. They were imaged and published, becoming available to the public

in spring 1994 and winter of 1995 (Waldby 2000; Spitzer et al. 1996). The scans were stored on the VHP FTP site, access to which is gained through the application of a license from the National Library of Medicine, approved on 10<sup>th</sup> of April 2015. The images used in the development of this project were adapted from this data set by the University of Iowa carver college of medicine, magnetic resonance research facility

Once the cadavers had been identified they were scanned using both CT and MRI, prior to freezing and then again once the cadaver had been placed in a gelatine block and frozen at -160°F. The two cadavers had axial magnetic resonance scans of the head/neck region and longitudinal sections of the rest of the body at intervals of 4mm.

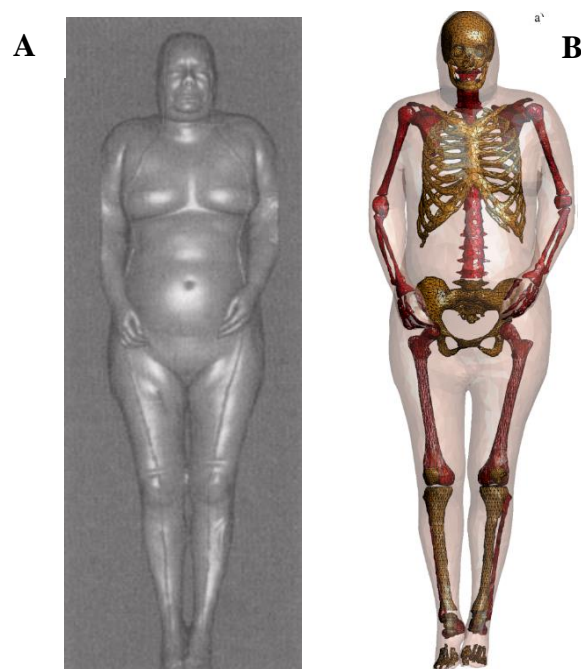


**Figure 36: A; Visible Human Female three-dimensional image reconstruction. Taken from Waldby (2000) (image courtesy of Lorensen and G.E. Imaging and Visualisation Laboratory) B; The musculoskeletal reconstruction of the visible human female taken from Yanamadala (2014).**

The pixel resolution was 256 by 256 pixel with each pixel consisting of 12 bits of grey tone. The CT sections of the axial anatomy of the body were obtained at intervals of 1mm for the

male specimen and at 0.3mm for the female specimen (Juanes et al. 2003). This resulted in a resolution of 1048 x 1216 pixels with 24 bits of colour per pixel for the male dataset and a total 1,871 axial slices. The smaller intervals between scans within the female data set resulted in a 5,189 axial slices of 0.33mm in cubic volume, making the data a good source for 3D reconstruction (National Library of Medicine 2003) and hence were used for the development of a base model.

#### **4.4 Base Model Development**

The CT images of the lower leg and ankle were downloaded as Digital Imaging and Communications in Medicine (DICOM) files from the VHP intranet. The slices pertaining to the tibia only were extracted. These tibia slices were imported into the 3D imaging visualisation, processing and analysing software AVIZO, version 9.5 (Thermo-fisher Scientific, MA, USA). The resolution of the scans was 1mm isotropic resolution. The following details the process of conversion of (DICOM) files to a 3D finite element tibia model.

The first process was segmentation of the scan images. This allowed the different biological materials within each image slice to be separated and specific properties allocated. Each slice was displayed within the segmentation editor in four display windows; XY, XZ and YZ and the 3D model. This enabled the images to be analysed in inclusive increments, improving the quality of model. Two materials were created for assignment; cortical bone and trabecular bone. The cortical bone was assigned to the outer edge of the bone images, in accordance with its anatomical location. Trabecular bone was identified as the darker grey matter displayed inside this boundary (see Figure 31). For the purpose of the anatomical accuracy, any gaps in the cortical material were filled in, this included holes or breaks in the

external boundary. For any missing slices the geometry was interpolated using the slices either side. These automatically generated interpolated slices were manually checked to ensure viability of the geometry.

To simplify the model, the trabeculae was filled as a block at both epiphyses. In order to do this, the last slice in the views where trabeculae could be visually identified were selected. The cortical area was locked to prevent any misidentification of materials.

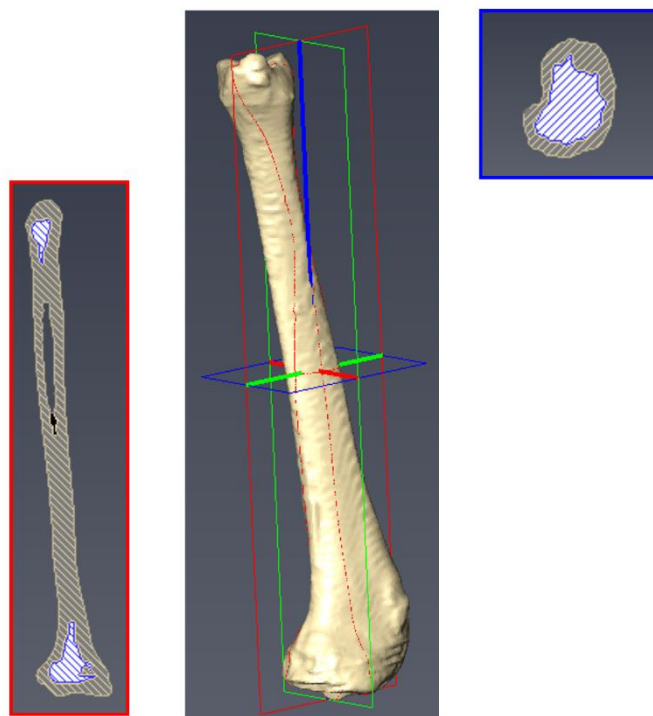


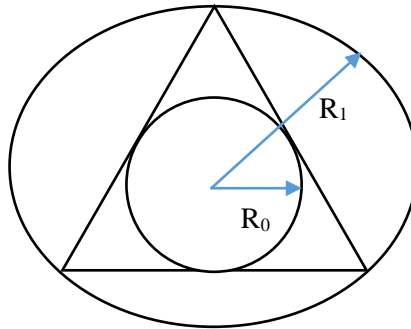
**Figure 37: The view of the tibia slices in the X direction (red boundary) and the Z direction (blue boundary). The checked blue area identifies trabecular bone and the checked yellow area is the cortical bone.**

In order to correct for the misidentification of voxels around the perimeter of the object, which leads to boundary irregularities, a smoothing function was applied. This function

changes the labelling file slightly by assigning probability weights to voxels. Probability weighting assigns a value to each voxel, averaged from the surrounding voxels, which identifies the probability the voxel belongs to an identified tissue, in this case either trabecular or cortical bone (Ashburner and Friston 2000; Haozhe et al. 2018). This assumes that surrounding voxels have been identified appropriately. Probability weighting assists in the smoothing of a generated surface.

Next the surface was generated, this function creates a 3D shape which represents the boundaries of all the materials, in this case the cortical and trabecular bone (where required). An '*existing weights*' smoothing algorithm was applied, which used the information from the probability weights generated previously. The boundary surface was extended to the edges of the identified materials, to mitigate any holes. However, the triangular elements generated from this step were not suitable for meshing. This is because the default sets an imbalanced distribution of triangle sizes, with smaller triangles in areas of high geometrical variation and larger in the plateaus. Although this helps maintain the detail of the model, it provides complication when simulating. The number of elements was reduced through the use of the '*simplify faces*' function, setting the maximum edge length to 1.5. This allowed for the reduction of triangles without the complications of intersecting triangles, as is often the case with an aggressive simplification. The surface editor was then used to perform quality checks, no intersections were found within the surface model. This was repeated for the aspect ratio, this is defined, for a triangular element, as the ratio of the radii of the circle on which all vertices lie (circumcircle) and the largest circle that fits within the triangle (incircle) (see Figure 38). It is recommended that the ratio of the radius of the circumcircle to radius of incircle be equal. For bone models, where there are areas of high curvature and low thickness this is not always possible. Therefore, research has stated that aspect ratio

values of up to 20 are acceptable as this is only applicable to a small percentage of elements within the model (Burkhart et al. 2013). This model had an aspect ratio <15 which is adhered to within previous publications (Quenneville et al., 2011).



$$\text{Aspect ratio} = \frac{R_1}{2R_0}$$

**Figure 38: Diagram to define aspect ratio of a triangular element.**

The final step is the generation of the volumetric tetrahedral grid, i.e. converting the volume within the surfaces to tetrahedral elements. This model is then taken forward for further analysis.

#### **4.4.1 Processing of base model images**

Once the model was constructed, the volume was converted back to slices and exported as .tifs. The scans at the 4%, 14%, 38% and 66% of total tibia length were selected and put through the image processing code (section 3.2). The slices generated from the visible human project have a 23° rotation factor. To control for this, a rotation factor was applied to the participant data to re-orientate the image to be in the same reference frame, see Figure 38.

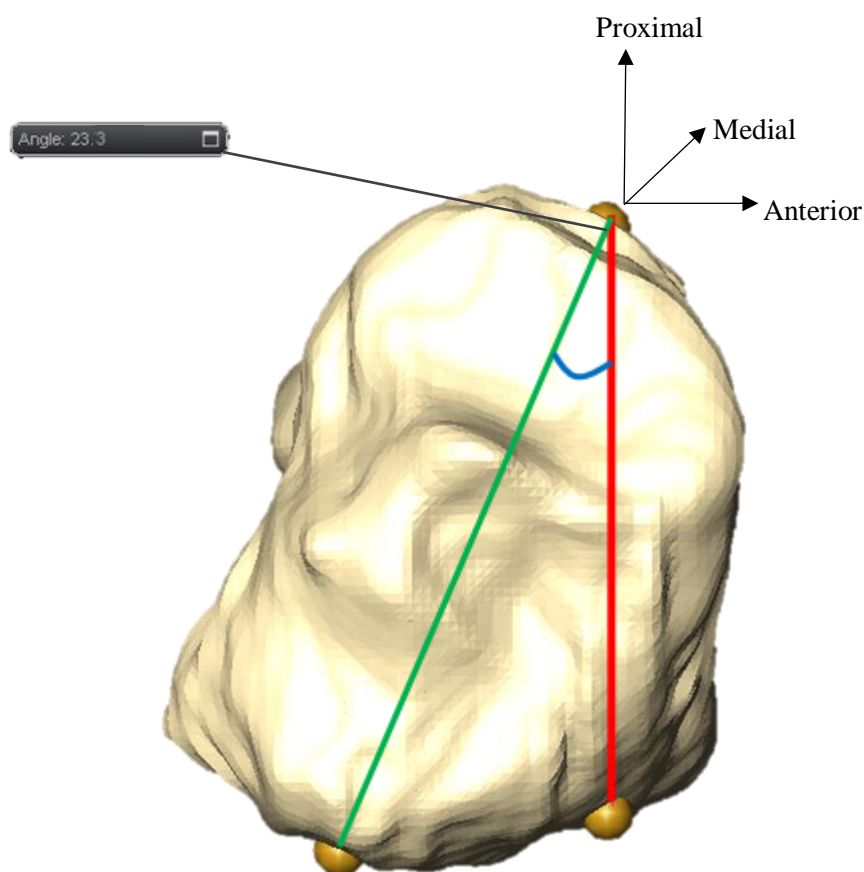


**Figure 39: Image of tibia from the proximal end to explain the rotation factor applied to the participant images.**

#### **4.4.2 Validity of the bone imaging acquisition and processing through assessments of accuracy and reliability**

##### **4.4.2.1 Model Specifications**

Validity was assessed through accuracy; the difference between the true diameter and pQCT derived diameter. Reliability was assessed through test-retest comparing diameter generated by pQCT and actual diameter.

In order to assess the validity of the image processing method, two Sawbones (Sawbones, MA, USA) models were scanned using the pQCT. The first, that of a uniform 3D shape, was

a fourth-generation composite cylinder; length of  $500\text{mm} \pm 2\text{mm}$ , outside diameter of  $40\text{mm}$  and wall thickness of  $5\text{mm} \pm 0.3\text{mm}$ . The cylinder was constructed of short fibre filled epoxy to simulate cortical bone, with a density of  $1.64\text{g/cc}$  and filled with 17PCF solid rigid polyurethane foam to simulate trabecular bone with a density of  $0.27\text{g/cc}$ .

The second model was a large left fourth generation tibia, length  $405\text{mm}$  and diameters of  $84\text{mm}$  across the tibial condyles,  $58\text{mm}$  across from the medial-lateral malleolus and approximately  $28\text{mm}$  diameter across the shaft (see Figure 40). This was constructed of short fibre filled epoxy to simulate cortical bone, with a density of  $1.64\text{g/cc}$  and filled with 17PCF solid rigid polyurethane foam at either end to simulate trabecular bone with a density of  $0.27\text{g/cc}$ . The geometry of this model was based on a male cadaver with height;  $1.83\text{m}$  and weight;  $91\text{kg}$ .

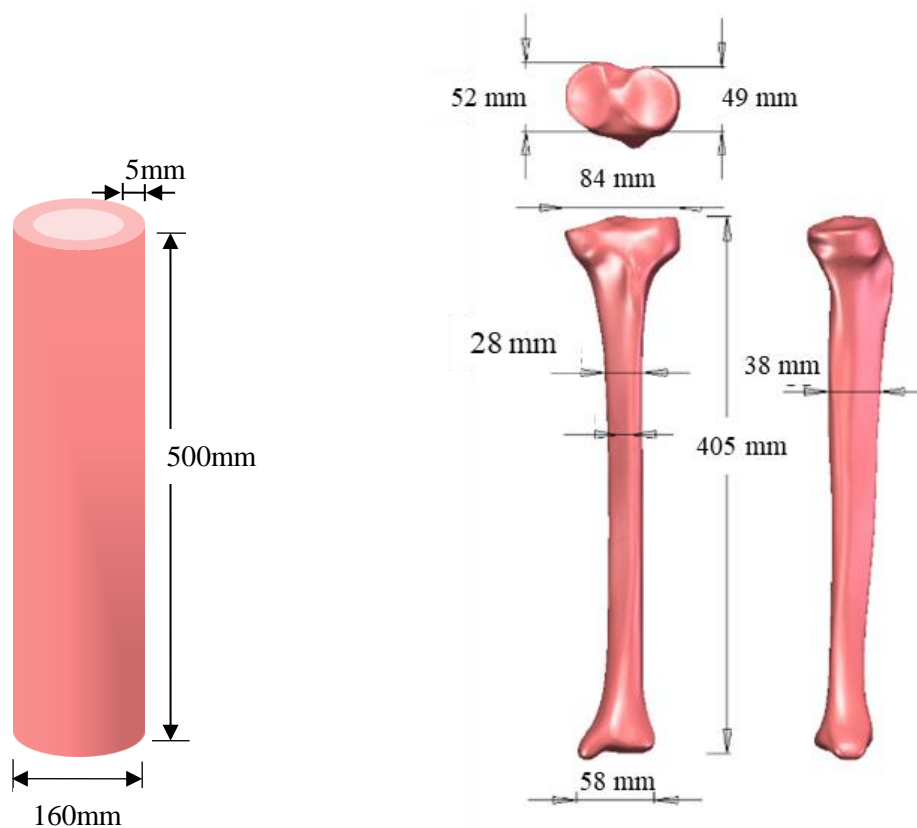


**Figure 40: Labeled diagram of cylinder model (Left) and tibia model (right) (Sawbones, Sweden)**

Accuracy was assessed by comparison of diameters generated through the image processing method to that provided by the manufacturer. Reliability was assessed using coefficient of variation of diameters from a direct test-retest and a test re-test a week apart.

#### **4.4.2.2 Model Positioning**

The models were scanned twice within the same session, without adjusting the positioning of the model. For the cylinder, due to its uniform shape there was no obvious features which could be identified by a scout scan. So instead the cylinder was positioned so the end of the cylinder was placed fully into heel support of the foot holder and secured at the other end in the thigh support, as seen Figure 41. The foot holder was at maximal extension and fed through so that the cylinder was level to the eye.

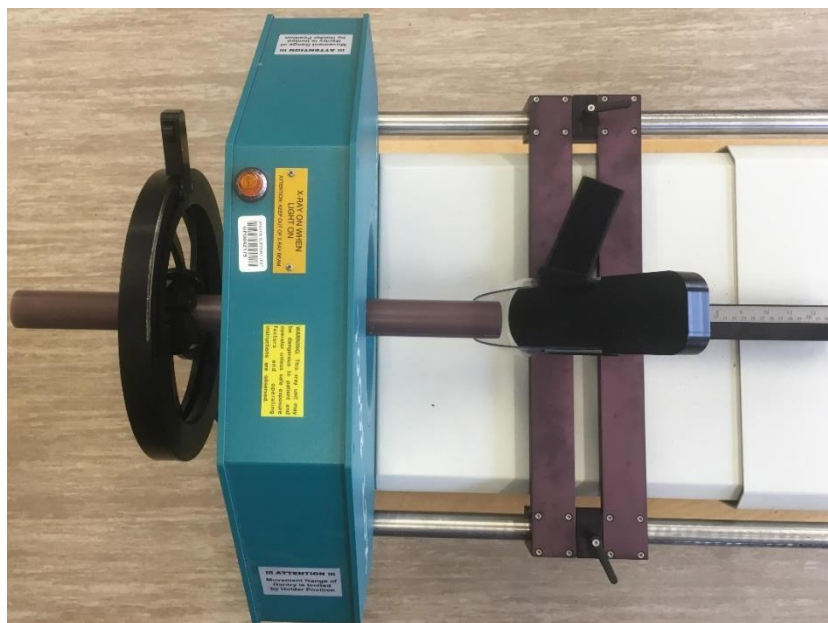


**Figure 41: Positioning of the cylinder model within the pQCT prior to scanning**

For the tibia there was no obvious change within the internal structure which could be identified during the scout scan. So, instead the end of the bone was used as a reference point. It was positioned within the scanner so that the reference laser was at the distal end of the model. In order to be able to scan at the 66% site, the model needed to be fixated in a

simulated thigh. In order to create this a 50mm deep section, slightly larger in diameter, but the same shape as the proximal tibia, was cut out of a foam cylinder (Figure 42). The tibia model was then secured into this cylinder so that there was no movement. The foot holder was then extended to its maximum height and the tibia was positioned so that it was a slight downward angle, which is more physiologically representative.

This scan for both the tibia and cylinder was conducted once (Scan1) then immediately repeated (Scan 2). The objects were removed and re-scanned a week later (Scan 3), keeping to the same positioning guidelines used in the first scan.



**Figure 42: Positioning of the tibia within the pQCT machine, with the reference laser (red line) at the distal end of the tibia. The proximal tibia is secured with a push fit within the blue foam cylinder (a simulated thigh) on the right of the image.**



**Figure 43: Scout scan laser and the resulting reference point for starting the scan**

#### **4.4.2.3 Data Acquisition**

Once scanned the region of interest was defined as the entire cylinder using the polygon selecting tool, see Figure 44.

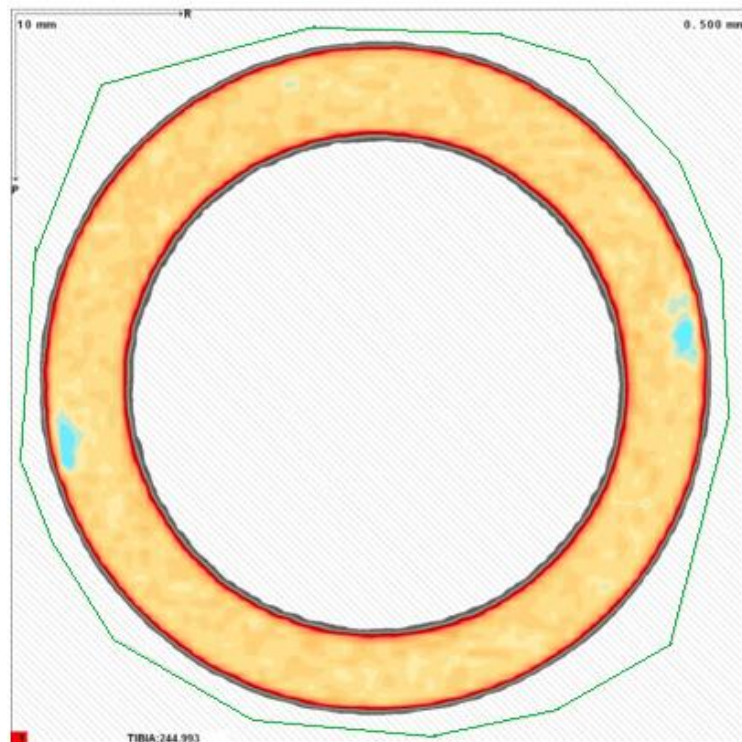


**Figure 44: Manual identification of the region of interest using the polygon tool (green line).**

Once the region of interest was defined, automated analysis was carried out. The pQCT was unable to identify density etc. due to material properties so, only the image files, exported in their .MO format, were used.

#### **4.4.2.4 Image processing**

The images were converted to their .tif and were processed through the image processing method described in Section 3.3. In order to make sure the accuracy and repeatability of the pQCT and not the image processing code was being assessed, the threshold value was chosen carefully. The threshold, which, when applied, yielded a diameter that was accurate to the diameter quoted by the manufacturer of  $160\text{mm} \pm 0.5\text{mm}$  was considered the most appropriate. At lower thresholds the solid rigid polyurethane foam, which represents trabecular bone, inside the cylinder, was incorrectly identified as the cylinder perimeter, which represents the cortical bone. If the image processing was continued with this mis-identification then the centre position, defined as centre of mass, would be inaccurate, as more 'mass' would be included in the calculation.

Figure 45 shows the result of the application of a range of thresholds. Once a threshold was decided the images could be processed to generate centre points, perimeter coordinates and therefore circumference and diameter.

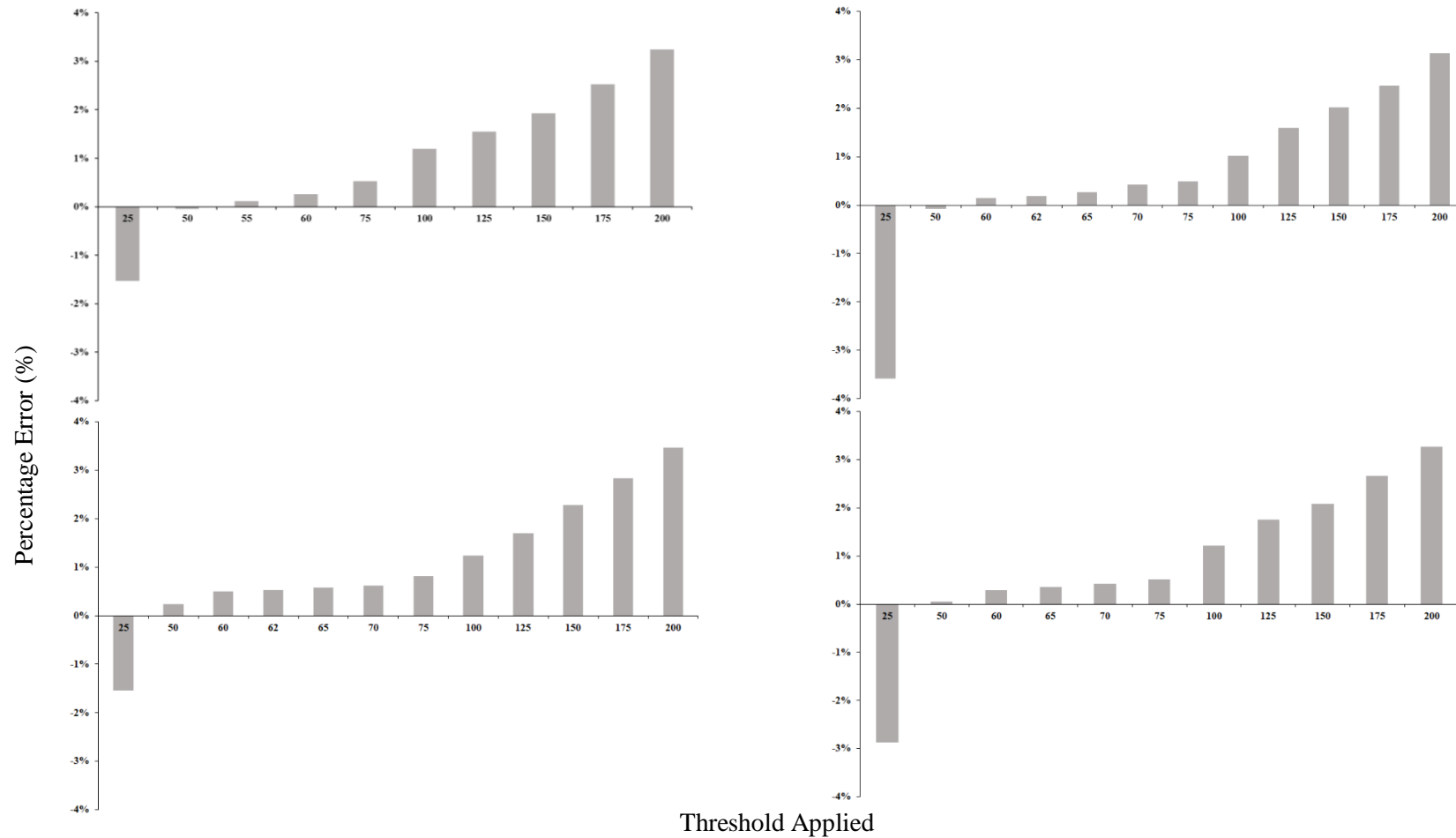


**Figure 45: Percentage error of the diameter, generated from varying the threshold within the image processing method. A is at the 4% site, B the 14% site, C the 38% site and D the 66% site. At 0% error the diameter is equal to the manufacturers provided measurement of 160mm.**

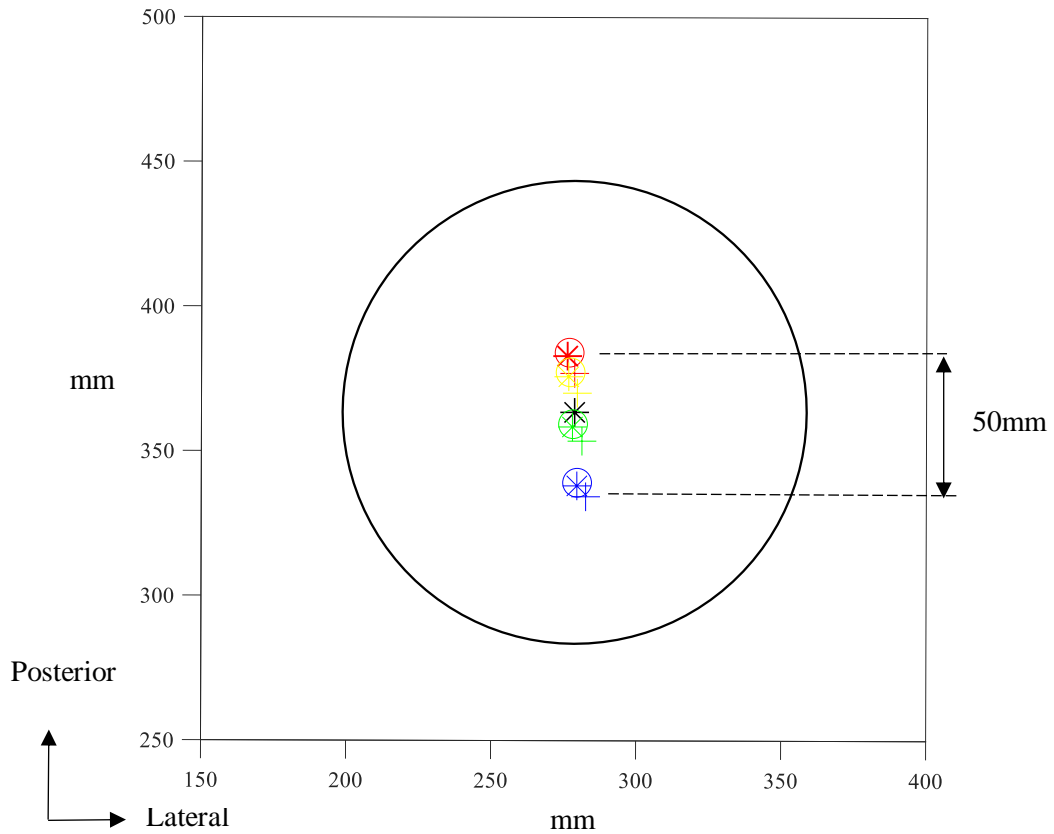


**Figure 46: Centre points generated through the image processing method. The centre point, based on manufactured diameter is represented by black \*. Each site is represented 4% (red), 14% (yellow), 38% (green), 66% (blue). The repeated scans are represented by symbols, scan 1 (\*), scan 2 (o) and scan 3 (+). The perimeter of the cylinder is represented by the black circle.**

In Figure 46, there is an average translation of 2.7mm in the x and 1.3mm in the y direction between repeated scans (represented through symbols). The translation between sites, reaches a maximum of 50mm between 4% and 66% sites. There is limited medial/lateral translation, translation occurs anterior/posterior in the direction, with maximum translation occurring at the 4% and 66% sites. This translation is considered to be as a result of the scanner movement rather than any error, therefore in order to see the absolute difference visually a translation factor was applied. This was the difference between the reference centre point and each individual site\*time centre point.

The following equation was used

$$x1 = X1 + (xc - xc1)$$

x1= translated perimeter co-ordinates

X1=Perimeter coordinates

xc=Reference centre point

xc1=centre point at time point one

*N.B. a separate code was used for each site with Scan 1, Scan 2 and Scan 3 being numbered sequentially within the code.*

### **3.4.2.3 Results**

Taking the average of all sites, the pQCT calculated the diameter of the cylinder to be 159.34 ± 0.27 mm. This was an average percentage error of 0.45%. This translates to an under-estimation of the diameter of the cylinder of between 0.35mm and 1mm. The largest percentage errors were seen at the 66% site, with smallest percentage errors at the 4% site (see Table 10). Table 11 and 12 show that there is more variation along the cylinder length *i.e.* between sites, than there was at a single site when the cylinder was removed and replaced.

**Table 11: Accuracy and reliability of the pQCT; the percentage error when comparing the diameter of the cylinder as derived from the pQCT to the 160mm diameter specified by the manufacturer.**

Scan Site	Scan Number	Coefficient of Variation (%)
	1	0.26%
4	2	0.22%
	3	0.43%
	1	0.27%
14	2	0.51%
	3	0.52%
	1	0.57%
38	2	0.50%
	3	0.47%
	1	0.43%
66	2	0.63%
	3	0.56%

**Table 12: Reliability of the pQCT Coefficient of variation of all scan sites (4, 14, 38 and 66%) at each scan time point (scan 1, scan 2 and scan 3).**

Scan time point	Coefficient of variation (%)
Scan 1	0.13
Scan 2	0.15
Scan 3	0.05

**Table 13: Reliability of the pQCT. Coefficient of variation between scan time points (scan 1, scan2 and scan 3) for each scan site (4, 14, 38 and 66%).**

Scan site (% of tibia length)	Coefficient of Variation (%)
4	0.09
14	0.12
38	0.04
66	0.08

The largest absolute differences in diameter were found between scan 1 and scan 2, *i.e.* immediately repeated scans. The maximum change in diameter as the scanner progresses along the cylinder was 0.65mm between the 4% site and the 66% site.

For the tibia model, a threshold value could not be quantified based on the accuracy to a known diameter. Instead, the threshold was determined when only the epoxy shell was visible. All sites had a threshold application of 50 except the 66% site where the threshold was 60. The centre points were plotted and a translation factor was determined. This was then applied to the outer perimeter points so that all sites and repeated time points could be

compared. As there is no reference geometry for the tibia model, the accuracy of the pQCT can-not be tested this way, however, the repeatability of the scanner can.

The theory of statistical shape analyses determines a shape to be the geometrical information that remains unchanged after the removal of location, scalar or rotational affects (Dryden and Mardia 2016). In order to reliably identify shape, literature has described the use of landmarks around the bodies boundary (Zhang and Golland 2016). So, in order to compare the outer geometry of the shape and determine any changes, the mathematical landmarks derived using the same method as described in section 3.3 within this chapter was used. Once the landmarks for each scan have been determined the average x and average y coordinate and the standard deviation across the scans was determined. From this the coefficient of variation can be determined for each landmark. The coefficient of variation was less than 1% at the majority of the threshold coordinates.

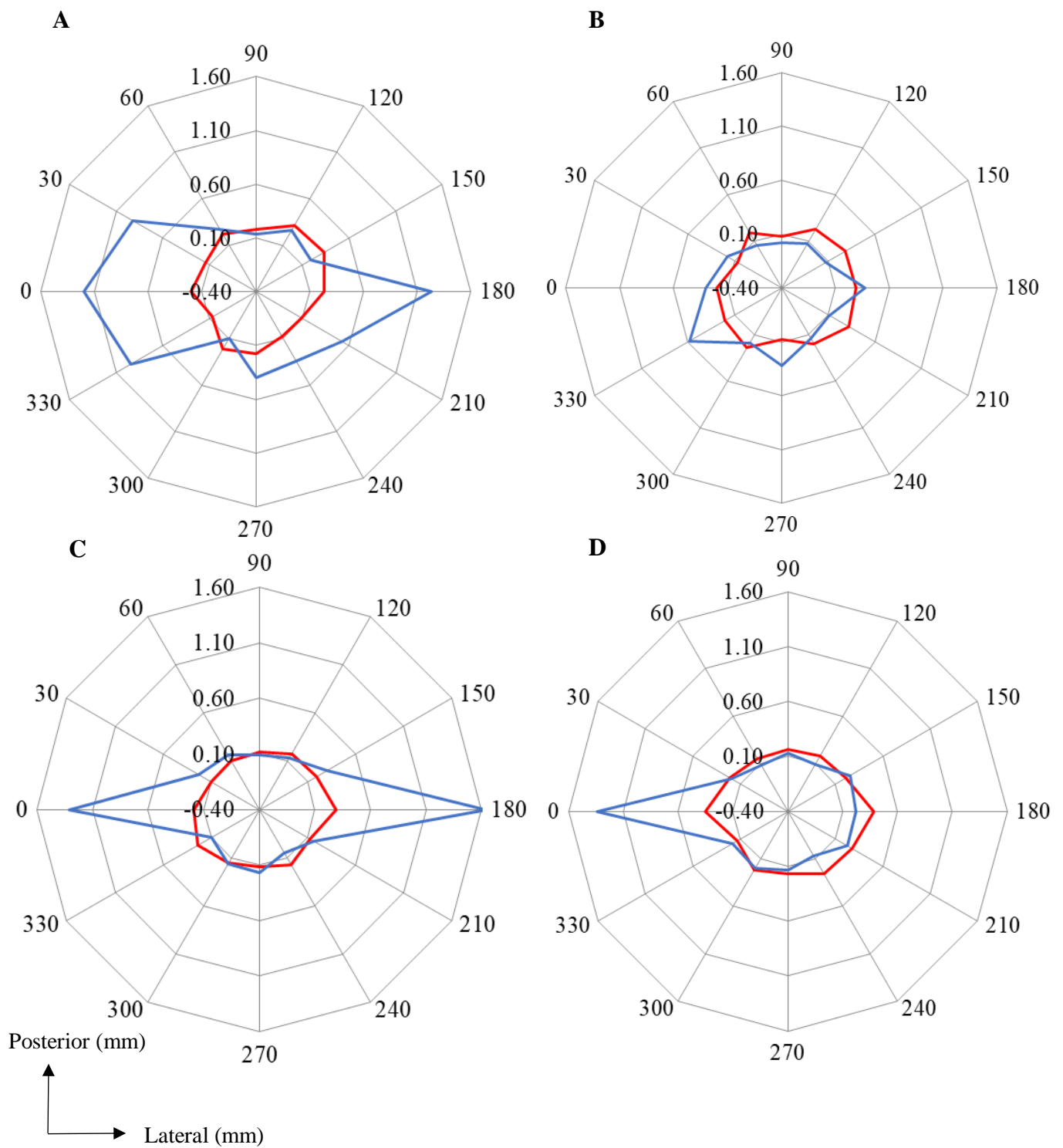


**Figure 47: The coefficient of variation in the x (red line) and y (blue line) coordinates of each landmark around the perimeter of the tibia. A is 4%, B is 14%, C is 38% and D is 66%.**

It cannot be determined how this would change the internal values of cortical/trabecular bone, due to the error in identification from the pQCT. So, to give this data physiological perspective the maximum medial/lateral (M/L) and anterior/posterior (A/P) diameter was used. The medial/lateral diameter shows most variation, with a coefficient of variation of 1.3% at the 14% site. The least variation is shown in the anterior/posterior with no change in the A/P diameter across repeated scans at the 38% site. As can be seen from Figure 47 the position of maximum M/L and A/P diameters changes between scans. There is a maximum of 15mm translation in the y coordinates for the medial/lateral direction at the 4% site.

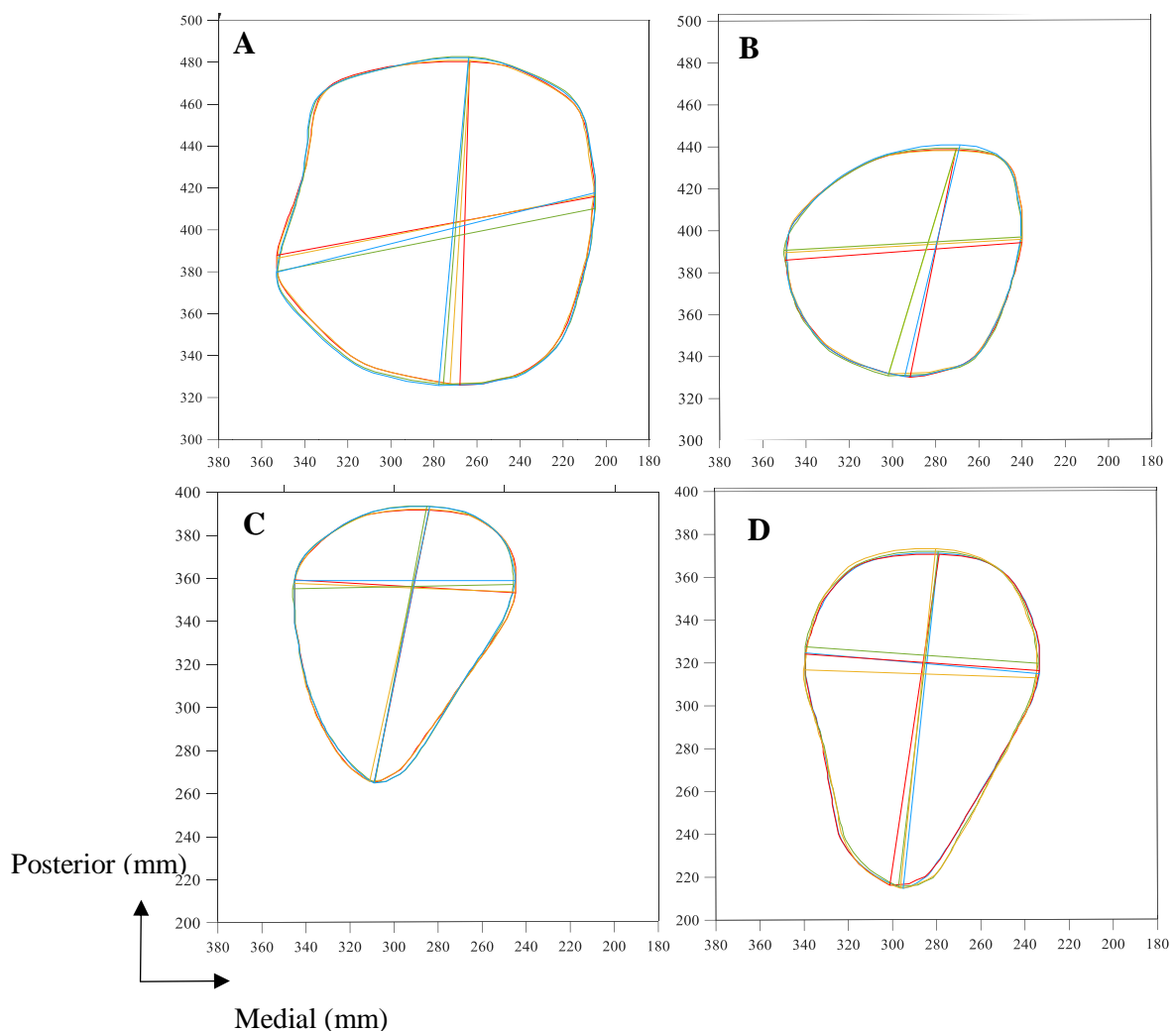


**Figure 48: The outer perimeter of the model tibia at the 4% (A), 14%(B); 38%(C) and 66% (D) sites. Red lines correspond to the first scan, yellow, scan2, green scan 3 and blue scan 4.**

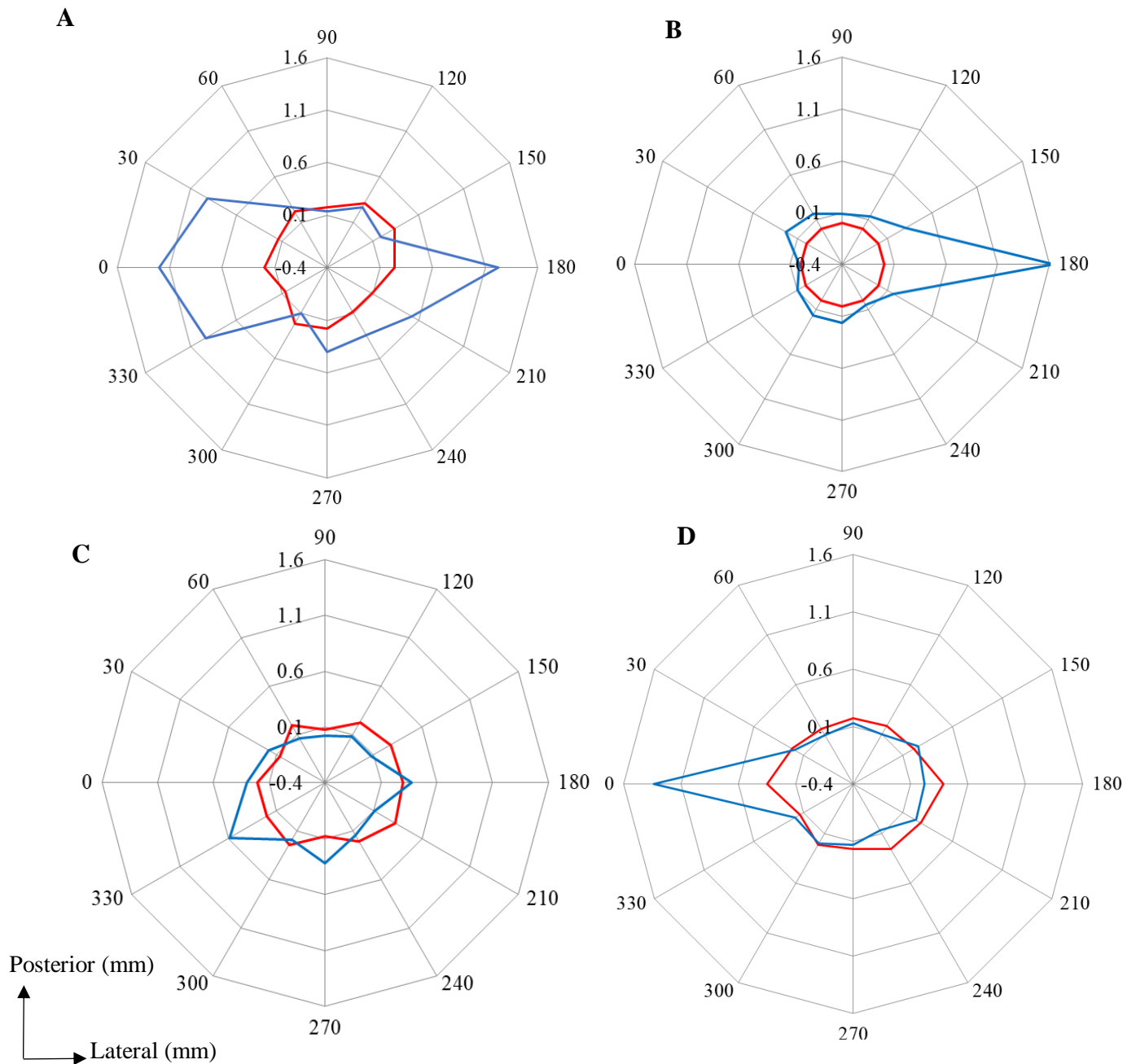


**Figure 49: The coefficient of variation of in the x (red) and y(blue) of the landmark coordinates around the perimeter of the tibia for each scan site 4% (A), 14%(B), 38%(C) and 66%(D).**

As with the cylinder the largest variation is in the y coordinate of the landmark, for physiological relevance this is the M/L in this orientation. The A/P direction is the x coordinate and show least change. The larger variations are seen at the most medial part of the tibia, or 0° in the diagram.

#### 4.4.3 Morphing of the base finite element model of the tibia

The outer coordinates generated from the image processing code were written into a text file, with the base model x, y, z coordinates for each of the landmarks listed first, followed by the x, y, z coordinates for the participant model. The origin of the image within MATLAB (Statistics Toolbox Release 2017a/2017b, The MathWorks, Inc., Natick, Massachusetts, United States) is at the bottom left of the image, where the origin in the Avizo software, is the bottom right of the image. Therefore, in generation of the coordinates of the landmarks the x coordinate generated by the MATLAB (Statistics Toolbox Release 2017a/2017b, The MathWorks, Inc., Natick, Massachusetts, United States) code was subtracted from the total length of the image (51.2 mm). The text file was then opened and the landmarks displayed, see Figure 50.

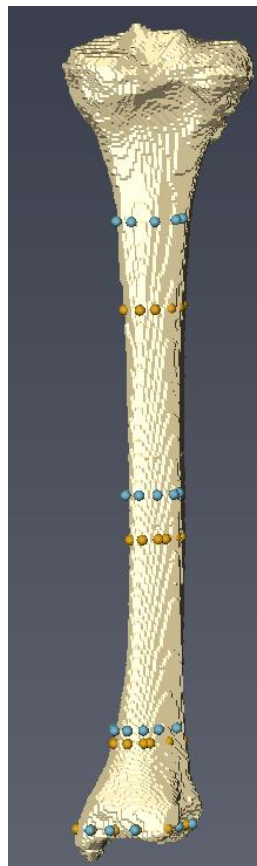


**Figure 50: Landmarks on the base tibia model. Yellow represents the landmarks generated from the base model and blue are those generated from participant data.**

The x and y coordinates were generated from the image processing code (section 3.3) and the z coordinate was generated from the total bone length and entered into a text file. Within the image processing software, Avizo, the x,y and z coordinates from the subject specific pQCT data was converted into landmarks.

The volume of the 3D model was then warped so that the surface of the base model was matched to the landmarks from the pQCT. As can be seen in Figure 51, this then generates a semi-subject specific finite element which is concurrent to the participant's tibia length and geometry at the four pQCT sites.

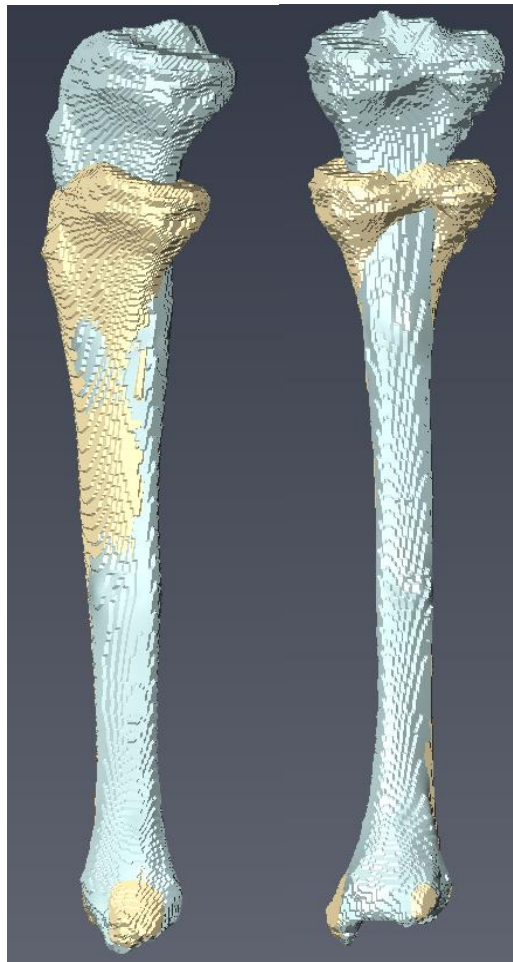


**Figure 51: Morphed model in the medial lateral and anterior posterior positions. Base surface model is presented in yellow and the semi-subject specific morphed model is presented in blue.**

#### 4.4.4 Subject-specific model generation

Once the surface of the base model had been morphed to the subject specific pQCT data, the semi-subject specific model was meshed. Similarly, to the base model, the number of faces was reduced using the ‘*simply faces*’ function (see section 4.4) within the simplification editor, each model was reduced to have 100,000 faces. The model was then smoothed using the ‘*surface transforms*’ function. The surface was edited to reduced tetra quality (ratio of the circumference and radius of the sphere within the triangle) and aspect ratio (the ratio between the circumcircle and the incircle within the triangular element), with the largest being 15 and 18 respectively, across all models.

In order to generate a mesh for the entire volume, the ‘*generate tetra grid*’ function was used. This function uses the surface model and fills the volume with tetrahedral elements. The .grid file is exported as an .unv file. The file ‘*unv. ansys*’ is used to convert the .unv file to be compatible with engineering simulation software (e.g. ANSYS).

#### 4.4.5 Model material properties

The material properties were assigned to each material within the pre-processor. For both the cortical and trabecular area’s materials were defined as linear, elastic and isotropic. In accordance with previous literature the materials were assigned the following properties.

**Table 14: Material properties for trabecular and cortical bone based on literature (Lai et al. 2015)**

	Elastic modulus	Poisson’s ratio
Trabecular bone	17 GPa	0.3
Cortical bone	350 MPa	0.25

## 4.5 Discussion

The first objective of this study was to establish an image processing method, which extracted tibial outer geometry coordinates. The pQCT scanner processes the bone scan but only analyses internal geometry *e.g.* cross sectional and cortical area. The novel image processing method developed within this thesis successfully identified the external geometry of a tibia, with coordinates generated at 30° segments around the perimeter. Previous literature has developed image processing methods, specifically the Bone Alignment and Measurement Package (BAMpack) software by Evans et al. (2007). The BAMpack software has been used to assess differences in geometry including cross sectional diameter between sexes (Evans et al. 2008) as well as used to assess the effect of exercise intervention protocols on cross sectional diameters (Evans et al. 2012). There has, however, been no publications to date that quantify the outer geometry plots for analyses, using BAMpack or any other image processing methods. Validation of the BAMpack software has stated a CV of less than 1% for trabecular and cortical density (Izard et al. 2016a), although the steps to achieve this CV remains an unpublished source. It is also not documented if BAMpack identifies a reference point for outer geometry *e.g.* a bone centre. This means replicated analyses by other researchers is difficult and repeated analyses of time points in an individual using BAMpack rely on the exact repeat placement of the individual within the scanner. Whilst the BAMpack software, has been used extensively for physiological assessment, due to its unavailability as an open source tool, these physiological assessments have been limited to the BAMpack author's research group. This provides an opportunity for the image processing method developed within this thesis to be further refined and made open to other researchers. Not only does this give opportunity for further analyses of bone, but, provides an accurate and reliable method that can be compared across studies.

The second objective was to construct a semi-subject specific FEM from the pQCT images and the base model tibia. The image processing method was successful for extracting a set of landmarks, at 30° sections which were used to morph a base model. This was justified on previous research that suggested that regional changes occur within the bone (Cheng et al. 2002). Previous research used the BAMpack software and sectioned the bone into sixty-degree sections. Increasing the number of sections for analyses using the image processing method developed in this chapter allows for increased specificity of bone analyses as well as providing enough information for morphing without becoming too computationally intensive.

Previous literature that has used pQCT scans to create FEM did so through interpolation (Mittag et al.,2017). Mittag et al. (2017) took pQCT scans of a cadaveric tibia at 1cm intervals. The image processing method then manually identified key reference points; centre point of the bone, the interpolation radius and radial lines. The greyscale values along this radial line were plotted for each slice and the values between two slices were interpolated to create a full data set. The conclusion of the Mittag et al. (2017) study produced a tibia model that was geometrically very accurate within the diaphysis region and although less accurate in the epiphyseal region, the method was successful in producing a FEM suitable for analyses. However, the method of manually identifying reference points reduces the repeatability and reliability of their method thus reducing its validity in producing a geometrically accurate bone. This study, was also conducted on an *in vitro* specimen with bone image scans taken every 1-2cm culminating in a higher number of images. If this was *in vivo*, the increased amount of radiation, additional to background radiation that the participant would be exposed to would not be ethically permissible. The benefit of only using four images, as in clinical pQCT, is the participant is exposed to reduced radiation. Further analyses is needed into the number of bone image scans from a pQCT is needed to generate

an accurate FEM and if the location associated with clinical assessment is the most anatomically appropriate for the development of a FEM.

To create a semi-subject specific finite element model a landmark based morphing technique was chosen. The other option for creating a semi-subject specific FEMs was mesh morphing (Sigal, et al., 2008; Caouette et al. 2015). Automatic mesh morphing as carried out by Sigal et al. uses a common surface of which both the source geometry and target geometry were morphed to. Once morphed the difference in their locations were calculated and a function was calculated for subject-specific morphing. The process of using landmarks, as in this study, was compared to automatic meshing by Sigal et al. (2015). Sigal et al. (2015) showed that automatic meshing provided a surface that was more accurate to the anatomy, however, the manual landmarks guaranteed correspondence between the two surfaces. The absolute differences between the morphed surface and the target natural surface was shown to be 32 $\mu$ m for the manual method compared to 18 $\mu$ m for the automated method. This relates to very small differences in strain and stress output, proving that the use of manual landmarks is viable for morphing finite element models. Also, automatic meshing, as described in Sigal et al. (2015) requires full bone geometry as well as a target model. In studies where this isn't possible, landmarks provide an advantageous solution and able the development of a semi-subject specific models.

The third objective was the validation and evaluation of the image processing method. This was assessed through reliability by repeating the scans to assess the consistency of the results and accuracy, by comparing the generated results to that of known geometry. The image processing method identified the outer geometry of a uniform object within a coefficient of variation of 0.57%,  $\sim$  0.9mm. For a non-uniform object the image processing method produced outer geometry coordinates within 1.6% of variation. Confirming the image

processing method is accurate and reliable at identifying outer tibial geometry. Previous research investigating the precision of pQCT in comparison to micro computed tomography ( $\mu$ CT) recorded CV in cross sectional area of 1.1% *in vitro* and up to 4.8% *in vivo* for mouse long bones (Schmidt et al. 2013). Similar values have been reported for density measurements at the human tibia of 3.2% (Groll et al. 1999). The reliability of the pQCT used by Groll et al. (1999) was assessed by taking three repeated measures taken days apart and did not take into consideration direct repeatability, as in clinical studies, participants do not have directly repeated scans. Another way to investigate the reliability in pQCT is through the comparison of studies that have reported the geometrical changes in the tibia. Intervention studies, across a 13 week period have reported no changes within some participant groups and others only displaying changes up to 1mm (Izard et al. 2016b). In another 12 week study in young footballers who maintained their active training, cross sectional area was shown to increase by a maximum of 10mm, although this was concluded as not statistically significant (Varley et al. 2019). The cortical cross sectional area was seen to significantly increase by 3mm at the 14 % site and by 5mm at the 38%. (Varley et al. 2019). Longitudinal studies investigating changes in bone structure over 20 months for a group of maturing children reported changes of up to 73% in some cohorts. (Macdonald et al. 2005). Although, within an actively growing population such as children and young adolescence, such as that in the Macdonald et al. (2005) and Varley et al.(2019) studies, you expect there to be changes in bone parameters. However, without validation studies, the data reported here cannot be assumed to be void of imaging error. Where validation of study methods to assess method error is not imperative and in cohorts where a variation larger than previously reported pQCT error is seen, it could be argued against. However, validation assures the studies reliability and accuracy of study results. This is especially important in cohorts where change is minimal, or very sensitive, knowing any image processing method associated errors is imperative for confidence in results.

#### **4.6 Limitations and Future directions**

The base tibia finite element model was based on the visible human project data. The female data set was used to generate this base model due to its high image quality. However, the participants within this study were male and therefore it is likely that the base geometry would be significantly different (Sherk et al. 2012). Further studies should be conducted using the same participant pQCT scans using two geometrical different base FEMs to identify how much the base model contributes to the geometry post morphing.

In setting up pQCT scanners, a calibration is carried out prior to scanning. However, the Stratec machine, which is commonly used in laboratory studies, doesn't employ a quantifiable calibration. Instead this is a coloured band system from dark red to green to light green. The lightest green determines a 'good' calibration, which manufacturers specify is within the 0.05mm tolerance. Published data does not divulge the value of the calibration so it is unknown if there is an error associated prior to scanning which could contribute to this. The results from the image processing will include any error associated with the calibration of the pQCT. The pQCT was not calibrated between directed re-tests but was between the tests a week apart, therefore there could be some error introduced from the calibration. However this will be less than the 0.05mm which is less than 0.03% of error. Although this seems small, when applying this to a biological structure, this variation would affect the significance of changes that have been reported in literature (Evans et al. 2012). Future development of the image processing code could also introduce a method of quantifying the calibration of the pQCT in order to incorporate the error into the image processing method.

The scans used to generate a semi-subject specific model were chosen based on the pQCT use within a clinical environment. This did not take into consideration sites within the bone

that have most anatomical subject specificity that would prove more informative to the finite element model. Further to this, previous studies have used an increased number of pQCT scans to build a subject specific model. Future research could investigate how sensitive the model is to the number of pQCT scans used to morph the model.

#### **4.7 Conclusion**

The novel image processing code developed in this chapter provides an accurate and repeatable method to extend the analysis on bone using a pQCT scanner. The identification of the outer geometry extracted from these pQCT scans provides an original contribution to literature. This process has enabled the successful construction of a semi-subject finite element model without the need for interpolation or high radiation exposure, making FEM more time efficient and easier to produce, without the risk to patient's health. The novel process determined and validated above can now be taken forward and subject specific data can be applied to physiologically validate the model in predicting bone strains.

# 5 STUDY TWO: VALIDATION AND EVALUATION OF A SEMI-SUBJECT SPECIFIC FINITE ELEMENT MODEL OF THE TIBIA

## 5.1 Introduction

Having developed a semi-subject specific FEM in the previous chapter, this chapter builds on the theory of finite element analysis (FEA) to evaluate and validate this method as a predictive tool. When these FEM of bones are loaded with forces each tetrahedral element deforms and results in a strain. For biological structures, such as bone, this strain can predict responses without invasive measures *e.g.* surgically implanted strain gauges. The ability of an FEM to predict a physiologically representative output relies on the anatomical and physiology accuracy of the model specifically material properties, geometry and loading, for further information see Chapter Two.

The experimental validation for FEM involves the replication of the finite element simulation environment on a biological specimen and comparing the results. Strain gauges have been used to measure strain in long bones within cadaveric and animal specimens (Lieberman et al. 2004; Gray et al. 2008; Taddei et al. 2006; Fung et al. 2017). The application of strain gauges to cadaveric tibia specimens is difficult, especially in the metaphysis, as the cortical bone is thin (Gray et al. 2008). It has also been reported that in those areas where there is high geometrical variation or irregularities, there is an increased risk of error in the measured strain output (Schileo et al. 2008; Taddei et al. 2006). The extent to which FEM's can be replicated *in vivo* is limited, so other validation and evaluation processes must be considered.

Where the entire simulation cannot be replicated, individual aspects of the model can be validated directly from the subject the model was generated from. Material properties, including Young's Modulus and Poisons ratio can be obtained directly from the original bone specimen the through nano-indentation and ultra-sonic methods (Zhang et al. 2008; Pithioux et al. 2002). Due to the invasiveness associated with the preparation and implementation of these processes, the values associated with the FEM can't always be validated using the bone specimen the FEM is modelled on. Instead, an informed assumption of these values has been established; Poisons ratio of 0.3 for cortical bone and 0.25 for trabecular bone and a Young's Modulus for trabecular and cortical bone within the range of 6 to 27.6GPa (Murphy et al. 2016; Niu et al. 2013; Wirtz et al. 2000). The Young's Modulus of bone gives it its anisotropic property, *i.e.* the bone behaviour changes dependent upon the load directions. Finite element models, which are isotropic, have only one set of mechanical elastic properties; Young's Modulus and a poisons ratio. Assigning anisotropy increases these properties to nine independent components; including three Young moduli, three shear moduli and three Poisson ratios (Vignoli and Kenedi 2016). The information for these properties comes from Computed Tomography (CT) data from the patient, which cannot always be provided (Kazembakhshi and Luo 2014).

Material composition is another property that is a determinate of output accuracy. Bone is considered a non-homogenous, or heterogeneous material, as evident from the varying density across the bone seen from CT scans. Studies comparing non-homogenous and homogenous FEM showed the former to be more accurate than the latter (Fung et al. 2017). However, the models ability to predict the measured strain has been reported to be similar with R<sup>2</sup> values of 0.91 and 0.89 for non-homogenous and homogenous models respectively (Taddei et al. 2006). The increased computational power that is associated with non-

homogeneity has resulted in researchers still using homogeneity to create simplified FEM (Kaze et al. 2017).

Validation of FEM can also be conducted through the analyses of the model properties *e.g.* mesh (the network of elements across the model). Burkhart et al. (2013) reports that over 90% of published literature does not present details of the models mesh, including convergence. Burkhart et al. (2013) also suggests verification through the assurance that the model adheres to the basic physical laws, through the reporting using energy balance equations. Although, this provides a stronger case for validation, researchers report adherence to basic laws through the presentation of constraints. Constraints within a model are implemented to limit the degrees of freedom within the model and prevent un-natural movement. This ensures model validity without extra time spent on the mathematical computational of energy balance.

When using semi-subject specific finite element models, such as that developed in Study One (Chapter Four), the model is derived from two, or more geometrical sources, therefore experimental validation using cadavers is not possible. Erdemir et al. (2012) suggests using experimental data where possible, but otherwise to use validated published literature as a comparison. However, due to differing modelling constraints, boundary conditions and load application, this may not be an accurate method of validation. Where experimental data can be used is by using bone remodelling and modelling theory. It is widely agreed that strain, or lack of, directly influences bone modelling and remodelling and subsequently the deposition and resorption of bone, affecting bone geometry. Therefore, the longitudinal changes in bone geometry can be used to infer location and magnitude of strain, which when compared to a semi-subject specific FEM can provide a non-invasive method of experimental validation.

The first objective of this study was to optimise the model developed in Study One by determining and applying physiologically accurate loading conditions generated from data produced in Study Three. The second objective of the study was to validate the FEM strain output against published experimental data. The third objective was to validate the strain values alongside longitudinal experimental data generated from Study Three.

## **5.2 Methods**

In order to produce a strain plot, the model has to be loaded. The FEM for each participant, generated in Chapter Four were used and loaded with experimental data generated in Chapter Six.

### **5.2.1 Musculoskeletal modelling**

Muscle forces are one of the main contributors to mechanical loading of the bones, so it is important to include them when studying the transmission of loads across bones (Lu et al. 1997). Electromyography (EMG) provides a tool that records muscle activation, although some developments have inferred a relationship, EMG does not provide data on the muscle force (Kuriki, et al. 2012). Estimations of muscle force can be achieved by using computational replicas of the experimental system through musculoskeletal modelling. Musculoskeletal models are referred to as rigid systems due to their representations of bones as rigid bodies. Muscle actuators are modelled using one dimensional lines of action, with intermediate points. (Dao 2017). There are a number of musculoskeletal modelling software, AnyBody modelling system, OpenSim and Biomechanics of Bodied (BOB), all which have been reviewed within literature (Langholz et al. 2016; Trinler et al. 2017; Dao 2017). All were developed based on the geometry of cadaver data and are all used widely within literature (Horsman et al. 2007).

### **5.2.1.1 OpenSim model**

For this thesis OpenSim (version 3.3), gait model 2392 was used. As OpenSim is an open source software the model has been validated in previous research. The gait 2392 model is one of the three dimensional, 23 degrees of freedom models. (Delp et al. 2007). Gait 2392 includes 92 musculotendon actuators that model the 76 muscles within the torso and lower limbs. The model is default scaled to represent an average subject at 1.8m tall with a mass of 75.16kg. The anatomy of the lower limb musculoskeletal model was taken from a dataset published by Klein Horsman et al. (2007), implemented into OpenSim by Delp et al. (2007). The muscles are represented by line segments with insertion and origin points mapped onto the bone using anatomical landmarks

### **5.2.1.2 OpenSim Bone definitions**

The gait 2392 model is anthropometrically defined based on the digitisation of bones collected in cadaver studies (Delp et al., 1990, Stredney et al., 1982, Anderson and Pandy, 1999). The lower limbs of the model include seven segments; the pelvis, femur, knee, shank, ankle, foot and toes. The hip joint is modelled as a ball and socket joint. The knee, first modelled by Yamaguchi and Zajac (1989) as a simple single planar knee model, was developed by Delp et al., (1990). The Delp model defined the translation between the femur, tibia and patella as a function of the knee angle, specifying that the femoral condyles

represented as ellipses) remain in contact with the tibial plateau (represented as a line) throughout the knee motion.

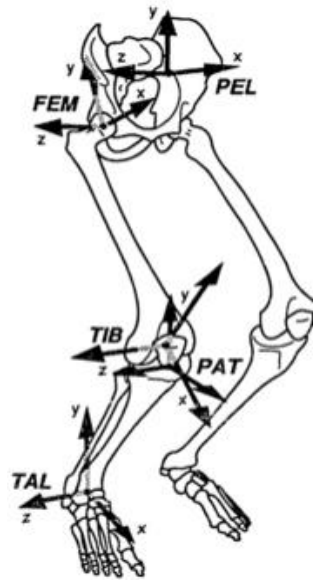


**Figure 52: The seven segment, lower extremity model developed by Delp et al (1990) taken from OpenSim documentation.**

**Table 15: Definitions of the location of the reference frame for each segment of the model.**

**Adapted from the OpenSim documentation**

Segment	Reference frame definition
Pelvis	Midpoint of the anterior iliac spines
Femur	Centre of femoral head
Knee	Distal most point of the patella
Shank	Midpoint between medial and lateral condyles
Ankle	On the talus at the midpoint between medial and lateral malleoli
Foot	On the calcaneus, most posterior, lateral point
Toes	At the base of the second metatarsal



**Figure 53: The gait2392 model taken directly from OpenSim**

### **5.2.1.3 OpenSim Muscle definitions**

Each muscle is represented by a line segment from the point of origin to insertion. The origin and insertion site location were identified through notches in the bone identified through cadaveric studies (Wickiewicz et al. 1983; Rajagopal et al. 2015). The muscle pennation angles and fibre lengths were then taken from Wickiewicz *et al.*, (1983). Lumbar muscles were defined by Anderson and Pandy (1999) due to the strength output being more physiologically representative. Intermediate or ‘via’ points were also used, these attach the muscle to other points along the bone to map the muscles action path. In some instances, a wrapping point was also used, which when the joint angle is large, prevents the muscle from seemingly going through the bone. OpenSim states three actuators which, despite the preventative measures, do go through the bone, the Gluteus Maximus at its most interior, superior and middle components when the hip flexion exceeds 60 °and 80° respectively. The muscles that were of interest in this thesis were those that had origin or insertion sites on the tibia.

The attachment sites of these muscles were determined on the model within the software, AVIZO. The position of the insertion and/or origin of the muscles on the tibia were modelled using landmarks. The positioning of the muscle attachment sites was placed on each model using reference from the OpenSim model and Sobotta Atlas (2006).

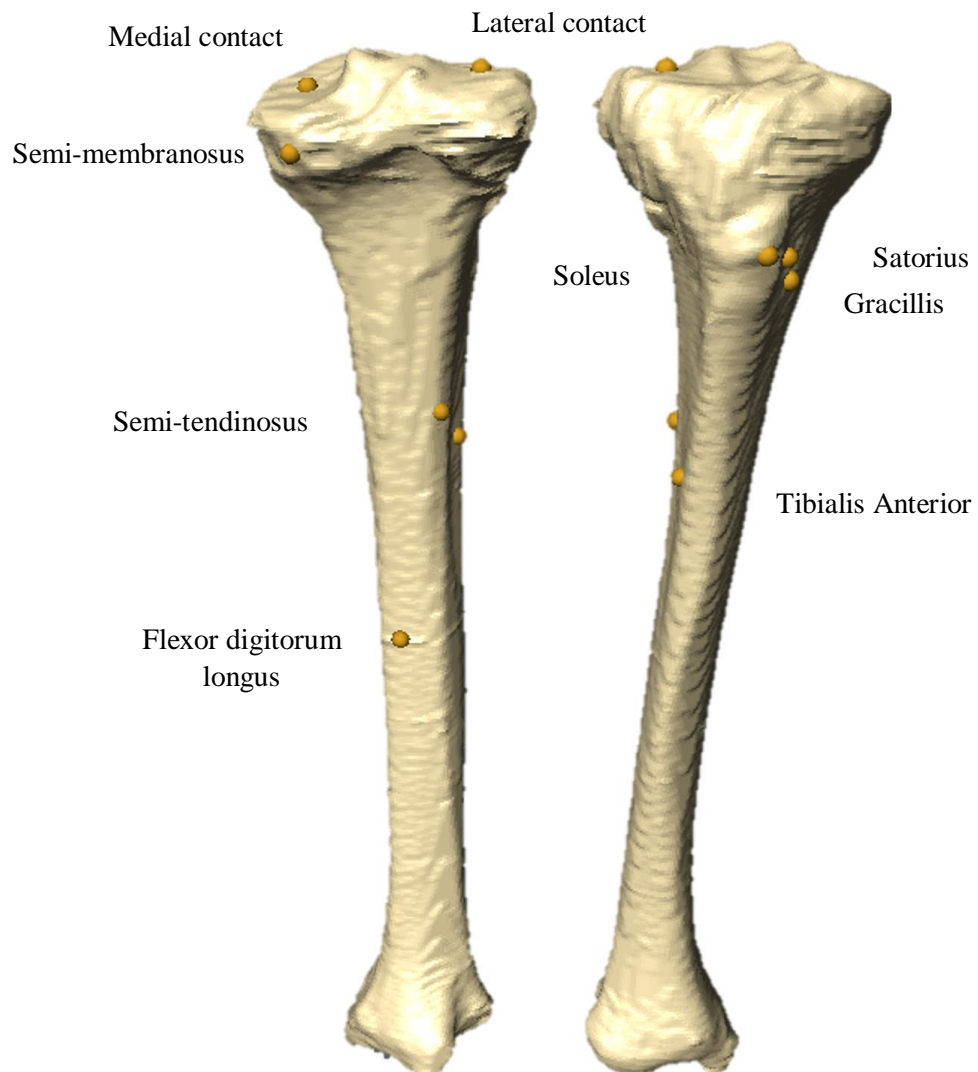


**Figure 54: Semi-subject specific participant model with muscle attachment sites represented as landmarks. The semitendinosus, gracillis and Sartorius and tibialis anterior can be seen on the anterior view. The flexor digitorum longus, soleus, tibialis anterior and semimembranosus can be identified on the posterior view. The joint reaction force application landmarks (Medial and lateral contact) can also be seen on the medial and lateral condyles.**

### 5.2.2 Muscle force output

The input for musculoskeletal modelling is dynamic movement, in the form of a motion file recorded using 3D motion capture. The data used to drive these simulations is that collected in Chapter Six. In order to make the dynamic movement files (in c3D format) compatible with OpenSim, the model had to fulfil specific requirements. This included altering the segment coordinate system so as the anterior/posterior axis was negative Y and the distal/proximal axis was set to negative Z. The participant also had to be facing and walking in the positive Y direction in both the static and dynamic files. In order to account for this a virtual lab segment was created, with a positive Y in the anterior direction, a positive Z in the vertical direction and positive X to the right. The c3D file can then be exported as a .mot (motion) file, which is compatible with OpenSim software. When exporting the files, the frames where only the right foot is in contact with the ground are exported. The files referred to in the following were downloaded as part of the Visual3D to OpenSim integration.

#### *Scaling*

When exporting the c3D file into a .mot file, the scaling information from the motion capture data was saved within the scale file, '*Visual3d\_Setup\_Scale.xml*'. This file saved the scaling factors calculated from the static file and the information within the '*gait2392 simbody.osim*' file. Specifically, the pelvis was scaled based on the distance between the hip joint centres \* 0.167 rather than based on the left and right ASIS, as the latter is not required for scaling within the biomechanics analysis tool, visual 3D , thus overcoming this potential problem. The thigh was 0.396 \* distance between hip and knee joint centres, the shank was 0.43\* distance between the knee and ankle joint centres, both these constants are based on the data within the '*gait 2392 simbody.osim*' file. The height was scaled based on the thigh length, which in accordance to anthropometry, is 0.245 \*height of the participant (Winter et al. 2009).

### ***Inverse Kinematics***

When the scale file was generated, the next step was to match the marker locations from the movement file within the static pose. The inverse kinematics tool implemented within Opensim analyses each step of the movement file and computes the coordinate values which best match the experimental marker coordinates for the same static pose. This was calculated using a least squares method with the aim to minimize any errors associated with marker or coordinate errors (Boyd and Vandenberghe 2009). There are two mathematical theorems implemented within Visual 3D for pose estimation, the six DOF method adapted from Spoor & Veldpaus (1980) and inverse kinematic method developed from Lu and O'Connor (1999). The inverse kinematic method for pose estimation within visual 3D is similar to that used within OpenSim, in that it uses a least squares regression equation with segment specific weightings to correct for any marker movement due to soft tissue artefact (Lu and O'Connor 1999). When applying the inverse kinematic method each segments movement and orientation is measured using the local and global coordinate systems. Then to reduce soft tissue artefacts and measurement errors, joint constraints which are consistent with that of the gait 2392 OpenSim model definitions are applied to the model which create a more physiologically accurate movement. These constraints are; the hips were defined with a 3DOF ball joint, the knee is defined as a hinge joint as a function of knee joint angle and the ankle and subtalar joints are hinge joints. The metatarsophalangeal joints are fixed and set at zero throughout the movement. Once in OpenSim the gait 2392 simbody model was opened and the scale file was applied to the model, with the only manual specification being the participants mass.

### ***Residual Reduction Algorithm (RRA)***

The next step was the application of a residual reduction algorithm. Residual forces and moments are applied to computer models to maintain dynamic stability and are defined using Newton's 2<sup>nd</sup> law, see equation below (Anderson et al. 2006)

$$\bar{F}_{exp} + \bar{F}_{residual} = \sum_{i=1}^{segments} m_i (a_i - \bar{g})$$

Where  $F_{exp}$  and  $F_{residual}$  are the expected and residual forces with  $m_i$  and  $a_i$  being mass and acceleration of body segment  $I$  due to gravity. The residuals are computed for every 0.1 seconds of movement, calculating what actuator forces are needed to move the model forward each step and into the configuration generated by the inverse kinematics. The actuators are calculated based on minimizing a function, specifically the acceleration errors, thus the resulting kinematics are slightly altered compared to the original. At the end of the simulation the average residuals are calculated. The torso is adjusted based on the results of the x and z moments to account for any inaccuracies in the distribution of mass or geometry. The aim is to have these residuals as small as possible, to maintain the desired kinematics, with recommended maximum forces being below 25N and maximum moments being below 75Nm (Delp et al. 2007)

### ***Computed Muscle Control (CMC)***

The next stage is to compute the muscle excitation that is needed to drive the model in accordance to the desired kinematics. To calculate these accelerations the anatomical joint (excluding the pelvis, as this is related to foot-floor contact) accelerations, velocities and positions as well as the ground reaction forces are fed into the system. A set of tracking errors are applied that minimise any errors to zero. These tracking errors are reduced, as part

of a feedback loop, through a set of feedback gains;  $k_v$  (velocity feedback gain) and  $k_p$  (positional feedback gain). To reduce any tracking errors,  $k_v$  and  $k_p$  were set to  $20\text{m}\cdot\text{s}^{-1}$  and  $100\text{m}$  respectively (Thelen and Anderson 2006).

After this the actuator controls are calculated through the static optimisation, producing the desired muscle forces. These can then be fed into the forward dynamics to obtain the desired kinematics. This is calculated for every 0.010 seconds of the movement as this allows the muscles to change whilst still being under control. A schematic representation of this can be found in Figure 55.

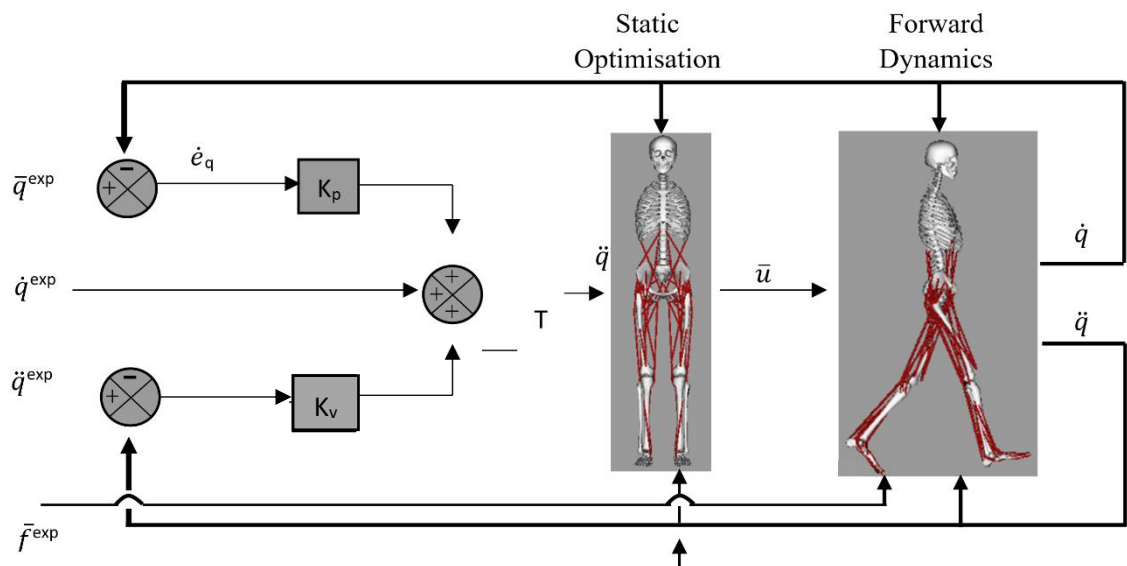


**Figure 55: A schematic of the feedback loop that is used to compute muscle control based on (Thelen and Anderson 2006) The first half details the PD control law with inputs being joint accelerations;  $\ddot{q}^{\text{exp}}$ , joint velocities;  $\dot{q}^{\text{exp}}$ , and joint positions;  $\bar{q}^{\text{exp}}$  with tracking errors  $\dot{e}_q$  and  $\ddot{e}_q$ .  $K_v$  and  $K_p$  are the feedback gains. Muscle excitations, represented by  $\bar{u}$  are calculated through the input of expected muscle forces  $\bar{f}^{\text{exp}}$  into the static optimisation.**

### *Muscle forces*

The gait 2392 model was used as a base model for the semi-subject specific musculoskeletal model. Only one c3d file was used to influence the musculoskeletal model, which was

determined from participant's biomechanics data from Study 3. The vertical ground reaction profiles were compared for all visits and the visit with the lowest RMS, compared to the average, was taken forward. The trials within this visit were averaged and the process repeated until one trial was chosen.

This c3d file was exported and processed in OpenSim as described in the general methods section. After the RRA and CMC were conducted, the muscle forces were calculated. The right knee joint reaction forces (JRF) were generated from visual 3d to account for the entirety of stance phase, rather than just between toe off and heel strike of the left leg. The maximum joint reaction force (JRF) was taken and the time and the percentage of stance phase were noted down.

The resultant muscle forces were calculated from the CMC, in order to determine their x, y, z and z components to apply to the finite element model, the origin and insertion coordinates were needed. These were generated using the 'MuscleForceDirection' plugin (Van Arkel et al. 2013). For each of the muscles, an excel spreadsheet was constructed to calculate the components of the force. The following details the calculations that were used to determine the resultant muscle force.

The length of the muscle path in each x, y and z is defined as

$$\textit{Length} = \textit{the insertion location} - \textit{The origin location}$$

The resultant of the length is calculated as

$$\textit{Resultant length} = \sqrt{\textit{Length}_x^2 + \textit{Length}_y^2 + \textit{Length}_z^2}$$

The resultant load is divided by the length in each direction to give a value of each component as a portion of the resultant. So, for x,

$$Lengthcomponent_x = Resultant\ length / Length_x$$

To then calculate the force component for each x, y and z as a ratio, the x component

$$Force_x = Lengthcomponent_x * Muscle\ Force$$

This is repeated for each of the muscles on the tibia. The location of the muscle on the bone along with the force was then input into a text file. Below is the breakdown of the text.

	Muscle name		X component of force
Location	<span style="color: magenta;">!Tibalis Anterior</span> <span style="color: cyan;">F,NODE(-28.695, -18.1455,-37.4251),FX,-19.8403</span> <span style="color: cyan;">F,NODE(-28.695, -18.1455,-37.4251),FY,560.9459</span> <span style="color: cyan;">F,NODE(-28.695, -18.1455,-37.4251),FZ,-134.171</span>		Y component of force
			Z component of force

### **5.2.3 Finite element model**

As a method of validation, the following section provides details on the loading and constraints placed on the finite element model, to adhere with the physiological range of motion associated with each joint. For further FEM properties, please see Study One (Chapter Four).

#### ***Model properties***

Previous studies have discussed using the mesh techniques as a validation process, by reporting the model's mesh characteristics i.e. the elements and nodes, more accurate comparisons can be made. In mesh generation, an edge length of 1.5mm was assigned, this is in agreement with Harrigan et al., (1988) who recommend an element size of between 1-2mm in order to maintain the continuum assumption, i.e. that the stress and strain response will be fluid across the model. All aspect ratios were below fifteen and for two participants this was improved to be below ten. Although it has been reported that aspect ratios of less than four produce the least errors (Tsukerman et al., 1998). The achievement of such low aspect ratio can become quite difficult, so other authors have instead ensured that the percentage of elements of higher than an aspect ratio of 4 does not exceed 5% (Burkhart et al. 2013). The other reported measure is angle within the tetrahedral elements, this is defined through the tetra quality property of the mesh. For all participant models, the tetra quality was less than 15 (see Chapter 4, Section 4.4). It is advised that the angles should be between 30 and 150 degrees (Burkhart, et al. 2013).

The elements were first order tetrahedral elements, which have been used in a number of experimental and validation studies (Ulrich et al. 1998; Niu et al. 2013; Zysset, et al. 2013). It has been suggested that for more complex models, second order tetrahedral elements are better suited for large variation in stress contours (Perillo-Marcone, et al. 2003). These

properties are reported on the guidelines of other validation publications (Anderson et al. 2008; Burkhart, et al. 2013; Erdemir et al. 2007).

### ***Loading and constraints***

In order to determine the contact forces across the knee as accurately as possible, previous research has used instrumented prosthetics, contact pressure maps, dynamic stereoradiography and MRI (Carey et al. 2014; Varadarajan et al. 2008; Zhao et al. 2007; DeFrate et al. 2004). However, these methods occur a high cost and/or exposes the participant to high amounts of radiation and invasive surgeries. The specifics of the knee contact are individual and very much dependant on the degree of flexion that the knee is under. To control for this studies have summed these forces to one in a resultant force, or used one contact point as a simplification technique (Kutzner et al. 2010; Wretenberg, et al. 2002). Therefore, landmarks were placed on the medial and lateral condyles to act as a position reference for joint loads. These landmarks were placed at 25% of the width of the distal tibia away from the knee joint centre in accordance to published data on tibio-femoral contact regions (see Figure 56) (Schipplein and Andriacchi 1991).

Originally a landmark was identified at the distal end of the tibia to apply a constraint to simulate the ankle joint. However, this created a pivot and the finite element model would therefore not solve. Perez et al. (2009a) constrained the ankle using three nodes however which nodes chosen was not divulged. So, for this study the nodes were arranged in a straight line, but that still allowed for excessive movement, and a failure to solve. So, three nodes were chosen at the base of the tibia as a response to the physiological bone contact found at the ankle. One in the medial malleolus, to simulate the deltoid ligament. One under the lateral face; to simulate constraint imposed by the fibula and one in the centre posterior of the tibia to simulate the articulating contact with the talus bone. (See Chapter 2, Figure 3) This is a triangle formation, and accurately represents the physiological constraints and contact points

seen at the human ankle (See Figure 57). For the purpose of the finite element, the ankle will be constrained in all degrees of freedom.

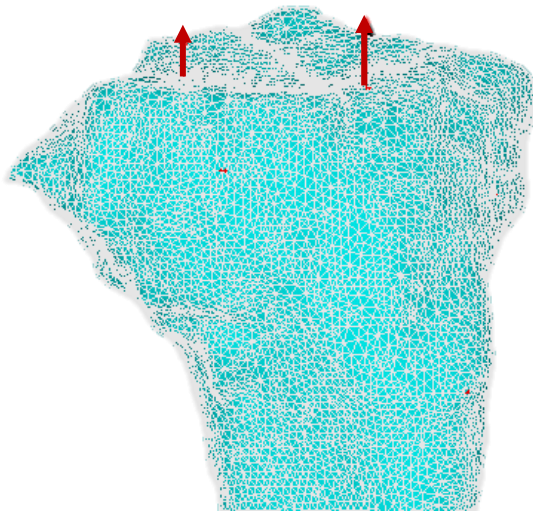


**Figure 56: Locations of the point loading on the condyles at the type of the tibia. The size of the arrow shows the larger distribution of load 60% on the medial c-ondyle compared to 40% on lateral condyle.**

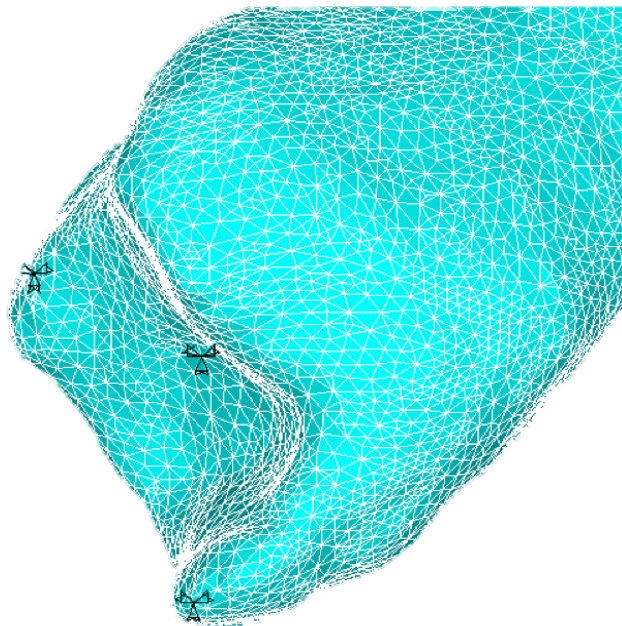


**Figure 57: The triangular formation of the constraints at the distal end of the tibia to simulate the ankle.**

### ***Deflection***

The deflection shows the models response to load, in regards to this FEM the deformation can be used to compare the model's responses but should not be related to any bone physiology. This is because within a human body the 'deflection' as it is described in reference to FEM would be minimised by the presence of the fibula as well as tendons, neither are modelled here. Changing the geometry of the model, varies the deflection by only 2% showing the models response to the loads is similar regardless of the geometry.

### ***Strain***

The output from the finite element is strain (dimensionless unit). As demonstrated in Figure 56 and 57, at either end of the bone there are constraints (distally) or loads (proximally) were placed. These constraints and loads create localised artefacts within the model (Richmond et al., 2005). These responses do not affect the rest of the plot, as can be explained by the Saint-Venants principle which states

*'...the difference between the effects of two different but statically equivalent loads become very small at sufficiently large distances from load.'*

This explains that despite the type of loading, e.g. distributed or point loading, that at a certain distance away from this the response will be the same. As a result, the maximum strains are not considered for the whole model but instead within the shaft, i.e. the areas that show true bone response. The minimum strains are plotted to show the magnitude of the strains, but due to a bone response not being elicited by such small strains, there will be no further evaluation.

#### **5.2.4 Subject-specific physiological data application to semi-subject specific finite element model.**

The first objective of this study was to optimise the semi-subject specific FEM developed in Study One by investigating the most physiologically accurate loading conditions using data collected in Study Three. Study Three was a longitudinal study where level walking kinetic and kinematic data was collected at six time points (every three months) and bone imaging scans were collected at three time points (at six month intervals) (see Figure 84). The bone imaging scans collected from time point one in Study Three (Chapter Six) were processed through the image processing method described in Chapter Four and a semi-subject specific FEM was created for each participant. A set of dynamic walking trials, from time point 1, 3 and 6 from Study Three were also collected. Ground reaction force profiles were extracted from each of the ten gait trials recorded at each level walking gait data collection time point. These ten GRF profiles were averaged to create one time point representative GRF profile. Each individual GRF profile was then compared to the time representative GRF profile. The individual gait trial which produced a GRF profile which had the lowest RMS when compared to the time representative GRF profile was the trial taken forward through the process described 5.2.1 and 5.2.2 of this chapter to generate muscle forces.

The other input into the model was the joint reaction force, *i.e.* the force experienced at the joint which is not related to muscle forces. The gait trial identified with the lowest RMS was taken forward in the calculation of joint reaction force. The joint reaction force was calculated through the use of inverse dynamics within the 3D motion capture analyses software visual 3D (see Figure 58).

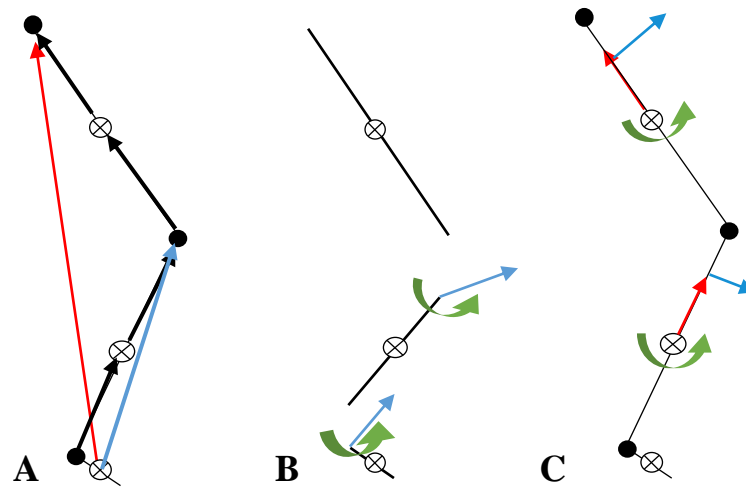


**Figure 58: The breakdown of the inverse dynamic's procedure used by Visual 3d. A; The definition of vectors for distance between centre of mass of the distal joint to proximal joint (red and blue arrows). B; The joint torques (green arrows) and forces at the proximal joint (blue arrows). C; the external forces (blue arrow), their location in relation the segment mass (red arrow) and external couples (green arrow).**

The joint reaction force at the proximal end of the joint was calculated through the shank and foot segment. The formula used to calculate these forces is the following;

$$F_{Proximal} = \sum_{i=1}^n m_i(a_i + g) + \sum_{j=1}^q F_q$$

$m_i$  = mass of segment i

$a_i$  = acceleration of segment i

$n$  = number of distal segments in the chain

$q$  = the number of external forces

$F_q$  = applied external forces

The joint reaction force was output for the right knee in its x, y and z components for all time points across the gait cycle. The maximum joint reaction force was then identified and

its time point recorded. The values of the component parts were divided according to the ratios of force across the condyles.

The joint reaction force was output for the right knee in its x, y and z components for all time points across the gait cycle. The maximum joint reaction force was then identified and its time point recorded. The values of the component parts were divided according to the ratios of force across the condyles.

### **5.2.5 Effect of subject-specific physiological data application to the semi-subject specific finite element model**

#### **Introduction**

The six participants recruited into Study Three were able bodied, it has previously been assumed that the pattern of mechanical loads and geometry of the tibia would experience little variation. As this method of validation is novel it was important to consider the effect of different iterations of loading and geometry, which may affect the validation of the model. The first objective was to investigate the effect of varying the geometry with the same load application. The second objective was to investigate the effect of varying the load application to two models with the same geometry.

#### **Methods**

The reference JRF data (as explained in 5.2.4) was applied to models generated from each of the three scan points to investigate how the change in geometry affected the strain pattern. Then the model generated from bone scans from the first time point were loaded with JRF generated from two gait trials at different time points. The iterations explained here can be demonstrated in Table 15.

**Table 16: To investigate the effect of variation of geometry, three FEM generated from bone imaging data from scan time point 1 (FEM1), scan time point 2 (FEM2) and scan time point 3 (FEM3) were loaded with a reference set of loads (column 4). To investigate the effect of varying loads, each FEM was loaded with the corresponding time specific loads and a set of reference loads.**

	<b>Loading from time point 1 (L1)</b>	<b>Reference Loads (RL)</b>
<b>FEM 1</b>	<b>X</b>	<b>X</b>
<b>FEM 2</b>		<b>X</b>
<b>FEM 3</b>		<b>X</b>

## **Results**

When comparing FEM that were loaded with data taken from the same time point to when they were loaded with the reference loading data, greater variation was seen. The coefficient of variation was 12% in FEM 1, 7% and FEM 2 and 3% at FEM 3. When looking at the individual sites, most variation occurs at the distal end of the bone.

The variations in micro strain ( $\mu\epsilon$ ) across the tibial shaft were minimal, therefore, to display the changes effectively, non-uniform contours were applied. The largest strain value was taken to be the highest contour decreasing in equal steps until the strain value was in the form of  $x \cdot 10^{-3}$ . The contours are then decreased in equal increments until the minimum strain value is reached. As strain is very small, it is often reported as micro strain ( $\mu\epsilon$ ) where  $\epsilon \cdot 10^{-6}$ . The values presented in these models are in strain with micro strain being reached within the dark blue plots of the model. Due to the localised strain values at the distal and proximal end of the tibia the strains were analysed for the tibia shaft only.

Figure 59 shows how varying the geometry and keeping the loading profile constant, visually shows very little difference in the strain plot. The largest strain values occur at the distal end of the tibia shaft. Comparing across models, the strain value, as displayed by the coloured contours, is similar across all models. The area where strain occurs does change slightly across the varying geometries. Figure 60 shows how having consistent geometry and varying the loading profile affects the strain output. The magnitude of strain was higher in the FEM when the FEM was loaded with biomechanical data collected from the same time point the scan was generated *e.g.* FEM 1 and Loading time point 1.

These results demonstrate that when loading a FEM generated from geometry from different time point with biomechanics from different time points can have an effect on the strain outcome. Therefore, FEM used in 5.2.6 were loaded with biomechanical data collected from the same time point as the scan used to create the FEM.

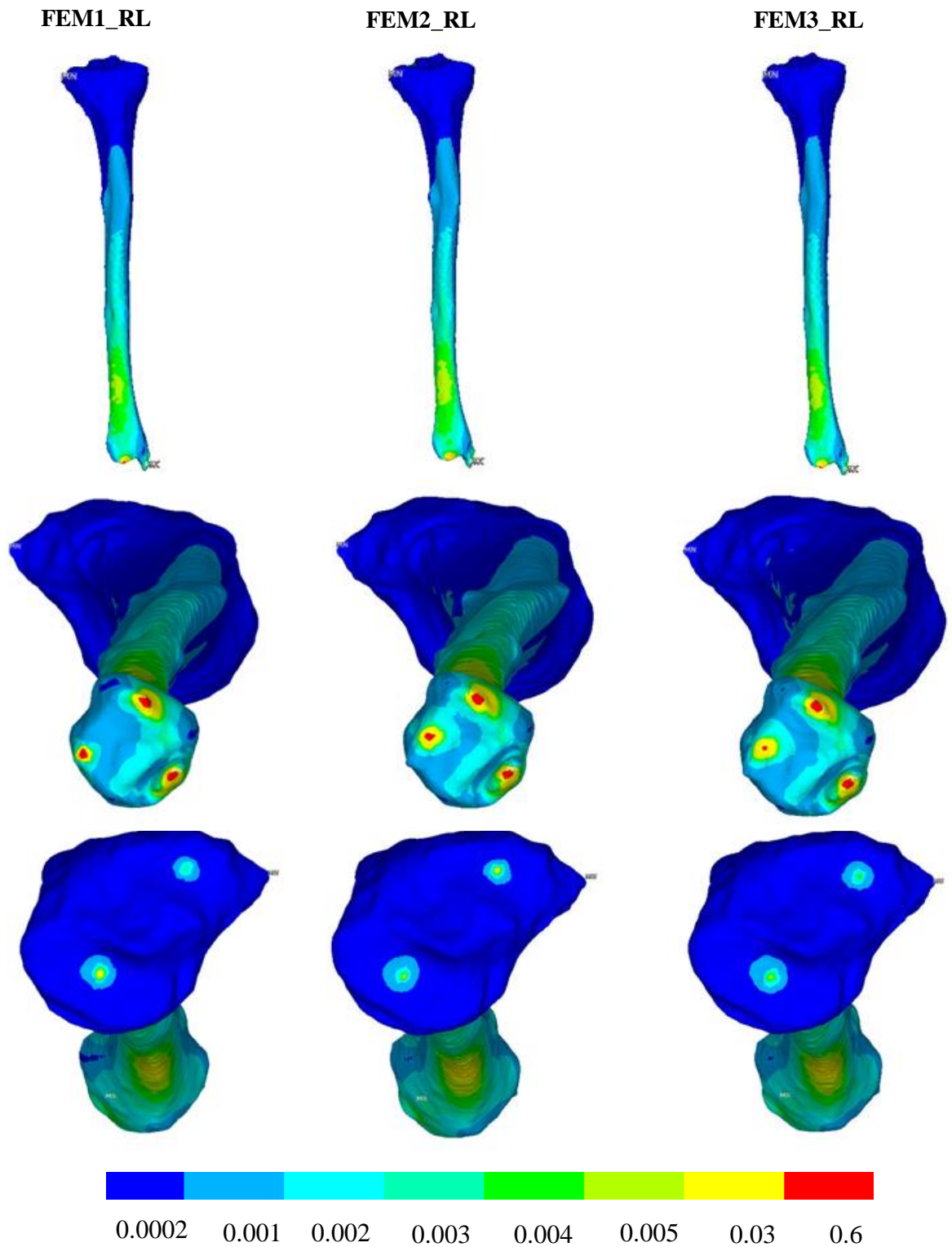
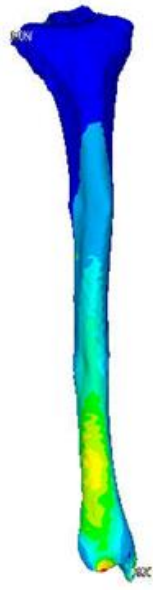


**Figure 59: Resultant strain plot from the application of loads to finite elements models generated from different bone image scan data. From top; full length tibia, from distal end of tibia, proximal end of tibia.**

FEM1\_Loading  
time point 1



FEM1\_Loading  
time point 2

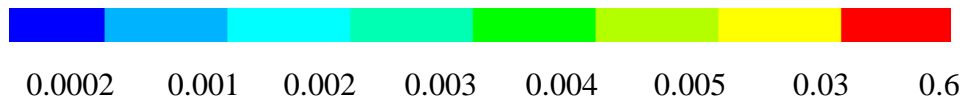
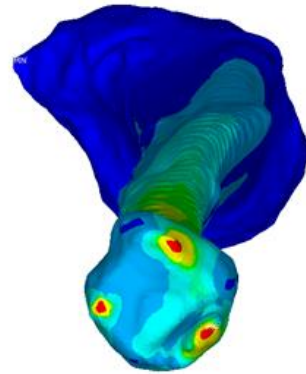
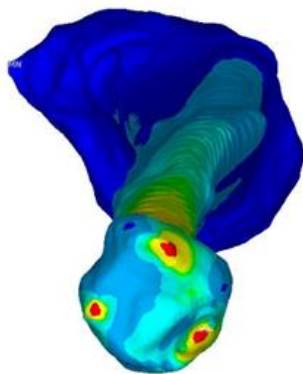
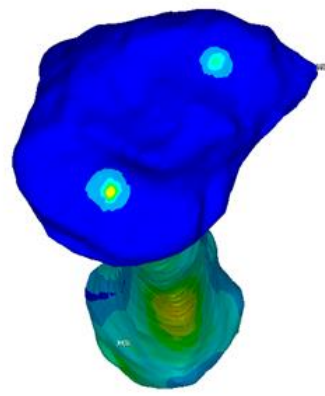
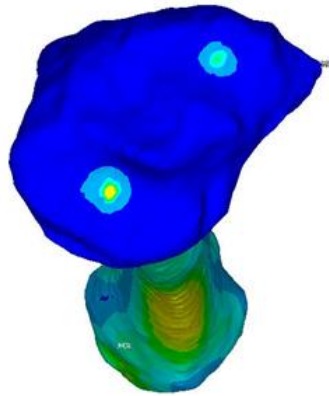
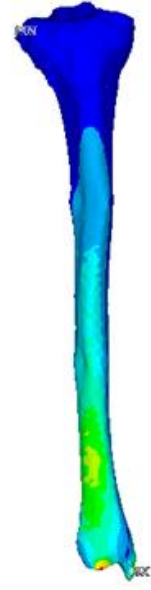


Figure 60: The same FEM geometry with application of loads generated from different biomechanics

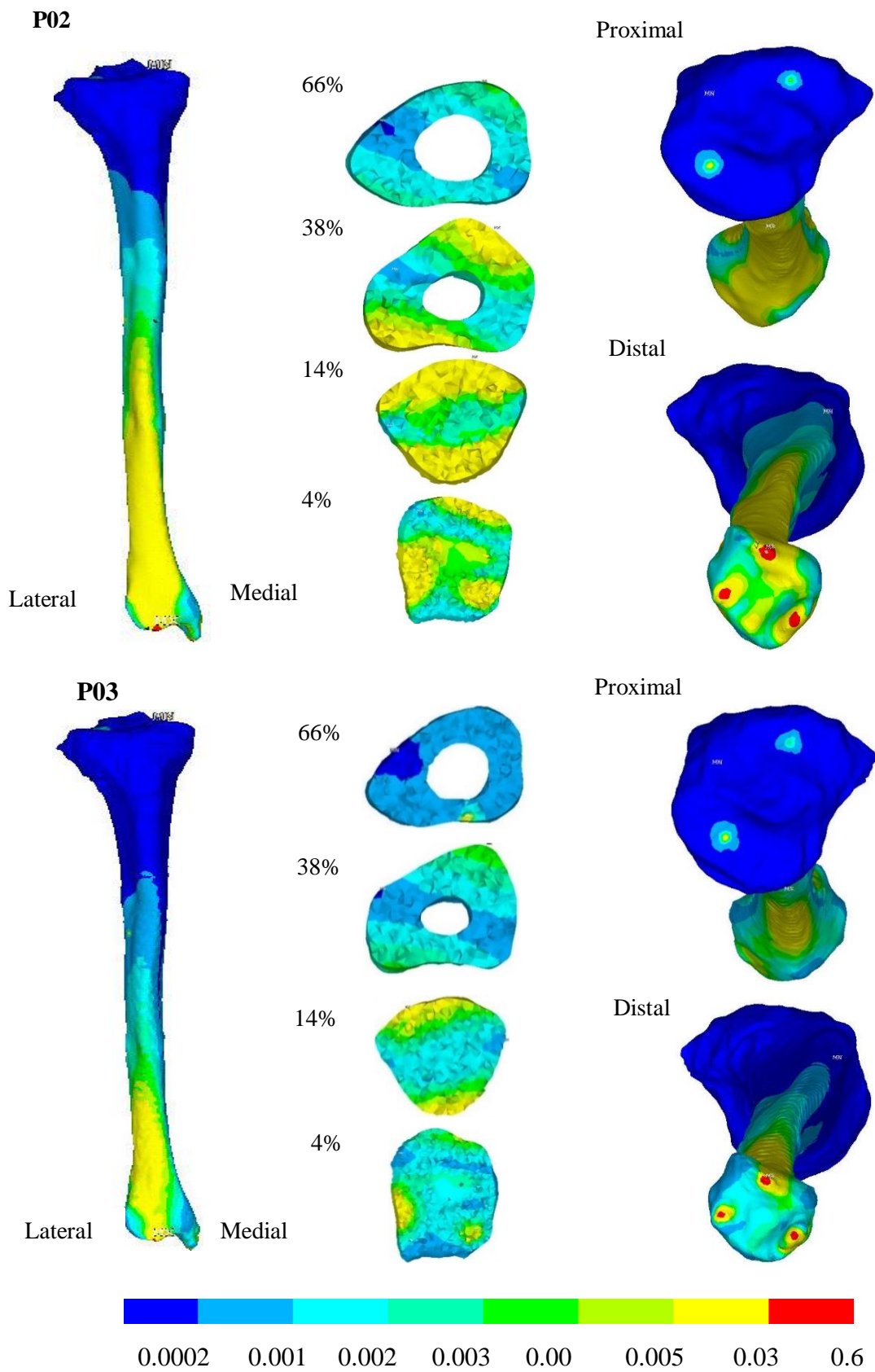
## **5.2.6 Validation and evaluation of the semi-subject finite element model using subject specific longitudinal physiological data**

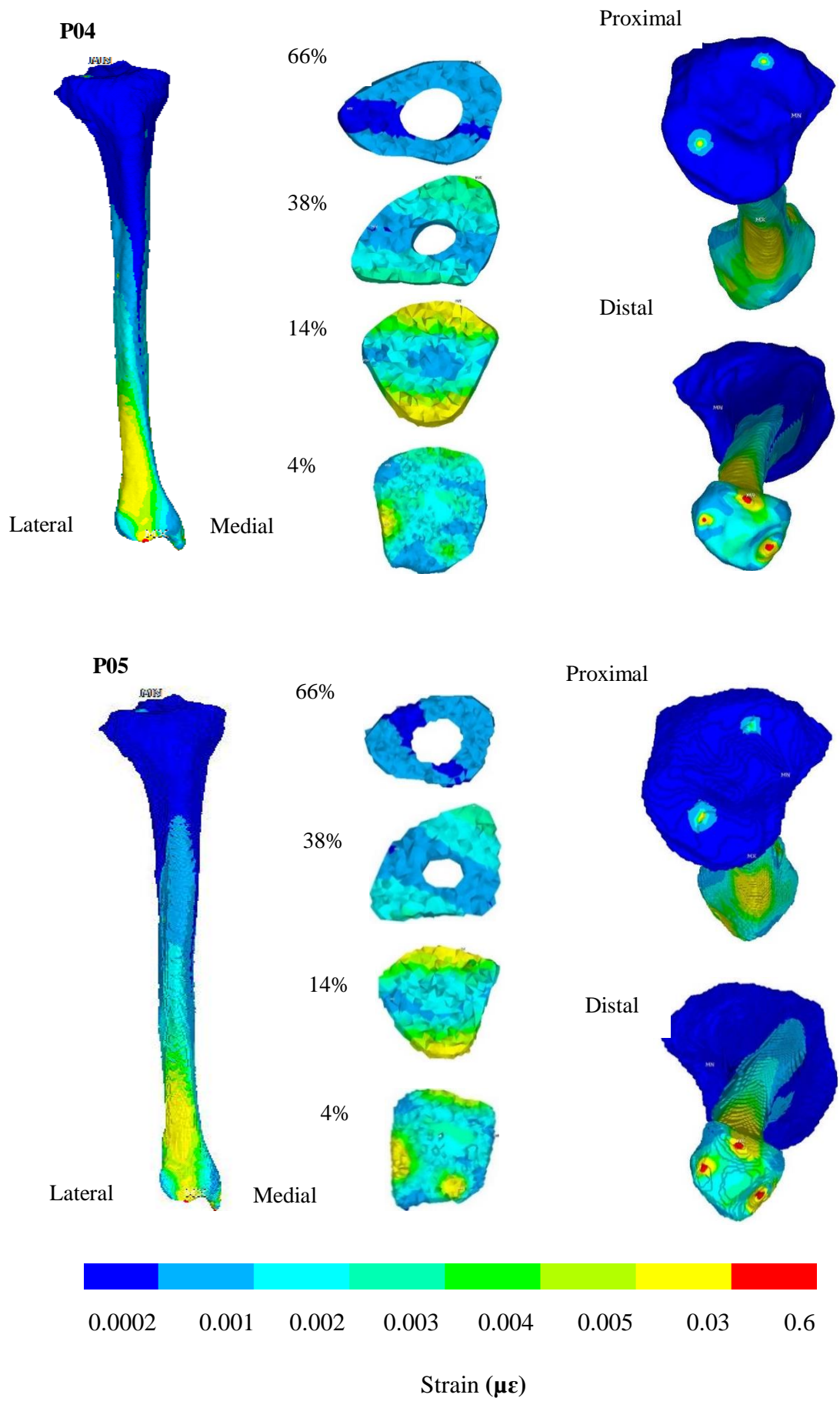
### **Introduction**

The third objective of this study was to validate the strain values generated from the semi-subject finite element model using the subject specific bone geometry and structure data generated from Study Three. It is known from the mechanostat theorem that bone formation and resorption are driven by strains within the bone (Cointry et al. 2004; Al Nazer et al. 2012) therefore the change in bone deposition and resorption can be identified through negative and positive bone geometry changes respectively. However, research has not yet to date used longitudinal bone changes to validate the strain plots produced from finite element models.

### **Methods**

The strain plot generated from the semi-subject finite element model was analysed for locations of both high and low strain magnitudes. The equivalent locations on the subject specific bone outer geometry plot was analysed and compared to identify if the bone geometry changes correlate with the strain plot. The strains for each participant are displayed on pages 151-153, in Figure 61. This includes the overall strains as well as a strain plot for each cross section in concurrence with the locations of the pQCT scanner, *i.e.* 4,14 38 and 66% of tibia length. Then a proximal and distal view of the bone is also displayed. All strain plots were contoured based on the same coloured contour scale which is presented at the bottom of each page.





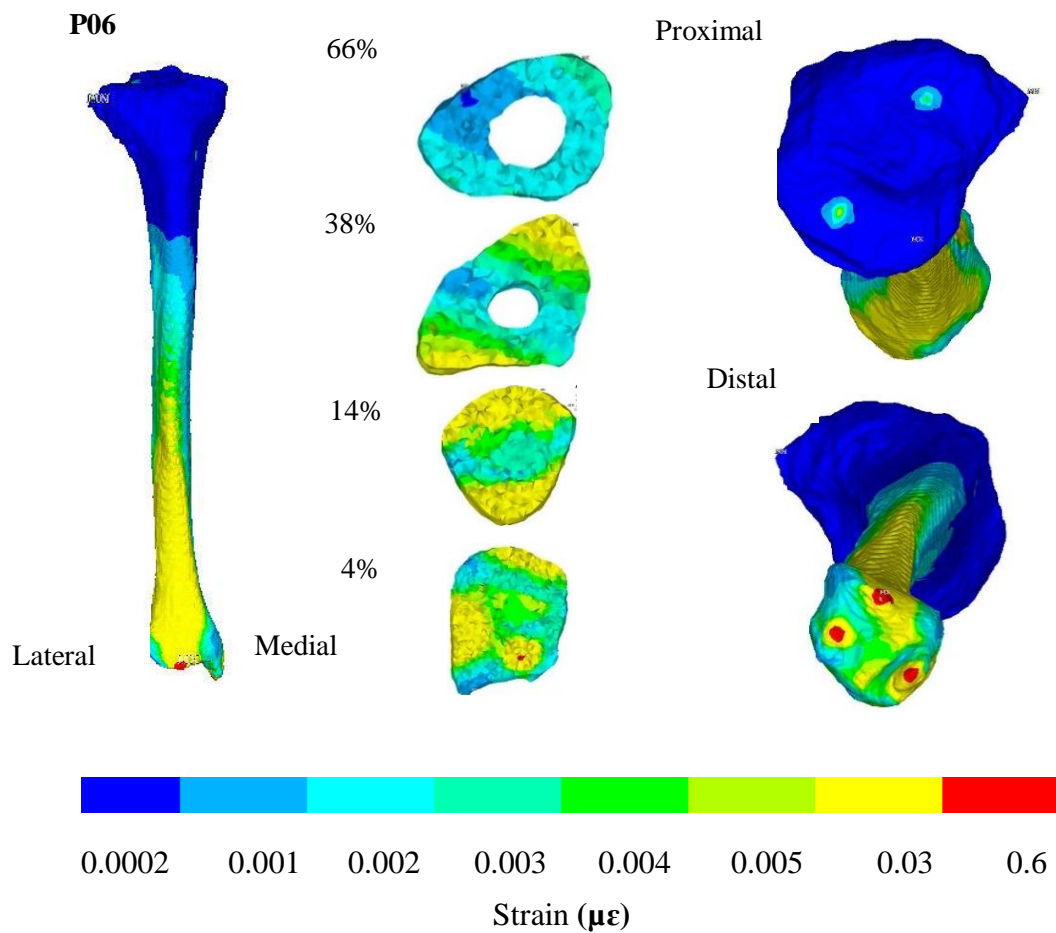


**Figure 61: All Participant strain ( $\mu\epsilon$ ) plots across the tibia alongside 4, 14, 38 and 66% cross sections.**

Due to the 4% site being in close physiological proximity to constraints applied to the FEM on some participants, areas of very high strain can be seen at the 4% cross section. This is a localised artefact and therefore was considered as so in the analyses. Therefore, the shaft of the tibia was the only part analysed for strain magnitude. All participants showed greatest strains at 14% of tibia length, (shown in Figure 63). The least strain was at the proximal end of the tibial diaphysis, specifically at the 66% site.

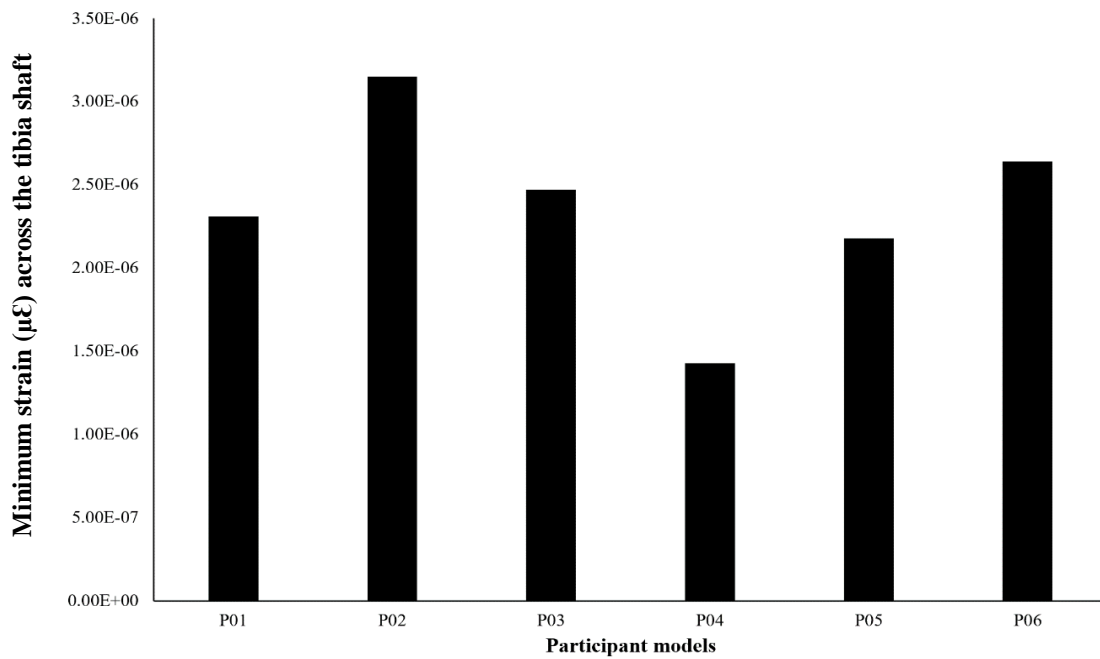


**Figure 62: The minimum strain (µε) across the tibia for all participant models.**

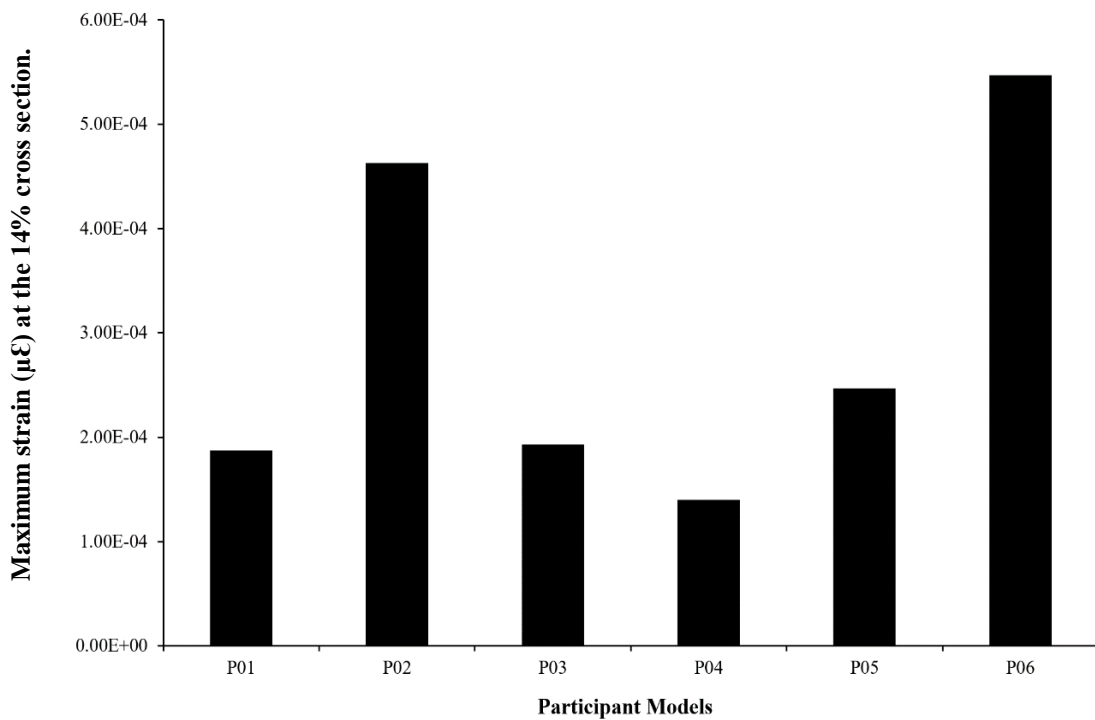


**Figure 63: The maximum strain (µε) at the 14% of tibia length for each semi-subject specific model.**

Individual comparisons were then made between the semi-subject specific finite element model cross sections and the outer geometry bone plots generated from the subject specific bone imaging scans. For all participants at 14% of the tibia length the highest levels of strain were shown, therefore the 14% site was taken forward in this next section.

### 5.2.6.1 Geometrical comparisons

The output from the pQCT was rotated to reflect the orientation of the cross section of the FEM. The landmarks were identified for the areas of highest and lowest strain, according to the FEM.

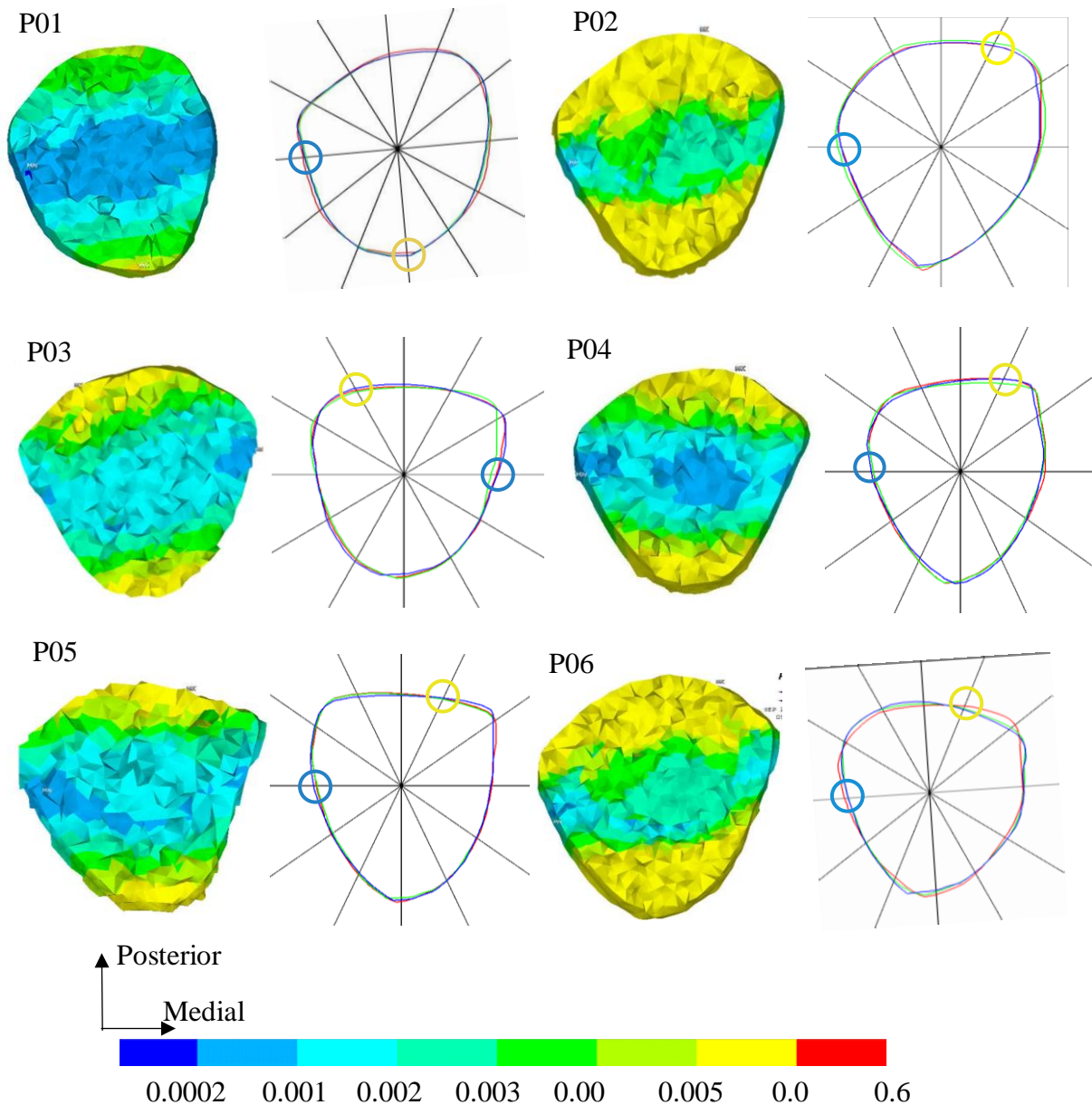


**Figure 64: Cross section of the finite element model at 14% tibia length and the pQCT external geometry plots for baseline (red), visit 2 (green) and visit 3 (blue). Yellow represents higher strain and blue, areas of lower strain. Landmarks at the highest and lowest strain points are identified by a circle in the corresponding colour.**

The coordinates for each of the landmarks that corresponded to areas of high strain and low strain on the FEM, were recorded at each scan time point. Table 16 shows the change in location for those time points.

**Table 17: The coordinates of the landmarks which correspond to the location where the FEM has identified highest strain levels and lowest strain levels. The X, Y coordinates are presented for each of the three time points. The positive X is Medial and positive Y is Posterior.**

Participant	Level of strain	X			Y		
		Scan1 (Baseline)	Scan 2	Scan 3	Scan 1 (Baseline)	Scan 2	Scan 3
P01	Highest	194	190	200	228	240	266
	lowest	248	244	254	168	184.8	210.8
P02	Highest	317.6	329.6	311.6	206.8	197.6	204.4
	lowest	270	280	264	282.8	276.8	280.4
P03	Highest	278	312	274	296	285.6	327.6
	lowest	232	266	228	214.8	209.2	246
P04	Highest	316.4	306.4	344.4	242	216	222.4
	lowest	258	252	288	294.4	268	277.6
P05	Highest	270	250	344.4	244.8	264	222.4
	lowest	230	210	308	313.2	331.2	288
P06	Highest	288	272	266	258	250.4	263.6
	lowest	242	226	222	346.8	331.6	345.2

Highest strain was located on the lateral side of the tibia for the majority of participants. Lowest strain was located posteriorly and medially for the majority of participants. For participant P01, the geometrical changes at the landmark located in an area of higher strain on the FEM were similar to the geometrical changes that occurred at the landmark located in an area of lower strains on the FEM. Across the time points participant P01 displayed minimal geometrical changes. For participants P02 and P04, there were higher geometrical changes at the landmark located at areas of higher strain on the FEM, compared to the geometrical changes at the landmark located in areas of lowest strains on the FEM. For participant P03, there was greater geometrical change in the anterior/posterior direction at the landmark located in an area of higher strain on the FEM. For participant P05, at the landmark located at areas of lowest strain location, there was minimal variation across the entire outer geometry perimeter, with only visit 3 (blue in Figure 64) showing small variation. For participant P06 there were larger geometrical changes in the medial/lateral direction, at the landmark located in an area of higher strain on the FEM. Participant P06 showed visit 2 (green) and 3 (blue) to have similar geometry at the point where lowest strain is reported.

#### **5.2.6.2 Literature validation of the finite element model**

The results from this study found a maximum compressive micro strain across participants ranging from 200 to 600  $\mu\epsilon$  at 14% of tibial length. For validation through literature a number of *in vivo* studies, which through the use of strain gauges have investigated tibial strain during walking were compared (Lieberman et al. 2004; Burr et al. 1996; Funk and Crandall 2006). These studies used strain gauges bonded to the bone surgically through adhesive or via bone staples. The recorded values range from 30 to 700 micro strain ( $\mu\epsilon$ ) across the tibia with 430 $\mu\epsilon$  reported during walking (Yang et al. 2011; Lanyon 1982; Burr et al. 1996).

The strain within the FEM were generated by the theoretical maximum joint reaction force and muscle forces at the same point within the gait cycle, which could account for their larger values. Also the strains within literature reported here were reported for the medial aspect of the tibia shaft. The strains that were higher for this study were located at the lateral aspect of the tibia shaft. Despite the differing location, the values are within previously reported ranges found *in vivo*, these models can be considered theoretically validated.

The strains in the semi-subject specific FEM were validated using outer geometry changes generated through the image processing method. The results from this were that most participants exhibit a positive geometrical change at a point where higher strains occur, specifically at strain values above 0.005. *In vivo* studies within animals have shown that above values of 0.001 inner geometrical values of bone increase e.g. periosteal and endosteal bone mass (Rubin and Lanyon 1985). However, there is no literature which has compared outer geometry values to *in vivo* strain values. This is because the outer geometry variables are not automatically generated from bone imaging scans such as pQCT. The image processing method developed within this thesis provides option for further geometrical analyses and has been proven to a valuable method in validating strains generated from semi-subject specific FEM's.

#### **5.2.6.3 Experimental validation of the finite element model.**

The third objective was to provide a method of validation using the strain values alongside longitudinal experimental data generated from Study Three. Experimental validation usually involves the simulation of the finite element environment on cadavers or animal subjects. When neither of these are possible the afore-mentioned method of comparison to literature is used. However, with knowledge provided by the Mechanostat theory; above a certain

strain magnitude bone will be encouraged to form and thus positively change the geometry. Therefore the strains generated from the FEM can be validated by comparing them to changes in outer bone geometry, a higher strain value should elicit a positive bone geometry change. This novel process provides a new method of validation, which is less invasive than using cadavers and animal studies, also means that individual participant models can be validated using participant specific geometry.

Figure 64 and Table 16 showed the strains across the cross section at 14% of tibial length and the analyses output of the outer geometry generated from the pQCT images. The FEM was plot for the first visit, so geometry changes were compared between Scan 1 to Scan 2 (the red and green plots). Positive bone changes, or reduced negative bone changes are seen at the highest strain location compared to the lowest strain location in the majority of participants. This would validate the strain in the FEM to conform to the theory that higher strain values encourage bone formation and thus positive bone changes.

This study used loads generated from walking to apply to the bone, which is not a high strain inducing activity. The participants between the study collection days were also instructed to maintain a healthy active lifestyle and so bone geometry changes are expected to be small, making analyses in geometry changes difficult. However, the location of highest strains and thus increased bone changes is in agreement with previous literature of outer geometry plots taken at 14% of tibial length (Izard et al. 2016a).

This method would be appropriate in a clinical environment as patients are monitored anyway. A semi-subject specific model can be easily created from a low radiation pQCT scanning (as previously described, see Chapter Four). The model can be loaded with JRF and muscle forces generated from 3D biomechanics taken at each health visit and validated

using results from subsequent visits. Once validation the participants would not have to have bone imaging scans in order for the clinician to be able to be informed of bone changes. Not only does this reduce the radiation exposure to the participant, but is more time efficient for clinicians.

### **5.3 Limitation and Future directions**

In studying a healthy able-bodied population, the limitation is that the loading magnitude or pattern is not expected to change over the course of a year and so the geometrical changes that are being investigated might not be obvious. The participants that were recruited were all healthy and active, therefore any geometrical changes observed might have been the result of activities conducted outside of the laboratory testing environment. All participants at the start and at the end of the testing session, recorded any changes in their physical activity, by filling out a bone physical activity questionnaire. Future directions would be to take this validation process into a population where there are expected changes in bone geometry over the course of a year *e.g.* lower limb amputees.

The limitation in using a semi subject specific FEM was that the geometry of the FEM was not always consistent with that generated by the pQCT. Therefore, the landmarks chosen may not be precise to the location of the highest strains within the participant. In some participants this was evident when the landmarks weren't in the same position as highest and lowest strains and therefore the geometry changes could not be validated. However, the overall plot of the outer tibia was still achieved and so overall changes could be identified. To improve the validation, a further sensitivity study could be carried out to investigate how the shape varied depending on how many landmarks were extracted using

The semi-subject specific FEM used in this study was a simplified model, research has discussed the advantages and disadvantages of using a simplified mesh and material properties (Taddei et al. 2006; Burkhart et al. 2013). The other simplification used was the loading and constraints. Loading was applied as two point loads on each condyles. *In vivo* studies have shown that the contact area at the knee is distributed over is in the range of 100 to 600 mm<sup>2</sup> (Périeré and Hobatho 1998; Fukubayashi and Kurosawa 1980; Gilbert et al. 2014) with 60/40% loading shared between the medial and lateral condyles. The contact area has also been shown to move depending on the level of flexion in the knee (Wretenberg, et al., 2002). Therefore, it can be argued that point loading at one element is not physiologically representative. To measure an individual's contact area, MRI, dynamic fluoroscopy as well as instrumented implants have been used. These are expensive, highly invasive or expose participants to high levels of radiation. So, the contact area would have to be estimated from other literature, potentially introducing error. Future development can include sensitivity analysis in reference to the limitations, comparing models with different material and mesh properties to investigate the change in strain. Investigating how varying the load across a larger area would affect the strain magnitude and pattern.

The loading that was applied to this model was walking, which is a low strain inducing activity. Future directions would include activities which are known to induce higher strains *e.g.* running and jumping (Al Nazer et al. 2012). Alternatively the model could be created and validation with participants within a population where a change in loading and changes in bone geometry have been found *e.g.* speed skaters (Varley, Greeves, and Sale 2019).

## **5.4 Conclusion**

This study optimised the loading of the FEM constructed in Study One. The semi-subject FEM displayed highest strain values at the 14% site, along the lateral side of the shaft.

Maximum strain values for participants ranged between 200 and 600  $\mu\epsilon$ . These values were within the range of published in vivo strain data. This study also proved a new method of validated the FEM through using participant own experimental data. Not only does this novel method of validation provide researchers with another method that is a lot less invasive but also provides an efficient method for clinicians. In validating participants FEM with data from routine appointments, clinicians can have confidence in the models predictions whilst not subjecting the patient to any more investigation than what would be routine. This can then lead to a FEM which confidently predicts bone geometry changes and subsequent bone health without the need to expose participants to radiation through bone imaging scans.

The data obtained to validate the FEM was done so through a longitudinal study, study three. Study three builds on the theory that bone in healthy able-bodied people is maintained through physical activity including a symmetrical walking pattern (Horst et al. 2017) to compare the variation in tibial bone health and lower limb biomechanics across a 12-month period.

## **6 STUDY THREE: THE VARIATION IN TIBIAL BONE HEALTH AND LOWER LIMB BIOMECHANICS ACROSS A 12-MONTH PERIOD**

### **Dissemination of Research**

#### **Conference proceedings**

**Brown, O.**, Sale, C., Barnett, C. T., (2017) Does the method used to locate force platform centre of pressure affect biomechanical measures obtained during stair walking on an instrumented staircase? Biomechanics Interest Group (BIG) meeting, Portsmouth, UK

## 6.1 Introduction

The validated semi-subject specific FEM constructed from landmarks identified from pQCT scans using an image processing method were taken forward to investigate the relationship between movement and bone health. It is known that bone responds to the loading imposed upon it by constant adaptation. The cellular modelling and remodelling processes which determine the deposition and absorption of bone material are stimulated by growth factors, hormones and strains (Boyce et al. 2009; Frost 1987). Strains are generated through mechanical loading of the bone, both through muscle loads and external forces generated through movement. There is a postulated optimum strain range at which a healthy bone is maintained (Forward and Tuner, 1995). A change in the mechanical loading can lead to an imbalance in the modelling and re-modelling processes subsequently affecting bone health.

Bone health can be defined through structure, (*i.e.* bone mineral content and density) geometry (*i.e.* area and shape) and subsequent strength through second moment of area (distribution of bone about its neutral axis). Non-invasive methods of imaging bone to determine its health include CT, MRI, DXA and pQCT. Computed tomography can image the full length of the bone and provide high levels of detail on the internal structure as well as outer geometry. The radiation dose associated with these scans, is comparatively large, thus only making them practical for cadaveric studies or for a specific clinical need. Magnetic Resonance Imaging uses magnetic radio waves, thus, not exposing the patient to radiation. The ability to image the differing bone materials is limited, to the point where the presence of cortical bone in MRI results in an absence of a signal (Faulkner et al. 1991). Where MRI is advantageous is in the accurate imaging of muscles and tendons and their bone attachment sites, leading to its use in joint articulation studies (Wretenberg et al. 2002). In comparison to the previously mentioned modalities, DXA, is less expensive and exposes participants to minimal radiation (Nana et al. 2015; Buxsein and Seeman 2009).

Comparison studies have also shown the DXA to be accurate to both MRI and CT scans in measuring body composition in adults of normal weight (Bredella et al. 2010). Where it could be argued that body composition is not directly related to analyses of bone properties, body composition is associated with bone characteristics through bone loading and muscle contributions (Cointry et al. 2004). Internal bone properties used for clinical measurements, such as bone mineral density, DXA is considered to be the gold standard (Yazicioglu et al. 2008). The disadvantage of a DXA scan is that a 2D scan image is produced so, is limited to singular plane analyses, thus making bone geometry assessments difficult. As a result of the inability to generate geometry and analyse bone material properties, studies have suggested that, as a research method, DXA should be used in conjunction with another method (Cointry et al. 2004; Bouxsein and Seeman 2009). Peripheral Quantitative Computerized Tomography uses a step scan process to image the peripheral bone at certain points along its length. The radiation dosage associated with this scan is comparatively low to that of CT and provides a scan with higher resolution than CT, enabling the analyses of cortical and trabecular bone independently (Liu et al. 2007, Stagi et al. 2016). The measurements obtained from a pQCT scan include geometrical properties *e.g.* cross sectional area, trabecular area and structural properties *e.g.* bone mineral content and bone mineral density. The disadvantage of using pQCT is the scanner can only scan peripheral limbs, *e.g.* the tibia can be measured. However, as the tibia is one of the weight bearing long bones, mechanical loading effects on bone health can be inferred.

Level walking within an able-bodied population has been studied extensively, with the first established gait cycle published in 1836 by the Weber brothers (Maquet et al. 1991). For simplification purposes, able-bodied gait is assumed, especially within a clinical environment, to be symmetrical and remain constant over time (Horst et al. 2017; Sadeghi et al. 2000). Within research, gait variability has previously been due to data collection error,

with a reduction in variability thought to be attributed to an improved research method (Gorton et al. 2009). Variations in GRF from experimental data using force platforms have been reported to be acceptable if within a level of variation of 12.5% (Wang and Watanabe 2000; White et al. 1999). Classification rates (how well a subsequent measure is predicted) have shown  $67.8 \pm 8.8\%$  for GRF and  $86.3 \pm 7.9\%$  for joint angles (Horst et al. 2017). This concludes that both GRF and joint angles have some variation. In order to assess changes in gait as a measure of health deterioration as well as rehabilitation improvements it is imperative that a baseline level of variation for an able-bodied population is established.

One clinical population where changes in gait occur and there is increased risk of bone health degradation is lower limb amputees. Research has found that lower limb amputees present with reduced bone mineral density at both the hip and distal end of the residual limb (Sherk et al. 2008; Leclercq et al. 2003; Royer and Koenig 2005). Amputees are also at an increased risk of developing osteoarthritis, a reduction in joint cartilage, in both the residual and intact limb (Melzer et al., 2001). In terms of geometry, there are a limited number of studies which investigate bone geometry in LLA's. Sherk et al. (2008) found that at the distal end of the residual limb, there was a decreased total bone area and cortical bone thickness, this is in agreement with an early study by Sevastikoglou et al. (1969). The justification provided for this degradation in bone health is the mechanical adaptations developed by amputees (Sherk et al. 2008; Royer and Koenig 2005).

Dependant on their level of mobility prior to surgery, vascular LLA's i.e. those as a result of complications with the blood vessels including diabetes, will often experience a prolonged period of reduced activity both prior and post amputation surgery. Then, as part of the rehabilitation process, LLA will start load bearing, gradually increasing this in the aim to restore both mobility and stability (Schaarschmidt et al. 2012). In adapting to the loss of

biological structures, patients will alter their walking pattern. Adopting a variety of temporal, spatial, kinetic and kinematic characteristics, resulting in gait, which is considered asymmetrical (Nolan et al. 2003; Sadeghi et al. 2000; Sagawa et al. 2011). The temporal, spatial adaptations include a slower walking speed, longer step length and proportionally more time spent on the intact limb in stance than on the prosthetic (Sadeghi et al. 2000; Schulz et al. 2010; Kovac et al. 2010; Schaarschmidt et al. 2012; Roerdink et al. 2012). Kinetic asymmetries for able-bodied ambulators are typically less than 10% whereas in LLA's up to 23% GRF asymmetry has been reported (Gailey et al. 2008). The magnitude of GRF are seen to be reduced in the residual limb and increased in the intact limb (Nolan et al. 2003; Silverman et al. 2008; Lloyd et al. 2010; Sanderson and Martin 1997; Royer and Koenig 2005; Silverman and Neptune 2014; Levine et al. 2012). Kinematic adaptations include an increased plantar flexor ankle angle in the intact limb, to compensate for the smaller range of motion at the ankle of the prosthetic limb (Winter and Sienko 1988; Silverman and Neptune 2014; Sanderson and Martin 1997; Bateni and Olney 2002). It is also well documented that transtibial amputees have a smaller knee flexion in their residual limb during stance (Bateni and Olney 2002; Powers et al. 1998; Sanderson and Martin 1997; Breakey 1976). Other compensatory mechanisms used by amputees include the use of hip extensors to reduce hip flexion during early to mid-stance (Winter and Sienko 1988; Seroussi et al. 1996; Soares et al. 2009). These adaptations allow for the thigh to remain more vertical and knee more extended reducing the requirements of the muscles to prevent knee buckling and providing greater stability for the amputee (Sanderson and Martin 1997).

Explanations as to why lower limb amputee's use these compensatory mechanisms are that by loading their intact limb more, the residual limb is protected (Nolan et al. 2003; Sanderson and Martin 1997; Hurley et al. 1990). Distributing more of their body weight over the intact limb, the centre of gravity is closer to the intact limb, improving the sense of stability and

balance (Nolan et al. 2003). The change in mechanical loading as a result of a prolonged period of reduced use and adoption of asymmetrical movement pattern affects the mechanical stimulus on the bone. This subsequently could affect the modelling and remodelling processes that maintain a healthy bone.

The aim of this study was to analyse the variation in tibial bone geometry and structure, level walking gait and stair ambulation over a 12-month period. The specific objectives were to analyse tibial bone geometry and structure and walking gait in able-bodied subjects (1 & 2) in order to determine a level of variability. As well as tibial bone geometry, structure and walking gait in lower limb amputees in order to further investigate the link between asymmetrical gait and poor bone health (3). The fourth objective was to collect subject specific bone imaging and biomechanical data to apply to the FEM developed in Study One and Study Two (4).

## 6.2 Methods

### 6.2.1 Participants

The sample size was calculated using the equation in the general methods (section 3.2.3). The value of 1.96 was selected for  $z\alpha$  as this represented the setting of a 0.05 alpha level of statistical significance for a two tailed hypothesis test. The value of 0.842 was selected for  $z\beta$  as this represents the setting of a power value of 0.8 that provided the study with good sensitivity with regards to false negatives. The number of time points represented the number of visits to the lab (visit 1, baseline, visit 2, at 3 months, visit 4, 6 months, visit 5, 9 months and visit 6, 12 months). The stated value of the assumed correlation of repeated measures ( $\rho$ ) was selected as it was anticipated that there would be a large interaction effect within the proposed study. The effect size was based on the outcomes of (Sherk et al. 2008) using the total body bone mineral density of unilateral transfemoral and transtibial amputees who were physically active as the main outcome measure.

**Table 18: Variables values used to determine required sample size**

Variable	$z\alpha$	$z\beta$	n	$\rho$	ES
Value	1.96	0.842	6	0.5	0.7

Figure 65 details the process behind recruiting into both participant groups. Able-bodied subjects were recruited based on the age of potential amputee participants. As a result, of this six able bodied participant's (mean  $\pm$  1S.D. height  $1.82 \pm 0.05\text{m}$ , weight  $90 \pm 12\text{kg}$ ) volunteered for this study.

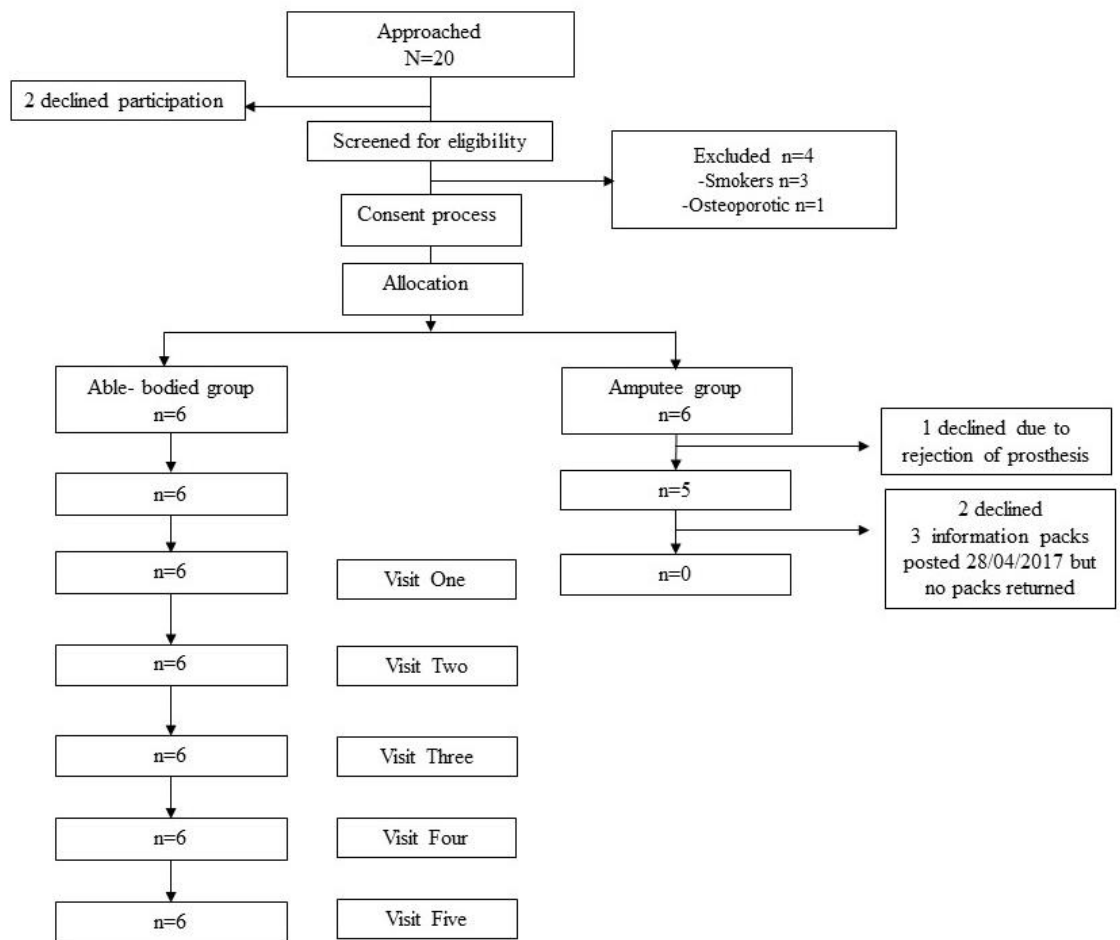


**Figure 65: Participant recruitment progress. A; recruitment of controls and their progression through the study. B; progression of recruitment of LLA into the study, culminating in no LLA**

### 6.2.2 Experimental design

This study employed a longitudinal repeated measures design. This design was selected for its scientific rigour in assessing changes in movement and bone health in an able-bodied population. Participants attended five time points across the 12-month study. Baseline levels were assessed at the first visit (Visit 1), and then repeated measures occurred at 3-month intervals until the final visit, at 12 months post baseline (Visit 5). The protocol for each visit is seen in Figure 66.

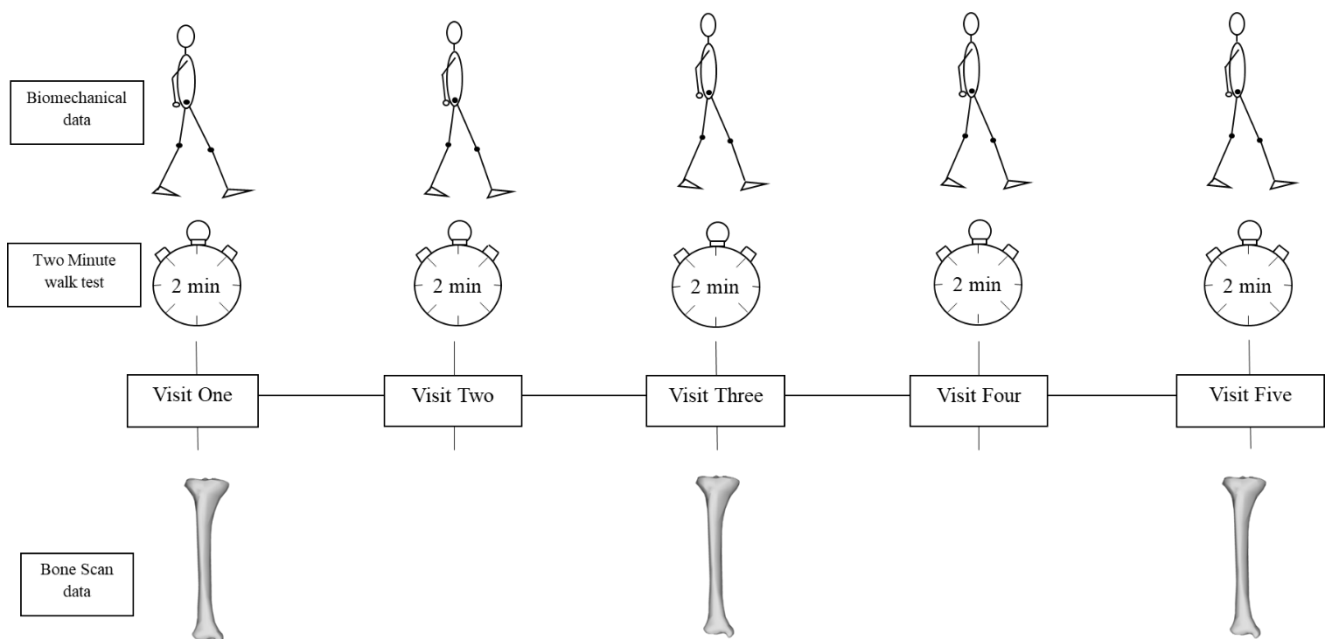


**Figure 66:** The experimental protocol for each visit across the 12-month period. The two-minute walk test and movement analysis are carried out at every time point. The bone imaging is carried out at visits 1, 3 and 5.

The following explains the processes of bone imaging and biomechanics data collection including two-minute walk test and movement analysis. At Visit 1, 3 and 5 participants underwent bone imaging scans. This included a peripheral quantitative computed tomography scan of the dominant tibia and a whole-body dual energy x-ray scan.

## **6.2.3 Bone Imaging**

### **6.2.3.1 Peripheral Quantitative Computed Tomography**

#### *Tibia scan analyses*

Analyses of the tibia bone was determined through the CALCBD (to determine cancellous bone properties) and CORTBD (to determine cortical bone properties) options within the software. For CORTBD the default threshold of 710 mg/cm<sup>3</sup> was used and for CALCBD a contour mode 1 and peel mode of 2 were both used with a default threshold of 280 mg/cm<sup>3</sup> and a trabecular bone area percentage of 45%. The contour mode detected the edge of the outer bone whereas the peel mode differentiated between subcortical and trabecular bone. For each of the 4, 14 and 38% sites the bone mass (g/cm<sup>3</sup>), area (mm<sup>2</sup>) and density (mg/cm<sup>3</sup>) was automatically analysed. For the 66% site, data on muscle total area (mm<sup>2</sup>), density (mg/cm<sup>3</sup>) and bone muscle, fat and fat muscle area ratio (%). The image processing and analysing software, Image J (Schneider et al. 2012) was then used to convert the files into a RGB format and then into .tifs. Details of further image processing can be found in Study one. For Study 3 bone image scans were taken at three time points; baseline, 6 months follow up and at the 12 months follow up.

### **6.2.3.2 Dual-Energy X-Ray Absorptiometry**

#### *Whole body DXA Analyses*

The DXA results were generated in report form automatically. The analysis depends on regions which can be edited post-scan. For Study 3 the bone was analysed as the head, spine, left and right arm, trunk, pelvis and leg. For body composition the left and right arm, trunk, pelvis and leg and Android and Gynoid regions. The former was the area between the arms, with the lower bound at the pelvis and upper bound 20% of the distance from the pelvis to the neck. The latter was the area between the legs, positioned 1.5 times the height of the android below the pelvis line, extended down by a height two times that of the android

region. Analyses of the total body include total mass, bone mass index ( $\text{kg}/\text{m}^2$ ), total percentage fat (%), and for both total body and individual regions; bone mineral density ( $\text{g}/\text{cm}^2$ ), bone mineral content (g), total mass (kg), fat (g), tissue (% fat) and lean mass (g). Further details of the results of these can be found in Chapter six.

### **6.2.3.3 Assessment of bone health**

The lunar iDXA (GE healthcare, IL, USA) and Stratec XCT 2000 pQCT (STRATEC Medizintechnik, Germany) were used to assess bone health. In this study, bone health was assessed through the measurement of bone structure through bone mineral density, bone mineral content and bone geometry through cortical and trabecular bone area and second moment of area. For these studies a used to analyse body composition and BMD.

## **6.2.4 Questionnaires**

### **6.2.4.1 Assessment of Quality of Life, activity levels and lifestyle**

On arrival for each testing session, participants completed a number of questionnaires which provided detail on participant's lifestyle which could influence changes in bone. To determine quality of life and lifestyle each participant filled in a Short form 36 (Ware and Gandek 1998) and an ARTD lifestyle questionnaire. The international physical activity questionnaire (Craig et al. 2003) and respectively to determine mobility and normal levels of activity. A bone specific physical activity questionnaire (BPAQ) (Weeks and Beck 2008) was also completed to quantify a baseline level of bone health for each individual. This was repeated at the conclusion of the study to be able to monitor any changes in levels of activity. The Short form 36 and international physical activity questionnaire were filled out at every visit, to control for self- negated physical and mental health.

### **6.2.5 Movement Analysis**

Prior to any movement analysis the participant's height and mass was recorded using a free-standing height measure and digital scales (Seca, Birmingham, UK). Spherical reflective markers were then attached to participant's body, to identify anatomical landmarks used to track movement (see Chapter Three, General methods). Participants completed all assessments wearing form fitting shorts and top and their normal everyday activity footwear, no heels were allowed. Participants completed a two-minute walk test as an assessment of gait functionality (Bohannon et al. 2014). This involves walking at as far as possible in two minutes along a set out route recording the amount of ground covered and number of strides taken to do this. Participants were also required to complete two activities for movement analysis. The first required participants to walk along a 10m level walkway making contact with a force plate with each limb until 5 complete trials are recorded for each limb. They were then asked to walk up and down a set of three steps, with each leg making contact with one step at a time. Participants were asked to repeat the stair ascent and descent until 5 complete trials are recorded for each limb under each condition. During this time, a nine-camera motion capture system (Qualisys, Gothenburg, SE) sampled movement (kinematic) data at 100Hz, whilst the force platform sampled synchronous force (kinetic) data at 500Hz. By participating in stair climbing, data was collected for a comparatively higher biomechanically demanding task than level walking. This was then compared to current literature to ensure that participants are displaying a 'normal' gait pattern, thus making the bone variation more representative of the general population.

#### **6.2.5.1 Staircase**

Biomechanical analysis of stair climbing using instrumented staircases is relatively commonplace (Andriacchi et al. 2008), although space restrictions often necessitate a

portable staircase design. The staircase used for this study was designed and commissioned especially for the use in the lab at Nottingham Trent University.

### *Set-up*

The staircase was constructed of six hollow wooden blocks (Figure 67), stacked and secured using heavy duty latch clamps. Recesses were cut into the bottom two steps of one side and each step on the other side to allow for a variation in force plate placement and staircase configuration. For the purpose of this study the two portable Kistler (Model 9286B and Model 9260AA3, Kistler, Winterthur, Switzerland respectively) force plates sat in recesses in the bottom two steps where the top step is void of recess (Figure 67). The motion of the markers was tracked in three-dimensional motion capture using eight walls mounted motion capture cameras (Oqus; Qualisys AB, Gothenburg, Sweden) cameras and five tripods mounted portable motion capture (Oqus; Qualisys AB, Gothenburg, Sweden) cameras, including one high-speed camera at a capture rate of 100HZ. Forces were recorded across a floor embedded AMTI force plate (Model OR6-7-200, AMTI, Advanced Mechanical Technology, Inc. Watertown, MA, USA) and two portable Kistler force plates (Model 9286B and Model 9260AA3, Kistler, Winterthur, Switzerland respectively). The staircase was placed against the edge of the ground embedded AMTI force plate so as not to interfere with the force plate. A validation study was conducted to determine the most accurate method of identifying the location of the portable force plates within the staircase (See appendix A for further details).

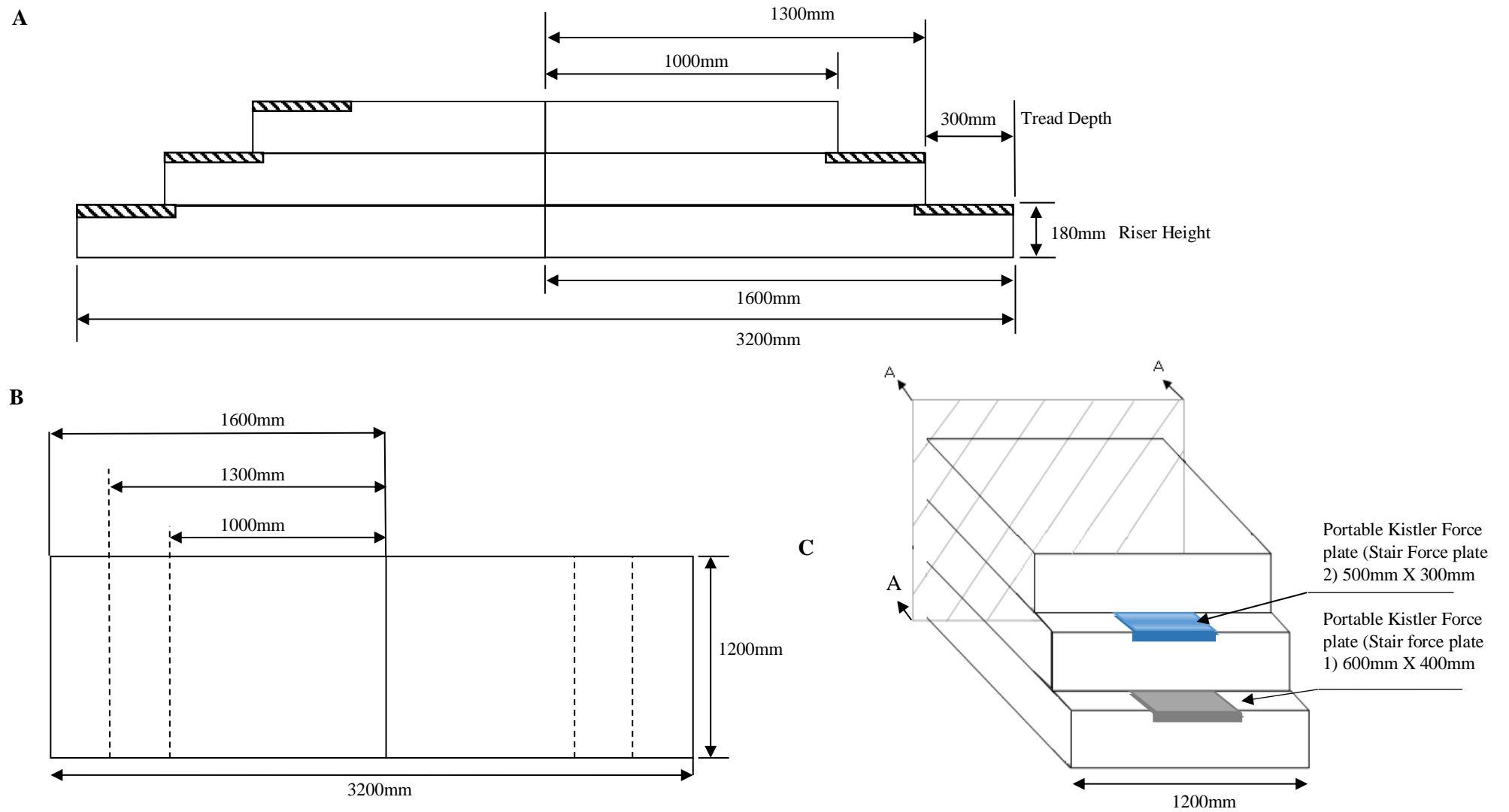


**Figure 67: Engineering drawings for the staircase. A; the side view of the staircase with  sections detailing the recesses. B; the plan view and C; the isometric view of the staircase with the two force plates placed in the recesses.**

It was concluded from the validation study that, due to the minimal difference in kinetic variables between the two different kinematic methods to the reference method (Cal-Tester), either method can be implemented to accurately identify location. It was decided that Method B, using two markers placed at the front corners of the force plates and using platform dimensions to generate the remaining coordinates, would be used during a testing session. This enabled efficient testing set-up whilst still obtaining accurate locations for the force plates.

### **6.2.6 Processing of data**

All biomechanics data was processed as described in the general methods section. The loading rate was calculated from time (s) it took from foot contact to reach the maximum GRF force (N) normalised to body weight in the first half of stance phase, see equation below

$$\text{Loading Rate} = \frac{\text{Max GRFv} \left(\frac{N}{BW}\right)}{\text{time (s)}}$$

GRFv= maximum vertical Ground Reaction Force normalised to body weight.

Time (s) = the time taken to reach the maximum vertical Ground Reaction Force in early stance.

### **6.2.7 Dependant variables**

In order to determine changes in bone health, total bone mineral density ( $\text{mg}/\text{cm}^3$ ) and total bone area (%) was measured at the 4, 14, 38 and 66% tibial length sites. Bone scan images taken from the pQCT were used to investigate outer geometry using the landmarks generated by the image processing method described in Study One (Chapter Three).

In order to measure gait variability, the two minute walk test was used. This has been used in previous publications investigated clinical gait, as a way to assess the variation (Brooks et al. 2002; Grimpampi et al. 2015). In repeating this in an able bodied population, gait functionality can be analysed and variation assessed to ensure consistency of healthy gait.

The variability in vertical GRF (N) was also investigated. As the GRF is a measure of the forces exerted on the body by the ground and is equal and opposite of that from the limb. As bone changes are driven by strains which are generated by forces exerted onto the bone, variation in GRF could also infer variability in bone parameters. The original study design allowed for comparisons of joint kinematics between the able-bodied cohort and LLA. These were not analysed due to LLA not being recruited into the study.

### **6.2.8 Statistical analysis**

As a result of LLA not being recruited into the study, data is presented on an individual basis. Each participant's kinetics and bone health parameters were analysed as a case study. The coefficient of variation was used to determine the individual variation across the duration of the study.

## **6.3 Results**

### **6.3.1 Variation in bone structure and geometry**

All participants had a T and Z score that determined their bone mineral density to be healthy as defined by the world health organised (see Chapter Two for further information). At an individual site level, the CV for total bone mineral density was below 5% for the majority of participants. Only one participant, P02 showed more variation, with 11% variation at the

4% site. Figure 68 and 69 show the individual variation across the scan sites for each participant.

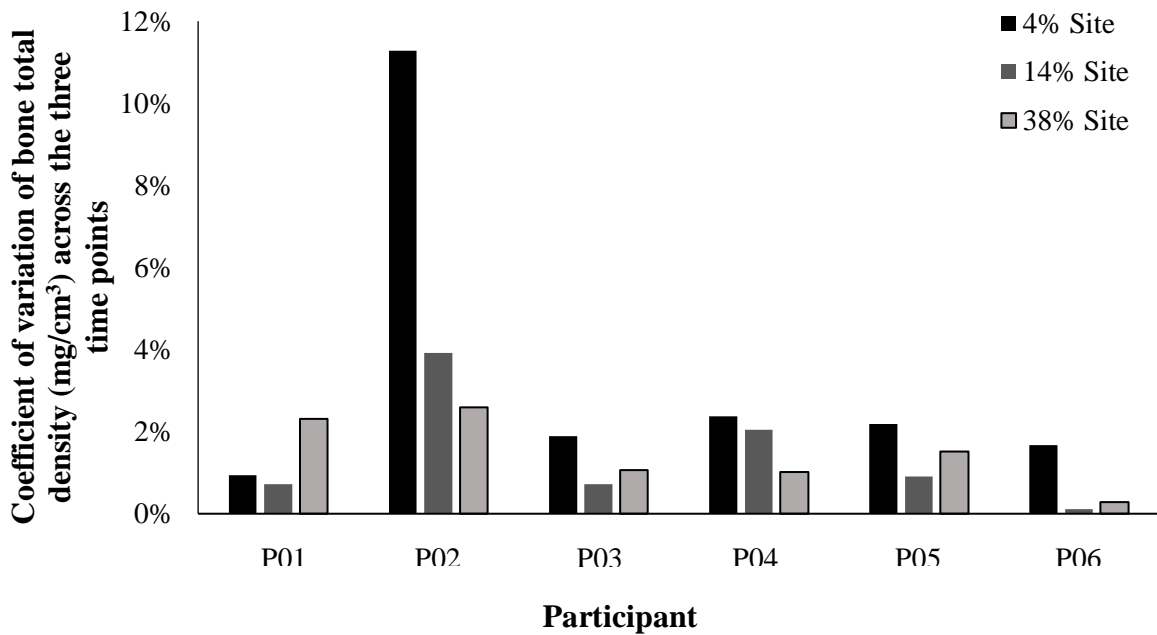


**Figure 68:** The coefficient of variation across for the total bone density across all three time points for each participant. At the 66% the muscle mass is the main measurement and therefore no bone density was processed.

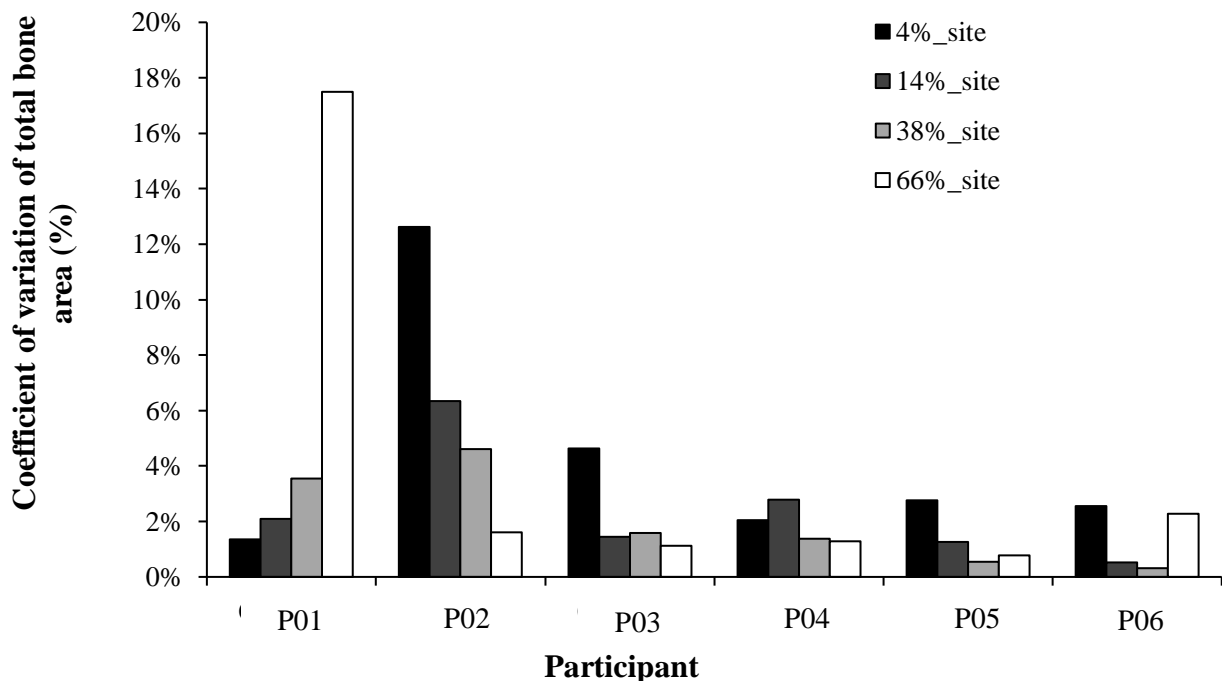


**Figure 69:** The coefficient of variation of total bone area, calculated from the mean and standard deviation across the three time points. The solid black bar denotes 4% and the white bar denotes 66% and the shades of grey in between show the 14 and 38% sites respectively.

For the majority of participants, the greatest variation was in the 4% site, where there is mostly trabecular bone. In participant P01 the greatest variation was at the 66% site, with 18% variation across the time points.

There was no trend across the time points, concluding this to be variation rather than an absolute change. Bone mass can also be used to assess this change. The trend in bone mass does not follow that shown in the bone total area across all participants. Participant 4, 4% site, visit 3 and 5, had a consistent total bone mass value of  $3.84\text{g/cm}^3$  and yet the bone area decreased from  $11.32\text{ cm}^2$  to  $11.165\text{ cm}^2$ . Further explanations can be derived from the outer cortical perimeter plotted from the image processing.

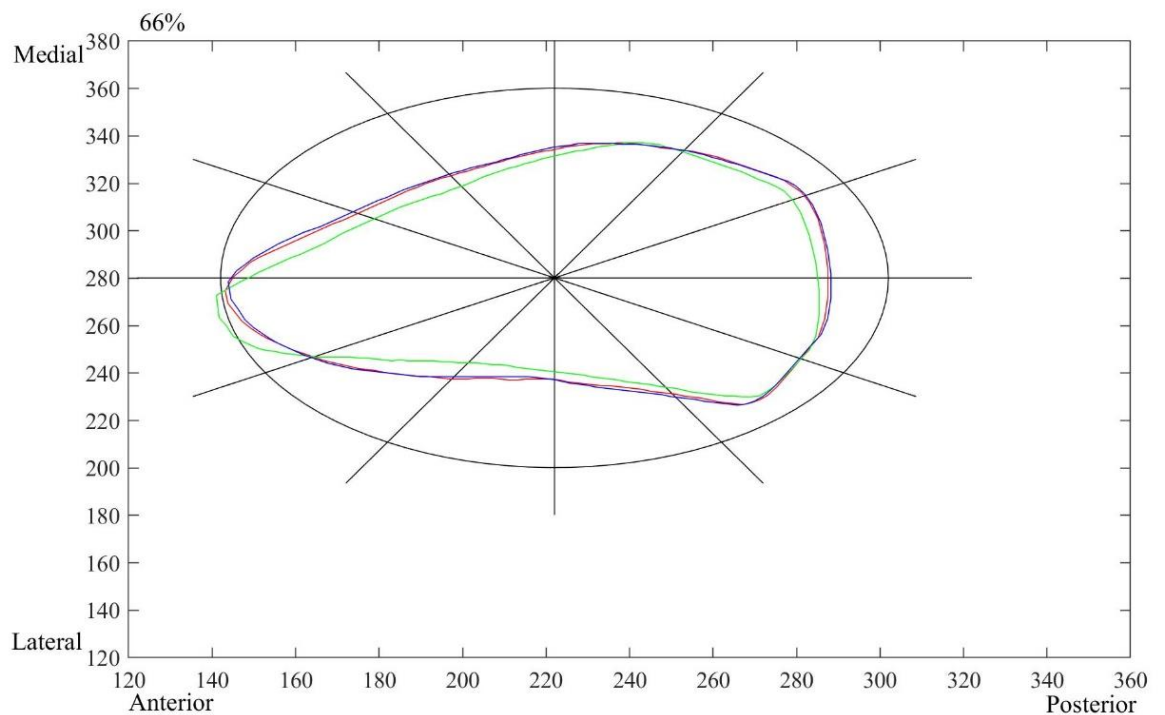


**Figure 70: The outer perimeter of P01 tibia at the 66%, generated from the pQCT and image processing method as developed in study one and two. The Red line represents scan 1, green line scan 3 and blue line scan 5. The black line is a circle and us used as a reference shape.**

Figure 70 shows the scan1 and scan 5 outer perimeter plot to have low geometrical variation, where-as scan 3 has visible differences. Table 4 shows the values for the total bone area, which reflects the differences seen.

**Table 19: The total bone area across all scan time points for participant one, P01 at the 66% site.**

	Scan time point	Total Bone Area (mm <sup>2</sup> )
P01_66%	1	918.25
	3	1107.75
	5	932

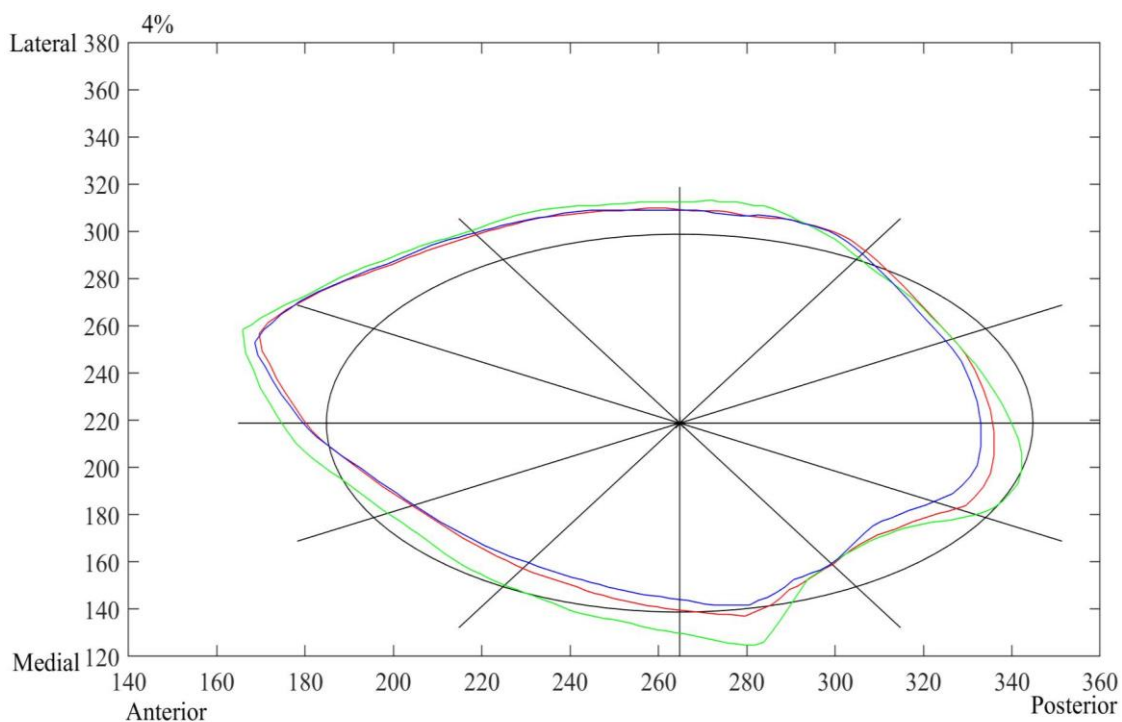


**Figure 71: The outer perimeter of the P02, at the 4% site. The red line represents scan 1, green line is scan 3 and the blue line is scan 5.**

The other participant where high variation in bone area was seen was participant P02. The geometrical plot shows that scan1 and scan 5 to be geometrically similar, whereas, scan 3 has a higher geometrical variation. The larger variation seen in outer geometry is reflected in the same pattern of variation in both total bone area and bone trabecular area. The trabecular density however showed the opposite pattern with a decrease in density at the same time point there was an increase in total bone area and trabecular bone area.

**Table 20: The Total Bone area for each scan time point, for participant P02, scan site 4%.**

	Scan time point	Bone Area (mm <sup>2</sup> )
	Total	
P02_4%	1	1340.25
	3	1465.75
	5	1300.25

### 6.3.2 Variation in biomechanics

#### *Two-minute walk test*

Table 21 shows the coefficient of variation for both the distance covered and the number of strides taken across repeated two- minute walk tests.

**Table 21: Coefficient of Variation (%) for distance covered and strides taken by each participant across the five visits.**

Participant	Distance covered (m)	Strides taken
P01	6%	3%
P02	3%	1%
P03	5%	2%
P04	10%	5%
P05	4%	3%
P06	4%	2%

The values of coefficient of variation are low, especially in number of strides taken. The largest coefficient of variation is related to a standard deviation of 12m, which is just over one lap of the 2-minute walk test circuit. The general trend of the distance covered over the number of visits was negative in all but one participant. This was not reflected in the number of strides taken, with a general trend not expressed with the same clarity.

### Ground reaction force

Figure 72 displays the max GRF for the dominant leg of all participants across each time point. P02 displays the greatest variation in max GRF, with a coefficient of variation of 15%. This is larger than the variation seen in the other participants where a maximum CV of 10% is seen. There was no consistent trend between time points, but overall all participants showed a decreased in GRF at visit 5 compared to visit 1.

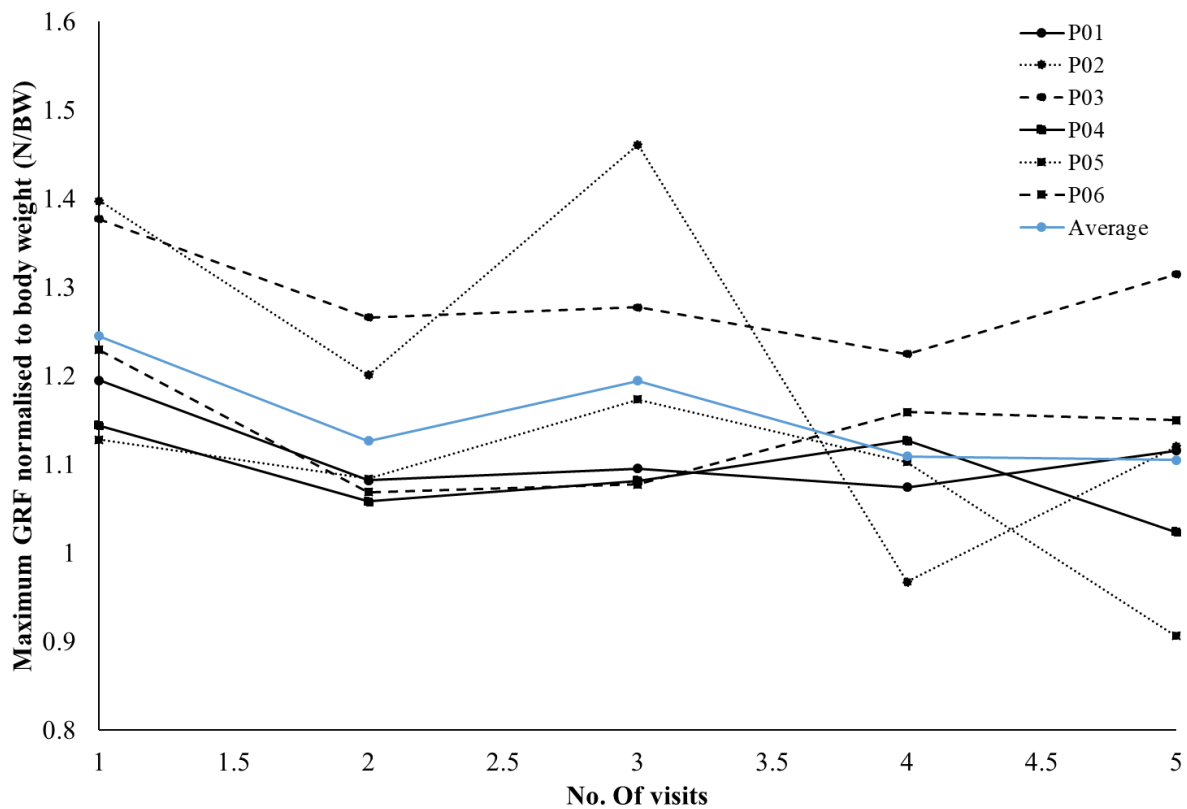


**Figure 72: Max vertical GRF across the gait cycle for each visit. The overall average across all participants is also presented.**

## Stair Walking

Figure 73 shows the max GRF for the right leg across all force plates. The CV for individual force plates across time points can be seen in Table 23 and 24.

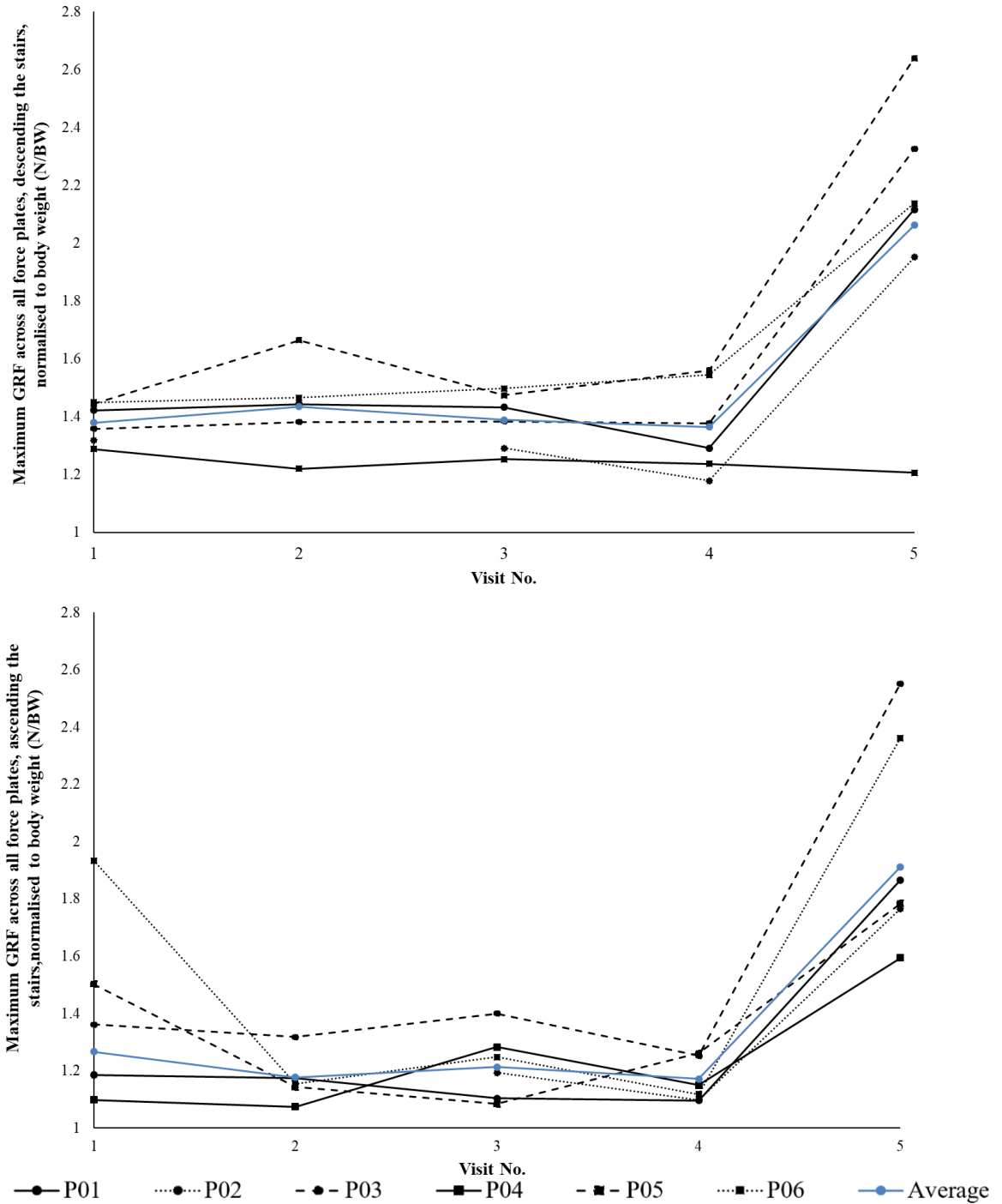


**Figure 73: The average maximum ground reaction force across all force plates (ground force plate, first step force plate and second step force plate) for both ascending and descending the staircase.**

All participants had a considerably higher maximum ground reaction force at the last visit of the study for both ascending and descending the staircase. The variation across the cohort for maximum ground reaction force was smaller when participants descended stairs than ascended. Table 22 and Table 23 show that there is increased variation in the force when recorded for the force plates within the stairs, specifically the first step.

**Table 22: The coefficient of variation across all visits for right leg contact on each force plate when ascending the staircase.**

Participant	Coefficient of variation		
	Ground force plate	Stair force plate one	Stair force plate two
P01	6%	33%	33%
P02	9%	30%	35%
P03	34%	32%	27%
P04	17%	25%	26%
P05	5%	32%	32%
P06	35%	35%	35%

**Table 23: The coefficient of variation across all visits for right leg contact on each force plate when descending the staircase**

Participant	Coefficient of variation		
	Ground force plate	Stair force plate one	Stair force plate two
P01	15%	32%	11%
P02	23%	35%	3%
P03	18%	38%	19%
P04	6%	2%	4%
P05	7%	26%	23%
P06	28%	7%	39%

## 6.4 Discussion

The aim of this study was to analyse the variation in tibial bone geometry and structure, level walking gait and stair ambulation over a 12-month period. The first objective was to analyse tibial bone geometry and structure, this was assessed through internal bone area measurements as well as outer geometry generated from the image processing code developed in Study One and bone mineral density. Highest variation in bone properties was seen at 4% of tibial length, for the majority of the participants. The two participants who demonstrated the largest variation in bone area were also processed through the image processing code from Study one. The outer geometry plots reflect the same trends seen in the bone area, providing further validation to the image processing code. The changes seen in this study measure larger than the 2mm error associated with the image processing code, concluding that this natural variation and not as a result of error associated with the image processing code. Studies, which have investigated bone geometry changes using outer geometry plots, have reported much smaller changes. A ten-week military training intervention found increases in tibial area of up to 2mm (Izard et al. 2016b) with changes almost reaching significance at the 14% and 38% sites with no changes seen at the 66% site. However, this investigation was only over ten weeks and the natural bone remodelling cycle is on average 200 days with 20-40 days of bone resorption followed by bone remodelling (Eriksen 2010). Therefore, the bone may have not had sufficient time to adapt to the training intervention. The participants within this study that showed greatest amount of variation also showed greatest difference in the follow up bone physical activity questionnaire (BPAQ) score, suggesting that their level of exercise had changed over the course of the year. As bone remodelling is dependent on mechanical stimulus, the fluctuation of loads needs to also be considered (Ruff et al. 2006).

The second objective was to investigate the change in walking gait in able-bodied subjects over a twelve-month period. Two-minute walk tests were used to assess mobility, as within a clinical population, measuring distance covered and strides taken (Reid et al. 2015). Maximum GRF was analysed to determine if the magnitude of loading is subjected to significant change over the course of a year. The results from this study show that within an able bodied population, there was less than 10% coefficient of variation in distance covered and less than 5% variation in strides taken within the two minute walk test. In comparison to other studies, the variation found here is greater than reported (Bohannon 2017; Selman et al. 2014). The consistent stride number but higher variation in distance covered suggests that self-selected walking speed is more varied. Walking speed has been found to have a negatively linear relationship to variability in stride intervals across all ages. (Chien et al. 2016). However, stride to stride variability, a measure of stability was seen to deteriorate above the age of 50 years, although this was reported to not change significantly with increasing age beyond 50 years. The participants within this study were not grouped based on their age, but with variability being reported to be a factor of age, further analyses should take this into consideration.

Maximum GRF was analysed to determine if the magnitude of loading is subjected to significant change over the course of a year. All participants were right leg dominant, although this did not reflect a larger max vertical ground reaction force, as loading was found to be within 0.01N/BW across limbs. The coefficient of variation was below 10% for all but one participant. Previous studies have stated that a CV value of below 12.5% for gait data is an acceptable level of force data variability (Wang and Watanabe 2000). The variation in ground reaction force cannot be explained by a change in participant mass or be identified by any changes in the participant's 2MWT data, therefore it can be concluded to be as a result of natural variation. Previous literature researching GRF variability in gait is limited.

So this study provides a novel insight into the natural variation of GRF in able-bodied subjects for level walking.

Ground reaction force variability was also assessed for stair walking. The variation in vertical GRF for stair walking was found to be higher than that when level walking. This is in agreement with previous literature (Luder et al. 2007). Although the variability reported here was considerably higher, maximum of 38% compared to 12.4% reported by Luder et al. (2007). They recorded variability as a measure of clinical rehabilitation in participants post hip surgery with a third group acting as control. Also their staircase had smaller dimensions, therefore would be a less demanding task. Other publications which report variability in stair climbing, use it as measure of reliability of their repeated measures rather than as an independent variable (Leitner et al. 2011). The high variability in gait parameters associated with stair climbing is stated within publications as justification for not including it in their research, resulting in limited data for comparison (Saxer et al. 2015).

Gait variability research, specifically GRF variability is limited. Measures of gait variability provide insight into a person's stability and potential muscle function. In understanding the natural variation within an able-bodied group a deterioration can be easily identified. Not only is this useful in the management of age and the known decrease in proprioception but within clinical populations.

### **6.5 Limitations and Future directions**

The activity levels outside out of the laboratory visits could not to be controlled. Therefore it cannot be guaranteed that changes in bone geometry and structure were due to natural variation and not as a result of changes in activity levels or activity type. A bone physical activity questionnaire was filled in at the start and end of the study to monitor if the activity

levels had changed over the year. The other way to monitor this would be an exercise diary as well as a pedometer to track the activity levels of all participants.

This study used previously validated gait measures, including the two minute walk test. The methods that were used in previous studies include instructing participants to walk as fast as possible, or cover as much ground as possible (Bohannon 2017). This study instructed participants to walk with purpose, therefore the 2MWT reported could be an underestimation.

This study only investigates a small cohort of able-bodied subjects, this first needs to be expanded in order to establish a normative variation margin. The results from the study can then be analysed further to understand the variation of each aspect of bone. Further to this, objectives 3 and 4 was to investigate the variation in bone structure and geometry as well as gait in lower limb amputees. The reason this was not fulfilled in this study was due to reasons stated in Figure 65. To overcome these issues whilst still maintaining scientific rigour, LLA participants could be recruited post the originally stated *up to a year after receiving their definitive prosthesis*. By increasing this, the number of potential participant's would be increased and thus increasing the likelihood of recruitment into the study. The most common reason for exclusion was that participants were smokers. Smoking in itself is a risk factor for amputation, therefore it is more likely that a LLA would also be a smoker. In order to recruit this population, the increased bone fracture risk must be included as a limitation or a method of smoking related changes must be introduced.

## **6.6 Conclusion**

Within a healthy able-bodied population there is a natural variation in gait across a 12-month period. Potentially as a result of this, there is also variation in bone mineral density and bone

area. In previous literature these bone geometry and structural measures have been used to define bone health without consideration for natural variation. Therefore, natural variation in bone gait changes and bone changes must be taken into consideration when investigating bone health within clinical populations or populations undergoing intervention.

# **7 STUDY FOUR: THE USE OF JOINT RESTRICTION IN ABLE BODIED INDIVIDUALS TO SIMULATE THE TEMPORAL- SPATIAL, GROUND REACTION FORCES AND KNEE ADDUCTION MOMENT ADAPTATIONS SEEN IN LOWER LIMB AMPUTEES.**

## **Dissemination of research**

### **Conference presentations**

Brown, O., Sale, C., Barnett, C. T., (2018) Investigating the effects of joint restriction to simulate prosthetic gait on loading and movement asymmetries in able-bodied individuals.

World Congress of Biomechanics Dublin Ireland

## 7.1 Introduction

When investigating amputation related mobility adaptations and subsequent bone health, the influence of the co-morbidities and the participant's prior health state needs to be considered. Lower limb amputations are most often as a result of dysvascular diseases, including diabetes related complications, atherosclerosis and peripheral arterial disease (PAD) (Ahmad et al. 2016; Stewart, 2008; Glaser et al. 2013). The majority of amputations within the UK and USA are as a result of dysvascular diseases (Moxey et al. 2011; Stewart, 2008). Risk factors of developing these diseases include aging, smoking and a poor diet, which independently have an effect on bone health. The incident of amputation increase in those over 50 years of age, with the average age of an amputation in the UK in 2015 was 68-70 years old (Davie-Smith et al. 2015; Stewart 2008). At the age of 25, bone reaches its peak mass, after which natural bone degradation occurs (Campbell, 2012). So irrespective of amputation, those in their advanced years are already at a higher risk of poor bone health. Smoking impairs the bone's ability to form bone, leading to a decrease in bone mineral density. The lower BMD has been linked to an increase of fracture risk by 25% in a general population (NCSCCT 2012). Diabetes related complications have been reported to contribute to over two thirds of vascular amputations (Ziegler-Graham et al. 2008). As an independent health condition, diabetic patients have increased BMD compared to non-diabetic patients, although they also have increased incident of bone fracture (Lecka-Czernik 2010). It is postulated that the increased bone fracture risk is due to biomechanical adaptations within the bone (Lecka-Czernik 2010). Specifically, the increased insulin levels caused an increase in bone mass by decreasing both bone resorption and formation results in an increase in bone fragility and stiffness (Huang et al. 2010).

It is also known that amputees have a higher risk of developing osteoporosis and osteoarthritis in their intact limb (Smith et al. 2011; Sherk et al. 2008; Lemaire et al. 1994)

with knee osteoarthritis the most prevalent form of the disease (Chehab et al. 2014). Research has found that an increased GRF, loading rates and knee adduction moments are contributing factors to the progression of osteoarthritis (Chehab et al. 2014; Lloyd et al. 2010; Brandon and Deluzio 2011, Esposito and Wilken 2014). The increased magnitude and rate of loading compresses the cartilage and impedes its ability to distribute the forces across the knee evenly (Radin and Paul 1971). Studies have also shown progression of the osteoporosis to increase by almost 7 times when the adduction moment increases by 1% (Miyazaki et al. 2002). Medial lateral knee moment is a key determinant of the distribution of the forces across the condyles of the tibia (Shelburne et al. 2005) and an increased knee adduction moment has shown to have a larger distribution of forces across the medial compartment of the knee. The increased load has been associated with the reduced cartilage thickness, seen in osteoarthritic patients (Chang et al. 2012; Bennell et al. 2011; Chehab et al. 2014).

It is therefore important to know if the negative changes in bone health are as a result of pre-existing conditions, lifestyle or gait adaptations including increased GRF, loading rates and knee adduction moment. With the concept of symmetrical loading pattern being beneficial for amputees being challenged, the clinical need to establish a link between biomechanical loading pattern and the maintenance of a positive bone health is imperative (Hak et al. 2014). However, the ability to mitigate or control for any of these diseases of comorbidities within an amputee population is difficult. To investigate this, there needs to be a control of bone health or gait adaptations, allowing the other measure to be manipulated.

Research has shown that using the restrictive orthotics, able bodied gait can be manipulated to reflect both transtibial and transfemoral amputee gait (Lemaire et al., 2000;

Nepomuceno et al., 2017; Vanicek et al., 2007). Specifically, the temporal-spatial gait compensations that occur as a result of amputation have been found within groups who use a prosthetic simulator, including shorter step length and a slower walking speed (Vanicek et al. 2007; Nepomuceno et al. 2017). Whilst the time taken to learn to use a prosthesis is variable depending on the individual (Baker and Hewison 1990) it has been reported to be slower in amputees than in able-bodied subjects using simulators (Vanicek et al. 2007). This allows researchers to conduct studies on able-bodied subjects after a shorter familiarisation period than would be seen within a clinical environment with those who have experience lower limb amputation.

To simulate amputee gait, researchers have used a rigid ankle-foot orthosis (Ota et al. 2014; Gulgin et al. 2017), a cast (Nepomuceno et al. 2017) and a rigid boot (Böhm and Hösl 2010) to restrict the ankle and thus simulate transtibial amputees. For simulation of transfemoral amputees researchers have used simulators (Vanicek et al. 2007) which fix the knee at approximately 90 degrees of flexion. The research presented to date does not use the same cohort to investigate both transtibial and transfemoral simulation. Across the studies there are reports of kinetic, kinematic and temporal-spatial changes, however, these do not address the simulated 'intact' limb.

The aim of this study was to investigate the changes in temporal/spatial, ground reaction force, loading rate and knee adduction moment when able bodied subjects are restricted at the ankle and both the ankle and knee through the use of a rigid ankle-foot orthotics and a transfemoral simulator respectively. Previous research has found that when walking in restrictive orthotics and prosthetics participants adopt gait similar temporal-spatial gait characteristics to lower limb amputees. Therefore it was hypothesised that (1) participants would adopt a shorter step length, slower walking speed when in restricted conditions.

Lower limb amputees have been shown to rely on their intact limb more displaying an increased vertical GRF and loading rate (Nolan et al. 2003, Gabrowski and D'Andrea 2013). Therefore, it was also hypothesised that (2) there would be an increased vertical GRF vector and loading rate in the intact limb when walking with in the restricted conditions. Lower limb amputees are also at a higher risk of developing osteoarthritis, which is thought to be as a result of a higher knee adduction moment (Gerus et al. 2013). Therefore, the final hypothesis (3) was that participants would display greater internal knee adduction when in the restricted conditions.

## **7.2 Study Methods**

### **7.2.1 Ethical approval**

Ethical approval for this study was granted by the research ethics committee and Nottingham Trent University (reference 427).

### **7.2.2 Participants**

The sample size was calculated as is defined in the general methods (section 3.2.3). The value of 1.96 was selected for  $z\alpha$  as this represents the setting of a 0.05 alpha level of statistical significance for a two-tailed hypothesis test. The value of 0.842 was selected for  $z\beta$  as this represents the setting of a power value of 0.8 which provides the study with good sensitivity with regards to false negatives. The number of time-points represents the number of visits to the lab, two familiarisation trials and then a final testing session. The stated value of the assumed correlation of repeated measures ( $\rho$ ) was selected as it was expected that there would be a high interaction effect. Specifically, the level of mobility of both the ankle-foot orthosis and the transfemoral simulator conditions are expected to improve across the study period. Whereas there isn't any expected changes in biomechanical measures within the control condition.

No previous studies have been conducted comparing two restrictive devices in order to simulate amputee gait. Instead the effect size was based on a paper by Vanicek et al., (2007) who collected temporal-spatial and kinematic data in ten able bodied participants, over three time points, investigating the learning effect of the prosthetic simulator. The effect size was calculated below:

$$\theta = \frac{(\mu_1 - \mu_2)}{\sigma}$$

Where

$\mu_1$  = The value for the walking speed under a control condition.

$\mu_2$  =The value for the final walking speed with the Prosthetic simulator

$\sigma$  = The mean value of the standard deviations for above,

Using the outcomes from this an effect size (ES) of was calculated.

**Table 24: Variables values used to determine required sample size.**

Variable	$z\alpha$	$z\beta$	n	$\rho$	ES
Value	1.96	0.842	12	0.5	5.3

Twelve healthy able bodied (mean  $\pm$  1S.D.; 21.8  $\pm$  2.5 years; 1.81  $\pm$  0.09 m; 75.4  $\pm$  9 kg) participated in this study. Inclusion and exclusion criteria were in line with those stated in the general methods section. Also, participants had to be considered active, *i.e.* they took part in physical activity, defined as “vigorous activities which made them sweat, puff or pant” (Paterson et al., 2011) at least once a week for around thirty minutes.

### 7.2.3 Experimental Set-up

This study employed randomised repeated measures, within group design. This design was selected for its scientific rigour in assessing the effect of a restrictive condition on gait, taking into account practice effects. Participants were familiarised with each condition through repeated 2-minute walk tests (2MWT). This was chosen as it is commonly used as a familiarisation test and often, the first to be used within a clinical setting (Gremeaux et al. 2012). Literature has found the 2MWT to be a good test of ambulation within the amputee cohort whilst also being a predictor of longer mobility tests such as the 6 minute walk test (Brooks et al., 2002; Brooks et al, 2001; Loyd et al., 2016; Reid et al., 2015). Once the distance covered during the 2MWT showed statistic similarity, higher than 95%, *i.e.* the difference between 2MWT distances were less than 5% participants will commence testing through three-dimensional motion capture. If, after 15 minutes of walking and participants were not within 5% of the previous 2MWT distance, but within 10% of the previous 2MWT distance, participants were considered familiarised.

Participants carried out a level walking test around a set of cones placed 10m apart. They repeated the walking trial under three conditions, which were randomised; Control (CON) in their own trainers, constraint at the ankle (TT) wearing the rigid ankle-foot orthosis and whilst constrained at the knee (TF), whilst wearing the transfemoral prosthesis simulator. Both the latter conditions restricted the left leg; therefore, the left leg within the control condition was also referred to as restricted despite its lack of restriction. In the current study, the use of a control condition was required to separate the effects of ankle/knee joint restriction on the gait from those that may be present in the participant's normal walking pattern.

## 7.2.4 Experimental Protocol

### 7.2.4.1 Simulators

For Study Three, restrictive orthotics was used to simulate LLA gait. The following details the specifications of these orthoses. To simulate transtibial gait a rigid foot-ankle orthosis was fitted to each participant. This was an Air step Walker boot in size; medium, length; long made of lightweight plastic (Promedics Orthopaedic Ltd, Glasgow, UK). The rigid foot-ankle orthosis had two sections and instead of the fitted liner, foam was permanently fixed to the inside of the shell. The participant placed their lower limb including foot into the back



shell of the boot and the participant's heel was pushed into the boot. The front section of the boot was then placed on top of the shank, this extended to the top of the foot. The three straps were then tightened around the participant's lower leg to secure the orthosis in place. The original product had air bladders on the inside of the back shell, with the option to 'inflate' the boot for individual fitting but due to the boot being used for simulating amputation rather than medical assistance, these bladders were removed. See Figure 74 for reference.

**Figure 74: The Air step walker boot used as the rigid ankle-foot orthoses, side and front view.**

To simulate trans-femoral gait, participants had an adapted trans-femoral prosthesis fitted. The trans-femoral prosthesis consisted of a carbon fibre shell which fixes the knee in 90 degrees of flexion. Four straps were then used to secure the knee and thigh segments into this shell. Attached to this was a four-bar linkage knee joint and pylon, this pylon was adjusted in length to account for the participants height. At the distal end of this pylon was a multi-flex ankle with a spring- leaf prosthetic foot which fits a UK size 7 shoe.



**Figure 75: The components on the trans-femoral simulator; A; the carbon fibre shell, B; spring-leaf prosthetic foot, C; four bar linkage knee and pylon.**

Prior to fitting, the participants left shoe was put onto the prosthetic foot to provide the same surface area and environment as the right foot. A tubular bandage was placed around the participants left leg from their mid-thigh down to shank to provide extra comfort and a more secure fit of the prosthetic simulator. The participant was also placed in a harness that secured around their pelvis and attached over their shoulders. This had a clip that attached to the ceiling that employed a locking mechanism to prevent the participant from injuring themselves if they fell.

To fit the trans-femoral prosthesis to the participant, the prosthesis was placed next to the participants left leg whilst they were standing and adjusted so that the shell sat just above the knee. The participant was then asked to place their left leg into the simulator whilst standing, using a counter as support. The straps on the carbon fibre shell were tightened

around the participant's thigh so that there was no movement at the top of the simulator. The participant was then asked to stand with their un-restricted thigh fully extended and their foot in its neutral position. According to previous literature the best fit for a trans-femoral prosthesis is when the prosthetic foot is orientated to match the intact foot and then the prosthesis is at the correct height when the pelvis was level (Long 1985). Based on this knowledge, the foot was adjusted to reflect the participant's natural stance and the height of the pylon was adjusted so when the participant was stood their pelvis was level.

Participants completed all trials in the biomechanics lab at Nottingham Trent University. Upon arrival investigators went through the participant information sheet (see appendix H), giving opportunity for participants to ask any final questions. Prior to any movement analysis the participant's height and mass was recorded using a free-standing height measure and digital scales (Seca, Birmingham, UK). Participants completed all assessments wearing form fitting shorts and top and their normal everyday activity footwear. Participants carried out the movement analysis under three randomised conditions; control (CON), transtibial simulator (TT) and in a transfemoral simulator (TF).

The transtibial simulation restricted movement at the ankle through a rigid ankle-foot orthosis (Figure 76) constructed of a rigid thermos-plastic shell with Velcro securing straps. The transfemoral condition restricted movement at the knee by fixing it in 90° of flexion, with the thigh sitting within a carbon fibre shell. Attached to this was a four-bar linkage knee joint and pylon. A standard multiflex ankle and spring leaf prosthetic foot were then attached to the distal end (Figure 77).



**Figure 76: Rigid ankle-foot orthosis worn in the TT condition, view from the side and from the front**



**Figure 77: Participant wearing the harness attached to the ceiling and fitted to the trans-femoral prosthesis. The pelvis is level (red dashed line) and prosthetic foot orientation mirroring the orientation of un-restricted foot.**

Participants were fitted to the rigid foot ankle orthosis based on the level of comfort and observation of no foot movement. The same sized rigid foot-ankle orthosis was used by all participants, with the manipulation of the boot to ensure comfort using foam and tape. The trans-femoral prosthesis was fitted to the participants whilst they were standing, this allowed for the prosthetic foot to be placed directly under the femoral head. The length of the pylon was then adjusted to ensure the pelvis was level when the participants had their non-restricted leg extended. The foot of the prosthesis was rotated to mirror the participant's abduction/adduction present in their un-restricted foot.

#### **7.2.4.2 Familiarisation**

Once these devices were fitted to the participant, they underwent a period of familiarisation. For the control condition, this consisted of one lap of the 10m walkway. For the TT condition, prior to familiarisation, participants completed one lap of the 10m walkway un-

assisted to ensure the orthosis was fitted appropriately. In the TF condition, participants were assisted by the researcher until they completed one lap of the 10-meter walkway, this was then repeated a second time un-assisted but still supported by the ceiling harness. Following this, participants then carried out a 2MWT where they were instructed to walk along a marked route for a period of two minutes. These 2MWTs were repeated until the distance covered was within 5% of the previous distance. The first lab session required a two-minute walk test, where the distance covered was within 10% of the previous distance. To prevent fatigue, participants stopped this period of familiarisation if the total duration of repeated 2MWT exceeded fifteen minutes. When this occurred in participants, they fulfilled the requirements of a less than 5% distance change within the required time frame within the next lab visit.

#### **7.2.4.3 Three-dimensional motion capture**

The set-up of the motion capture is as described in the general methods section, including process of calibration. To summarise a nine-camera motion capture system (Qualisys, Gothenburg, SE) will sample movement (kinematic) data at 100Hz, whilst the force platform, model AMTI OR6-7-2000 (dimensions: 464mm by 508mm) will sample synchronous force (kinetic) data at 500Hz.

#### **7.2.5 Data Collection**

Upon completion of familiarisation with each condition, spherical reflective markers were attached to the participant's body at anatomical landmarks. For the control condition this is consistent with the marker set defined in the general methods. Marker placement on the restrictive prosthesis/orthosis was estimated from those on the intact limb in order to track the three-dimensional motion of the body. Two visual 3D models were created to incorporate the differing masses of the two simulators and the effect this would have on body centre of mass.

### 7.2.5.1 Transtibial simulator segment definition

The upper body marker set is consistent with that defined in the general methods (see section 3.2.3.1). For the transtibial condition, the markers were named consistently with that in the control condition. Their positioning reflected that of the control condition; see Figure 78 below for diagrammatic representation of this.

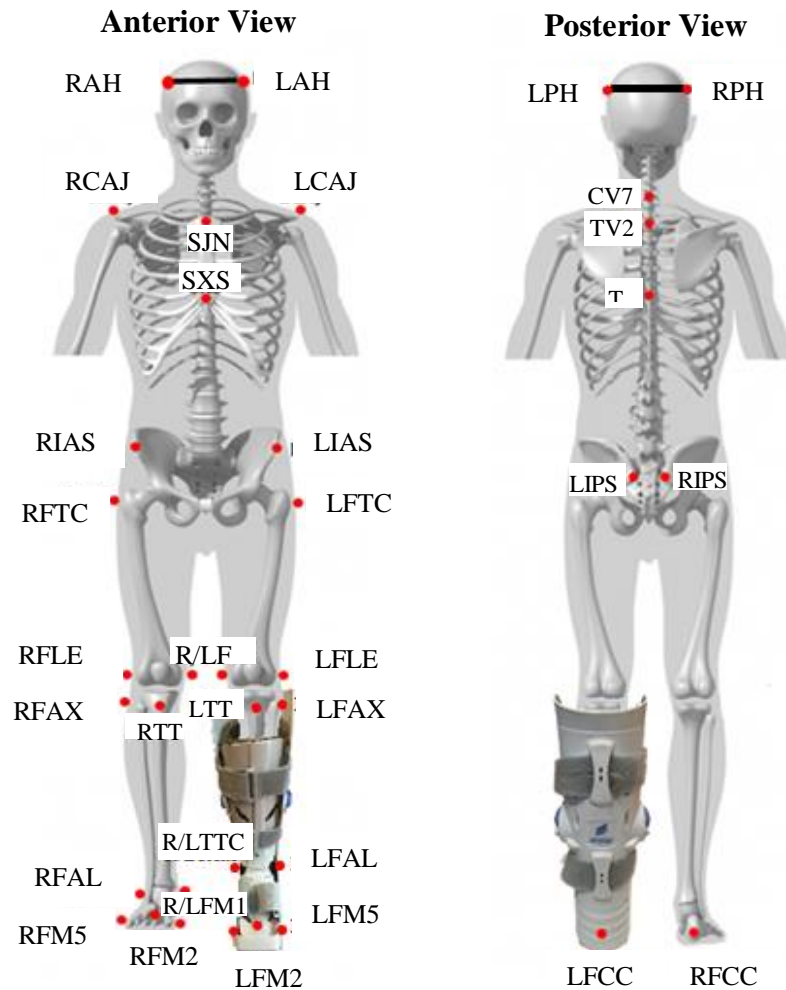


**Figure 78: The marker definitions for the transtibial condition.**

The mass of the boot was added to the shank and foot segment of the model so as the segment masses were defined as follows;

Foot

$$(0.0145 * \text{body mass}) + 0.25\text{kg}$$



**Table 25: The additional definitions of the marker set included in the prosthetic simulator.**

Abbreviation	Expansion	Description
LPC1	Left Prosthetic Cluster 1	Cluster is placed on the front of the
LPC2	Left Prosthetic Cluster 2	prosthetic thigh segment and markers are
LPC3	Left Prosthetic Cluster 3	identified from top left and labelled
LPC4	Left Prosthetic Cluster 4	clockwise.
LPFME	Left Prosthetic Medial Femoral Epicondyle	Markers placed on the thigh prosthetic segment where the distal aspect of the medial part of the knee as it sits inside the prosthetic simulator.
LPFLE	Left Prosthetic Lateral Femoral Epicondyle	Markers placed on the thigh prosthetic segment where the distal aspect of the lateral knee as it sits inside the prosthetic simulator.
LPTTC	Left Prosthetic Tibial Tuberosity	Marker is placed on the shank prosthetic segment in line with the tibial tuberosity as it sits inside the prosthetic
LPmidT	Left Prosthetic mid Tibia	Marker is placed at the midpoint of the length of the pylon section of the prosthetic.
LPTAM	Left Prosthetic Medial Malleolus	Marker is placed on the distal aspect of the medial prosthetic pylon as it connects to the prosthetic foot.

LPFAL	Left Prosthetic Apex of the lateral Malleolus	Marker is placed on the distal aspect of the lateral prosthetic pylon as it connects to the prosthetic foot.
LPFM1	Left Prosthetic first metatarsal head	The base of the ‘Big toe’ of the prosthetic foot
LPFM2	Left Prosthetic second metatarsal head	The base of the ‘second toe’ of the prosthetic foot
LPFM5	Left Prosthetic fifth metatarsal head	The base of the ‘little toe’ of the prosthetic foot
LPFCC	Left Prosthetic Calcaneus	The most distal part of the prosthetic foot

Prior to defining each segment, Figure 80 shows the complete lower half of the model of including the prosthetic simulator.

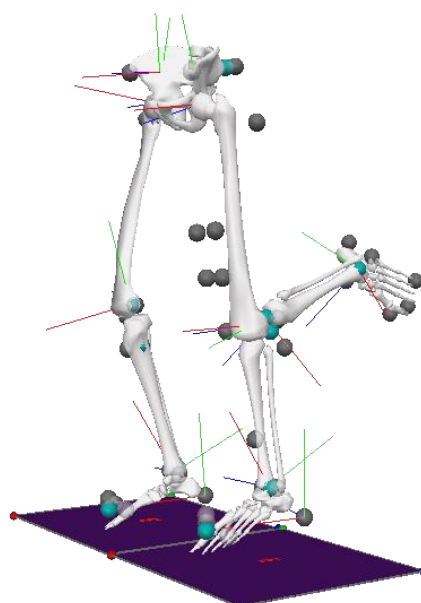


**Figure 80: The visual 3D model, where the prosthetic simulator is represented by an anatomical shank and anatomical foot in the correct physiological orientation for standing. The ‘real’ shank and foot are represented by those at 90-degree flexion from the anatomical knee.**

The following defines the segments for the left side of the body as the right-hand segments, as with the upper body, were consistent with the definitions stated in the general methods.

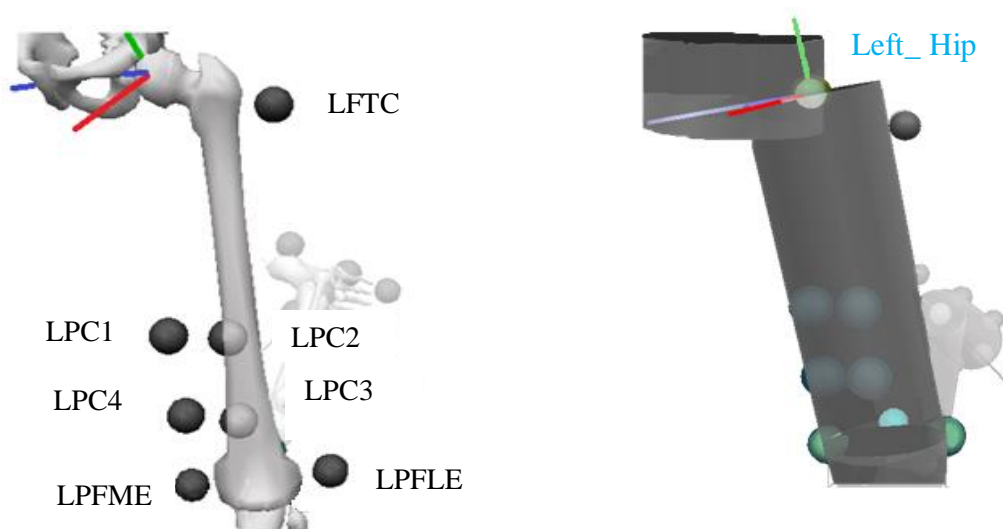


**Figure 81: Anatomical thigh segment. Markers in black and landmarks in blue.**

The definition of the left hip landmark is consistent with that in general method. The mass of the segment was defined as follows;

Thigh

$$(0.10 * \text{body mass}) + 1.85\text{kg}$$

**Anatomical shank**

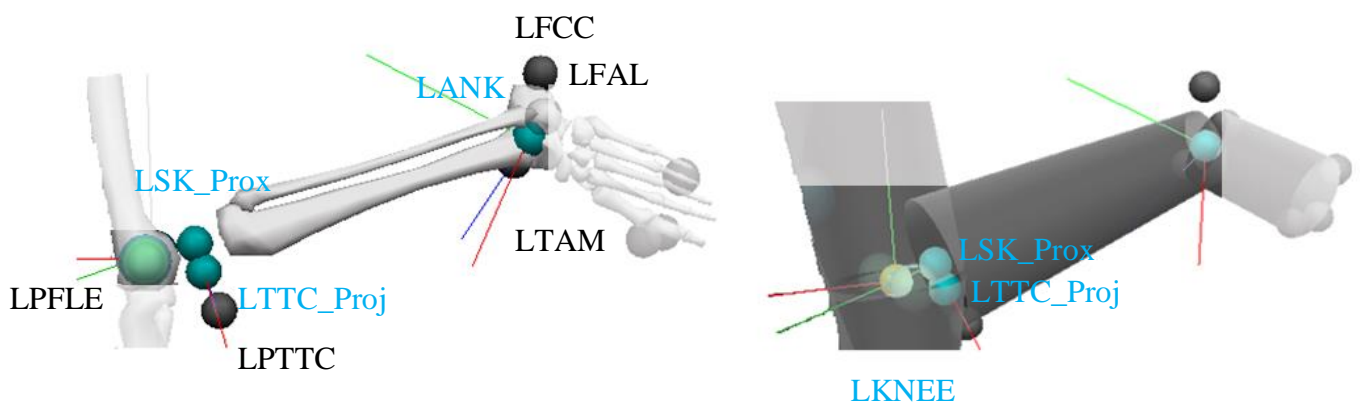


**Figure 82: Anatomical shank segment. Markers in black and landmarks in blue.**

**Anatomical Foot**



**Figure 83: Anatomical foot segment. Markers in black and landmarks in blue.**

**Table 26: Landmark definitions used to define the anatomical shank and foot.**

Landmark	Starting Point	End Point	Projected from
LKNE	LPFLE	LPFME	
LSK_Prox	LANK	LKNE	LTTC_PROJ
LTTC_Proj	LPFLE	LFAL	LPTTC
LANK	LFAL	LTAM	

**Prosthetic shank**

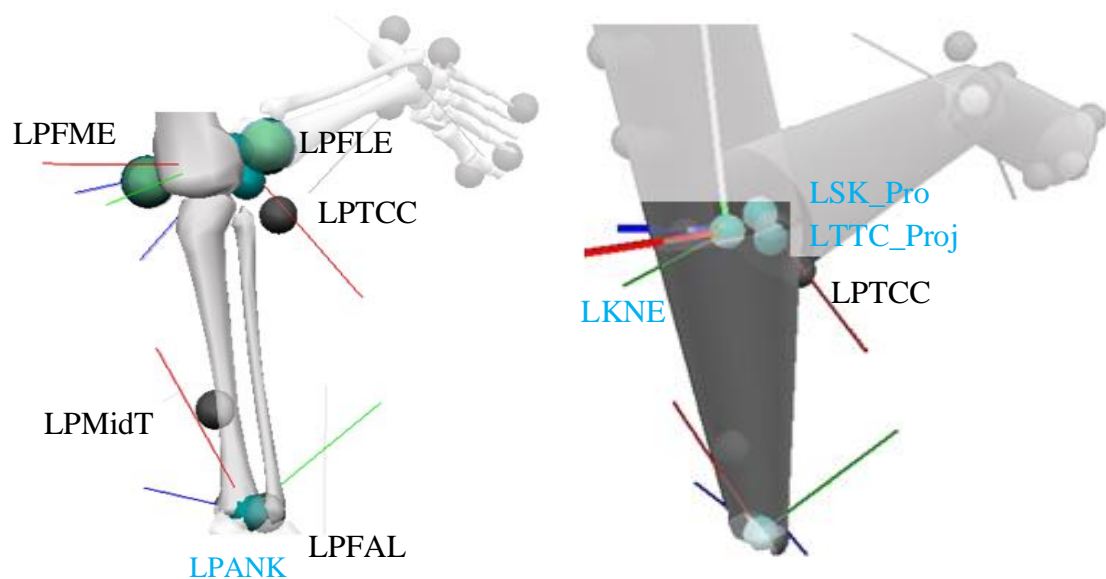


**Figure 84: Prosthetic shank segment. Markers are in black and landmarks in blue.**

**Prosthetic foot**

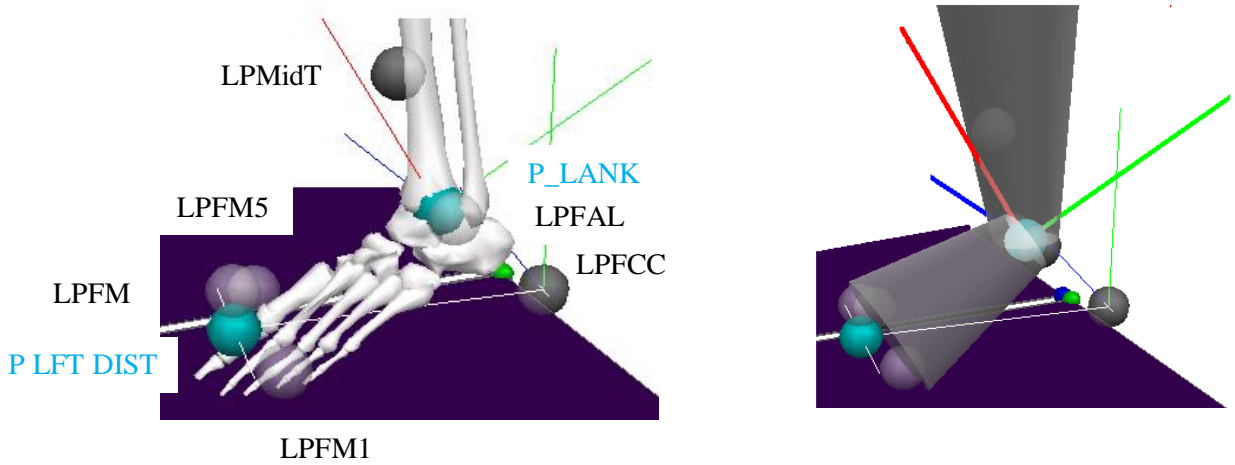


**Figure 85: Prosthetic foot segment. Markers are in black and landmarks are in blue.**

Landmark	Starting Point	End Point	Lateral object	Projected from
P_LANK	LPFAL	LPTAM		
P_LFT_DIST	LPFCC	LPFM5	LPFM1	LPFM2

**Table 27: Landmark definitions for the prosthetic segments**

The mass of the prosthetic segments was defined based on the mass of the prosthetic components themselves;

Shank = 0.90kg

Foot = 0.65kg

**7.2.6 Data processing**

Static and dynamic data was exported as a c3D file from the motion capture Qualisys and then imported into visual 3D. The dynamic data was then interpolated with a third order polynomial with a maximum frame gap of 10. A low pass butterworth filter was applied to force data with a frequency cut off of 25Hz and to kinetic data with a cut off of 6Hz.

### **7.2.6.1 Temporal-spatial Parameters**

In order to define the gait events, the kinematic method as described by De Asha et al. (2012) was used. This assumes the legs act like a pendulum and that peak hip extension occurs at the same time as heel contact. The markers at the distal and proximal foot, FCC and MF2 are transformed into the pelvis segment using the target path command. For the transfemoral condition the markers on the prosthetic foot, MPF2 are transformed. The maximum and minimum anterior components of this are used to define the heel strike and toe off within an eight-frame section of the gait cycle.

### **7.2.6.2 Loading Rate**

Loading rate was calculated using the same formula as the previous study and was defined as the time (s) it took to reach the maximum GRF force (N) normalised to body weight in the first half of stance phase, see equation below

$$\text{Loading Rate} = \frac{\text{Max GRFv} \left( \frac{N}{BW} \right)}{\text{time (s)}}$$

GRFv= maximum vertical Ground Reaction Force normalised to body weight.

Time (s) = the time taken to reach the maximum vertical Ground Reaction Force in early stance.

### **7.2.6.3 Knee Adductor Moment**

The knee adductor moment was calculated using the inverse dynamics approach, as explained in the general methods. The right hand rule was used, so the knee adduction moment was defined as a positive knee moment in the frontal plane.

### **7.2.7 Statistical Analyses**

Statistical analyses were carried out in SPSS version 23 (SPSS Inc, Chicago, USA). The analyses carried out were described in the general methods. A Shapiro Wilks test of normality was conducted and upon satisfaction of this, a parametric, analyses of variance (ANOVA) was performed. Mauchly's test of sphericity was then conducted, where the assumption of sphericity was violated, a greenhouse geisser correction was applied. Post Hoc analysis was performed with the Bonferroni correction, as a robust method for controlling for type 1 error (Field, 2013). For this study a comparison of the main effects of conditions (CON, TT and TF), legs (restricted and un-restricted) and the interaction effect between condition \* leg was analysed. Statistical significance was set at a p value of  $\leq 0.05$ .

## **7.3 Results**

### **7.3.1 Familiarisation**

All twelve participants were familiarised to the control condition within three repeats of the two-minute walk test. Eighty four percent of participants were familiarised after seven trails with the transtibial simulator condition. It took ten trials before the majority of participants, 66%, were familiarised with the transfemoral and a further three trials for 92% of participants to become comfortable with the simulator.

Figure 86 shows the change in distance covered during consecutive two-minute walk tests for the TT and TF conditions. For the control condition all participants were familiarised within two consecutive two minute walk tests. The last two trials of the TF condition show an increase in distance covered outside of the stipulated threshold of 5%. This was due to the participant reaching the point of fatigue and so the two-minute walk test no longer reflected familiarity.

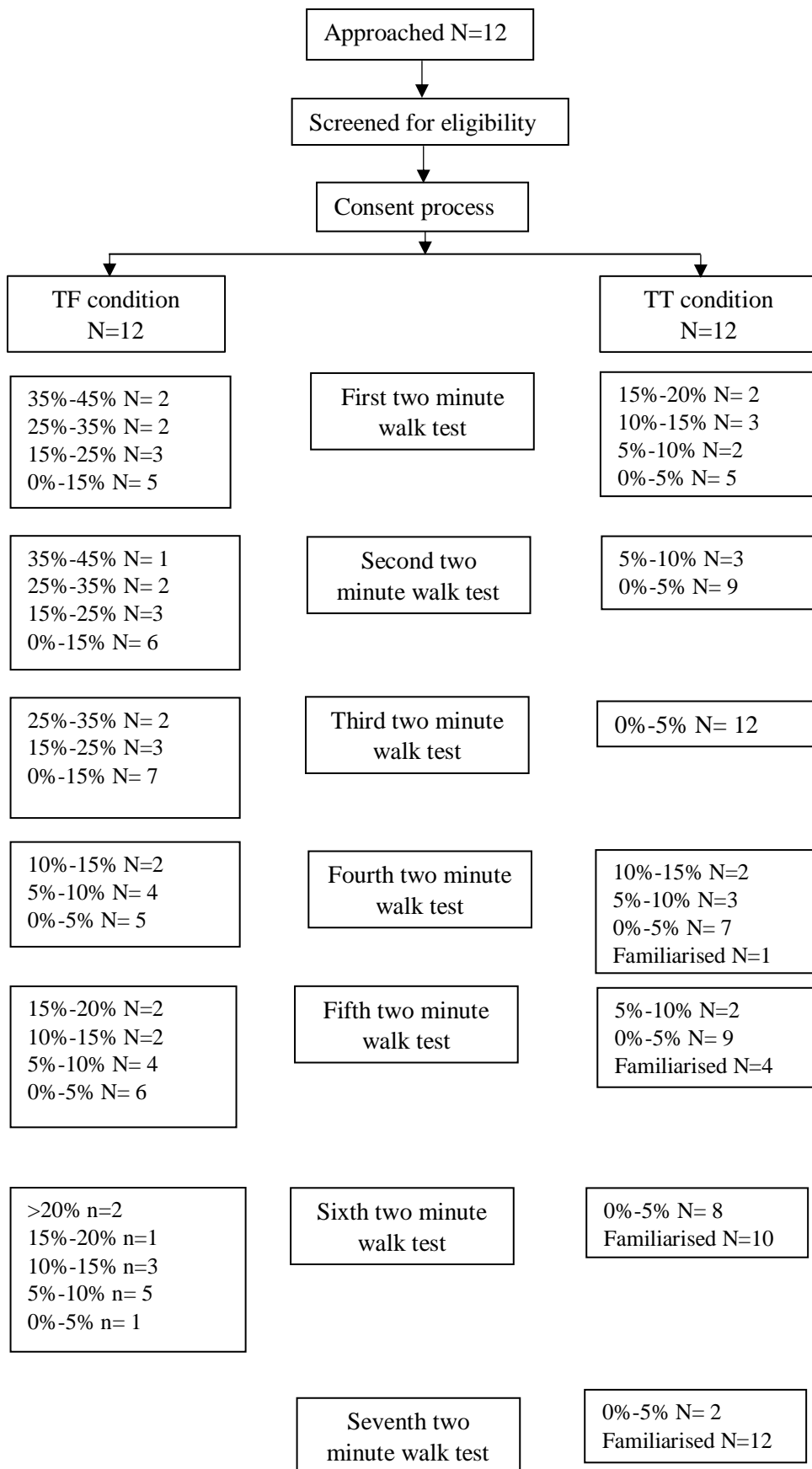


**Figure 86: Percentage change in distance walked between consecutive two-minute walk tests in meters in the transtibial condition (grey) For the TT condition (A) and TF condition (B) participants were familiarised to 5% for both lab visits for the TT condition and to 10% at lab visit one and to 5% at lab visit for the TF condition (5% and 10% familiarisation denoted by the red lines).**

### **7.3.2 Temporal-Spatial**

The temporal-spatial variables and results for each condition and limb are presented in table 12 and the breakdown of statistics including the F and p values are presented in Table 29.

There was a statistically significant difference in walking speed between condition (main effect of condition,  $F(2, 22) = 55.4$ ;  $p < 0.01$ ,  $\eta_p^2 = 0.834$ ). The walking speed was significantly greater in the control condition ( $1.47 \pm 0.14$  m/s) compared to the TF condition ( $0.76 \pm 0.16$  m/s,  $p < 0.01$ ). The walking speed was also significantly greater in the TT condition ( $1.33 \pm 0.16$  m/s) compared to the TF condition ( $p < 0.01$ ).

There was a significant difference in step length between limbs and between conditions resulting in an interaction effect (limb \* condition  $F(2, 22) = 622.735$ ,  $p < 0.01$ ,  $\eta_p^2 = .983$ ). Specifically, participants took a longer step with their unrestricted limb in the TF condition ( $102.32 \pm 14.03$ cm) compared to both the control condition ( $79.99 \pm 7.84$  cm;  $p < 0.01$ ) and TT condition ( $76.18 \pm 6.64$ cm;  $p < 0.01$ ). In the TF condition, participants took a significantly longer step with their unrestricted limb compared to their restricted limb ( $p < 0.01$ ). This also results in a statistically significant difference in step length based on the condition ( $F(2, 22) = 20.361$ ,  $p < .001$ ,  $\eta_p^2 = .649$ ), limb ( $F(1, 11) = 770.031$ ,  $p < .001$ ,  $\eta_p^2 = .986$ ). There was also a statistically significant difference in stance time between limbs and between conditions resulting in an interaction effect (limb \* condition  $F(2, 22) = 33.122$ ,  $p < 0.01$ ,  $\eta_p^2 = .751$ ). Participants spent significantly longer time in stance on their unrestricted limb ( $73.7\% \pm 0.04$ ) compared to their restricted limb ( $61.3\% \pm 0.02$ ,  $p < 0.01$ ). Participants spent more time in stance in the TF condition compared to both other conditions ( $F(2, 22) = 10.057$ ,  $p < 0.01$ ,  $\eta_p^2 = .478$ ) as well as in their restricted limb compared to their unrestricted limb (main effect of limb,  $F(1, 11) = 82.414$ ,  $p < 0.01$ ,  $\eta_p^2 = .882$ ).

**Table 28: Group mean (SD) temporal/ spatial parameters for each condition and leg**

	Control Condition		Transtibial Condition		Trans-Femoral Condition	
	Restricted	Un-restricted	Restricted	Un-restricted	Restricted	Un-restricted
Walking Speed (m/s)	1.47 (0.14)		1.33 (0.16)		0.76 (0.16)*+	
Step Length (cm)	79.78(5.89)	79.99 (7.84)	77.39(6.05)	76.18 (6.64)	12.58(10.91)	102.32(14.03)*+×
Stance time (% of cycle time)	64.2 (0.03)	65.1(0.01)	63.4 (0.02)	63.1 (0.05)	61.3 (0.02)	73.7(0.04)*+×
Swing time (% of cycle time)	35.8 (0.03)	34.9 (0.01)	37.5(0.02)	36.9(0.05)	38.7 (0.02)	25.3 (0.03)*+×
Double support time (s)	0.17 (0.02)	0.16 (0.02)	0.18 (0.02)	0.16(0.02)	0.21(0.05)	0.35(0.08)*+×
Cadence (step/min)	115.95 (17.46)	118.28 (24.19)	106.39 (12.64)	102.47 (8.97)	67.37 (7.97)	101.65 (11.36)*+×

Key; \*comparison to control, + comparison to TT condition and × between leg. Statistical significance (p< 0.05).

### 7.3.3 Ground reaction forces

The limbs were loaded at a quicker rate in the control and TT conditions compared to the TF condition ( $F(2, 22) = 27.538, P < 0.01, \eta_p^2 = .715$ ). The loading rate is higher in the restricted limb although not significantly ( $F(1, 11) = 4.487, p = 0.058, \eta_p^2 = .290$ ).

The maximum ground reaction force in the first half of stance was not significantly different between conditions ( $F(1.348, 14.828) = .397, p = 0.6, \eta_p^2 = 0.035$ ). There was a significant difference between limbs ( $F(1, 11) = 13.097, p = 0.004, \eta_p^2 = .249$ ) with the maximum GRF higher in the unrestricted limb in both the TT condition ( $1.36 \text{ N/BW} \pm 0.14, p = 0.045^*$ ) and the TF condition ( $1.27 \text{ N/BW} \pm 0.19, p = 0.126$ ).

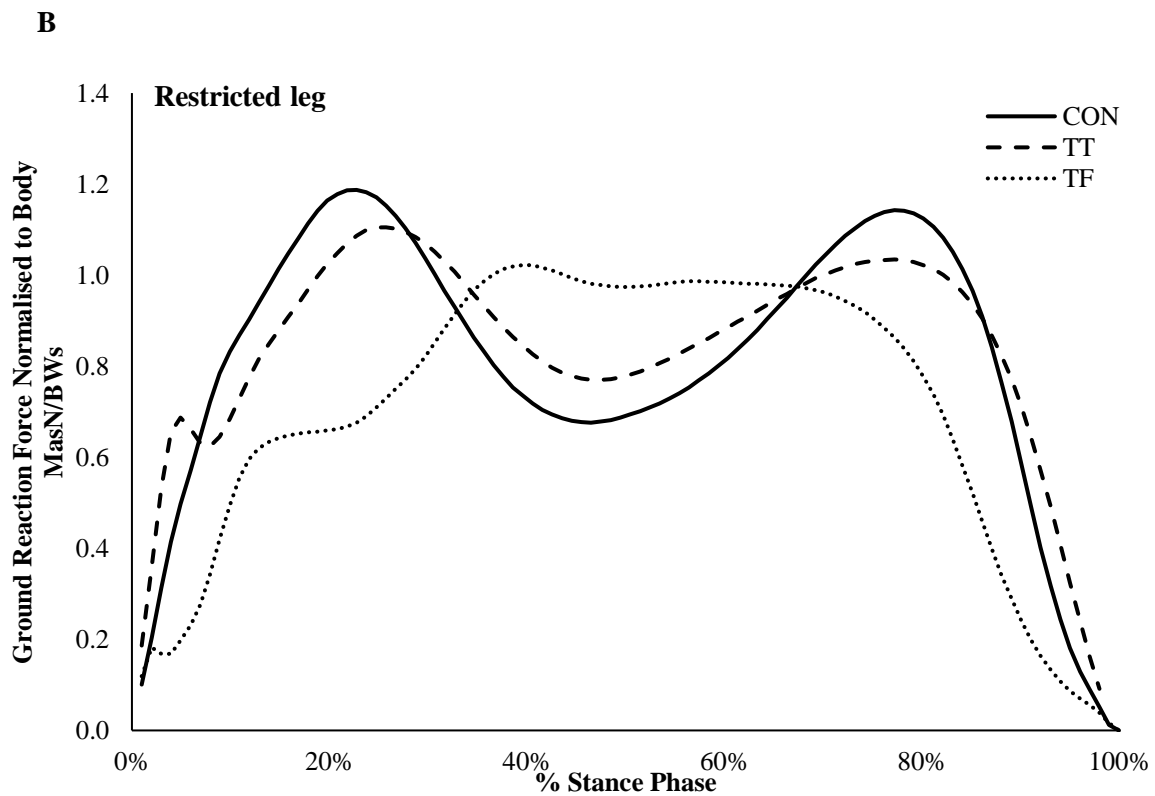
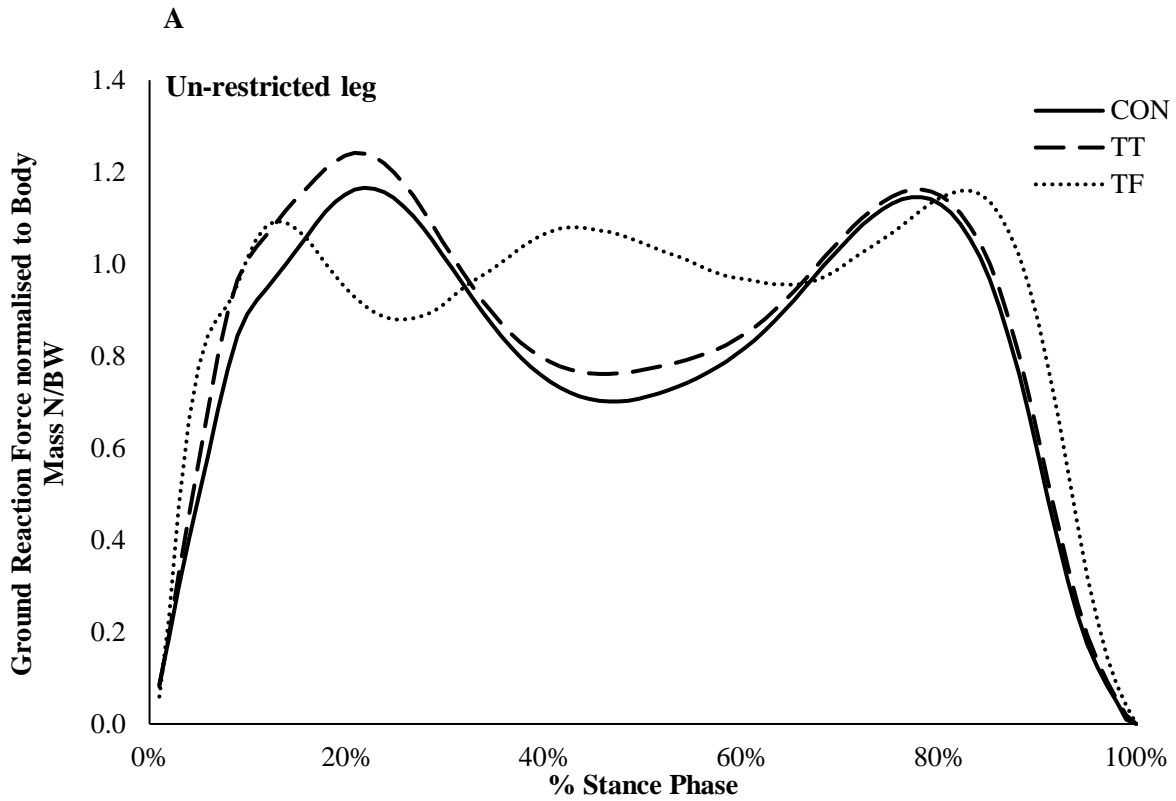


**Figure 87: The vertical ground reaction force normalised for body weight across the stance phase. A; the unrestricted leg and B; the restricted leg,**

### 7.3.4 Knee adduction moment

The average knee adductor moment was calculated for the un-restricted leg across all conditions. Larger knee adduction moments were seen in the first half of stance across the TT and CON conditions, with the maximum knee adductor moment 1 (KAM1) was greatest in the TT condition ( $F(2, 22) = 7.478$   $p = .003^*$ ). The second peak knee adductor moment (KAM2) in the TF condition occurred in the first half of stance. For statistical analysis the KAM2 for the TF condition was compared to the KAM2 for the TT and control condition which occurred in the second half of stance. In the second half of stance the maximum knee adductor moment 2 (KAM2) was greatest in the control condition ( $F(1.157, 12.723) = 6.884$ ,  $p = 0.018^*$ ).

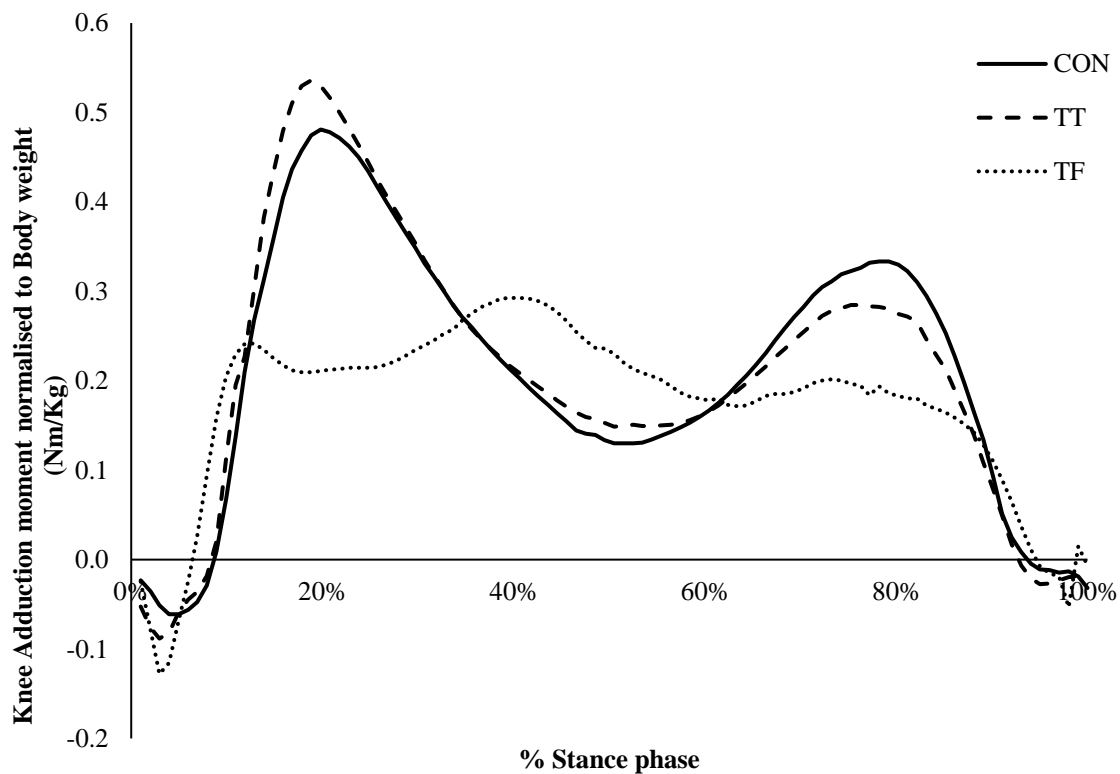


**Figure 88: Knee adduction moment normalised for body weight and walking speed for the unrestricted limb across stance phase. The first peak was KAM1 and the second peak as KAM2. For the TF condition, the first peak was KAM1 and the second peak (at ~40%) was KAM2.**

**Table 29 : Statistical properties of the temporal-spatial parameters and ground reaction force across both limbs and knee moment in the unrestricted limb. Results are presented as F and p value with \*denoting significance.**

	Main effect		Limb		Interaction effect Condition*Limb	
	Condition F	P	F	P	F	P
<b>Temporal-spatial</b>						
Walking Speed	(2,22) =55.392	<0.01*				
Step Length	(2,22) =20.361	< 0.01*	(1,11) =770.031	<0.01*	(2,22) =622.735	<0.01*
% Stance time	(2,22) =10.057	<0.01*	(1,11) =82.414	<0.01*	(2,22) =33.133	<0.01*
% Swing time	(2,22) =42.046	<0.01*	(1,11) =14.951	0.03*	(2,22) =53.560	<0.01*
Double support time	(1.097,22) =34.332	<0.01*	(1,11) =32.578	<0.01*	(1.126,22) =65.769	<0.01*
Cadence	(2,22) =22.628	<0.01*	(1,11) = 73.622	<0.01*	(2,22) =26.577	<0.01*
<b>Ground Reaction Force</b>						
Loading Rate	(2,22) =27.538	<0.01*	(1,11) =4.487	0.058	(2,22) =1.592	0.226
Max. VGRF	(1.348,14.828) =.397	0.6	(1,11) =13.097	0.004*	(2,22) =3.647	0.043*
<b>Unrestricted limb knee moment</b>						
Max KAM1	(2,22) =7.478	0.003*				
Max KAM2	(1.157,12.723) =6.884	0.018*				

## *Discussion*

Research within amputee populations have shown that an altered loading pattern results in poor bone health. However, the majority of amputations are due to dysvascular disease e.g. diabetes related complications, which independently are associated with a degradation in bone health. This questions the direct causation relationship which suggests the degradation in bone health is a result of the change in loading profiles within an amputee population. Therefore, the aim of this study was to investigate if able-bodied subjects i.e. those with healthy bone displayed the same temporal/spatial, GRF and knee adduction moment as lower limb amputees when in restricted conditions.

The first hypothesis was that participants would adopt a shorter step length and slower walking speed when in the restricted conditions. This hypothesis was fully supported in the TF condition, where the restricted limb displayed a significantly shorter step length compared to the un-restricted limb ( $p < 0.01$ ). Within the TF condition participants also had a statistically significant slower walking speed compared to both control and TT conditions ( $0.76 \pm 0.16$  m/s,  $p < 0.01$ ). This hypothesis was partially supported within the TT conditions. The step length in the TT condition is shorter than in the control condition, however not significantly. The participants walking speed in the TT condition was slower than the control condition although this did not reach significance. In literature, participants when walking in a transfemoral simulator often had a negative step length, i.e. their step did not progress past the contra lateral leg (Vanicek et al. 2007), this was experienced by some of the participants within this study, hence the short restricted leg average step length. The step length in the TT group was 77cm and 76cm for the restricted and unrestricted respectively, which is longer than those reported in literature (Lemaire et al. 1993; Schulz et al. 2010). The walking speed of participants transfemoral simulator speed was slower than the 0.96-1.04 meters/second reported for transfemoral amputees (Boonstra et al. 1993; Schulz et al. 2010). This has been found in

previous transfemoral simulation gait when compared to the equivalent amputee group (Vanicek et al. 2007; Lemaire et al. 2000). The considerably reduced walking speed within the TF condition could be as a result of the lack of forward progression seen in step length. When comparing the TT simulated walking speed, these data showed a slightly higher walking speed than the 1.20-1.22 m/s reported within literature for transtibial gait (Lemaire et al. 2000; Schulz et al. 2010; Doane and Holt 1983) and in fact reflected the speed seen within control subjects. However, the walking speed within the control condition was also higher than previously reported 1.30-1.45 meters/second for able bodied individuals (Schulz et al. 2010; Nepomuceno et al. 2017; Boonstra et al. 1993) suggesting this population had a higher level of stability compared to those within literature and could explain the higher walking speed seen in the restricted conditions, specifically in the TT condition. The increased walking speed and longer step length shown by the participants within the TT simulated condition suggest that the rigid foot/ankle orthosis boot was not sufficient in simulating amputee temporal/spatial gait characteristics. This rigid foot-ankle restrictive orthotic is given to patients as part of the rehabilitation practice for healing of fractures and thus participants may already be familiarised by this and so can suitably adapt.

The second hypothesis was that there would be an increased vertical GRF vector in the non-restricted limb when walking in the restricted conditions. This hypothesis was fully supported within both restricted conditions ( $p=0.004$ ). Of the studies which have used restrictive devices, investigation into ground reaction force is limited. These studies concluded that the unrestricted limb had a decreased GRF compared to the restricted limb (Gulgin et al. 2017; Nepomuceno et al. 2017). This opposes the findings of this study, however, the Gulgin et al (2017) study concluded this based on a 2% difference in max GRF that was determined significant. This study was conducted from one 3D motion capture test and did not require any familiarisation.

Also as this study aimed to investigate leg discrepancy and not ankle restriction thus the fitting of the boot might not restrict the ankle as much as is done in this study. The Nepomuceno et al (2017) also found a decrease in vertical GRF for the unrestricted condition. Although the differences between the restricted and unrestricted conditions was very similar, 1.15 (N/BW) for no restriction versus 1.19 (N/BW) for restricted. The participants within this study were restricted using a cast condition, which allowed some movement. In LLA the average vertical ground reaction forces have been found to be greater in the intact limb than the prosthetic limb (Nolan et al. 2003; Royer and Koenig 2005). The values reported in these studies, are for the prosthetic side, with the first peak being larger than the second peak. When comparing between amputation levels literature has shown greater vertical ground reaction forces in transfemoral amputees (Nolan et al. 2003). This is not reflected within the transfemoral simulated gait in this study; however, this could be as a result, as seen by the reduced walking speed and step length, participants were more cautious in the simulator.

The final hypothesis (3) was that participants would display greater internal knee adduction in the restricted conditions. This hypothesis was fully supported in the TT condition with participants displayed a higher knee adduction moment peak in early stance (KAM1) ( $p=0.03$ ). In the TF condition, the hypothesis was not supported. Knee adduction moments have not been investigated within simulated gait, but within an amputee population it has been found that transtibial amputees have an increased knee adduction moment on their intact limb (Chang et al. 2012; Royer and Wasilewski 2006b) which reflects the results reported here within the first half of stance. The reason why the knee adduction moment could be reduced was that the walking speed was significantly reduced in the TF condition. Once the walking speed is taken into consideration, the knee adduction moment would increase and potentially becomes larger than the control condition. Although there was a period of familiarisation for all participants,

the slower walking speed could be due to participants still adapting to the use of the simulator. The participants increasing the time in the transfemoral simulator prior to testing could increase the walking speed.

An increased knee adduction moment has been correlated to increase medial knee force and progression of knee osteoarthritis (Brandon and Deluzio 2011; Chehab et al. 2014). Increased risk of osteoporosis and osteoarthritis could be explained by this increase in knee adduction moment. In vivo implantation studies have found that a decrease in KAM1 does not necessarily decrease medial contact forces however a decrease in KAM2 values do (Walter et al. 2010).

#### **7.4 Limitations**

One limitations of this study was that all participants used the same transfemoral and transtibial simulator, whereas prosthetic prescription is individualised. The results maybe that the simulator is not an optimal fit for some participants and therefore the adaptations are due to ill-fit rather than the simulator itself. However, the adaptations are also presented on an individual level, as well as across the groups and so the researcher believes that the results are still relevant.

#### **7.5 Conclusion**

To conclude, when the participants were wearing the rigid ankle-foot orthosis, an increased ground reaction force and knee adduction moment at KAM1 on the intact limb were displayed. However, the walking speed and shorter step length seen in transtibial amputees was not replicated. So, the TT simulating condition can be used to investigate loading magnitude and distribution of forces within lower limb amputees. The TF prosthetic simulator showed temporal-spatial adaptations similar to that adopted by TF amputees. The reduced GRF and knee does not replicate the loading magnitude. The increase in KAM2 shows that the force distribution found in transfemoral amputee gait can be replicated using a simulator.

Using restrictive orthotic and prosthetic devices means that research can investigate some effects of amputation without the interference of co-morbidities or previous health. In reference to previous chapters, the movement data collected from able-bodied subjects using prosthetic simulators can be applied to FEM to investigate how movement adaptations as a result of the removal of a biological structure independently affects bone health. This can also be used in conjunction with rehabilitation programmes to investigate which activities that benefit bone, in accordance to the predictive FEM, are feasible for an amputee. This combats the time constraints and recruitment difficulties often associated with scientific research whilst adding to knowledge, benefiting amputees, clinicians and the general health care industry.

## 8 GENERAL DISCUSSION

### 8.1 Introduction

Applying the Mechanostat theory, it is known that bone responds to strains produced as a result of mechanical loading through movement (Lanyon 1982; Wolff 1986; Boyce et al. 2009). A change in this mechanical loading, such as that in the adoption of an asymmetrical gait, can imbalance the bone remodelling and modelling processes subsequently resulting in poor bone health. This has been shown in clinical populations, such as LLAs (Sherk, et al. 2008; Nolan et al. 2003). However, LLAs are one population where the aetiology of the amputation can be as a result of disease (such as diabetes) or lifestyle choices (such as smoking), which independently affect bone (Jiao et al. 2015). The use of FEMs to predict bone responses to mechanical loading is well reported within literature (Brekelmans et al. 1972; Poelert et al. 2013; Schileo et al. 2007; Shim et al. 2007; Zysset et al. 2013). The migration toward subject-specific models has facilitated the manipulation of loading and the accurate prediction of bone responses without the interference of comorbidities. Participant specificity in FEM requires high radiation exposure and expensive equipment, resources that are not always possible in research or clinical environments (Poelert et al. 2013).

The overall aim of this Ph.D was to establish a method to investigate the relationship between bone health and asymmetrical loading *e.g.* in LLA through semi-subject specific FEM, and restrictive lower limb devices. This aim was addressed through five objectives detailed in Chapters Four to Eight. The current chapter provides a summary of each of these objectives followed by critical analysis in fulfilment of the overall Ph.D aim.

## 8.2 Summation and critical analysis of research objectives

The objectives of Study one were to construct a base tibia finite element model from a set of open-source bone scans (1) and to use anthropometric data extracted from subject specific tibial pQCT scans using a novel image processing method to create a semi subject- specific finite element model (2). The base tibial finite element model was successfully developed using the open source scans from the female the visible human project specimen (National Library of Medicine 2003). In order to create a semi-subject specific model, the base model was morphed using set landmarks from 30 degree intervals around the external geometry of the participant's tibial pQCT scan. The image processing method was assessed for accuracy through coefficient of variation (CV) using known diameters of a uniform object. Results concluded  $<0.15\%$  CV between scan time points across all scan sites and  $<0.12\%$  CV between scan sites across all time points. Repeatability was assessed through CV using a non-uniform object, a tibia. The CV  $<1.6\%$  between time points at all sites. Thus, it was concluded that the novel method of image processing developed provided an accurate and repeatable method of processing pQCT bone scan images across multiple time points and scan sites.

Subject-specific FEM have previously been achieved through scanning participants bone using bone-imaging techniques, such as CT scans (Taddei et al. 2006; Schileo et al. 2007a; Viceconti et al. 2004). Within a clinical environment, the imaging of a full long bone is rarely required, therefore to obtain the information needed to construct a subject specific FEM, participants must be exposed to additional radiation through further CT scans (Messmer et al. 2007). Peripheral quantitative computed tomography offers an advantageous alternative with comparatively low radiation exposure. Within a clinical environment, pQCT imaging of the tibial bone occurs most commonly at four sites along bone length (4, 14, 38 and 66%) as these represent varying proportions of trabecular and cortical bone whilst minimising radiation

exposure ( Evans et al. 2012). Previous studies have used the four pQCT bone scans in conjunction with a 2D planar radiograph to morph a base model (Caouette et al. 2015). Other studies that used pQCT to create subject specific FEM increased the scan intervals so that images were taken every 10mm (Mittag et al. 2017). An interpolation algorithm was applied to the Mittag et al. (2017) data set, which used the grey scale plot of two adjacent pQCT slices to determine the values of those in-between (Mittag et al. 2017). Both methods within these studies were time intensive, with manual identification of areas, increasing the risk of introducing human error. The image processing method developed within this Ph.D used a novel approach in using only these four pQCT scans to influence a base finite element model. The automated analysis of the image processing method developed within this study would allow for multiple scans to be analysed efficiently, if more detail was required.

The image processing method developed within this Ph.D was in fulfilment of objective (2) to create a semi-subject specific FEM, in the extraction anthropometric data. Therefore, a rotation factor of  $23^{\circ}$  was applied to register with the cadaver scan image. Previous image processing software, specifically the Bone Alignment and Measurement package (BAMpack) developed by Evans et al. (2012) used an automatic image registration and rotating process in order to compare across time points and control for any positional error within the scanner. The automatic registration and rotation factor was based on the 66% site only and required manual manipulation on some participants. The next stage of the image processing method developed in this Ph.D was the application of threshold analysis to convert the image into binary. This ensured that the objects within the image were distinguishable and removed the risk of including transitional pixilation i.e. pixels which could not be identified as either trabecular or cortical bones. As previous studies have proven that tibial changes can differ within sections of the bone (Bankoff 2012), the image processing method developed within this thesis used

sectional analyses. The image processing method used within this thesis dissected the image at 30° sections in order to provide enough geometrical data to morph the model without increasing computational time. Where previous image processing methods sectioned the image at every 10° degrees in order to investigate shape properties ( Evans et al. 2012), the image processing method developed here allows for full perimeter analyses and easy manipulation of sectioning. This enables more detailed analysis of the bone shape with the ability for personalised section analyses. In order to create an anatomically accurate outer geometry, the image processing method developed within this study used a three point moving average as a smoothing technique, which was also used within the Evans et al., (2008) study to create an average tibial geometry.

To validate the image processing method, Study one used two models, one with known outer geometry to assess accuracy and another with non-uniform geometry to assess repeatability. A CV of <0.6% was shown for the uniform object and a CV of < 1.6% was shown for the non-uniform object. The BAMpack software was reported to be validated through a test-retest method measuring the trabecular and cortical density and geometry in a sample of 31, achieving a coefficient of variation of less than 1% (Evans et al. 2012). The image processing method developed within this Ph.D showed marginally higher CV for the non-uniform object. However, further analyses cannot be made as the method used to assess variation for the BAMpack was not disclosed. Producing a non-disclosed method of validation will enable researchers to replicate this and produce data that can be confidently compared worldwide.

The objective of Study Two was to optimise and validate the semi-subject specific finite element model by applying muscle and joint reaction forces outputs from subject-specific biomechanics and comparing results to longitudinal bone geometry changes (3). A sensitivity

study was conducted to investigate the effect of application of forces derived from different time points on semi-subject FEM developed from the equivalent and non-equivalent data collection time points. Due to the variation in strain outputs from loading the semi-subject FEM with differing GRF, it was concluded that semi subject-specific FEM was loaded with force data generated from movement data collected at the equivalent time point. Maximum strain occurred at the 14% of the tibial shaft with maximum values across participants ranging from 200 to 600  $\mu\epsilon$ . These strains were validated by comparing to published *in vivo* studies which attached strain gauges to the medial tibial shaft. The average results from this study were toward the top end of the 30-700  $\mu\epsilon$  strain previously reported for *in vivo* walking gait studies (Burr et al. 1996; Yang et al. 2011). The location of these strains were reported in the medial shaft of the tibia, due to its ease of surgical access (Lanyon et al. 1975). This study showed higher strain magnitudes at the lateral side of the tibia, this could explain the strain levels being toward the higher end of the range reported *in vivo*. Further validation was conducted using the participant's longitudinal bone geometry data. Areas of higher strain from the semi subject specific FEM developed from time point one were consistent with areas of higher bone geometry changes from time point one to time point two. This novel method of validation means that experimental validation using *in vivo* implantation of strain gauges is no longer needed. This reduces the invasiveness of validating FEM, making them more accessible to researchers and clinicians alike. This validation also concludes that semi-subject specific FEM are an accurate and valid method of predicting strain magnitudes from walking in able-bodied subjects, removing the need for radiation exposure and reducing the computational time associated with subject-specific modelling.

Following on from the optimisation and validation of the finite element model from one participant, the methods developed in Study One were used to investigate the changes in bone

geometry and gait longitudinally. The objective of Study Three was to analyse the variation in tibial bone structure and geometry and walking gait in lower limb amputees and able-bodied subjects over a 12-month period (4). Unfortunately, for this study lower limb amputees were unable to be recruited into the study, due to not fulfilling the inclusion criteria as well as a high drop-out rate. The most common reason for exclusion was the presence of other bone debilitating diseases such as osteoporosis. These exclusion criteria were enforced to control for any bone degradation independent of amputation. However, as those who smoke are at a higher risk of developing peripheral arterial disease and thus at a higher risk of amputation, there is a higher probability that an amputee will be also be a smoker (Nosova et al. 2015). The advantage of investigating able-bodied gait longitudinal is it is often assumed that able-bodied participants display a consistent symmetrical gait, which enables the maintaining of healthy bone. As a result clinical studies often assume that positive changes in gait parameters or bone properties are due to movement interventions through rehabilitation. Study four concluded that there is a level of natural variation in gait parameters and bone properties within an able-bodied population, which need to be given consideration within a clinical environment.

Bone geometry was determined through the automatically generated pQCT measures, including bone area as well as the image processing method output namely outer geometry. Total bone area and total bone density was most varied at the 4% site. Bone total density varied by a maximum of 12%, although was <4% for the majority of participants. Bone total area had a maximum variation of 12%, with the majority of participants had a CV <5%. The outer geometry was also shown to increase as the bone area increased. Bone area is one measure of bone health, as an increase in bone area and outer geometry will increase the mass around the neutral axis of the bone, thus making it more resistant to bending and stronger (Cristofolini et al. 2013). Bone mineral density is a measure of the porosity of the bone, a reduced bone density

means the bone will be less able to absorb energy and the bone will be at a higher risk of fracture (Leali et al. 2011; Royer and Koenig 2005). This study shows that there is a natural variation in bone structural and geometrical properties within able bodied subjects across a twelve month period that exceeds measurement error. Only small changes (in the region of 2 mm) in outer bone geometry have been shown in current studies (Izard et al. 2016a). The maximum CV value shown from studies within this Ph.D was 18%, this translates to natural variation in outer bone geometry changes in excess of 2mm. This might be explained by the much shorter intervention period utilised by Izard et al, who aimed to determine the effects of the first 10 weeks of basic military training on bone mass and geometry. In contrast, the present study investigated changes over three month periods for a year total. On the other hand the study conducted by Izard et al. (2016) was in a controlled environment where researchers were able to control the exercise between visits. In Study Three, participants were not controlled for exercise outside of the lab but instead were asked to fill out the bone specific physical activity questionnaires (BPAQ) to quantify their activity (Weeks and Beck 2008). This recorded any changes in activity that could result in changes in bone geometry and structure.

Walking gait was measured over level ground and stair ambulation in order to investigate the variation in forces in different common activities of daily living. Each participant also performed a two minute walk test, as this is used in clinical environments to assess gait functionality and levels of mobility (Grimpampi et al. 2015). The variation, as determined by CV shown for the distance walked was <10% across all participants and <5% for number of strides taken across the 2MWT. The increased variability in distance walked over number of strides demonstrates that participants are varying the self-selected walking speed over the 12 months. Higher walking speeds within clinical populations are associated with increased functionality, with a decrease being associated with increased risk of morbidity (Batten et al.

2018). However, the change in gait speed may be as a result of natural variation. Maximum vertical ground reaction forces varied by up to 10%, which is less than the 12.5% previously reported within the literature as a threshold of variability (Wang and Watanabe 2000). There was a higher variability in vertical ground reaction forces when participants were traversing stairs, <35% for stair ascent and <39% for stair descent. An increase in variability has previously been used to exclude staircase activities from studies. This is because an increased variation is associated with decreased stability and subsequent higher risk of falls (Stacoff et al. 2005). On the other hand studies have concluded that gait variability is independent of stability (Li, et al. 2005). This study showed a high level of variability within an able-bodied population, none of whom had reported any falls or indications of instability. The benefit of staircase ambulation increases ground reaction forces in comparison to level walking. The increased forces result in increased strains, which encourage bone formation and have the potential to improve bone health. Therefore, this study adds to the current data for staircase ambulation, with variability data supporting studies that gait variation is independent of stability.

To investigate the relationship between asymmetrical loading and bone health whilst eliminating the complications associated comorbidities and pre-existing conditions often seen in clinical population with asymmetrical gait, e.g. LLA restrictive devices within able-bodied participants were used. Specifically, the objective of Study Four was to simulate the gait characteristics of lower limb amputates in able-bodied participants by restricting their ankle with a rigid ankle-foot orthosis and ankle and knee concurrently and a trans-femoral simulator. The results showed that when able-bodied participants were restricted, walking speed was reduced. In the TF condition step length on the restricted limb was significantly shorter, with less time spent in stance. These results show that the transfemoral condition was able to fully

simulate and the transtibial conditions were able to partially simulate the temporal-spatial adaptations seen in lower limb amputees. There were increased GRF and knee adduction moments in the TT condition compared to the control, although not in the TF condition. The walking speed was, however, significantly slower in the TF condition and a decrease in walking speed has been shown to decrease the compressive forces acting on the tibia along with knee adduction moments (Riaz et al. 2016). Therefore, if the walking speed was matched to the control walking speed, both conditions would show larger GRF's and knee adduction moments than is displayed in the control condition. Lower limb amputees have an increased knee adduction moment in their intact limb (Royer and Wasilewski 2006a; Chang et al. 2012), demonstrating that the restriction conditions can be used to simulate amputee gait. In using healthy able-bodied participants the pain that are associated with the removal of the biological supporting structure and the complications surrounding the comorbidities, which could influence walking patterns were controlled for. This enabled the independent investigation into the asymmetrical gait pattern. Upon the conclusion that these restrictive devices can be used to simulate the asymmetrical gait pattern, rehabilitation techniques can be applied to reduce compensatory mechanisms that are detrimental to bone health *e.g.* larger knee adduction moments. This provides clinicians with knowledge that can be applied to lower limb amputees in early rehabilitation to encourage a gait mechanism that maintains bone health, reducing reliance on NHS and other health care systems longitudinally. Another advantage of these restrictive devices is that the time taken for an able-bodied participant to familiarise to these conditions was achievable across two familiarisation sessions. Whereas research has shown significant changes in gait within 12 months post amputation (Czerniecki et al. 2012). So, in using restrictive devices, amputee gait can be investigated without interrupting a participant's rehabilitation or waiting for participants to become familiarised to their prosthesis. This enables

research to be carried out within a smaller time frame, enabling the results to be implemented into clinics and benefit patients sooner.

**Table 30: An overview of the objectives addressed throughout the Ph.D and the key outcomes from the respective objectives.**

Objective No.	Study No.	Key study outcomes
1		A novel image processing method was developed to extract anthropometric landmarks from
2	Study 1, Chapter 3	participant pQCT scan. Landmarks were then used to successfully construct a semi-subject specific FEM.
3	Study 2, Chapter 4	Longitudinal bone geometry data can be used to validate semi-subject specific FEMs.
4	Study 3, Chapter 5	There is a natural variation in bone geometry and maximum GRF experienced in level walking in able-bodied participants over a 12 month period.
5	Study 4, Chapter 6	LLA temporal-spatial characteristics can be simulated using a TF prosthetic simulator. LLA knee adduction moments and GRF characteristics can be simulated using a rigid foot-ankle orthosis.

## 9. LIMITATIONS AND FUTURE DIRECTIONS

The base FEM developed in Study One was constructed using the female visible human project (National Library of Medicine 2003). Both sex and age effect tibial geometry, with studies finding significantly higher endosteal and periosteal circumferences for men compared to women (Sherk et al. 2012). Also, it is known that bone reaches its peak mass at 25 years of age, after which point circumferences, cortical thickness and BMD are also seen to decrease (Campbell 2012; Sherk et al. 2012). Those recruited into Study One were all male whose age ranged from 30 years old up to 60 years old. In morphing the model, the outer geometry of the shaft and the length of the tibia were the only parts that were scaled. So, bone properties including cortical thickness and BMD remain specific to the female cadaveric specimen from the VHP. It is therefore likely that the cortical thickness was reduced in the FEM when compared to the studies' younger participants' actual cortical thickness. In mice it has been shown that a decrease in cortical thickness results in a significantly greater tibial strain magnitude (Patel et al., 2015). Therefore, the model may have overestimated strains for those participants who were younger than the visible human project specimen. The advantage of the image processing method is that Future directions could use the image processing method to identify cortical thickness and add another level of participant specificity to the FEM.

For study three, the objective was to investigate changes in tibia bone and walking gait within both an able bodied and a lower limb amputate population. Due to potential participants being smokers or experiencing bone degradation diseases such as osteoporosis, they were excluded from the study. The able-bodied participants were recruited based on being age matched to potential amputee participants, as a result there were only six able-bodied participants who volunteered for Study Three. This was half of the participants that had been calculated as needed through a power calculation (see 6.2.1). With only six participants recruited into the

study, inferential statistics is not appropriate, as it may wrongly produce statistical significance when there is no significant differences across the population (Hackshaw 2008). The data collected allowed for analyses at an individual level, in case study format. In future, greater participant numbers should be recruited in order to allow a statistical conclusion for the population. Also, as mentioned in section 6.7 and in the discussion, future studies will recruit LLA who are over a year post the assignment of the definitive prosthesis.

Study Four used restrictive devices to simulate lower limb amputee gait. The participants recruited into this study were young healthy individuals and therefore do not age match the average LLA. This could explain the reduced time taken for participants to be familiarised with the restrictive devices. Also all participants were placed in a harness for health and safety. Amputees would not have a harness when ambulating in a community environment, so the results from this study may have a more optimistic conclusion. If this method would be used to assist physiotherapists, it would be important to investigate simulated gait in an age group that reflects an amputee cohort, as well as in a more ecologically valid environment.

## **10. CONCLUSION**

This thesis developed a novel method of identifying anthropometric landmarks around the outer geometry of a participant's tibia. This new method allowed the development of a semi-subject specific FEM from only four pQCT scans. The semi-subject specific FEM were self-validated; areas of higher strain within the FEM correlated to positive bone geometry changes, recorded over a 12 month period in able-bodied subjects. This new method of non-invasive self-validation means that FEM can now be validated without the need of cadavers, making them an accessible tool to clinicians and the wider research community. The longitudinal study showed that able-bodied participants have a natural variation in bone geometry properties and gait characteristics. This challenges previous knowledge that able-

abled subjects maintained a symmetrical walking pattern than maintained consistent positive bone health. Similar values to the CV shown within this thesis have previously been used as evidence for successful intervention studies, rehabilitation or response to exercise. This evidence may be incorrect and it is important that a level of natural variation be established to enable accurate future investigations. Finally this thesis showed that restrictive devices can be used to simulate LLA gait characteristics. Restrictive orthotics and prosthetics therefore allow further investigation into asymmetrical loading without the complications of comorbidities, as is often the case with LLA.

Overall this thesis provides a novel and valid approach of constructing a semi-subject specific FEM for the investigation into a participant's long term bone health as a result of their loading conditions. These FEM can then be used to manipulate loading profiles generated from differing movements without risk to the participant. Not only is this safer but can be used to educate clinicians into the best method of rehabilitating amputees to give them the best quality of life. The knowledge that able-bodied subjects have some natural variation will provide new information to clinicians in the assessment of clinical groups, taking into consideration that natural variation in movement is positive for bone health. Further research directions within other clinical populations who present with asymmetrical gait demonstrates the wide applicability of this research.

## 11. REFERENCES

- Ackerman, M, J., 1999. "The Visible Human Project." *Academic Medicine* 74:667-70.
- Adouni, M, Shirazi-Adl, A & Shirazi, R. 2012. "Computational Biodynamics of Human Knee Joint in Gait: From Muscle Forces to Cartilage Stresses." *Journal of Biomechanics* 45: 2149–56.  
<https://doi.org/10.1016/j.jbiomech.2012.05.040>.
- Ahmad, N.G., Thomas, N., Gill, P., Chan, C., & Torella, F. 2014. "Lower Limb Amputation in England: Prevalence, Regional Variation and Relationship with Revascularisation, Deprivation and Risk Factors. A Retrospective Review of Hospital Data." *Journal of the Royal Society of Medicine* 107 (12): 483–89. <https://doi.org/10.1177/0141076814557301>.
- Ahmad, N, G., Thomas,N., Gill, P., Chan, C., and Torella. F. 2016. "The Prevalence of Major Lower Limb Amputation in the Diabetic and Non-Diabetic Population of England 2003-2013." *Diabetes and Vascular Disease Research* 13 (5): 348–53.  
<https://doi.org/10.1177/1479164116651390>.
- Alcock, L., O'Brien, T.D & Vanicek, N. 2015. "Biomechanical Demands of the 2-Step Transitional Gait Cycles Linking Level Gait and Stair Descent Gait in Older Women." *Journal of Biomechanics* 48 (16): 4191–97. <https://doi.org/10.1016/j.jbiomech.2015.09.020>.
- Alcock, L., O'Brien, T.D & Vanicek, N. 2015. "Biomechanical Demands of the 2-Step Transitional Gait Cycles Linking Level Gait and Stair Descent Gait in Older Women." *Journal of Biomechanics* 48: 4191–97. <https://doi.org/10.1016/j.jbiomech.2015.09.020>.
- Merkur, A., Fradet, L., Braatz, F., Gerner, H. J & Wolf, S.I. 2009. "Kinematics and Kinetics with an Adaptive Ankle Foot System during Stair Ambulation of Transtibial Amputees." *Gait and Posture* 30 (3): 356–63. <https://doi.org/10.1016/j.gaitpost.2009.06.009>.
- Anderson, D ., Goldsworthy, J., LiWendy, B.S., Rudert, J., Tochigi, Y & Brown, T.D. 2008. "Physical Validation of a Patient-Specific Contact Finite Element Model of the Ankle." *Biomedical Engineering* 40 (8): 1662–69.

- Anderson, F. C & Pandy, M.G. 1999. "A Dynamic Optimization Solution for Vertical Jumping in Three Dimensions." *Computer Methods in Biomechanics and Biomedical Engineering* 2 (3): 201–31. <https://doi.org/10.1080/10255849908907988>.
- Anderson, F.C ., Chand, J. T., Guendelman, E., Arnold, S.A & Delp, S.L. 2006. "SimTrack: Software for Rapidly Generating Muscle-Actuated Simulations of Long-Duration Movement." *International Symposium on Biomedical Engineering*, 3–6.
- Andriacchi, T. P., Andersson, G.B., Fermier, R.W., Stern, D & Galante, J.O. 1980. "A Study of Lower-Limb Mechanics during Stair-Climbing of Lower-Limb." *The Journal of Bone & Joint Surgery* 62: 749–57.
- Van Arkel, R. J ., Modenese, L., Phillips, A.T.M & Jeffers, J.R.T.2013. "Hip Abduction Can Prevent Posterior Edge Loading of Hip Replacements." *Journal of Orthopaedic Research : Official Publication of the Orthopaedic Research Society* 31 (8): 1172–79. <https://doi.org/10.1002/jor.22364>.
- Ashburner, J. & Friston, K.J. 2000. "Voxel-Based Morphometry - The Methods." *NeuroImage* 11 (6 D): 805–21. <https://doi.org/10.1006/nimg.2000.0582>.
- Baker, P. A & Hewison, S.R. 1990. "Gait Recovery Pattern of Unilateral Lower Limb Amputees during Rehabilitation." *Prosthetics and Orthotics International* 14: 80–84. <https://doi.org/10.3109/03093649009080327>.
- Bankoff, A. 2012. "Biomechanical Characteristics of the Bone." In *Human Musculoskeletal Biomechanics*, 154–57.
- Batani, H. & Sandra J. Olney. 2002. "Kinematic and Kinetic Variations of Below-Knee Amputee Gait." *JPO Journal of Prosthetics and Orthotics* 14 (1): 2–10. <https://doi.org/10.1097/00008526-200203000-00003>.
- Heather R. B., McPhail, S.M., Mandrusiak, A.M., Varghese, P.N. & Kuys, S.S. 2018. "Gait Speed as an Indicator of Prosthetic Walking Potential Following Lower Limb Amputation." *Prosthetics*

*and Orthotics International*, August, 030936461879272.

<https://doi.org/10.1177/0309364618792723>.

Beillas, P., Papaioannou, G., Tashman, S & Yang, K.H. 2004. "A New Method to Investigate in Vivo Knee Behavior Using a Finite Element Model of the Lower Limb." *Journal of Biomechanics* 37 (7): 1019–30. <https://doi.org/10.1016/j.jbiomech.2003.11.022>.

Bell, A. L., Pedersen, D.R & Brand, R.A. 1990. "A Comparison of the Accuracy of Several Hip Center Location Prediction Methods." *Journal of Biomechanics* 23 (6): 617–21. [https://doi.org/10.1016/0021-9290\(90\)90054-7](https://doi.org/10.1016/0021-9290(90)90054-7).

Bell, A.L., Brand, R.A. & Pedersen, D.R. 1989. "Prediction of Hip Joint Centre Location from External Landmarks." *Human Movement Science* 8 (1): 3–16. [https://doi.org/10.1016/0167-9457\(89\)90020-1](https://doi.org/10.1016/0167-9457(89)90020-1).

Bemben, D.A., Sherk, V.D., Ertl, W. J. J. & Bemben, M.G. 2017. "Acute Bone Changes after Lower Limb Amputation Resulting from Traumatic Injury." *Osteoporosis International*. <https://doi.org/10.1007/s00198-017-4018-z>.

Bennell, K.L., Bowles, K-A., Wang, Y., Cicuttini, F., Davies-Tuck, M. & Hinman. R.S. 2011. "Higher Dynamic Medial Knee Load Predicts Greater Cartilage Loss over 12 Months in Medial Knee Osteoarthritis." *Annals of the Rheumatic Diseases* 70 (10): 1770–74. <https://doi.org/10.1136/ard.2010.147082>.

Berger, A. 2002. "Bone Mineral Density Scans." *Bone and Mineral* 325: 484.

Berger, C., Goltzman, D., Langsetmo, L., Joseph, J., Kreiger, N., Tenenhouse, A., Davison, K.S. & Robert G Josse. 2016. "Peak Bone Mass From Longitudinal Data : Implications for the Prevalence , Pathophysiology , and Diagnosis of Osteoporosis." *Journal Bone Mineral Research* 25 (9): 1948–57. <https://doi.org/10.1002/jbmr.95.Peak>.

Bohannon, R. W. 2017. "Normative Reference Values for the Two-Minute Walk Test Derived by Meta-Analysis." *Journal of Physical Therapy Science* 29 (12): 2224–27.

<https://doi.org/10.1589/jpts.29.2224>.

- Bohannon, R.W., Bubela, D., Magasi, S., McCreath, H., Wang, Y-C., Reuben, D. & Rymer, W.Z. 2014. "Comparison of Walking Performance over the First 2 Minutes and the Full 6 Minutes of the Six-Minute Walk Test." *BMC Research Notes* 7 (1): 269. <https://doi.org/10.1186/1756-0500-7-269>.
- Böhm, H. & Hösl, M. 2010. "Effect of Boot Shaft Stiffness on Stability Joint Energy and Muscular Co-Contraction during Walking on Uneven Surface." *Journal of Biomechanics* 43 (13): 2467–72. <https://doi.org/10.1016/j.jbiomech.2010.05.029>.
- Boonstra, A.M, Fidler, V. & Eisma, W.H. 1993. "Walking s p e e m t m k u b j e c t s and Amputees : Aspects of Validity of Gait Analysis," 78–82.
- Bouxsein, M.L, & Seeman, E. 2009. "Quantifying the Material and Structural Determinants of Bone Strength." *Best Practice & Research Clinical Rheumatology* 23 (6): 741–53. <https://doi.org/10.1016/j.berh.2009.09.008>.
- Boyce, B ., Yao, Z. & Xing, L. 2009. "Osteoclasts Have Multiple Roles in Bone in Addition to Bone Resorption." *Critical Reviews in Eukaryotic Gene Expression* 19 (3) 171-180.
- Boyd, S.K. & Vandenberghe, L. 2009. *Convex Optimization*. Cambridge University Press.
- Brandon, S.C,E, & Deluzio.K, J. 2011. "Robust Features of Knee Osteoarthritis in Joint Moments Are Independent of Reference Frame Selection." *Clinical Biomechanics* 26 (1): 65–70. <https://doi.org/10.1016/j.clinbiomech.2010.08.010>.
- Brassey, C.A., Margetts, L., Kitchener, A.C., Withers, P.J., Manning, P.L & Sellers, W.I. 2012. "Finite Element Modelling versus Classic Beam Theory: Comparing Methods for Stress Estimation in a Morphologically Diverse Sample of Vertebrate Long Bones." *Journal of the Royal Society Interface*. <https://doi.org/10.1098/rsif.2012.0823>.
- Breakey, J. 1976. "GAIT OF UNILATERAL BELOW-KNEE AMPUTEES." *Orthotics and Prosthetics* 30: 17–24. [http://www.oandplibrary.org/op/pdf/1976\\_03\\_017.pdf](http://www.oandplibrary.org/op/pdf/1976_03_017.pdf).

- Brooks, D., Hunter, J.P., Parsons, J., Livsey, E., Quirt, J & Devlin, M. 2002. “Reliability of the Two-Minute Walk Test in Individuals with Transtibial Amputation.” *Archives of Physical Medicine and Rehabilitation* 83 (11): 1562–65. <https://doi.org/10.1053/apmr.2002.34600>.
- Brooks, D., Parsons, J., Hunter, J.P., Devlin, M. & Walker, J., 2001. “The 2-Minute Walk Test as a Measure of Functional Improvement in Persons with Lower Limb Amputation.” *Archives of Physical Medicine and Rehabilitation* 82 (10): 1478–83. <https://doi.org/10.1053/apmr.2001.25153>.
- Burke, M.J., Roman, V. & Wright, V. 1978. “Bone and Joint Changes in Lower Limb Amputees.” *Annals of the Rheumatic Diseases* 37 (3): 252–54. <https://doi.org/10.1136/ard.37.3.252>.
- Burkhart, T.A., Andrews, D.M. & Dunning, C.E. 2013. “Finite Element Modeling Mesh Quality, Energy Balance and Validation Methods: A Review with Recommendations Associated with the Modeling of Bone Tissue.” *Journal of Biomechanics* 46 (9): 1477–88. <https://doi.org/10.1016/j.jbiomech.2013.03.022>.
- Burr, D.B., Milgrom, C., Fyhrie, D., Forwood, M., Nyska, M., Finestone, A., Hoshaw, S., Saiag, E., & Simkin, A. 1996. “In Vivo Measurement of Human Tibial Strains during Vigorous Activity.” *Bone* 18 (5): 405–10. [https://doi.org/10.1016/8756-3282\(96\)00028-2](https://doi.org/10.1016/8756-3282(96)00028-2).
- Burra, S., Nicolella, D. P., Francis, W. L., Freitas, C. J., Mueschke, N. J., Poole, K. & Jiang, J. X. 2010. “Dendritic Processes of Osteocytes Are Mechanotransducers That Induce the Opening of Hemichannels.” *Proceedings of the National Academy of Sciences* 107 (31): 13648–53. <https://doi.org/10.1073/pnas.1009382107>.
- Caeiro, J.R., González, P. & Guede, D. 2013. “Biomechanics and Bone (& II): Trials in Different Hierarchical Levels of Bone and Alternative Tools for the Determination of Bone Strength.” *Revista de Osteoporosis y Metabolismo Mineral* 5 (2): 99–108. <https://doi.org/10.4321/S1889-836X2013000200007>.
- Campbell, B. 2012. “Healthy Bones at Every Stage.” American Academy of Orthopaedic Surgeons.

2012.

- Canavan, R., Unwin, N., Kelly, W. & Connolly, V. 2008. "Diabetes- and Nondiabetes-Related Lower Extremity Amputation Incidence Before and After the Introduction of Better Organized Diabetes Foot Care." *Diabetes Care* 31 (3): 459–63. <https://doi.org/10.2337/dc07-1159>. Abbreviations.
- Caouette, C., Ikin, N., Villemure, I., Arnoux, P.-J., Rauch, F. & Aubin, C.-E. 2015. "Geometry Reconstruction Method for Patient-specific Finite Element Models for the Assessment of Tibia Fracture Risk in Osteogenesis Imperfecta." *Medical & Biological Engineering & Computing*. <https://doi.org/10.1007/s11517-016-1526-5>.
- Carbone, V., Fluit, R., Pellikaan, P., Van Der Krogt, M.M., Janssen, D., Damsgaard, M., Vigneron, L., Feilkas, T., Koopman, H.F.J.M & Verdonschot, N. 2015. "TLEM 2.0 – A Comprehensive Musculoskeletal Geometry Dataset for Subject-Specific Modeling of Lower Extremity." *Journal of Biomechanics* 48: 734–41. <https://doi.org/10.1016/j.jbiomech.2014.12.034>.
- Carey, R.E., Zheng, L., Aiyangar, A.K., Harner, C.D. & Zhang, X. 2014. "Subject-Specific Finite Element Modeling of the Tibiofemoral Joint Based on CT, Magnetic Resonance Imaging and Dynamic Stereo-Radiography Data in Vivo." *Journal of Biomechanical Engineering* 136 (4): 041004. <https://doi.org/10.1115/1.4026228>.
- Cervinka, T., Hyttinen, J. & Sievanen, H. 2010. "Enhanced Bone Structural Analysis through PQCT Image Preprocessing." *Medical Engineering and Physics* 32 (4): 398–406. <https://doi.org/10.1016/j.medengphy.2010.02.003>.
- Chang, Y.H., Bae, T.S., Kim, S.S., Kim, S.B., Mun, M.S., & Lee, W.H. 2012. "Relationship Between Ankle Inversion Angle and Knee Adduction Moment on the Intact Limb in Unilateral Transfemoral Amputees During Walking." *International Journal of Precision Engineering and Manufacturing*. <https://doi.org/10.1007/s12541-012-0078-3>.
- Chehab, E.F., Favre, J., Erhart-Hledik, J.C. & Andriacchi, T.P. 2014. "Baseline Knee Adduction and Flexion Moments during Walking Are Both Associated with 5 Year Cartilage Changes in

- Patients with Medial Knee Osteoarthritis.” *Osteoarthritis and Cartilage* 22: 1833–39.  
<https://doi.org/10.1016/j.joca.2014.08.009>.
- Cheng, S., Sipilä, S., Taaffe, D.R., Puolakka, J. & Suominen, H. 2002. “Change in Bone Mass Distribution Induced by Hormone Replacement Therapy and High-Impact Physical Exercise in Post-Menopausal Women.” *Bone* 31 (1): 126–35. [https://doi.org/10.1016/S8756-3282\(02\)00794-9](https://doi.org/10.1016/S8756-3282(02)00794-9).
- Cheung, C., Wall, J.C. & Zelin, S. 1983. “A Microcomputer-Based System for Measuring Temporal Asymmetry in Amputee Gait.” *Prosthetics and Orthotics International* 7 (3): 131–40.  
<http://ovidsp.ovid.com/ovidweb.cgi?T=JS&PAGE=reference&D=med2&NEWS=N&AN=6647009>.
- Chien, J.H., Yentes, J., Stergiou, N & Siu, K-C. 2016. “The Effect of Walking Speed on Gait Variability in Healthy Young, Middle-Aged and Elderly Individuals.” *Journal of Physical Activity, Nutrition and Rehabilitation* 2015 (Cv).  
<http://www.ncbi.nlm.nih.gov/pubmed/26929929><http://www.pubmedcentral.nih.gov/articlerender.fcgi?artid=PMC4768759>.
- Clarke, P., Gray, A., Legood, R., Briggs, A., and Holman, R. 2003. “The Impact of Diabetes-Related Complications on Healthcare Costs: Results from the United Kingdom Prospective Diabetes Study (UKPDS Study No. 65).” *Diabetic Medicine* 20 (6): 442–50.  
<http://ovidsp.ovid.com/ovidweb.cgi?T=JS&PAGE=reference&D=emed6&NEWS=N&AN=2003259556>.
- Cointry, G. R., Capozza, R.F., Negri, A.L., Roldán, E.J.A & Ferretti, J.L. 2004. “Biomechanical Background for a Noninvasive Assessment of Bone Strength and Muscle-Bone Interactions.” *Journal of Musculoskeletal Neuronal Interactions* 4 (1): 1–11.
- Costigan, P.A., Deluzio, K.J. & Wyss, U.P. 2002. “Knee and Hip Kinetics during Normal Stair Climbing.” *Gait and Posture* 16: 31–37. [www.elsevier.com/locate/gaitpost](http://www.elsevier.com/locate/gaitpost).

- Couteau, B., Yohan, P., & Lavallee, S., 2000. "The Mesh-Matching Algorithm: An Automatic 3D Mesh Generator for Finite Element Structures." *Journal of Biomechanics* 33 (8).  
<https://hal.archives-ouvertes.fr/hal-00082218>.
- Cowen, S. 1990. *Bone Mechanics. Clinical Biomechanics*. Vol. 5. [https://doi.org/10.1016/0268-0033\(90\)90036-6](https://doi.org/10.1016/0268-0033(90)90036-6).
- Craig, C.L., Marshall, A.L., Bauman, A.E., Booth, M.L., Ainsworth, B.E., Pratt, M. 2003.  
"International Physical Activity Questionnaire: 12-Country Reliability and Validity." *Medicine and Science in Sports and Exercise* 35 (8): 1381–95.  
<https://doi.org/10.1249/01.MSS.0000078924.61453.FB>.
- Cristofolini, L., Angeli, E., Juszczak, J.M. & Juszczak, M.M. 2013. "Shape and Function of the Diaphysis of the Human Tibia." *Journal of Biomechanics* 46: 1882–92.  
<https://doi.org/10.1016/j.jbiomech.2013.04.026>.
- Croce, U.D. & Bonato, P. 2007. "A Novel Design for an Instrumented Stairway." *Journal of Biomechanics* 40: 702–4. <https://doi.org/10.1016/j.jbiomech.2006.01.020>.
- Currey, J. 2002. *Bones Structure and Mechanics*. Princeton: Princeton University Press.
- Currey, J. 2005. "Structural Heterogeneity in Bone: Good or Bad?" *Journal of Musculoskeletal Neuronal Interactions*.
- Curtis, N., Jones, M.E.H., Shi, J., O'Higgins, P., Evans, S.E. & Fagan, M.J. 2011. "Functional Relationship between Skull Form and Feeding Mechanics in *Sphenodon*, and Implications for Diapsid Skull Development." *PLoS ONE* 6 (12): 31–33.  
<https://doi.org/10.1371/journal.pone.0029804>.
- Czerniecki, J.M., Turner, A.P., Williams, R.M., Hakimi, K.N. & Norvell, D.C. 2012. "Mobility Changes in Individuals with Dysvascular Amputation from the Presurgical Period to 12 Months Postamputation." *Archives of Physical Medicine and Rehabilitation* 93 (10): 1766–73.  
<https://doi.org/10.1016/j.apmr.2012.04.011>.

- Dalla, A. & Bankoff, P. 2012. *Biomechanical Characteristics of the Bone, Human Musculoskeletal Biomechanics*. 61-86 [www.intechopen.com](http://www.intechopen.com).
- Damsgaard, M., Rasmussen, J., Christensen, S.T., Surma, E. & De Zee, M. 2006. "Analysis of Musculoskeletal Systems in the AnyBody Modeling System." <https://doi.org/10.1016/j.simpat.2006.09.001>.
- Dao, T.T. 2017. "Rigid Musculoskeletal Models of the Human Body Systems: A Review." *Journal of Musculoskeletal Research* 19 (03): 1630001. <https://doi.org/10.1142/s0218957716300015>.
- Davie-Smith, F., Heberton, J., & Scott, H. 2015. "A Survey of the Lower Limb Amputee Population in Scotland, 2008," 58.
- De Oliveira, S.D. & Rodrigues, S. 2013. "Biomechanics of the Total Ankle Arthroplasty: Stress Analysis and Bone Remodeling." <https://fenix.tecnico.ulisboa.pt/downloadFile/395145522891/Tese.pdf>.
- DeFrate, L.E., Sun, H., Gill, T.G., Rubash, H.E. & Li, G.. 2004. "In Vivo Tibiofemoral Contact Analysis Using 3D MRI-Based Knee Models." *Journal of Biomechanics* 37 (10): 1499–1504. <https://doi.org/10.1016/j.jbiomech.2004.01.012>.
- Delp, S.L., Loan, P., Hoy, M.G., Zajac, F.E., Topp, E.L. & Rosen, J.M. 1990. "An Interactive Graphics-Based Model of the Lower Extremity to Study Orthopaedic Surgical Procedures." *IEEE Transactions on Biomedical Engineering*. <https://doi.org/10.1109/10.102791>.
- Delp, S.L., Anderson, F.C., Arnold, A.S., Loan, P., Habib, A., John, C.T., Guendelman, E. & Thelen, D.G. 2007. "OpenSim: Open Source to Create and Analyze Dynamic Simulations of Movement." *IEEE Transactions on Bio-Medical Engineering* 54 (11): 1940–50. <https://doi.org/10.1109/TBME.2007.901024>.
- Dennis, D.A., Mahfouz, M.R., Komistek, R.D. & Hoff, W. 2005. "In Vivo Determination of Normal and Anterior Cruciate Ligament-Deficient Knee Kinematics." *Journal of Biomechanics* 38 (2): 241–53. <https://doi.org/10.1016/j.jbiomech.2004.02.042>.

- Detrembleur, C., Vanmarsenille, J.M., De Cuyper, F. and Dierick, F. 2005. "Relationship between Energy Cost, Gait Speed, Vertical Displacement of Centre of Body Mass and Efficiency of Pendulum-like Mechanism in Unilateral Amputee Gait." *Gait and Posture* 21 (3): 333–40. <https://doi.org/10.1016/j.gaitpost.2004.04.005>.
- Dickinson, A.S., Steer, J.W. & Worsley, P.R. 2017. "Finite Element Analysis of the Amputated Lower Limb: A Systematic Review and Recommendations." *Medical Engineering and Physics* 43: 1–18. <https://doi.org/10.1016/j.medengphy.2017.02.008>.
- Doane, N.E., & Holt, L.E. 1983. "A Comparison of the SACH and Single Axis Foot in the Gait of Unilateral Below-Knee Amputees." *Prosthetics and Orthotics International*, 33–36. [http://www.oandplibrary.org/poi/pdf/1983\\_01\\_033.pdf](http://www.oandplibrary.org/poi/pdf/1983_01_033.pdf).
- Donlagic, D., Cigale, B. & Heric, D. 2008. "A Patient-Specific Knee Joint Computer Model Using MRI Data and 'in Vivo' Compressive Load from the Optical Force Measuring System." *CIT. Journal of ...*, 209–22. <https://doi.org/10.2498/cit.1001126>.
- Dragomir-Daescu, D., Salas, C., Uthamaraj, S. and Rossman, T. 2015. "Quantitative Computed Tomography-Based Finite Element Analysis Predictions of Femoral Strength and Stiffness Depend on Computed Tomography Settings." *J Biomech* 48 (1): 153–61. <https://doi.org/10.1016/j.jbiomech.2014.09.016>.
- Dryden, I.L. & Mardia, K.V. 2016. *Statistical Shape Analysis with Applications in R*. Edited by David J Blading, Noel A c Cressie, Garrett M Fitzmaurice, Geof H Givens, Harvey Goldstein, Geert Molenberghs, David W Scott, Adrian F M Smith, Ruey S Tsay, and Sanford Weisberg. Second. John Wiley and Sons Ltd. <http://www.victoriawwy.com/wp-content/uploads/2017/12/SSA2.pdf>.
- Duda, G.N., Mandruzzato, F., Heller, M., Goldhahn, J., Moser, R., Hehli, M., Claes, L. & Haas, N.P. 2001. "Mechanical Boundary Conditions of Fracture Healing: Borderline Indications in the Treatment of Unreamed Tibial Nailing." *Journal of Biomechanics* 34 (5): 639–50. [https://doi.org/10.1016/S0021-9290\(00\)00237-2](https://doi.org/10.1016/S0021-9290(00)00237-2).

- Erdemir, A., Mclean, S., Herzog, W., & Van Den Bogert, A.J. 2007. "Model-Based Estimation of Muscle Forces Exerted during Movements." *Clinical Biomechanics* 22: 131–54.  
<https://doi.org/10.1016/j.clinbiomech.2006.09.005>.
- Eriksen, E.F. 2010. "Cellular Mechanisms of Bone Remodeling." *Reviews in Endocrine and Metabolic Disorders* 11 (4): 219–27. <https://doi.org/10.1007/s11154-010-9153-1>.
- Evans, R.K., Negus C.H., Centi., A.J., Spiering B.A., Kraemer, W.J. & Nindl, B.C. 2012. "Peripheral QCT Sector Analysis Reveals Early Exercise-Induced Increases in Tibial Bone Mineral Density." *J Musculoskelet Neuronal Interact* 12 (3): 155–64.  
<http://www.ncbi.nlm.nih.gov/pubmed/22947547>.
- Evans, R.K., Negus, C., Antczak, A.J., Yanovich, R., Israeli, E., & Moran, D.S. 2008. "Sex Differences in Parameters of Bone Strength in New Recruits." *Medicine & Science in Sports & Exercise* 40 (Suppl 1): S645–53. <https://doi.org/10.1249/mss.0b013e3181893cb7>.
- Farahmand, F., Rezaeian, T., Narimani, R. & Dinan, H. 2006. "Kinematic and Dynamic Analysis of the Gait Cycle of Above-Knee Amputees." *Scientia Iranica* 13 (3): 261–71.
- Fernandez, J.W. & Pandy, M. G. 2006. "Integrating Modelling and Experiments to Assess Dynamic Musculoskeletal Function in Humans." *Experimental Physiology* 91 (2): 371–82.  
<https://doi.org/10.1113/expphysiol.2005.031047>.
- Fey, N.P. & Neptune, R.R. 2012. "3D Intersegmental Knee Loading in Below-Knee Amputees across Steady-State Walking Speeds." *Clinical Biomechanics* 27 (4): 409–14.  
<https://doi.org/10.1016/j.clinbiomech.2011.10.017>.
- Frossard, L., Stevenson, N., Sullivan, J., Uden, M. & Percy, M. 2011. "Categorisation of Activities of Daily Living of Lower Limb Amputees during Short Term Use of a Portable Kinetic Recording System : A Preliminary Study." *Brain Research* 23 (1): 1–17.
- Frost, H.M. 1994. "Wolff's Law and Bone's Structural Adaptations to Mechanical Usage: An Overview for Clinicians." *Angle Orthodontist*. <https://doi.org/10.1043/0003->

3219(1994)064<0175:WLABSA>2.0.CO;2.

- Frost, H.M. 1987. "The Mechanostat: A Proposed Pathogenic Mechanism of Osteoporoses and the Bone Mass Effects of Mechanical and Nonmechanical Agents." *Bone and Mineral* 2 (2): 73–85.  
<http://www.ncbi.nlm.nih.gov/pubmed/3333019>.
- Fukubayashi, T. & Kurosawa, H 1980. "THE CONTACT AREA AND PRESSURE DISTRIBUTION PATTERN OF THE KNEE A Study of Normal and Osteoarthrotic Knee Joints." *Acta Orthop. Wand* 51: 871–79. <http://www.tandfonline.com/doi/pdf/10.3109/17453678008990887>.
- Fung, A ., Loundagin, L.L. & Edwards, W.B. 2017. "Experimental Validation of Finite Element Predicted Bone Strain in the Human Metatarsal." *Journal of Biomechanics* 60: 22–29.  
<https://doi.org/10.1016/j.jbiomech.2017.06.010>.
- Funk, J. R. & Crandall, J.R. 2006. "Calculation of Tibial Loading Using Strain Gauges." *Biomedical Sciences Instrumentation* 42: 160–65.
- Grabowski, A.M., D'Andrea, S., 2013. Effects of a powered ankle–foot prosthesis on kinetic loading of the unaffected leg during level-groundwalking. *Journal of Neuro engineering and Rehabilitation* 10, 49
- Gailey, R., Allen, K., Castles, J., Kucharik, J. & Roeder, M. 2008. "Review of Secondary Physical Conditions Associated with Lower-Limb Amputation and Long-Term Prosthesis Use." *Journal of Rehabilitation Research and Development*. <https://doi.org/10.1682/JRRD.2006.11.0147>.
- Gerus, P., Sartori, M., Besier, T.F., Fregly, B.J., Delp, S.L., Banks, S.A., Pandy, M.G., D’Lima, D.D. & Lloyd, D.G. 2013. "Subject-Specific Knee Joint Geometry Improves Predictions of Medial Tibiofemoral Contact Forces." *Journal of Biomechanics* 46 (16): 2778–86.  
<https://doi.org/10.1016/j.jbiomech.2013.09.005>.
- Gilbert, S., Chen, T., Hutchinson, I.D., Choi, D., Voigt, C., Warren, R.F. & Maher, S.A., 2014. "Dynamic Contact Mechanics on the Tibial Plateau of the Human Knee During Activities of Daily Living." *Journal of Biomchanics* 47 (9): 2006–12.

<https://doi.org/10.1016/j.jbiomech.2013.11.003>.

Glaser, J., Bensley, R., Hurks, R., Dahlberg, S., Hamden, A., Wyers, M., Chaikof, E. & Schermerhorn, M. 2013. "Fate of the Contralateral Limb after Lower Extremity Amputation."

*Journal Vascular Surgery* 58 (6): 220–31.

<https://doi.org/10.1016/j.freeradbiomed.2008.10.025>.The.

Gorton, G.E., Hebert, D.A. & Gannotti, M.E. 2009. "Assessment of the Kinematic Variability among 12 Motion Analysis Laboratories." *Gait and Posture* 29 (3): 398–402.

<https://doi.org/10.1016/j.gaitpost.2008.10.060>.

Gray, H.A., Taddei, F., Zavatsky, A.B., Cristofolini, L. & Gill, H.S. 2008. "Experimental Validation of a Finite Element Model of a Human Cadaveric Tibia." *Journal of Biomechanical Engineering*

130 (3): 031016. <https://doi.org/10.1115/1.2913335>.

Gregor, R.J., Roy, R.R., Whiting, W.C., Lovely, R.G., Hodgson, J.A. & Edgerton, V.R. 1988.

"Mechanical Output of the Cat Soleus during Treadmill Locomotion: In Vivo vs in Situ Characteristics." *Journal of Biomchanics* 21: 721–32.

Gremeaux, V., Damak, S., Troisgros, O., Feki, A., Laroche, D., Perennou, D., Benaim, C. & Casillas, J.M. 2012. "Selecting a Test for the Clinical Assessment of Balance and Walking Capacity at the Definitive Fitting State after Unilateral Amputation: A Comparative Study." *Prosthetics and Orthotics International*. <https://doi.org/10.1177/0309364612437904>.

Grimpampi, E., Oesen, S., Halper, B., Hofmann, M., Wessner, B. & Mazzà, C. 2015. "Reliability of Gait Variability Assessment in Older Individuals during a Six-Minute Walk Test." *Journal of Biomechanics* 48 (15): 4185–89. <https://doi.org/10.1016/j.jbiomech.2015.10.008>.

Groll, O., Lochmüller, E.M., Bachmeier, M., Willnecker, J. and Eckstein, F. 1999. "Precision and Intersite Correlation of Bone Densitometry at the Radius, Tibia and Femur with Peripheral Quantitative CT." *Skeletal Radiology* 28 (12): 696–702.

Gulgin, H., Hall, K., Luzadre, A. & Kayfish, E. 2017. "3D Gait Analysis with and without an

- Orthopedic Walking Boot.” *Gait & Posture* 59: 76–82.  
<https://doi.org/10.1016/j.gaitpost.2017.09.024>.
- Hackshaw, A. 2008. “Small Studies: Strengths and Limitations.” *European Respiratory Journal* 32 (5): 1141–43. <https://doi.org/10.1183/09031936.00136408>.
- Haeufle, D. F.B., Günther, M., Bayer, A. & Schmitt, S. 2014. “Hill-Type Muscle Model with Serial Damping and Eccentric Force-Velocity Relation.” *Journal of Biomechanics* 47 (6): 1531–36.  
<https://doi.org/10.1016/j.jbiomech.2014.02.009>.
- Xie, H., Yao H., Zhou X., Sun S. & Tong, X. 2018. “Weighted Voxel: A Novel Voxel Representation for 3D Reconstruction.” In *ICIMCS '18 Proceedings of the 10th International Conference on Internet Multimedia Computing and Service*. <https://doi.org/10.1145/3240876.3240888>.
- Hashemi, J., Schutt, R., Chandrashekar, N. & Dabezies, E. 2004. “53rd Annual Meeting of the Orthopaedic Research Society Poster No : 0801” 76 (5): 2004.
- Haut Donahue, T.L., Hull, M.L., Rashid, M.M., Jacobs, C.R., Donahue, T.L.H., Hull, M.L., Rashid, M.M. and Jacobs, C.R. 2002. “A Finite Element Model of the Human Knee Joint for the Study of Tibio-Femoral Contact.” *Journal of Biomechanical Engineering* 124 (3): 273.  
<https://doi.org/10.1115/1.1470171>.
- Obara, H., Yoshiyuki Kobayashi, Y., Nakamura, T., Yamasaki, N, Nakazawa, K., Akai, M. & Ogata, T. 2011. “Lower Extremity Joint Kinematics of Stair Ascent in Transfemoral Amputees.” *Prosthetics and Orthotics International* 35 (4): 467–72.  
<https://doi.org/10.1177/0309364611425564>.
- Hobara, H., Baum, B.S., Kwon, H.J., Linberg, A., Wolf, E.J., Miller, R.H., Shim, J.K., 2014. Amputee locomotion: lower extremity loading using running-specific prostheses. *Gait and Posture* 39, 386-390
- Holden, J.P., Selbie, S.W. & Stanhope, S.S. 2002. “A Proposed Test to Support the Clinical Movement Analysis Laboratory Accreditation Process.” *Gait and Posture* 17: 205–13.

<http://www.c-motion.com/download/CalTester/CalTesterArticle2003.pdf>.

- Holick, M. F. 1998. "Perspective on the Impact of Weightlessness on Calcium and Bone Metabolism." *Bone* 22 (5 SUPPL.): 105S-111S. [https://doi.org/10.1016/S8756-3282\(98\)00014-3](https://doi.org/10.1016/S8756-3282(98)00014-3).
- Horsman, K., M. D., H. F.J.M. Koopman, F. C.T. van der Helm, L. Poliacu Prosé, and H. E.J. Veeger. 2007. "Morphological Muscle and Joint Parameters for Musculoskeletal Modelling of the Lower Extremity." *Clinical Biomechanics* 22 (2): 239–47. <https://doi.org/10.1016/j.clinbiomech.2006.10.003>.
- Horsman, K. & Martijn D. 1979. *The Twente Lower Extremity Model*.
- Horst, F., Eekhoff, A., Newell, K.M. & Schöllhorn. W.I. 2017. "Intra-Individual Gait Patterns across Different Time-Scales as Revealed by Means of a Supervised Learning Model Using Kernel-Based Discriminant Regression." *PLoS ONE* 12 (6). <https://doi.org/10.1371/journal.pone.0179738>.
- Huang, S., Kaw, M., Harris, M., Ebraheim, N., McInerney, Najjar, S., & Lecka-Czernik, B. 2010. "Decreased Osteoclastogenesis and High Bone Mass in Mice with Impaired Insulin Clearance Due to Liver-Specific Inactivation to CEACAM1." *Bone* 46 (4): 1138–45. <https://doi.org/10.1038/mp.2011.182>.
- Huiskes, R., & Chao, E.Y.S.1983a. "A Survey of Finite Element Analysis in Orthopedic Biomechanics: The First Decade." *Journal of Biomechanics* 16 (6): 385–409.
- . 1983b. "A Survey of Finite Element Analysis in Orthopedic Biomechanics: The First Decade." *Journal of Biomechanics* 16 (6): 385–409. [https://doi.org/10.1016/0021-9290\(83\)90072-6](https://doi.org/10.1016/0021-9290(83)90072-6).
- Hurley, G R., McKenney, R., Robinson, M., Zadavec, M. & Pierrynowski, M.R. 1990. "The Role of the Contralateral Limb in Below-Knee Amputee Gait." *Prosthetics and Orthotics International* 14 (1): 33–42. <https://doi.org/10.3109/03093649009080314>.

- Inman, V.T. 1966. "Human Locomotion." *Can Med Assoc J* 94 (20): 1047–54.  
[https://doi.org/10.1016/S0021-9290\(07\)70004-0](https://doi.org/10.1016/S0021-9290(07)70004-0).
- Isakov, E., Burger, H., Krajnik, J., Gregoric, M., & Marincek, C. 1996. "Influence of Speed on Gait Parameters and on Symmetry in Trans-Tibial Amputees." *Prosthetics and Orthotics International* 20 (3): 153–58. <https://doi.org/10.3109/03093649609164437>.
- Izard, R.M., Fraser, W.D., Negus, C., Sale, C., & Greeves, J.P. 2016a. "Increased Density and Periosteal Expansion of the Tibia in Young Adult Men Following Short-Term Arduous Training." *Bone* 88: 13–19. <https://doi.org/10.1016/j.bone.2016.03.015>.
- . 2016b. "Increased Density and Periosteal Expansion of the Tibia in Young Adult Men Following Short-Term Arduous Training." *Bone* 88: 13–19.  
<https://doi.org/10.1016/j.bone.2016.03.015>.
- Jiao, H., Xiao, E. & Graves, D.T. 2015. "Diabetes and Its Effect on Bone and Fracture Healing Compliance with Ethics Guidelines Conflict of Interest Statement The Authors Must Submit Their Disclosure Forms Human and Animal Rights and Informed Consent HHS Public Access." *Curr Osteoporos Rep* 13 (5): 327–35. <https://doi.org/10.1007/s11914-015-0286-8>.
- Johansson, J.L., Sherrill, D.M., O. Riley, P., Bonato, P., & Herr, H. 2005. "A Clinical Comparison of Variable-Damping and Mechanically Passive Prosthetic Knee Devices." *American Journal of Physical Medicine & Rehabilitation* 84 (8): 563–75.  
<https://doi.org/10.1097/01.phm.0000174665.74933.0b>.
- Jones, S. F., Twigg, P. C., Scally, A. J., & Buckley, J. G. 2006. "The Mechanics of Landing When Stepping down in Unilateral Lower-Limb Amputees." *Clinical Biomechanics* 21 (2): 184–93.  
<https://doi.org/10.1016/j.clinbiomech.2005.09.015>.
- Juanes, J. A., Prats, A., Lagándara, M. L., & Riesco, J. M. 2003. "Application of the 'Visible Human Project' in the Field of Anatomy: A Review." *European Journal of Anatomy* 7 (3): 147–59.
- Kaufman, K.R., Levine, J.A., Brey, R.H., Iverson, B.K., McCrady, S.K., Padgett, D.J., & Joyner, M.J.

2007. "Gait and Balance of Transfemoral Amputees Using Passive Mechanical and Microprocessor-Controlled Prosthetic Knees." *Gait & Posture* 26 (4): 489–93.  
<https://doi.org/10.1016/j.gaitpost.2007.07.011>.
- Kaufman, K.R., Frittoli, S., & Frigo, C.A. 2012. "Gait Asymmetry of Transfemoral Amputees Using Mechanical and Microprocessor-Controlled Prosthetic Knees." *Clinical Biomechanics (Bristol, Avon)* 27 (5): 460–65. <https://doi.org/10.1016/j.clinbiomech.2011.11.011>.
- Kazakia, G.J., Tjong, W., Nirody, J.A., Burghardt, A.J., Carballido-Gamio, J., Patsch, J.M., Link, T., Feeley, B.T. & Ma, B.C. 2014. "The Influence of Disuse on Bone Microstructure and Mechanics Assessed by HR-PQCT." *Bone* 63: 132–40. <https://doi.org/10.1016/j.bone.2014.02.014>.
- Kaze, A.D., Maas, S., Arnoux, P-J., Wolf, C., & Pape, D. 2017. "A Finite Element Model of the Lower Limb during Stance Phase of Gait Cycle Including the Muscle Forces." *BioMedical Engineering OnLine*. <https://doi.org/10.1186/s12938-017-0428-6>.
- Kazembakhshi, S. & Lu, Y. 2014. "Constructing Anisotropic Finite Element Model of Bone from Computed Tomography (CT)." *Bio-Medical Materials and Engineering*.  
<https://doi.org/10.3233/BME-141078>.
- Kazemi, M., Dabiri, Y. & Li, L.P. 2013. "Recent Advances in Computational Mechanics of the Human Knee Joint." *Computational and Mathematical Methods in Medicine* 2013 (November 2015): 718423. <https://doi.org/10.1155/2013/718423>.
- Kerr, M. 2017. "Improving Footcare for People with Diabetes and Saving Money: An Economic Study in England." *Diabetes UK*.
- Kim, J. 2017. "The Effect of Bone and Ligament Morphology of Ankle Joint Loading in the Neutral Position." Old Dominion University.
- Komi, P V. 1990. "Relevance of in Vivo Force Measurements to Human Biomechanics." *J Biomech*.
- Kovac, I., Medved, V. & Ostojić, L. 2010. "Spatial, Temporal and Kinematic Characteristics of Traumatic Transtibial Amputees' Gait." *Collegium Antropologicum* 34 (1): 205–13.

<http://www.ncbi.nlm.nih.gov/pubmed/20402320>.

- Kulkarni, J., Adams, J., Thomas, E. & Silman, A. 1998. "Association between Amputation, Arthritis and Osteopenia in British Male War Veterans with Major Lower Limb Amputations." *Clinical Rehabilitation* 12 (4): 361–66. <https://doi.org/10.1191/026921598672393611>.
- Kuriki, F.M., Azevedo, H., Takahashi, L.S.O., Mello, E.M., de Faria Negro Filho, R. & Alves, N. 2012. "The Relationship Between Electromyography and Muscle Force, EMG Methods for Evaluating Muscle and Nerve Function." *EMG Methods for Evaluating Muscle and Nerve Function*, 31–54. <https://doi.org/10.5772/25381>.
- Kutzner, I., Heinlein, B., Graichen, F., Bender, A., Rohlmann, A., Halder, A., Beier, A. & Bergmann, G. 2010. "Loading of the Knee Joint during Activities of Daily Living Measured in Vivo in Five Subjects." *Journal of Biomechanics* 43 (11): 2164–73. <https://doi.org/10.1016/j.jbiomech.2010.03.046>.
- Lai, Y-S., Chen, W-C., Huang, C-H., Cheng, C-K., Chan, K-K., Chang, T-K. & Woloschak, G.E. 2015. "The Effect of Graft Strength on Knee Laxity and Graft In-Situ Forces after Posterior Cruciate Ligament Reconstruction." *PLOS ONE*. <https://doi.org/10.1371/journal>.
- Langholz, J. B., Westman, G. & Karlsteen, M. 2016. "Musculoskeletal Modelling in Sports-Evaluation of Different Software Tools with Focus on Swimming." *Procedia Engineering* 147: 281–87. <https://doi.org/10.1016/j.proeng.2016.06.278>.
- Lanyon, L. E., Hampson, W. G. J., Goodship, A. E. & Shah, J. S. 1975. "Bone Deformation Recorded in Vivo from Strain Gauges Attached to the Human Tibial Shaft." *Acta Orthopaedica* 46 (2): 256–68. <https://doi.org/10.3109/17453677508989216>.
- Lanyon, L.E. 1982. "Mechanical Function and Bone Remodeling." *Bone in Clinical Orthopaedics.*, p 273–304.
- Leali, P.T., Muresu, F., Melis, A., Ruggiu, A., Zachos, A. & Doria, C.2011. "Skeletal Fragility Definition." *Clinical Cases in Mineral and Bone Metabolism* 8 (2): 11–13.

[https://www.ncbi.nlm.nih.gov/pmc/articles/PMC3279077/pdf/ccmbm8\\_2p011.pdf](https://www.ncbi.nlm.nih.gov/pmc/articles/PMC3279077/pdf/ccmbm8_2p011.pdf).

- Lecka-Czernik, B. 2010. "Bone Loss in Diabetes: Use of Antidiabetic Thiazolidinediones and Secondary Osteoporosis." *Curr Osteoporos Rep* 8: 178–84. <https://doi.org/10.1007/s11914-010-0027-y>.
- Leclercq, M.M, Bonidan, O., Haaby, E., Pierrejean, C. & Sengler, J. 2003. "Étude de La Masse Osseuse Par Ostéodensitométrie Dans Une Population de 99 Amputés de Membre Inférieur." *Annales de Réadaptation et de Médecine Physique* 46 (1): 24–30. [https://doi.org/10.1016/S0168-6054\(02\)00350-1](https://doi.org/10.1016/S0168-6054(02)00350-1).
- Leitner, M., Schmid, S., Hilfiker, R., and Radlinger, L. 2011. "Test-Retest Reliability of Vertical Ground Reaction Forces during Stair Climbing in the Elderly Population." *Gait and Posture* 34 (3): 421–25. <https://doi.org/10.1016/j.gaitpost.2011.06.014>.
- Lemaire, E D, and Fisher, F.R. 1994. "Osteoarthritis and Elderly Amputee Gait." *Archives of Physical Medicine and Rehabilitation* 75 (10): 1094–99. <http://www.ncbi.nlm.nih.gov/pubmed/7944914>.
- Lemaire, E.D., Fisher, F.R. & Robertson, D.G.E. 1993. "Gait Patterns of Elderly Men W--Tibiai-Amputatiorr." *Prosthetics and Orthotics International*. Vol. 17. <http://journals.sagepub.com/doi/pdf/10.3109/03093649309164352>.
- Lemaire, E. D., Nielen, D., & Paquin, M.A. 2000. "Gait Evaluation of a Transfemoral Prosthetic Simulator." *Archives of Physical Medicine and Rehabilitation* 81 (6): 840–43. <https://doi.org/10.1053/apmr.2000.3853>.
- Lesso-Arroyo, R., Cesar, J., Jiménez, S., Castro, R.R., Instituto Tecnológico De Celaya, Grupo S S C De México, & Allende, S.M. 2004. Biomechanical Behavior of the Knee Joint Using ANSYS. *International ANSYS Conference Proceedings.*, issued 2004. <https://pdfs.semanticscholar.org/b0cd/dfeb9dd551f91db80af9141a5eeb6fbd6291.pdf>.
- Levenston, M.E., Beaupré, G.S. & Carter, D.R. 1998. "Loading Mode Interactions in Simulations of Long Bone Cross-Sectional Adaptation." *Computer Methods in Biomechanics and Biomedical*

- Engineering* 1 (April): 303–19. <https://doi.org/10.1080/01495739808936709>.
- Levine, D., Richards, J. & Whittle, M. 2012. *Whittle's Gait Analysis*.
- Guoan, L.A., Van de Velde, S.K. & Bingham, J.T. 2008. "Validation of a Non-Invasive Fluoroscopic Imaging Technique for the Measurement of Dynamic Knee Joint Motion." *Journal of Biomechanics* 41: 1616–22. <https://doi.org/10.1016/j.jbiomech.2008.01.034>.
- Li, L., Haddad, J.M. & Hamill, J. 2005. "Stability and Variability May Respond Differently to Changes in Walking Speed." *Human Movement Science* 24 (2): 257–67. <https://doi.org/10.1016/j.humov.2005.03.003>.
- Lieberman, D. E., Polk, J.D. & Demes, B. 2004. "Predicting Long Bone Loading from Cross-Sectional Geometry." *American Journal of Physical Anthropology* 123 (2): 156–71. <https://doi.org/10.1002/ajpa.10316>.
- Livingston, L.A., Stevenson, J.M. & Obey, S.J. 1991. "Stairclimbing Kinematics on Stairs of Differing Dimensions." *Archives of Clinical Neuropsychology* 72: 398–402. [https://www.archives-pmr.org/article/0003-9993\(91\)90174-H/pdf](https://www.archives-pmr.org/article/0003-9993(91)90174-H/pdf).
- Lloyd, C.H., Stanhope, S. J., Davis, I.S. & Royer, T.D. 2010. "Strength Asymmetry and Osteoarthritis Risk Factors in Unilateral Trans-Tibial, Amputee Gait." *Gait and Posture* 32 (3): 296–300. <https://doi.org/10.1016/j.gaitpost.2010.05.003>.
- Long, I. 1985. "Normal Shape-Normal Alignment (NSNA) Above-Knee Prosthesis." *Clinical Prosthetics and Orthotics* 9.
- Loyd, B. J., Fields, T.T., Stephenson, R.O., Stevens-Lapsley, J.E., Cory L Christiansen, and Brian Loyd. 2016. "Explaining Modified 2-Min Walk Test Outcomes in Male Veterans with Traumatic or Nontraumatic Lower-Limb Amputation HHS Public Access." *J Rehabil Res Dev. J Rehabil Res Dev* 53 (6): 1035–44. <https://doi.org/10.1682/JRRD.2015.03.0038>.
- Lu, T.W., & O'Connor, J.J., 1999. "Bone Position Estimation from Skin Marker Co-Ordinates Using Global Optimisation with Joint Constraints." *Journal of Biomechanics* 32: 129–34.

file:///D:/eric.desailly/Desktop/pdf en vrac/Lu, Connor - 1999.pdf.

- Lu, T-W., Taylor, S.J.G., O'connor, J.J. & Walker, P.S. 1997. "INFLUENCE OF MUSCLE ACTIVITY ON THE FORCES IN THE FEMUR: AN IN T/H/O STUDY." *Biomechanics* 30 (1): 1101–6. [http://ac.els-cdn.com/S0021929097000900/1-s2.0-S0021929097000900-main.pdf?\\_tid=7cfc59c-8337-11e7-9c84-00000aab0f01&acdnat=1502966180\\_0a2486912bc260c6d276d1262bbd1e75](http://ac.els-cdn.com/S0021929097000900/1-s2.0-S0021929097000900-main.pdf?_tid=7cfc59c-8337-11e7-9c84-00000aab0f01&acdnat=1502966180_0a2486912bc260c6d276d1262bbd1e75).
- Luder, G., Baumann, T., Jost, C., Schmid, S. & Radlinger, L. 2007. *Variability of Ground Reaction Forces in Healthy Subjects during Stair Climbing. Physioscience*. Vol. 3.
- Lund, M. E., Andersen, M.S., De Zee, M. & Rasmussen, J. 2015. "Scaling of Musculoskeletal Models from Static and Dynamic Trials." *International Biomechanics* 2 (1): 1–11. <https://doi.org/10.1080/23335432.2014.993706>.
- Lunn, D. E. 2013. "Musculoskeletal Modeling and Finite Element Analysis of the Proximal Juvenile Femur," no. October.
- Brekelmans, M.W.A., Poort, H.W., Slooff, T. J.J.H., Diaconessenziekenhuis, I., Chapchal, G., Janssen, J.D., Van Rens, P.P.T.G., Sanders, A.G., Tomesen, L.B.M & Zorge, S.D. 1972. "A New Method To Analyse the Mechanical Behaviour of Skeletal Parts." *Acta Orthop. Scandinav* 43: 301–17. <https://doi.org/10.3109/17453677208998949>.
- Macdonald, H.M., Kontulainen, S.A., MacKelvie-O'Brien, K.J., Petit, M.A., Janssen, P., Khan, K.M. & McKay, H.A., 2005. "Maturity- and Sex-Related Changes in Tibial Bone Geometry, Strength and Bone-Muscle Strength Indices during Growth: A 20-Month PQCT Study." *Bone* 36 (6): 1003–11. <https://doi.org/10.1016/j.bone.2004.12.007>.
- Maghraoui, A. 2012. "Interpreting a DXA Scan in Clinical Practice, Dual Energy X-Ray Absorptiometry." *Dual Energy X-Ray Absorptiometry*, no. Roux 1998: 146. <https://doi.org/10.5772/52807>.
- Maquet, P, and Furlong R. 1991. "Mechanics of the Human Walking Apparatus [Transl. of W. Weber

and E. Weber].”

Martin, J.A., Brandon, S.C.E., Keuler, E.M., Hermus, J.R., Ehlers, A.C., Segalman, D.J., Allen, M.S.

& Thelen, D.G. 2018. “Gauging Force by Tapping Tendons.” *Nature Communications* 9 (1).

<https://doi.org/10.1038/s41467-018-03797-6>.

Martini, F, Nath, J & Bartholomew, E. 2012. *Anatomy and Physiology*. San Francisco: Pearson.

Matijevich, E. S., Branscombe, L.M., Scott, L.R. & Zelik. K.E. 2019. “Ground Reaction Force

Metrics Are Not Strongly Correlated with Tibial Bone Load When Running across Speeds and

Slopes: Implications for Science, Sport and Wearable Tech.” *PLoS ONE* 14 (1): 1–19.

<https://doi.org/10.1371/journal.pone.0210000>.

Mcfadyen, B.J. & Winter, D.A. 1988. “AN INTEGRATED BIOMECHANICAL ANALYSIS OF

NORMAL STAIR ASCENT AND DESCENT.” *J. Biomechanics* 21 (9): 733–44.

<https://eurekamag.com/pdf/004/004731043.pdf>.

Messmer, P., Matthews, F., Ludwig, A.J., Kikinis, R., Regazzoni, P. & Noser, H. 2007. “A CT

Database for Research, Development and Education: Concept and Potential” 20 (1): 17–22.

<https://doi.org/10.1007/s10278-006-0771-9>.

Mitchell, M., Craig, K., Kyberd, P., Biden, E. & Bush, G. 2013. “Design and Development of Ankle-

Foot Prosthesis with Delayed Release of Plantarflexion.” *Journal of Rehabilitation Research*

*and Development* 50 (3): 409–22.

Mittag, U., Kriechbaumer, A. & Rittweger, J. 2017. “A Novel Interpolation Approach for the

Generation of 3D-Geometric Digital Bone Models from Image Stacks.” *J Musculoskelet*

*Neuronal Interact.* [http://www.ismni.org/jmni/accepted/jmni\\_aa\\_MITTAG.pdf](http://www.ismni.org/jmni/accepted/jmni_aa_MITTAG.pdf).

Miyazaki, T., Wada, M., Kawahara, H., Sato, M., Baba, H. & Shimada, S. 2002. “Dynamic Load at

Baseline Can Predict Radiographic Disease Progression in Medial Compartment Knee

Osteoarthritis.” *Ann Rheum Dis* 61: 617–22.

<https://www.ncbi.nlm.nih.gov/pmc/articles/PMC1754164/pdf/v061p00617.pdf>.

- Mooren, F. C. 2012. *Encyclopedia of Exercise Medicine in Health and Disease*. Berlin, Heidelberg: Springer Berlin Heidelberg. <https://doi.org/10.1007/978-3-540-29807-6>.
- Morgenroth, D.C., Gellhorn, A.C. & Suri, P. 2012. "Osteoarthritis in the Disabled Population: A Mechanical Perspective." *PM and R* 4 (5 SUPPL.): S20–27. <https://doi.org/10.1016/j.pmrj.2012.01.003>.
- Moxey, P. W., Gogalniceanu, P., Hinchliffe, R. J., Loftus, I. M., Jones, K. J., Thompson, M. M. & Holt, P. J. 2011. "Lower Extremity Amputations - a Review of Global Variability in Incidence." *Diabetic Medicine* 28 (10): 1144–53. <https://doi.org/10.5980/jpnjurol.106.255>.
- Murphy, W., Black, J. & Hastings, G. 2016. "Handbook of Biomaterial Properties, Second Edition." *Handbook of Biomaterial Properties, Second Edition*, 1–676. <https://doi.org/10.1007/978-1-4939-3305-1>.
- National Cancer Institute. 2009. "National Cancer Institute. Radiation Risks and Pediatric Computed Tomography (CT): A Guide for Health Care Providers." 2009. <http://www.cancer.gov/cancertopics/causes/radiation-risks-pediatric-CT>.
- National Library of Medicine, U.S. 2003. "The National Library of Medicines Visible Human Project." U.S. National Library of Medicine. 2003. [https://www.nlm.nih.gov/research/visible/visible\\_human.html](https://www.nlm.nih.gov/research/visible/visible_human.html).
- Nazer, R., Lanovaz, J., Kawalilak, C., Johnston, J. D. & Kontulainen, S. 2012. "Direct in Vivo Strain Measurements in Human Bone-A Systematic Literature Review." *Journal of Biomechanics* 45 (1): 27–40. <https://doi.org/10.1016/j.jbiomech.2011.08.004>.
- NCSCT. 2012. Executive summary Smoking and bone health, issued 2012. [http://www.ncsct.co.uk/usr/pub/smoking\\_and\\_bone\\_health.pdf](http://www.ncsct.co.uk/usr/pub/smoking_and_bone_health.pdf).
- Nepomuceno, A., Major, M.J., Stine, R. & Gard, S. 2017. "Effect of Foot and Ankle Immobilization on Able-Bodied Gait as a Model to Increase Understanding about Bilateral Transtibial Amputee Gait." *Prosthetics and Orthotics International*, 030936461769852.

<https://doi.org/10.1177/0309364617698521>.

NIH. 2015. "Bone Mass Measurement: What the Numbers Mean." 2015.

[www.niams.nih.gov/health\\_info/bone/bone\\_health/bone\\_mass\\_measure.asp](http://www.niams.nih.gov/health_info/bone/bone_health/bone_mass_measure.asp).

Niu, W. X., Wang, L. J., Feng, T. N., Jiang, C. H., Fan, Y. B. & Fan, Y. B. 2013. "Effects of Bone Young's Modulus on Finite Element Analysis in the Lateral Ankle Biomechanics." *Applied Bionics and Biomechanics* 10 (4): 189–95. <https://doi.org/10.3233/ABB-140085>.

Nolan, L., Wit, A., Dudziński, K., Lees, A., Lake, M. & Wychowański, M. 2003. "Adjustments in Gait Symmetry with Walking Speed in Trans-Femoral and Trans-Tibial Amputees." *Gait and Posture* 17 (2): 142–51. [https://doi.org/10.1016/S0966-6362\(02\)00066-8](https://doi.org/10.1016/S0966-6362(02)00066-8).

Nolte, D., Tsang, C. K., Zhang, K.Y., Ding, Z., Kedgley, A.E. & Bull, A.M.J. 2016. "Non-Linear Scaling of a Musculoskeletal Model of the Lower Limb Using Statistical Shape Models." *Journal of Biomechanics* 49 (14): 3576–81. <https://doi.org/10.1016/j.jbiomech.2016.09.005>.

Nordin, M. & Frankel, V.H. 2001. "Biomechanics of Bone." In *Biomechanics of Tissues and Structures of the Musculoskeletal System*, 3–29.

Nosova, E.V., Conte, M.S. & Grenon, S.M. 2015. "Advancing beyond the 'Heart-Healthy Diet' for Peripheral Arterial Disease." *Journal of Vascular Surgery* 61 (1): 265–74. <https://doi.org/10.1016/j.jvs.2014.10.022>.

Oliveira De Cerqueira Soares, A.S., Edward Yuji Yamaguti, Luis Mochizuki, Alberto Carlos Amadio, and Júlio Cerca Serrão. 2009. "Biomechanical Parameters of Gait among Transtibial Amputees: A Review." *Sao Paulo Medical Journal* 127 (5): 302–9. <https://doi.org/10.1590/S1516-31802009000500010>.

Orendurff, M.S., Raschke, S.U., Winder, L., Moe, D., Boone, D.A. & Kobayashi, T. 2015.

"Functional Level Assessment of Individuals with Transtibial Limb Loss: Evaluation in the Clinical Setting versus Objective Community Ambulatory Activity." *Journal of Rehabilitation and Assistive Technologies Engineering*. <https://doi.org/10.1177/2055668316636316>.

- Ota, S., Ueda, M., Aimoto, K., Suzuki, Y. & Sigward, S.M. 2014. “Acute Influence of Restricted Ankle Dorsiflexion Angle on Knee Joint Mechanics during Gait.” *The Knee*, 669–75. <https://doi.org/10.1016/j.knee.2014.01.006>.
- Subrata, P. 2014. “Design of Artificial Human Joints & Organs.” *Design of Artificial Human Joints & Organs* 9781461462: 1–419. <https://doi.org/10.1007/978-1-4614-6255-2>.
- Parker, K., Kirby, R.L., Adderson, J. & Thompson, K. 2010. “Ambulation of People With Lower-Limb Amputations: Relationship Between Capacity and Performance Measures.” *YAPMR* 91: 543–49. <https://doi.org/10.1016/j.apmr.2009.12.009>.
- Pérez, M.A., P Fornells, P., Doblaré, M. & García-Aznar, J.M. 2009a. “Comparative Analysis of Bone Remodelling Models with Respect to Computerised Tomography-Based Finite Element Models of Bone.” *Computer Methods in Biomechanics and Biomedical Engineering* 13 (1): 71–80. <https://doi.org/10.1080/10255840903045029>.
- . 2009b. “Computer Methods in Biomechanics and Biomedical Engineering Comparative Analysis of Bone Remodelling Models with Respect to Computerised Tomography-Based Finite Element Models of Bone Comparative Analysis of Bone Remodelling Models with Respect to Computerised Tomography-Based Finite Element Models of Bone.” *Computer Methods in Biomechanics and Biomedical Engineering* 13 (1): 71–80. <https://doi.org/10.1080/10255840903045029>.
- Périé, D. & Hobatho, M.C. 1998. “In Vivo Determination of Contact Areas and Pressure of the Femorotibial Joint Using Non-Linear Finite Element Analysis.” *Clinical Biomechanics* 13 (6): 394–402. [https://doi.org/10.1016/S0268-0033\(98\)00091-6](https://doi.org/10.1016/S0268-0033(98)00091-6).
- Perillo-Marcone, A., Alonso-Vazquez, A. & Taylor, M. 2003. “Assessment of the Effect of Mesh Density on the Material Property Discretisation within QCT Based FE Models: A Practical Example Using the Implanted Proximal Tibia.” *Computer Methods in Biomechanics and Biomedical Engineering* 6 (1): 17–26. <https://doi.org/10.1080/1025584031000064470>.

- Petit, M.A., Beck, T. J. & Kontulainen, S.A. 2005. “Examining the Developing Bone: What Do We Measure and How Do We Do It?” *Journal of Musculoskeletal Neuronal Interactions* 5 (3): 213–24.
- Phate, N., Nareliya, R., Kumar, V. & Francis, A. 2014. “Three-Dimensional Finite Element Analysis of Human Tibia Bone.” *International Journal of Scientific Research Engineering & Technology* 3 (1): 2278–2882. [www.ijret.org](http://www.ijret.org).
- Pickle, N.T., Wilken, J.M., Aldridge, J.M., Neptune, R.R. & Silverman, A.K. 2014. “Whole-Body Angular Momentum during Stair Walking Using Passive and Powered Lower-Limb Prostheses\*.” *Journal of Biomechanics* 47: 3380–89.  
<https://doi.org/10.1016/j.jbiomech.2014.08.001>.
- Pithioux, M., Lasaygues, P. & Chabrand, P. 2002. “An Alternative Ultrasonic Method for Measuring the Elastic Properties of Cortical Bone.” *Journal of Biomechanics* 35 (7): 961–68.  
[https://doi.org/10.1016/S0021-9290\(02\)00027-1](https://doi.org/10.1016/S0021-9290(02)00027-1).
- Poelert, S., Valstar, E., Weinans, H. & Zadpoor, A. A. 2013. “Patient-Specific Finite Element Modeling of Bones.” *Proceedings of the Institution of Mechanical Engineers, Part H: Journal of Engineering in Medicine* 227 (4): 464–78. <https://doi.org/10.1177/0954411912467884>.
- Portnoy, S., Yizhar, Z., Shabshin, N., Itzchak, Y., Kristal, A., Dotan-Marom, Y., Siev-Ner, I. & Gefen, A. 2008. “Internal Mechanical Conditions in the Soft Tissues of a Residual Limb of a Trans-Tibial Amputee.” *Journal of Biomechanics* 41 (9): 1897–1909.  
<https://doi.org/10.1016/j.jbiomech.2008.03.035>.
- Powers, C.M., Rao, S. and Perry, J. 1998. “Knee Kinetics in Trans-Tibial Amputee Gait.” *Gait and Posture* 8 (1): 1–7. [https://doi.org/10.1016/S0966-6362\(98\)00016-2](https://doi.org/10.1016/S0966-6362(98)00016-2).
- Prendergast, P J. 1997. “Finite Element Models in Tissue Mechanics and Orthopaedic Implant Design.” *Clinical Biomechanics Clin. Biomech* 12 (6): 343–66. [http://ac.els-cdn.com/S0268003397000181/1-s2.0-S0268003397000181-main.pdf?\\_tid=7fc19aa6-841f-11e7-](http://ac.els-cdn.com/S0268003397000181/1-s2.0-S0268003397000181-main.pdf?_tid=7fc19aa6-841f-11e7-)

be2b-00000aab0f6b&acdnat=1503065828\_467b296442423e45c3efcb1ac88e1063.

- Protopapadaki, A., Drechsler, W.I., Cramp, M.C., Coutts, F.J. & Scott, O.M. 2007. "Hip, Knee, Ankle Kinematics and Kinetics during Stair Ascent and Descent in Healthy Young Individuals." *Clinical Biomechanics* 22 (2): 203–10. <https://doi.org/10.1016/j.clinbiomech.2006.09.010>.
- Rajagopal, A., Dembia, C.L., Demers, M.S., Delp, D.D., Hicks, J.L. & Delp, S.L. 2015. "Full Body Musculoskeletal Model for Muscle Driven Simulation of Human Gait." *Transactions on Biomedical Engineering*, no. Table I.
- Rao, S.S. 2011. *The Finite Element Method in Engineering*. Elsevier/Butterworth Heinemann.
- Razi, H., Birkhold, A.I., Zehn, M., Duda, G.N., Willie, B.M. & Checa, S. 2014. "A Finite Element Model of in Vivo Mouse Tibial Compression Loading : Influence of Boundary Conditions" 12 (April 2015): 195–207.
- Reid, L., Thomson, P., Besemann, M & Dudek, N. 2015. "Going Places: Does the Two-Minute Walk Test Predict the Six-Minute Walk Test in Lower Extremity Amputees?" *Journal of Rehabilitation Medicine* 47 (3): 256–61. <https://doi.org/10.2340/16501977-1916>.
- Reid, S.M, Lynn, S.K., Musselman, R.P. & Costigan, P.A. 2007. "Knee Biomechanics of Alternate Stair Ambulation Patterns." *Med. Sci. Sports Exerc* 39 (11): 2005–11. <https://doi.org/10.1249/mss.0b013e31814538c8>.
- Rho, J.Y., Kuhn-Spearing, L. & Zioupos, P. 1998. "Mechanical Properties and the Hierarchical Structure of Bone." *Medical Engineering and Physics* 20 (2): 92–102. [https://doi.org/10.1016/S1350-4533\(98\)00007-1](https://doi.org/10.1016/S1350-4533(98)00007-1).
- Riaz, N., Wolden, S.L., Gelblum, D.Y. & Eric, J 2016. "The Effects of Walking Speed on Tibiofemoral Loading Estimated via Musculoskeletal Modeling." *Journal of Applied Biomechanics* 118 (24): 6072–78. <https://doi.org/10.1002/cncr.27633>. Percutaneous.
- Riener, R., Rabuffetti, M. & Frigo, C . 2002. "Stair Ascent and Descent at Different Inclinations." *Gait and Posture* 15: 32–44. [www.elsevier.com/locate/gaitpost](http://www.elsevier.com/locate/gaitpost).

- Robertson, G., Gordon E., & Dowling, J.J. 2003. "Design and Responses of Butterworth and Critically Damped Digital Filters." *Journal of Electromyography and Kinesiology* 13 (6): 569–73. [https://doi.org/10.1016/S1050-6411\(03\)00080-4](https://doi.org/10.1016/S1050-6411(03)00080-4).
- Robertson, G., Caldwell, G., Hamill, J., Kamen, G. & Whittlesey, S. 2014. "Musculoskeletal Modelling." In *Research Methods in Biomchanics*, 247–76.
- Robling, A.G. & Turner, C.H. 2009. "Mechanical Signaling for Bone Modeling and Remodeling." *Critical Reviews in Eukaryotic Gene Expression* 19: 319–38.  
<https://www.ncbi.nlm.nih.gov/pmc/articles/PMC3743123/pdf/nihms-281049.pdf>.
- Roerdink, M., Roeles, S., Van der Pas, S.C.H., Bosboom, O. & Beek, P.J. 2012. "Evaluating Asymmetry in Prosthetic Gait with Step-Length Asymmetry Alone Is Flawed." *Gait and Posture* 35 (3): 446–51. <https://doi.org/10.1016/j.gaitpost.2011.11.005>.
- Roewer, B., Ford, K., Myer, G. & Hewett, T. 2014. "The 'impact' of Force Filtering Cut-off Frequency on the Peak Knee Abduction Moment during Landing: Artefact or 'Artification'?" *British Journal Sports Medicine* 48 (6): 464–68. <https://doi.org/10.1136/bjsports-2012-091398.The>.
- Royer, T.D., and Wasilewski, C.A. 2006a. "Hip and Knee Frontal Plane Moments in Persons with Unilateral, Trans-Tibial Amputation." *Gait and Posture* 23 (3): 303–6.  
<https://doi.org/10.1016/j.gaitpost.2005.04.003>.
- . 2006b. "Hip and Knee Frontal Plane Moments in Persons with Unilateral, Trans-Tibial Amputation." *Gait & Posture* 23: 303–6. <https://doi.org/10.1016/j.gaitpost.2005.04.003>.
- Royer, T.D. & Koenig, M. 2005. "Joint Loading and Bone Mineral Density in Persons with Unilateral, Trans-Tibial Amputation." *Clinical Biomechanics (Bristol, Avon)* 20 (10): 1119–25.  
<https://doi.org/10.1016/j.clinbiomech.2005.07.003>.
- Rubin, C. & Lanyon, L. 1985. "Regulation of Bone Mass by Mechanical Strain Magnitude." *Calcified Tissue International*, no. 37: 411–17.

- Ruff, C., Holt, B. & Trinkaus, E. 2006. "Who's Afraid of the Big Bad Wolff?: 'Wolff's Law' and Bone Functional Adaptation." *American Journal of Physical Anthropology* 129 (4): 484–98. <https://doi.org/10.1002/ajpa.20371>.
- Sadeghi, H., Allard, P., Prince, F. & Labelle, H. 2000. "Symmetry and Limb Dominance in Able-Bodied Gait: A Review." *Gait & Posture* 12 (1): 34–45. [https://doi.org/10.1016/S0966-6362\(00\)00070-9](https://doi.org/10.1016/S0966-6362(00)00070-9).
- Sagawa, Y., Turcot, K., Armand, S., Thevenon, A., Vuillerme, N. & Watelain, E. 2011. "Biomechanics and Physiological Parameters during Gait in Lower-Limb Amputees: A Systematic Review." *Gait & Posture* 33 (4): 511–26. <https://doi.org/10.1016/j.gaitpost.2011.02.003>.
- Salathe, E.P., Arangio, G.A. & Salathe, E.P. 1989. "An Application of Beam Theory to Determine the Stress and Deformation of Long Bones." *Journal of Biomechanics* 22 (3). [https://doi.org/10.1016/0021-9290\(89\)90087-0](https://doi.org/10.1016/0021-9290(89)90087-0).
- Sanders, J.E. & Daly, C.H. 1993. "Normal and Shear Stresses on a Residual Limb in a Prosthetic Socket during Ambulation: Comparison of Finite Element Results with Experimental Measurements." *Journal of Rehabilitation Research and Development* 30: 191–204.
- Sanderson, D.J. & Martin, P.E. 1997. "Lower Extremity Kinematic and Kinetic Adaptations in Unilateral Below-Knee Amputees during Walking." *Gait & Posture* 6 (2): 126–36. [https://doi.org/10.1016/S0966-6362\(97\)01112-0](https://doi.org/10.1016/S0966-6362(97)01112-0).
- Saxer, S., Speich, R., Toigo, M., Mueller, S. M. & Ulrich S. 2015. "Reliability of Parameters during Stair Ascent Measured with Leonardo Mechanograph® Stair a in Healthy Subjects." *Journal of Musculoskeletal Neuronal Interactions* 15 (3): 257–63.
- Schaarschmidt, M., Lipfert, S.W., Meier-Gratz, C., Scholle, H-C. & Seyfarth, A. 2012. "Functional Gait Asymmetry of Unilateral Transfemoral Amputees." *Human Movement Science* 31 (4): 907–17. <https://doi.org/10.1016/j.humov.2011.09.004>.

- Schellenberg, F., Oberhofer, K., Taylor, W.R., Lorenzetti, S., Schellenberg, F., Oberhofer, K., Taylor, W.R. and Lorenzetti, S. 2015. "Review of Modelling Techniques for *In Vivo* Muscle Force Estimation in the Lower Extremities during Strength Training." *Computational and Mathematical Methods in Medicine* 2015: 1–12. <https://doi.org/10.1155/2015/483921>.
- Schileo, E., Taddei, F., Cristofolini, L. and Viceconti, M. 2008. "Subject-Specific Finite Element Models Implementing a Maximum Principal Strain Criterion Are Able to Estimate Failure Risk and Fracture Location on Human Femurs Tested *In Vitro*." *Journal of Biomechanics* 41 (2): 356–67. <https://doi.org/10.1016/j.jbiomech.2007.09.009>.
- Schileo, E., Taddei, F., Malandrino, A., Cristofolini, L. & Viceconti, M. 2007a. "Subject-Specific Finite Element Models Can Accurately Predict Strain Levels in Long Bones." *Journal of Biomechanics* 40: 2982–89. <https://doi.org/10.1016/j.jbiomech.2007.02.010>.
- . 2007b. "Subject-Specific Finite Element Models Can Accurately Predict Strain Levels in Long Bones." *Journal of Biomechanics* 40 (13): 2982–89. <https://doi.org/10.1016/j.jbiomech.2007.02.010>.
- Schipplein, O. D., and Andriacchi, T. P. 1991. "Interaction between Active and Passive Knee Stabilizers during Level Walking." *Journal of Orthopaedic Research* 9 (1): 113–19. <https://doi.org/10.1002/jor.1100090114>.
- Schmalz, T., Blumentritt, S. & Marx, B. 2007a. "Biomechanical Analysis of Stair Ambulation in Lower Limb Amputees." *Gait and Posture* 25 (2): 267–78. <https://doi.org/10.1016/j.gaitpost.2006.04.008>.
- . 2007b. "Biomechanical Analysis of Stair Ambulation in Lower Limb Amputees." *Gait & Posture* 25: 267–78. <https://doi.org/10.1016/j.gaitpost.2006.04.008>.
- Schmidt, C., Priemel, M., Kohler, T., Weusten, A., Muller, R., Amling, M. & Eckstein, F. 2013. "Precision and Accuracy of Peripheral Quantitative Computed Tomography (PQCT) in the Mouse Skeleton Compared with the Histology and Microcomputed Tomography." *Journal of Bone and*

*Mineral Research* 18 (8): 1486–96.

Schneider, C. A., Rasband, W. S., & Eliceiri, K.W. 2012. “NIH Image to ImageJ: 25 Years of Image Analysis.” *Nature Methods* 9 (7): 671:675.

Schofield, C. J., Libby, G., Brennan, G.M., Macalpine, R.R., Morris, A.D. & Leese, G.P. 2006. “Mortality and Hospitalization in Patients after Amputation: A Comparison between Patients with and without Diabetes.” *Diabetes Care* 29 (10): 2252–56. <https://doi.org/10.2337/dc06-0926>.

Schulz, B., Hart-Hughes, S., Latief, G., Phillips, S. & Highsmith, M.J. 2010. “109 Asymmetries in Spatiotemporal Gait Parameters of Transtibial and Transfemoral Amputees.” *American Academy of Orthotists and Prosthetists* 16 (1): S32. [https://doi.org/10.1016/S1353-8020\(10\)70110-3](https://doi.org/10.1016/S1353-8020(10)70110-3).

Segal, A.D., Orendurff, M.S., Klute, G.K., McDowell, M.L., Pecoraro, J.A., Shofer, J. & Czerniecki, J.M. 2006. “Kinematic and Kinetic Comparisons of Transfemoral Amputee Gait Using C-Leg and Mauch SNS Prosthetic Knees.” *Journal of Rehabilitation Research and Development* 43 (7): 857–70. <https://doi.org/10.1682/JRRD.2005.09.0147>.

Segal, D., Pick, R.Y., Klein, H.A. & Heskiaoff, D. 1984. “The Role of the Interosseous Membrane on Tibiofibular Weightbearing.” *Foot & Ankle International* 4 (6): 301–4. <https://doi.org/10.1177/107110078400400605>.

Selbie, S.W., Hamill, J. & Kepple, T.M. 2004. “Three-Dimensional Kinetics.” In *Research Methods in Biomechanics*, 2nd ed., 151–76. Human Kinetics.

Selman, J. P., De Camargo, A.A., Santos, J., Lanza, F.C. & Dal Corso, S. 2014. “Reference Equation for the 2-Minute Walk Test in Adults and the Elderly.” *Respiratory Care* 59 (4): 525–30. <https://doi.org/10.4187/respcare.02649>.

Seroussi, R.E., Gitter, A., Czerniecki, J.M. & Weaver, K. 1996. “Mechanical Work Adaptations of Above-Knee Amputee Ambulation.” *Archives of Physical Medicine and Rehabilitation* 77 (11): 1209–14. [https://doi.org/10.1016/S0003-9993\(96\)90151-3](https://doi.org/10.1016/S0003-9993(96)90151-3).

- Sevastikoglou, J.A., Eriksson, U. & Larsson, S-E. 1969. "Skeletal Changes of the Amputation Stump and the Femur on the Amputated Side: A Clinical Investigation." *Acta Orthopaedica Scandinavica* 40 (5): 624–33. <https://doi.org/10.3109/17453676908989528>.
- Shelburne, K.B., Torry, M.R. & Pandy, M.G. 2005. "Muscle, Ligament, and Joint-Contact Forces at the Knee during Walking." *Med. Sci. Sports Exerc* 37 (11): 1948–56. <https://doi.org/10.1249/01.mss.0000180404.86078.ff>.
- Sherk, V.D., Bemben, D.A., Bemben, M.G. & Anderson, M.A. 2012. "Age and Sex Differences in Tibia Morphology in Healthy Adult Caucasians." *Bone* 50 (6): 1324–31. <https://doi.org/10.1016/j.bone.2012.03.005>.
- Sherk, V.D., Bemben, M.G. & Bemben, D.A. 2008. "BMD and Bone Geometry in Transtibial and Transfemoral Amputees." *Journal of Bone and Mineral Research* 23 (9): 1449–57. <https://doi.org/10.1359/jbmr.080402>.
- Sheu, Y., Zmuda, J.M., Boudreau, R.M., Petit, M.A., Ensrud, K.E., Bauer, D.C., Gordon, C.L., Orwoll, E.S., Cauley, J.A. 2011. "Bone Strength Measured by Peripheral Quantitative Computed Tomography and the Risk of Nonvertebral Fractures: The Osteoporotic Fractures in Men (MrOS) Study." *Journal of Bone and Mineral Research : The Official Journal of the American Society for Bone and Mineral Research* 26 (1): 63–71. <https://doi.org/10.1002/jbmr.172>.
- Shim, V.B., Pitto, R.P., Streicher, R.M., Hunter, P.J. & Anderson, I.A. 2007. "The Use of Sparse CT Datasets for Auto-Generating Accurate FE Models of the Femur and Pelvis." *Journal of Biomechanics* 40 (1): 26–35. <https://doi.org/10.1016/j.jbiomech.2005.11.018>.
- Sigal, I.A., Hardisty, M.R. & Whyne, C.M. 2008. "Mesh-Morphing Algorithms for Specimen-Specific Finite Element Modeling." *Journal of Biomechanics* 41: 1381–89. <https://doi.org/10.1016/j.jbiomech.2008.02.019>.
- Silver-Thorn, M.B. & Childress, D.S. 1997. "Generic, Geometric Finite Element Analysis of the Transtibial Residual Limb and Prosthetic Socket." *Journal of Rehabilitation Research and*

*Development* 34 (2): 171–86.

Silverman, A.K., Fey, N.P., Portillo, A., Walden, J.G., Bosker, G. & Neptune, R.R. 2008.

“Compensatory Mechanisms in Below-Knee Amputee Gait in Response to Increasing Steady-State Walking Speeds.” *Gait and Posture* 28 (4): 602–9.

<https://doi.org/10.1016/j.gaitpost.2008.04.005>.

Silverman, A.K. & Neptune, R.R. 2014. “Three-Dimensional Knee Joint Contact Forces during

Walking in Unilateral Transtibial Amputees.” *Journal of Biomechanics* 47 (11): 2556–62.

<https://doi.org/10.1016/j.jbiomech.2014.06.006>.

Sinitski, E.H., Hansen, A.H. & Wilken, J.M. 2012. “Biomechanics of the Ankle-Foot System during

Stair Ambulation: Implications for Design of Advanced Ankle-Foot Prostheses.” *Journal of*

*Biomechanics* 45 (3): 588–94. <https://doi.org/10.1016/j.jbiomech.2011.11.007>.

Smith-Bindman, R., Lipson, J., Marcus, R., Kwang, P.K., Mahadevappa, M., Guold, R., Berrington de

Gonzalez, A. & Miglioretti, D. 2009. “Radiation Dose Associated with Common Computed

Tomography Examinations and the Associated Lifetime Attributable Risk of Cancer” 22: 2078–

86. <https://doi.org/10.1016/j.bbi.2017.04.008>.

Smith, É., Comiskey, C., Carroll, Á. & Ryall, N. 2011. “A Study of Bone Mineral Density in Lower

Limb Amputees at a National Prosthetics Center.” *JPO Journal of Prosthetics and Orthotics* 23

(1): 14–20. <https://doi.org/10.1097/JPO.0b013e318206dd72>.

Spitzer, V., Ackerman, M.J., Scherzinger, A.L. & Whitlock, D. 1996. “The Visible Human Male.”

*Technical Milestone* 3: 118–30. [https://watermark.silverchair.com/3-2-](https://watermark.silverchair.com/3-2-118.pdf?token=AQECAHi208BE49Ooan9kKhW_Ercy7Dm3ZL_9Cf3qfKAac485ysgAAAacwggGjBqkqhkiG9w0BBwagggGUMIIBkAIBADCCAYkGCSqGSIB3DQEHATAeBgIghkgBZQMEAS4wEQQMh9oYZNwsr0mMi56zAgEQgIIBWpF2dcJok5Oq2SPX55ISDJQKiPZOLVGmh_z_EKi7_JM48Ur)

[118.pdf?token=AQECAHi208BE49Ooan9kKhW\\_Ercy7Dm3ZL\\_9Cf3qfKAac485ysgAAAacwgg](https://watermark.silverchair.com/3-2-118.pdf?token=AQECAHi208BE49Ooan9kKhW_Ercy7Dm3ZL_9Cf3qfKAac485ysgAAAacwggGjBqkqhkiG9w0BBwagggGUMIIBkAIBADCCAYkGCSqGSIB3DQEHATAeBgIghkgBZQMEAS4wEQQMh9oYZNwsr0mMi56zAgEQgIIBWpF2dcJok5Oq2SPX55ISDJQKiPZOLVGmh_z_EKi7_JM48Ur)

[GjBqkqhkiG9w0BBwagggGUMIIBkAIBADCCAYkGCSqGSIB3DQEHATAeBgIghkgBZQME](https://watermark.silverchair.com/3-2-118.pdf?token=AQECAHi208BE49Ooan9kKhW_Ercy7Dm3ZL_9Cf3qfKAac485ysgAAAacwggGjBqkqhkiG9w0BBwagggGUMIIBkAIBADCCAYkGCSqGSIB3DQEHATAeBgIghkgBZQMEAS4wEQQMh9oYZNwsr0mMi56zAgEQgIIBWpF2dcJok5Oq2SPX55ISDJQKiPZOLVGmh_z_EKi7_JM48Ur)

[AS4wEQQMh9oYZNwsr0mMi56zAgEQgIIBWpF2dcJok5Oq2SPX55ISDJQKiPZOLVGmh\\_z](https://watermark.silverchair.com/3-2-118.pdf?token=AQECAHi208BE49Ooan9kKhW_Ercy7Dm3ZL_9Cf3qfKAac485ysgAAAacwggGjBqkqhkiG9w0BBwagggGUMIIBkAIBADCCAYkGCSqGSIB3DQEHATAeBgIghkgBZQMEAS4wEQQMh9oYZNwsr0mMi56zAgEQgIIBWpF2dcJok5Oq2SPX55ISDJQKiPZOLVGmh_z_EKi7_JM48Ur)

[\\_EKi7\\_JM48Ur](https://watermark.silverchair.com/3-2-118.pdf?token=AQECAHi208BE49Ooan9kKhW_Ercy7Dm3ZL_9Cf3qfKAac485ysgAAAacwggGjBqkqhkiG9w0BBwagggGUMIIBkAIBADCCAYkGCSqGSIB3DQEHATAeBgIghkgBZQMEAS4wEQQMh9oYZNwsr0mMi56zAgEQgIIBWpF2dcJok5Oq2SPX55ISDJQKiPZOLVGmh_z_EKi7_JM48Ur).

Stacoff, A., Diezi, C., Luder, G., Stüssi, E. & Kramers-De Quervain, I.A. 2005. “Ground Reaction

- Forces on Stairs: Effects of Stair Inclination and Age.” *Gait and Posture* 21 (1): 24–38.  
<https://doi.org/10.1016/j.gaitpost.2003.11.003>.
- Stefanyshyn, D.J., Engsborg, J.R., Tedford, K.G. & Harder, J.A. 1994. “A Pilot Study to Test the Influence of Specific Prosthetic Features in Preventing Trans-Tibial Amputees from Walking like Able-Bodied Subjects.” *Prosthetics and Orthotics International* 18: 180–90.  
[http://www.oandplibrary.org/poi/pdf/1994\\_03\\_180.pdf](http://www.oandplibrary.org/poi/pdf/1994_03_180.pdf).
- Stevens, P.M., Rheinstein, J. & Wurdeman, S.R. 2018. “Prosthetic Foot Selection for Individuals with Lower-Limb Amputation: A Clinical Practice Guideline.” *Journal of Prosthetics and Orthotics* 30 (4): 175–80. <https://doi.org/10.1097/JPO.0000000000000181>.
- Stewart, C. 2008. “Synopsis of Causation Lower Limb Amputation,” no. September 2008: 1–25.
- Taddei, F., Cristofolini, L., Martelli, S., Gill, H.S. & Viceconti, M. 2006. “Subject-Specific Finite Element Models of Long Bones: An in Vitro Evaluation of the Overall Accuracy.” *Journal of Biomechanics* 39: 2457–67. <https://doi.org/10.1016/j.jbiomech.2005.07.018>.
- Taylor, W.R., Heller, M., Bergmann, G. & Duda, G.N. 2004. “Tibio-Femoral Loading during Human Gait and Stair Climbing.” *Journal of Orthopaedic Research* 22: 625–32.  
<https://onlinelibrary.wiley.com/doi/pdf/10.1016/j.orthres.2003.09.003>.
- Thelen, D.G. & Anderson, F.C. 2006. “Using Computed Muscle Control to Generate Forward Dynamic Simulations of Human Walking from Experimental Data.” *Journal of Biomechanics* 39: 1107–15. <https://doi.org/10.1016/j.jbiomech.2005.02.010>.
- Turner, P.J. 2009. “Atomic Force Microscopy and Indentation Force Measurement of Bone.” *WIREs Nanomedicine and Nanobiotechnology* 1 (December): 624–49.  
<https://doi.org/10.1002/wnan.056>.
- Torburn, L., Schweiger, G.P., Perry, J. & Powers, C.M. 1994. “Below-Knee Amputee Gait in Stair Ambulation.” *Clinical Orthopaedics and Related Research* 303 (303): 185–92.  
<https://doi.org/10.1097/00003086-199406000-00024>.

- Trinler, U., Alexander, N., Schwameder, H. & Baker, R 2017. "Muscle Force Estimation in Clinical Biomechanics: Anybody vs OpenSim," no. June: 420–23.
- Turner, C. H. 1998. "Three Rules for Bone Adaptation to Mechanical Stimuli." *Bone*.  
[https://doi.org/10.1016/S8756-3282\(98\)00118-5](https://doi.org/10.1016/S8756-3282(98)00118-5).
- . 2006. "Bone Strength: Current Concepts." *Annual New York Academy of Science*, 429–46.  
<https://doi.org/10.1196/annals.1346.039>.
- Turner, C.H. & Robling, A.G. 2003. "Designing Exercise Regimens to Increase Bone Strength"  
 46202: 45–50.
- Ulrich, D., Van Rietbergen, B., Weinans, H. & Rü, P. 1998. "Finite Element Analysis of Trabecular Bone Structure: A Comparison of Image-Based Meshing Techniques." *Journal of Biomechanics*. Vol. 31. [https://ac.els-cdn.com/S0021929098001183/1-s2.0-S0021929098001183-main.pdf?\\_tid=171a2ba6-256c-47ef-9b9d-804818bb6daa&acdnat=1543958326\\_a7d7ccc2f08373c02b760ac69a1a6261](https://ac.els-cdn.com/S0021929098001183/1-s2.0-S0021929098001183-main.pdf?_tid=171a2ba6-256c-47ef-9b9d-804818bb6daa&acdnat=1543958326_a7d7ccc2f08373c02b760ac69a1a6261).
- US Department of Health and Human Services. 2004. *Bone Health and Osteoporosis: A Report of the Surgeon General. Bone Health and Osteoporosis*. <https://doi.org/10.2165/00002018-200932030-00004>.
- Vanicek, N., Sanderson, D.J., Chua, R., Kenyon, D. & Inglis, T. 2007. "Kinematic Adaptations to a Novel Walking Task With a Prosthetic Simulator." *JPO Journal of Prosthetics and Orthotics* 19 (1). <https://doi.org/10.1097/JPO.0b013e31802d4668>.
- Van Sint Jan, S. 2007. *Color Atlas of Skeletal Landmark Definitions*.
- Varadarajan, K.M., Moynihan, A., D'lima, D., Colwell, C.W. & Li, G. 2008. "In Vivo Contact Kinematics and Contact Forces of the Knee After Total Knee Arthroplasty During Dynamic Weight-Bearing Activities." *J Biomech*. July 19 (4110): 2159–68.  
<https://doi.org/10.1016/j.jbiomech.2008.04.021>.
- Varley, I., Greeves, J.P. & Sale, C. 2019. "Seasonal Difference in Bone Characteristics and Body

- Composition of Elite Speed Skaters.” *International Journal of Sport Medicine* 1: 9–15.
- Viceconti, M., Davinelli, M., Taddei, F. & Cappello, A. 2004. “Automatic Generation of Accurate Subject-Specific Bone Finite Element Models to Be Used in Clinical Studies.” *Journal of Biomechanics* 37: 1597–1605. <https://doi.org/10.1016/j.jbiomech.2003.12.030>.
- Vignoli, L.L. & Kenedi, P.P. 2016. “Bone Anisotropy – Analytical and Finite Element Analysis.” *Latin American Journal of Solids and Structures* 13 (1): 51–72. <https://doi.org/10.1590/1679-78251814>.
- Vilayphiou, N., Boutroy, S., Szulc, P., Van Rietbergen, B., Munoz, F., Delmas, P. D. & Chapurlat, R. 2011. “Finite Element Analysis Performed on Radius and Tibia HR-PQCT Images and Fragility Fractures at All Sites in Men.” *Journal of Bone and Mineral Research* 26 (5): 965–73. <https://doi.org/10.1002/jbmr.297>.
- Wagner, D.W., Stepanyan, V., Shippen, J.M., Demers, M.S., Gibbons, R.S., Andrews, B.J., Creasey, G.H. & Beaupre, G.S. 2013. “Consistency among Musculoskeletal Models: Caveat Utilitor.” *Annals of Biomedical Engineering* 41 (8): 1787–99. <https://doi.org/10.1007/s10439-013-0843-1>.
- Waldby, C. 2000. *The Visible Human Project- Informatic Bodies and Posthuman Medicine*. Routledge.
- Walter, J.P., D’lima, D.D., Colwell, C.W.B & Fregly, B.J. 2010. “Decreased Knee Adduction Moment Does Not Guarantee Decreased Medial Contact Force during Gait.” *J Orthop Res*. <https://doi.org/10.1002/jor.21142>.
- Wang, Y. & Watanabe, K. 2000. “Symmetry and Variability of Vertical Ground Reaction Force and Centre of Pressure in Able-Bodied Gait,” no. 1.
- Ward, S.R., Eng, C.M., Smallwood, L.H. & Lieber, R.L. 2009. “Are Current Measurements of Lower Extremity Muscle Architecture Accurate?” *Clinical Orthopaedics and Related Research* 467 (4): 1074–82. <https://doi.org/10.1007/s11999-008-0594-8>.
- Ware, J.E. & Gandek, B. 1998. “Overview of the SF-36 Health Survey and the International Quality

- of Life Assessment (IQOLA) Project.” *Journal of Clinical Epidemiology* 51 (11): 903–12.  
[https://doi.org/10.1016/S0895-4356\(98\)00081-X](https://doi.org/10.1016/S0895-4356(98)00081-X).
- Weeks, B.K, & Beck, B.R 2008. “The BPAQ: A Bone Specific Physical Activity Assessment Instrument.” *Osteoporosis Int.* 888: 3–4. <https://doi.org/10.1029/2005JE002426>.
- Whatling, G.M., Evans, S.L. & Holt, C.A. 2010. “Introducing a New Staircase Design to Quantify Healthy Knee Function during Stair Ascent and Descent.” *Computer Methods in Biomechanics and Biomedical Engineering* 13 (3): 371–78. <https://doi.org/10.1080/10255840903251296>.
- Wheless, C. 2011. *Wheless’ Textbook of Orthopaedics*.
- White, R., Agouris, I., Selbie, R. D. & Kirkpatrick, M. 1999. “The Variability of Force Platform Data in Normal and Cerebral Palsy Gait.” *Clinical Biomechanics* 14 (3): 185–92.  
[https://doi.org/10.1016/S0268-0033\(99\)80003-5](https://doi.org/10.1016/S0268-0033(99)80003-5).
- Whittle, M. 1996. “Clinical Gait Analysis: A Review.” *Human Movement Science* 15 (3): 369–87.  
[https://doi.org/10.1016/0167-9457\(96\)00006-1](https://doi.org/10.1016/0167-9457(96)00006-1).
- Wickiewicz, T.L., Roy, R.R., Powell, P.L. & Edgerton, V.R. 1983. “Muscle Architecture of the Human Lower Limb.” *Clinical Orthopaedics and Related Research*, no. 179 (October): 275–83.  
<http://www.ncbi.nlm.nih.gov/pubmed/6617027>.
- Wickiewicz, T., Roland, R., Powell, P. & Edgerton, R. 1983. “Muscle Architecture of the Human Lower Limb.” *Clinical Orthopaedics and Related Research*.
- Wiener, J. M., Hanley, R. J., Clark, R. & Van Nostrand, J. F. 1990. “Measuring the Activities of Daily Living: Comparisons Across National Surveys.” *Journal of Gerontology* 45 (6): S229–37.  
<https://doi.org/10.1093/geronj/45.6.S229>.
- Winter, D. & Sienko, S. 1988. *Biomechanics of below Knee Amputee Gait*.
- Wirtz, C.D., Schiffers, N., Pandorf, T., Radermacher, K., Weichert, D. & Forst, R. 2000. “Critical Evaluation of Known Bone Material Properties to Realize Anisotropic FE-Simulation of the

- Proximal Femur.” *Journal of Biomechanics* 33: 1325–30. [https://ac.els-cdn.com/S002192900000695/1-s2.0-S002192900000695-main.pdf?\\_tid=6e93c7c4-f489-11e7-8054-00000aab0f27&acdnat=1515425856\\_aff7e34a784ae9bb4e725f0066fde7ce](https://ac.els-cdn.com/S002192900000695/1-s2.0-S002192900000695-main.pdf?_tid=6e93c7c4-f489-11e7-8054-00000aab0f27&acdnat=1515425856_aff7e34a784ae9bb4e725f0066fde7ce).
- Wolff, J. 1986. *The Law of Bone Remodelling*. Springer-Verlag Berlin Heidelberg.  
<https://doi.org/10.1007/978-3-642-71031-5>.
- Wretenberg, P., Ramsey, D.K. & Németh, G. 2002. “Tibiofemoral Contact Points Relative to Flexion Angle Measured with MRI.” *Clinical Biomechanics* 17 (6): 477–85.  
[https://doi.org/10.1016/S0268-0033\(02\)00036-0](https://doi.org/10.1016/S0268-0033(02)00036-0).
- Yamaguchi, G.T. & Zajac, F.E. 1989. “A Planar Model of the Knee Joint to Characterize the Knee Extensor Mechanism.” *Journal of Biomechanics* 22 (1): 1–10. [https://doi.org/10.1016/0021-9290\(89\)90179-6](https://doi.org/10.1016/0021-9290(89)90179-6).
- Yang, P.F., Brüggemann, G-P. & Rittweger, J. 2011. “What Do We Currently Know from in Vivo Bone Strain Measurements in Humans ?” *J Musculoskelet Neuronal Interact* 11 (1): 8–20.
- Yao, H., Dao, M., Carnelli, D., Tai, K. & Ortiz, C. 2010. “Size-Dependent Heterogeneity Benefits the Mechanical Performance of Bone.” *Journal of the Mechanics and Physics of Solids* 59: 64–74.  
<https://doi.org/10.1016/j.jmps.2010.09.012>.
- Yassine, R.A., Elham, M.K., Mustapha, S. & Hamade, R.F. 2018. “Heterogeneous Versus Homogeneous Material Considerations in Determining the Modal Frequencies of Long Tibia Bones.” *Journal of Engineering and Science in Medical Diagnostics and Therapy* 1 (2): 021001.  
<https://doi.org/10.1115/1.4038448>.
- Yazicioglu, K., Tugcu, I., Yilmaz, B., Goktepe, A.S. & Mohur, H. 2008. “Osteoporosis: A Factor on Residual Limb Pain in Traumatic Trans-Tibial Amputations.” *Prosthetics and Orthotics International* 32 (2): 172–78. <https://doi.org/10.1080/03093640802016316>.
- Zachariah, S. G. & Sanders, J. E. 1996. “Interface Mechanics in Lower-Limb External Prosthetics: A Review of Finite Element Models.” *IEEE Transactions on Rehabilitation Engineering* 4 (4):

288–302. <https://doi.org/10.1109/86.547930>.

Zachazewski, J.E., O'Riley, P. & Krebs, D.E. 1993. "Biomechanical Analysis of Body Mass Transfer during Stair Ascent and Descent of Healthy Subjects." *Journal of Rehabilitation Research and Development* 30 (4).

<http://citeseerx.ist.psu.edu/viewdoc/download?doi=10.1.1.459.9179&rep=rep1&type=pdf>.

Zeni, J.A., Richards, J.G. & Higginson, J.S. 2008. "Two Simple Methods for Determining Gait Events during Treadmill and Overground Walking Using Kinematic Data." *Gait & Posture*, 710–14.

<https://doi.org/10.1016/j.gaitpost.2007.07.007>.

Zhang, J., Nieber, G. & Ovaert, T. 2008. "Mechanical Property Determination of Bone through Nano and Micro- Indentation Testing and Finite Element Simulation." *Journal of Biomchanics* 41 (2):

267–75. <https://doi.org/10.1038/mp.2011.182.doi>.

Zhang, M. & Golland, P. 2016. "Statistical Shape Analysis: From Landmarks to Diffeomorphisms."

*Medical Image Analysis* 33 (October): 155–58. <https://doi.org/10.1016/J.MEDIA.2016.06.025>.

Zhao, D., Banks, S.A., D'lima, D.D., Colwell, C.W. & Fregly, B.J. 2007. "In Vivo Medial and

Lateral Tibial Loads during Dynamic and High Flexion Activities." *J Orthop Res* 25: 593–602.

<https://doi.org/10.1002/jor.20362>.

Ziegler-Graham, K., MacKenzie, E.J., Ephraim, P.L., Travison, T.G. & Brookmeyer, R., 2008.

"Estimating the Prevalence of Limb Loss in the United States: 2005 to 2050." *Archives of Physical Medicine and Rehabilitation* 89 (3): 422–29.

<https://doi.org/10.1016/j.apmr.2007.11.005>.

Zysset, P.K., Dall'Ara, E., Varga, P. & Pahr, D.H. 2013. "Finite Element Analysis for Prediction of

Bone Strength." *BoneKEY Reports* 2 (August): 1–9. <https://doi.org/10.1038/bonekey.2013.120>.

## **Appendix A- Staircase Validation Study**

### **1.1 Introduction**

Stair climbing is a common activity within daily living. Research into of stair climbing biomechanics, however, is limited when compared to level walking gait (Pickle et al. 2014; Reid et al. 2007; Jones et al. 2006; Livingston et al. 1991; Protopapadaki et al. 2007). Stair climbing is considered more biomechanically demanding compared to level walking with increased joint moments and ground reaction forces (Whatling, Evans, and Holt 2010; Protopapadaki et al. 2007; Andriacchi et al. 1980). Stair climbing can be used within a clinical application to determine joint and muscle function especially in the improvement of pathological gait.

Biomechanical analysis of stair climbing using instrumented staircases is relatively commonplace (Andriacchi et al. 2008), although space restrictions often necessitate a portable staircase design. Previous staircase designs vary in force plate (FP) accommodation, either solid boxes sitting on top of floor embedded FPs, (Yu et al. 1996; Croce & Bonato 2007; Whatling et al. 2010) integrated force transducers within the steps (Riener et al. 1999) or portable FPs sitting within the staircase structure (Alcock et al. 2015). In such designs, FPs may be partially obscured by subsequent steps. Therefore, accurate location of FP position and resulting centre of pressure (COP) within the lab coordinate system is important to avoid errors in subsequent analyses.

There are a number of methods which could be considered in order to identify force plate positioning. One method for verifying the spatial synchronization used is that of the Cal-Tester (Motion-Lab Inc.), developed to provide repeatable lab quality assurance (Holden et al. 2002). The Cal-Tester requires a series of eight, twenty second, trials to obtain enough information to

generate a set of coordinates. This can be considered time consuming, especially during a lab session. The alternative is using a manual, marker placement method, more efficient, but as of yet unknown to its accuracy.

Therefore the aim of the current study was to compare two kinematic methods of determining instrumented staircase FP location to a widely accepted location determination reference method, namely the Cal-Tester.

## **1.2 Methods**

One healthy male completed one dynamic trial ascending and descending the staircase. The staircase set-up is as detailed in Chapter Six. With three dimensional motion capture collected using eight wall mounted motion capture cameras (Oqus; Qualisys AB, Gothenburg, Sweden) and five tripod mounted portable motion capture cameras (Oqus; Qualisys AB, Gothenburg, Sweden) including one high speed camera at a capture rate of 100HZ. Forces were recorded across a floor embedded AMTI force plate (Model OR6-7-200, AMTI, Advanced Mechanical Technology, Inc. Watertown, MA, USA) and two portable Kistler force plates (Model 9286B and Model 9260AA3, Kistler, Winterthur, Switzerland respectively)

Initially, spatial synchronization of the force plates was determined using a Cal-Tester Rod (Model MTD-3, Motion-Lab Inc. Germantown, MD) ( Holden et al. 2002). A base plate was placed on the force platform prior to zeroing. Once the data capture began the Cal-Tester rod was placed within the divot and a force of at least 200N was applied whilst the rod is moved through 30 degrees in all directions. A trial of 20 seconds was recorded and then repeated, moving the base plate around the force plate, until eight trials were recorded (for a detailed overview on using this method, as manufacturer's instructions please see (Holden, et al. 2002).

Once the Cal Tester markers were identified the files can be exported Visual 3D to determine FP corner locations (x, y, z) and the force plate centre location.

Two marker based methods were then carried out for comparison. Method A used four, nine diameter reflective markers placed at the corners of the force plate (At circle locations only in Figure 83). A 5 second trial was recorded and the x,y,z coordinates of the identified markers were input as coordinates for the corners of the force plates. Method B (At circle and triangle locations in Figure 85) used two markers placed at the front corners of the force plate, using the platforms dimensions to generate the remaining coordinates.

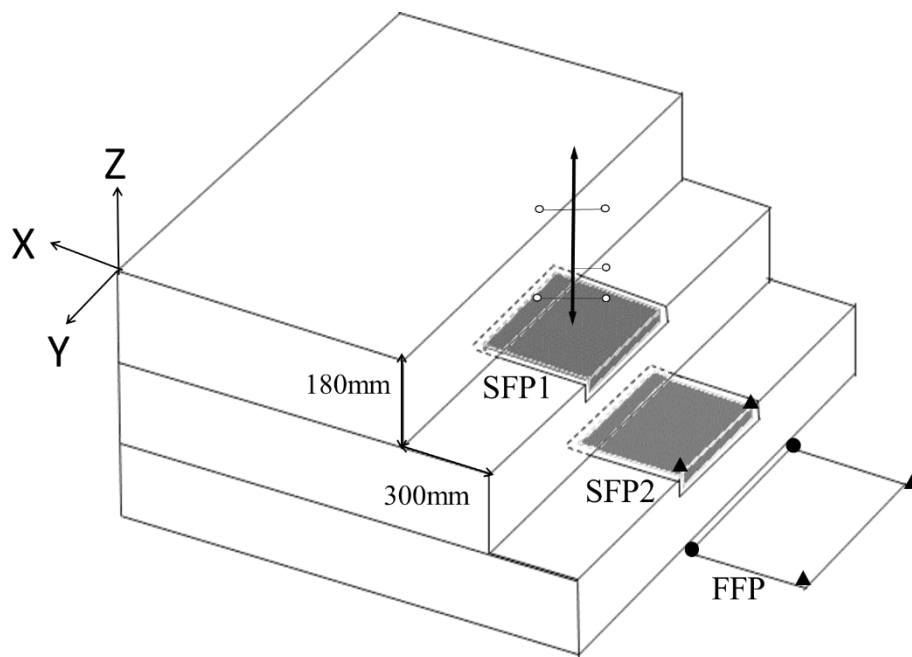


**Figure 89: Schematic of Portable staircase with portable force plates (SFP1,SFP2) next to the floor embedded force plate (FFP) FFP- Floor force plate (Model OR6-7-200, AMTI, Advanced Mechanical Technology Inc. USA), SFP1- Stair force plate 1(Model 9286B, Kistler, Winterhur, Switzerland), SFP2 - Stair force Plate 2 (Model 9260AA3 Kistler, Winterhur, Switzerland).**

### Data Analysis

Data was analysed from one steady state walking trial and normalised to the gait cycle. Kinematic data was interpolated and a low pass, butterworth filter was applied at a cut-off rate

of 6 Hz. The low-pass butterworth filter was also applied to the force data at a cut-off rate of 25 Hz. Gait events were using an event threshold as described in 3.2.5. The event was labelled ON when the vertical component of the GRF exceeded 20 Newtons and labelled as OFF when the vertical component of the GRF descends below 20 Newtons. Sagittal plane moments and powers for the ankle, knee and hip were calculated. The path of centre of pressure was also plotted for each condition. The same processing was used for each method, with the force platform parameters modified to reflect the change in force plate corner coordinates generated from each method (Table 31).

### **Statistical Analysis**

Root mean square error was used to analyse and compare each kinematic method with the reference method. The equation used to determine the RMSE was as follows:

$$\sqrt{\frac{\sum(x - y)^2}{n}}$$

X= value of measured variable

Y= predicted value of variable based on reference method

n= sample size

This was measured for static location of the force plate as well as dynamic centre of pressure.

### **1.3 Results of variation in force plate location as identified by differing methods**

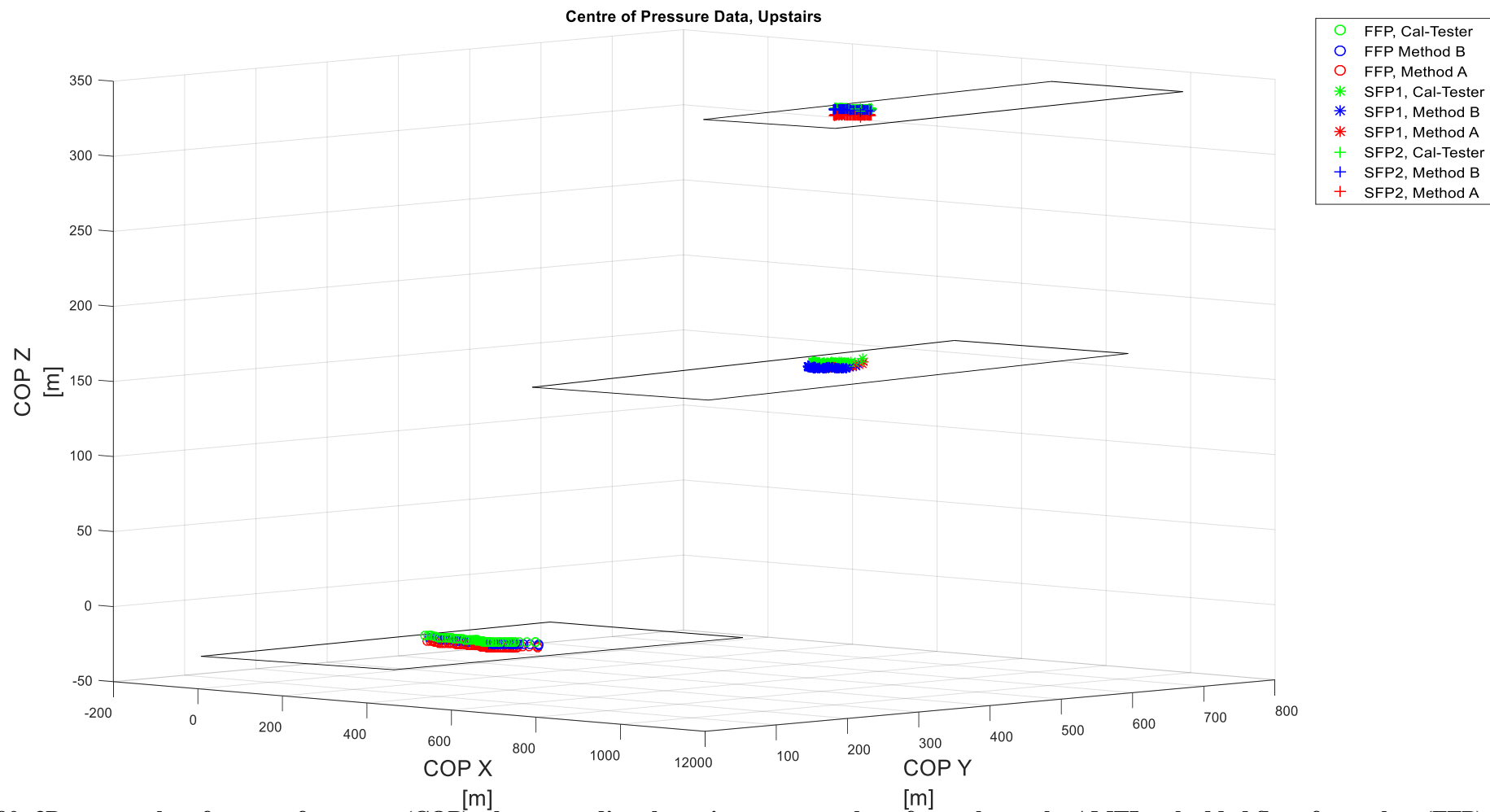
Coordinates seen in Table 30 were used to generated the location of the centre of the force plate (Table 31) A positive x reflects a more posterior coordinate, a positive y reflects a coordinate to the right and a positive z that the force plate coordinates are superior to that generated by the reference method. Neither method proves to be more accurate to the reference method when identifying the centre coordinate of the force plate.

**Table 31: Difference in force plate centre coordinate (mm) when compared to the reference method across the three force plates.**

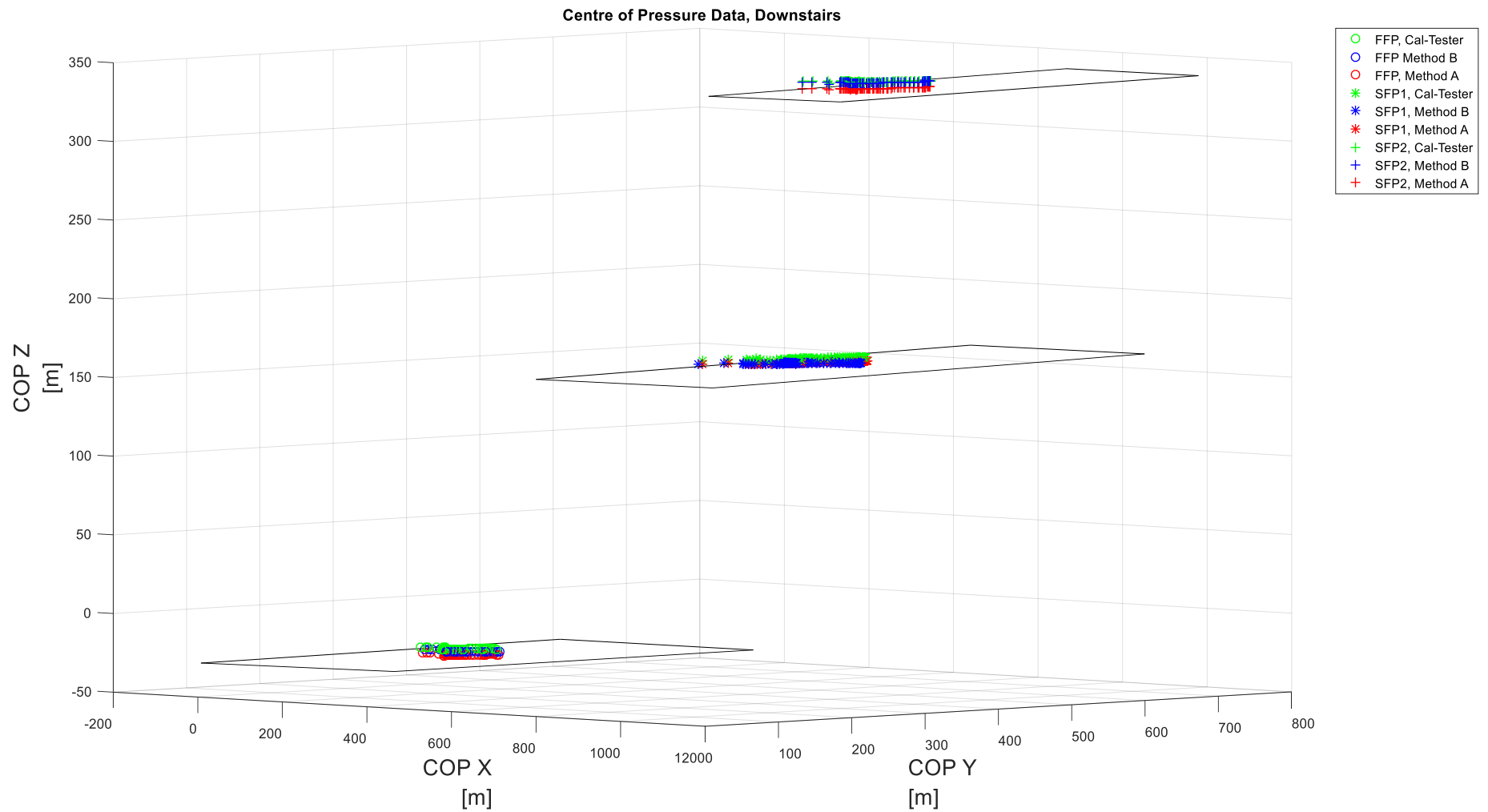
Force plate		Condition	
		Method A	Method B
Floor force Plate	x	1.14	-1.98
	y	2.34	-0.73
	z	-3.56	-2.05
Stair Force Plate 1	x	0.89	-2.39
	y	2.81	12.37
	z	-2.24	1.29
Stair Force Plate 2	x	1.63	-1.37
	y	-1.4	0.76
	z	-3.64	-3.42

Figure 86 and Figure 87 show the three dimensional scatter plot of the centre of pressure across the dynamic trial. The current view point demonstrates the lack of variation in Z between the three methods.

The COP for each method was compared to that generated from the reference method using root mean square (RMS) (Figure 88). A higher RMS was seen in method B in both the floor force plate (FFP) and the stair force plate one (SFP1). Conversely a higher RMS is shown for method A across stair force plate two (SFP2). This is seen in both stair ascent and descent.



**Figure 90: 3D scatter plot of centre of pressure (COP) when ascending the staircase across three force plates; the AMTI embedded floor force plate (FFP) and the two portable Kistler force plates, stair force plate one (SFP1) and stair force plate 2 (SFP2).**



**Figure 91: 3D scatter plot of centre of pressure (COP) when descending the staircase across three force plates; the AMTI embedded floor force plate (FFP) and the two portable Kistler force plates, stair force plate one (SFP1) and stair force plate 2 (SFP2).**

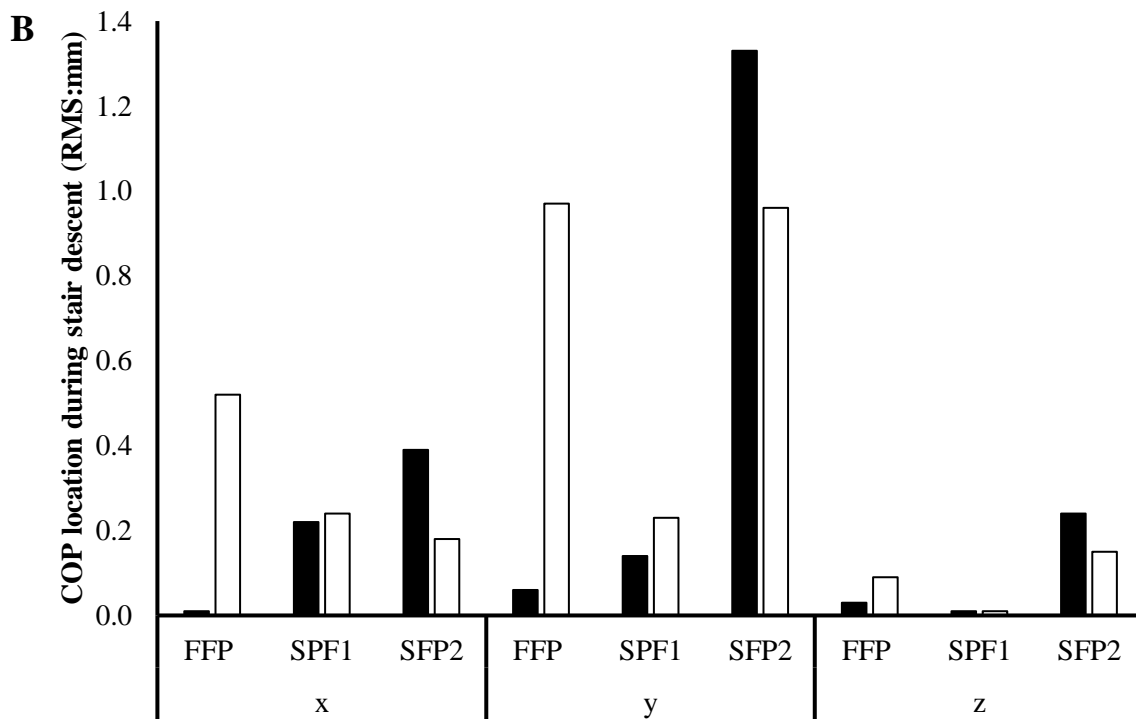
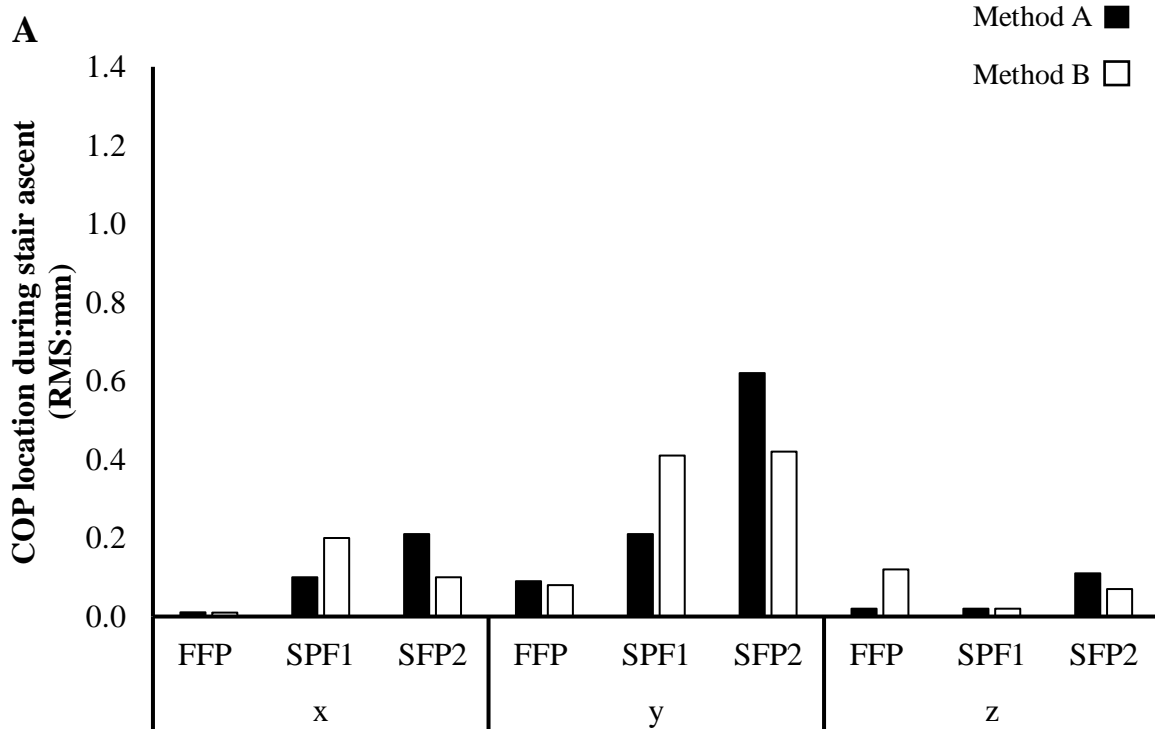


**Figure 92: Root mean square of dynamic COP across three force plates. A; when ascending the staircase and B; when descending the staircase. FFP; Floor force plate, SFP1; Stair force plate 1, SFP2; Stair Force plate 2.**

The profile for the moments and powers (Figure 89) shows no difference in the shape of the response. From looking at the graphs the difference between each method can be seen as minimal, so the RMS for each graph was also calculated (Figure 90, Figure 91). When ascending the staircase, a higher RMS in method B across FFP and SFP1 for moments and powers at all joint. Across SPF2 a higher RMS in method B is found in knee power, knee moment and hip moment.

When descending the staircase a higher RMS in method B across SFP1 is found for all joint moments and powers. A higher RMS in method B is also found in the knee and hip in FFP and at the knee in SPF2. The maximum RMS is found in hip moment when descending the staircase;  $0.0197\text{Nm/Kg}$  and knee power  $0.0261\text{ W/Kg}$  when descending the staircase.

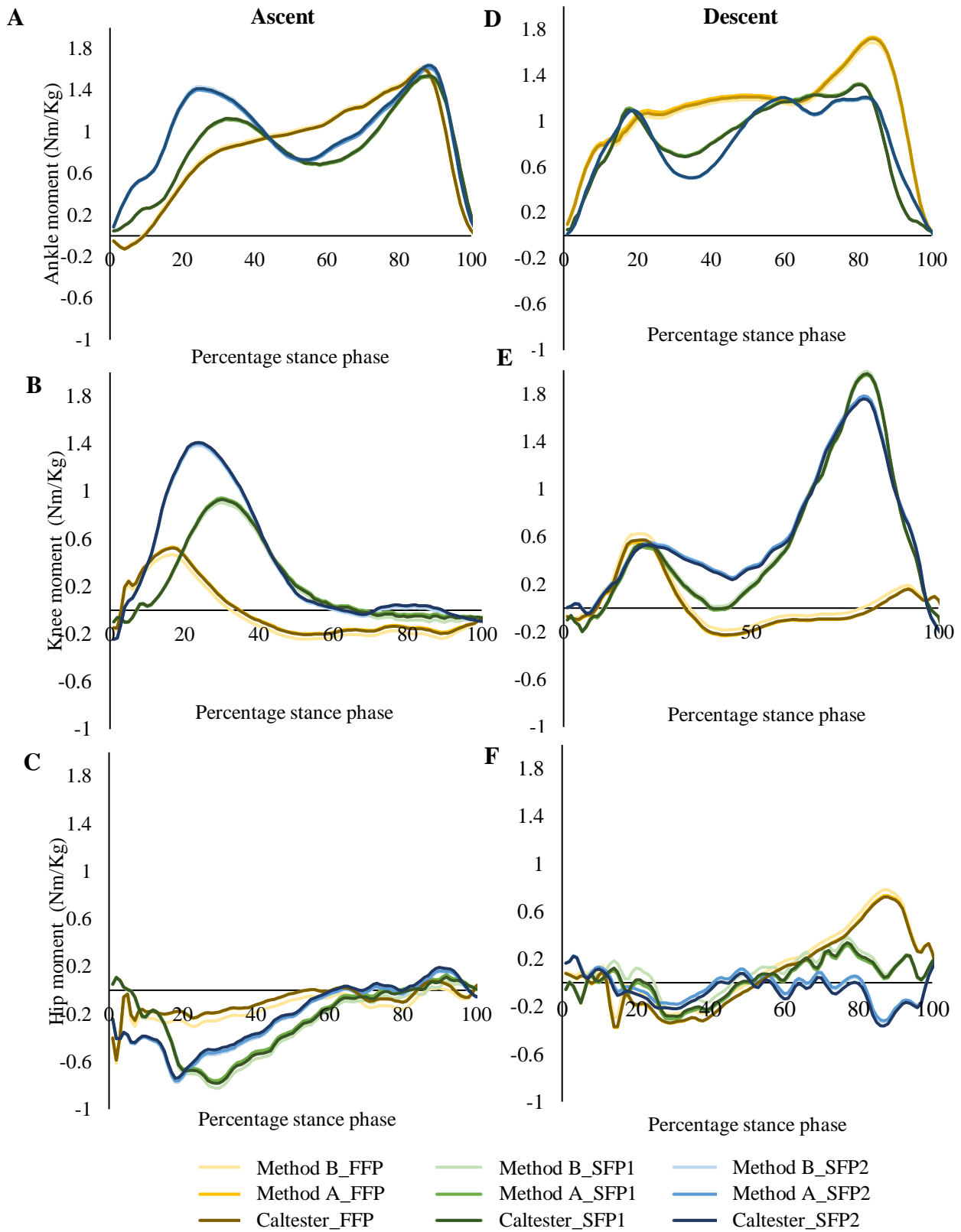


**Figure 93: Joint moments during stance phase for Ankle, Knee and Hip during stair ascent (A, B, C) and stair descent (D, E, F).**

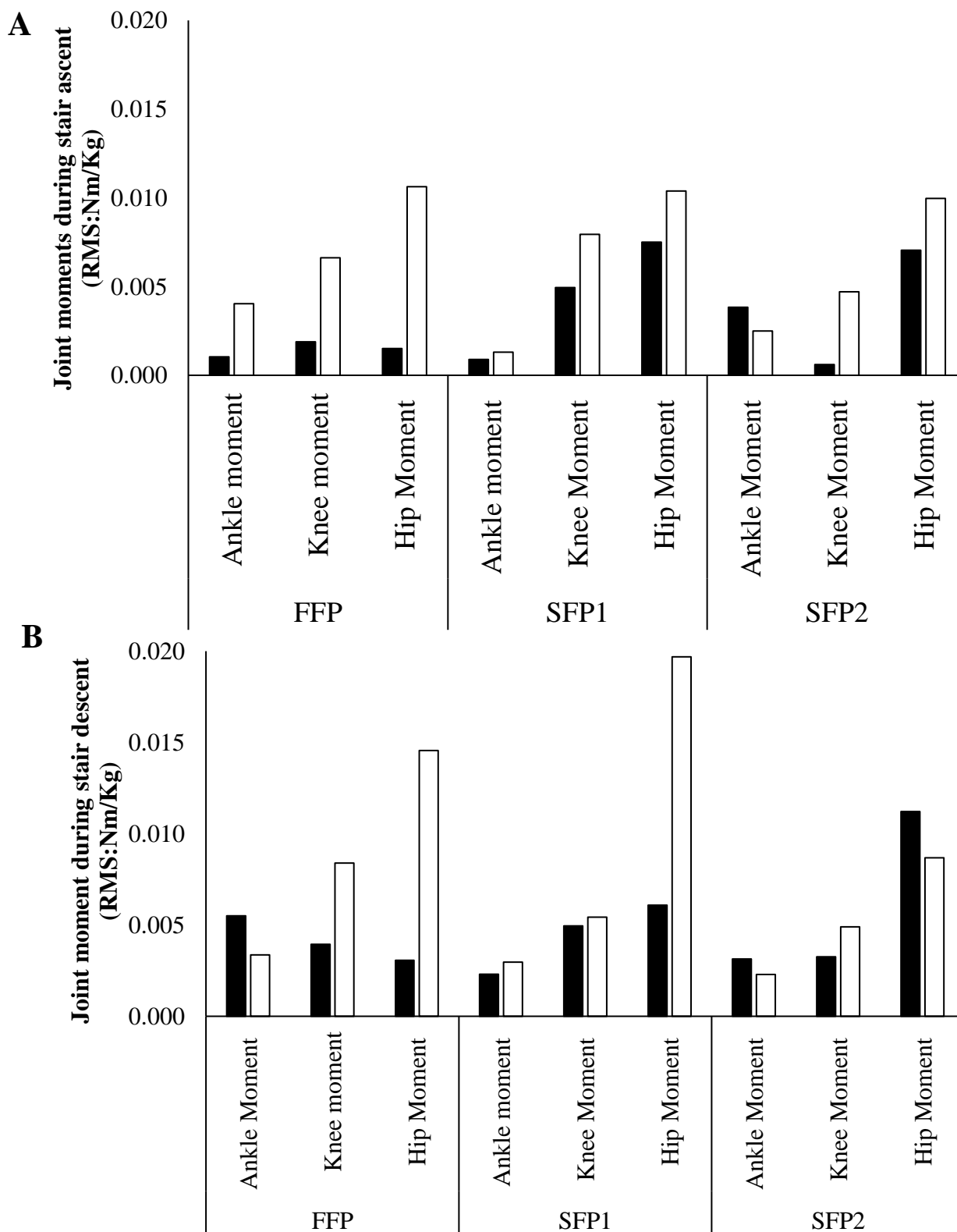


**Figure 94: Root mean square of the joint moments when Ascending the staircase (A) and descending the staircase (B) across the three force plates; Floor force plate (FFP), Stair force plate (SFP1) and stair force plate (SFP2).**

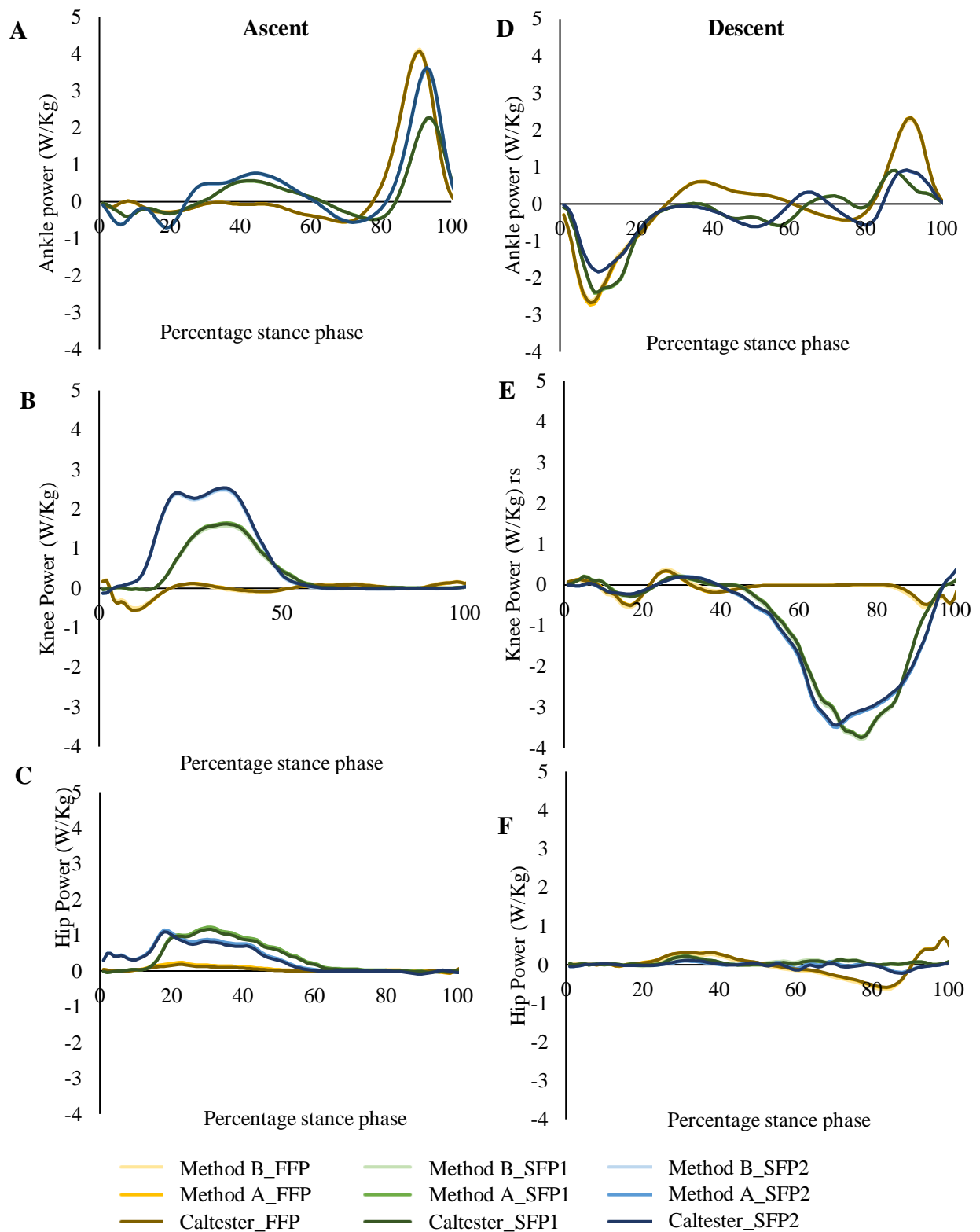


**Figure 95: Joint Powers for the Ankle, Knee and hip across the stance phase for both ascending (A, B, C) and descending (D, E, F) the staircase.**

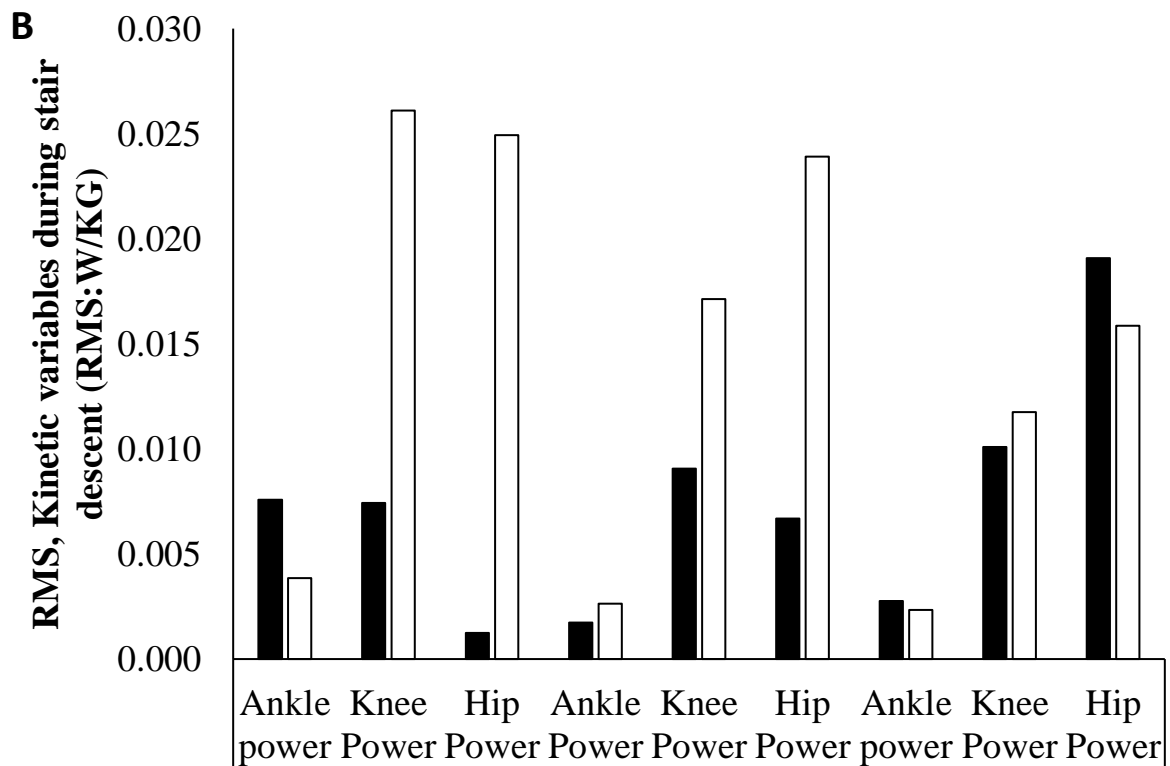
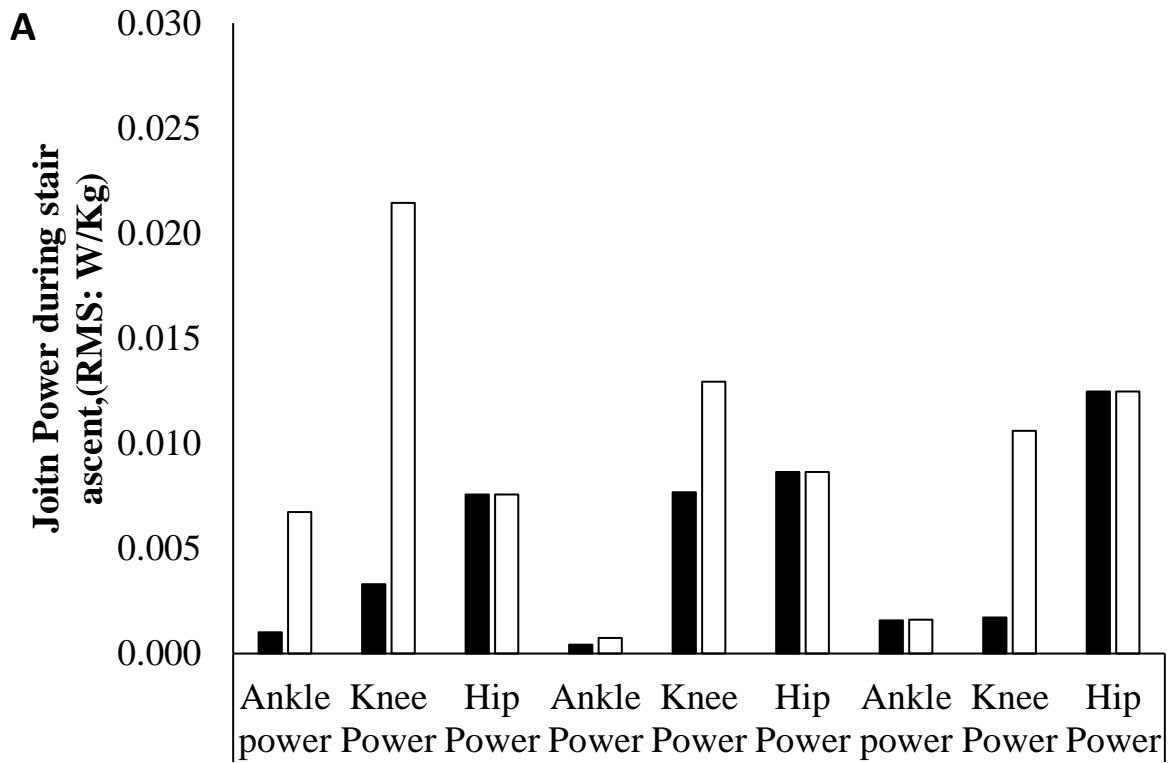


**Figure 96: Joint Powers for the Ankle, Knee and hip when ascending (A) and descending (B) the staircase, across three force plates; Floor force plate (FFP), Stair force plate 1 (SFP1) and stair force plate 2 (SFP2).**

## 1.4 Discussion

The COP variation shown between these differing techniques has shown to be between 0.01 and 1.33mm. Although literature has not yet investigated how a varying technique of force plate location identification affects accuracy, there has been some consideration of the COP accuracy between force plates within the staircase (Whatling et al. 2010; Croce and Bonato 2007). The errors that were found within these studies are similar to that in literature, which allows us to conclude that such small errors are acceptable.

Alike COP the largest RMS in joint moments, when ascending the stairs, is seen when using method B for both the FFP and the SFP1. However across SFP2 there is a larger RMS when using method A only in the ankle. When descending the staircase, higher RMS in method B, is seen across SFP1 only. Unlike the COP, in FFP method B is higher in the knee and hip only. Again in disagreement with the COP, the RMS during method A across SFP2, is only higher in ankle and hip.

For joint power method B shows largest RMS across FFP and SFP1, during both stair ascent and descent. When ascending, SFP1 shows highest RMS in method B for knee power, with the other two joints showing equal RMS values. When descending the staircase, method B shows higher RMS across SFP1 only. In FFP Method B shows higher RMS in knee and hip only. In SFP2, the higher RMS in method A seen in measure of COP is only demonstrated at the ankle and hip.

To summarise, the higher COP RMS seen in method B during ascent in FFP and SFP1 reflects a higher RMS for joint moment and joint power in these force plates. The higher COP RMS seen in method A in SFP2 during stair ascent is only reflected in ankle moment and knee power. When descending the staircase, only joint moments and powers across SFP2 agree with a

higher RMS in method B seen in COP. Opposing this is the moment and powers seen at the ankle and knee, i.e. they have a higher RMS in method B.

However, as shown by the lack of visible difference in the graphs, both methods show little variation from the reference method.

### **1.5 Conclusion**

The difference in kinetic variables between the two different kinematic methods to the reference method (Cal-Tester) is minimal, to the point where either method can be implemented to accurately identify location.

## Appendix B- Participant Information Sheet Study Three

Study Number:

Patient Identification Number for this trial:

---

### PARTICIPANT INFORMATION SHEET-ABLE-BODIED

---

**Title of Project:** How does the level of amputation influence movement asymmetry and subsequent bone health?

**Name of Researcher:** Miss Olivia Brown

**Contact Details:** email: [Olivia.brown022015@my.ntu.ac.uk](mailto:Olivia.brown022015@my.ntu.ac.uk)

We would like to invite you to take part in a research study. Before you decide, we would like you to understand why the research is being done and what it would involve for you.

Please take time to carefully read the following information and talk to others about the study if you wish.

**Part 1** will tell you about the purpose of the study and what will happen if you decide to take part.

**Part 2** gives you more detailed information about the conduct of the study.

Please ask us if there is anything that is not clear or if you would like more information. You have up to two weeks following your appointment to decide whether or not you would like to take part.

#### **PART 1**

*What is the purpose of this study?*

Research has shown that to compensate for the loss of a limb, individuals that have experienced lower limb amputation change the way they walk to rely more on the intact limb, resulting in a walking pattern

that is considered asymmetrical.. We know that bone formation is as a response to a physical stimulus e.g. exercise. Increased strain produced through exercise encourages bone formation (growth), where reduced use encourages bone resorption (loss). This change in walking pattern leads to unequal loading and an imbalance in the bone formation/resorption cycle. As a result of this, lower limb amputees (LLA) have been shown to suffer from poor bone health, such as the deterioration of joints (e.g. osteoarthritis) and a decrease in bone mineral density (e.g. osteoporosis). Understanding how this change in walking pattern is related to the deterioration in bone health has a number of benefits. Firstly, it will guide us on how to optimise walking patterns for the improvement and long term maintenance of good bone health. Not only will this improve the long term quality of life of amputees but can help to reduce the care costs and associated demand on healthcare services. Therefore, the main aim of the current study is to investigate how the level of amputation affects walking pattern and subsequent bone health.

*Why have I been invited?*

You have been invited to take part in this study as you are over 25 years of age, able bodied and fit the criteria required to participate in the current study e.g. do not experience any musculoskeletal pain during walking which would cause an individuals to stop walking at a normal speed.

*Do I have to take part?*

No. Participation in this study is entirely voluntary.

If you do decide to take part in this study, you will be free to stop taking part at any time without giving reason. This will not affect your care, your future treatment or your legal rights in any way.

*What will happen if I decide to take part?*

If you decide to take part in the study then great! You will need to contact Miss Olivia Brown (email:Olivia.brown022015@my.ntu.ac.uk) to let her know you are keen to take part and you will then be invited to the Sports department and Biomechanics Laboratory, at Nottingham Trent University. If you do not have your own transportation the University will be able to arrange a taxi for you. You will

be asked to bring along a pair of shorts, a t-shirt or vest and some comfortable shoes you can walk in, no high heels please! If you do not have shorts, they will be provided for you.

*Are there any costs involved?*

No. The University will reimburse any costs that you incur as a result of travelling to the University at a standard University rate of 45p per mile travelled if coming by car. If you come by public transport or taxi your fare will be reimbursed.

*What do I have to do?*

You will need to visit Nottingham Trent University on five occasions during a 12 month period as described in the diagram below.

**Table 32: Study Outline for controls**

	<b>Visit 1</b>	<b>Visit 2</b>	<b>Visit 3</b>	<b>Visit 4</b>	<b>Visit 5</b>
<b>Measure</b>	0 months	3 months	6 months	9 months	12 months
Bone Imaging	X		X		X
Two minute walk test	X	X	X	X	X
Movement analysis	X	X	X	X	X

When you arrive you will be taken to the biomechanics lab where your height and weight will be recorded. You will then complete your first mobility test, this involves you walking along a set route, non-stop for a period of 2 minutes.

You will then have some reflective markers place on your skin with double sided sticky tape. The markers are about the size of a marble, made of polystyrene and covered in reflective tape. The reflective

markers are used to see how the limbs move while you are performing these tasks using motion capture cameras that see the light from the markers only and not the person, so your identity is fully protected.

Once these markers are in place you will be asked to perform a three individual movement analysis tests:

1. Walking along a 10m level walkway.
2. Walking up and down a 5° slope.
3. Walking up and down a set of three steps.

You will then be taken to have your first bone imaging scans. You will be asked to remove all metal, including jewellery and belts, so please avoid wearing anything that is difficult to remove.

You will have two bone imaging scans. The first one will be a Dual Energy X-ray Absorptiometry (DXA) scan to measure your bone density. This involves you lying face up on the scanner, you will be positioned appropriately by the research team. The scanner passes over your body first to establish your position then again to take the measurement. You will be asked to close your eyes whilst it passes over your face but you won't feel anything. In total the scan only takes about ten minutes.



**Figure 97: DXA scanner**

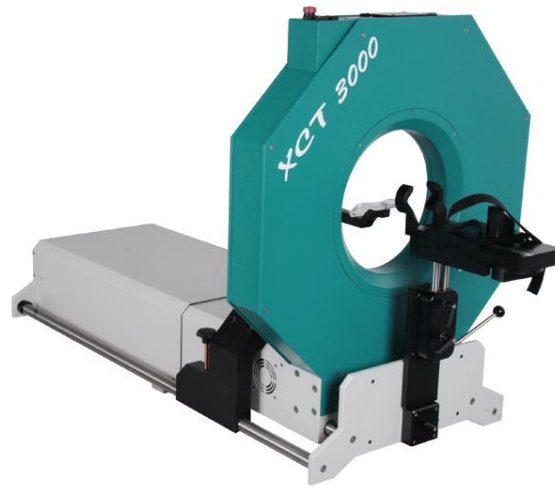


**Figure 98: pQCT scanner**

The second will be a Peripheral Quantitative Computed Tomography (pQCT) scan to take pictures in order to measure your bone geometry. This involves you sitting in front of the scanner and putting the lower half of your dominant leg through the scanner hole. The researcher will adjust your positioning so you are comfortable, gently securing you in with the straps. Again this scan moves to position itself before carrying out the scan. Again you won't feel anything and the scan lasts approximately 10 minutes.

The radiation dosage for both these scans are small, the equivalent of a flight to Europe. Safety precautions are in place and the scans will be carried out by a qualified and experienced practitioner. As mentioned previously each scan only takes about ten minutes, so a total of 30 minutes will be assigned to this element.

On your second and subsequent visits you will you will be first taken over to the biomechanics lab, where you will be asked to change into your shorts and t-shirt. You will be asked to repeat the mobility tests, you will then be taken, as shown in table 1, to have repeat bone imaging scans at visits 2, 4 and 6.

You will also be asked to complete a number of questionnaires during each visit to ask you about your activity levels, quality of life and lifestyle. Breaks will be offered regularly and whenever you feel you need them and Tea/coffee and biscuits will be provided. Each visit should last between 2 and 4 hours.

*Are there any risks involved?*

When performing the movement analysis tasks you may feel unstable. You will have access to a safety harness for all of these activities. However, you will not be asked to perform any tasks you feel are not within your capabilities. The correct health and safety measures are taken at all times in the Biomechanics Laboratory.

When undergoing the bone imaging scans there is a small radiation exposure, about the same as a flight to Europe. The total radiation exposure is well within the recommended yearly amount and precautions are in place to ensure your safety at all times.

It is extremely rare but one possible side effect of sticky tape being placed on the skin is a skin reaction to the tape. Your skin will be checked when the markers have been removed and, if there has been any reaction, appropriate treatment would be recommended.

*What happens when the research study stops?*

The results from the study will be published in scientific and clinical publications as well as being presented at international conferences. You will not be identified in any of this material to preserve your confidentiality. You may request a copy of any published results from Miss Olivia Brown.

*What if there is a problem?*

Any complaint about the way you have been dealt with during the study or any possible harm you might suffer will be addressed. Please contact professor Mary Nevill, Head of Sports Science department at Nottingham Trent University via email [mary.nevill@ntu.ac.uk](mailto:mary.nevill@ntu.ac.uk) or via phone on 011584883918 if this is the case.

If the information in Part 1 has interested you and you are considering taking part in the study, please read on to Part 2 for additional details.

## **PART 2**

### *Benefit*

As a participant you will receive no direct benefit from taking part in this study.

### *Confidentiality*

All information and data from the study will be kept strictly confidential. Your name and details will not be disclosed at any time and you will be assigned a code number to identify you in the study. All data and information will be kept on record electronically on a password protected computer and on paper in locked filing cabinets.

Miss Olivia Brown has responsibility to safeguard the data and information and only those individuals involved with the study will have access to these sources.

All data and information will be kept by Miss Olivia Brown at Nottingham Trent University for the duration of the study. Please be aware that, when giving consent to participate, you are agreeing with the conditions outlined above.

### *Your Rights*

Your participation in this study is voluntary. You are allowed to withdraw from the study at any time without reason. This will not affect any future treatment, or any legal rights. Withdrawal is totally without prejudice.

For more advice on the project please contact Miss Olivia Brown on email at [Olivia.brown022015@my.ntu.ac.uk](mailto:Olivia.brown022015@my.ntu.ac.uk)

### *Trial-Related Injury*

It is unlikely that you will experience an injury or illness as a result of taking part in this research study. However, indemnity is provided by the Nottingham Trent University and any compensation will be as per the University's usual standards. For more information please contact Miss Olivia Brown.

*Who is organising the study?*

Miss Olivia Brown, School of Science and Technology, Nottingham Trent University.

Thank you for your time and I look forward to speaking to you soon.

Miss Olivia Brown,

Ph.D in sports science,

School of Science and Technology

Nottingham Trent University

# Appendix C- Bone Scan Form, Study Three

Nottingham Trent University

IONISING RADIATIONS (MEDICAL EXPOSURE) REGULATIONS 2000

REQUEST FOR: **Peripheral Quantitative Computed Tomography Scan and Dual-energy X-ray absorptiometry**

ID#		Study number	203581
<b>1. INVESTIGATION REQUESTED:</b>  Dual-energy X-ray absorptiometry (DXA): Whole-body scan  Peripheral Quantitative Computed Tomography Scan (pQCT): Tibia Scan			
<b>2. PATIENT QUESTIONNAIRE</b>  Title: How does the level of amputation influence movement asymmetry and subsequent bone health?  NRES Approval: 16/EM/0316  <b>Exclusion Criteria</b>  <b>Please enter an X as appropriate</b>			
Does not have a pacemaker or automatic defibrillator		<input type="checkbox"/>	
Not pregnant, trying to become pregnant or breastfeeding		<input type="checkbox"/>	
Not had an X-ray (e.g. tooth, chest or bone scan) or MRI scan in the previous 30 days		<input type="checkbox"/>	
Does not have any metal implants (e.g. pins, artificial joints)		<input type="checkbox"/>	
<b>3. SCAN REQUEST</b>  I hereby state that I have carried out the above questionnaire with the patient and confirm that the answers given are an accurate record. I therefore request that a DXA scan is made on the above patient as requested in Section 1.  Name: _____ Signed: _____			

**4. CONFIRMATION OF SCAN PERFORMED AND REPORT GENERATED:**

**Pre scan:**

I hereby state that I have correctly identified the participant, checked the participant meets the inclusion/exclusion criteria and obtained a completed consent form for said participant.

Name:

Signed:

Appointed DXA and IRMER operator, Nottingham Trent University

**Post scan:**

I hereby state that I have performed the DXA scan on the above participant and confirm that I will analyse the results and produce a written report on the findings of the investigation as requested in Section 1.

Name:

Signed:

Appointed DXA and IRMER operator Nottingham Trent University

Number of scans (Side: Left or Right )

Signed: ..... Date: .....

Signed: ..... Date: .....

Signed: ..... Date: .....

Signed: ..... Date: .....



taking consent.

# Appendix E- SF 36 Questionnaire-Study Three

## SF 36 Questionnaire

ID#: \_\_\_\_\_

Date: \_\_\_\_\_

Visit No.: \_\_\_\_\_

This set of questions asks for your views about your health. This information will help keep track of how you feel and how well you are able to do your usual activities. Answer every question by marking the answer as indicated. If you are unsure about how to answer a question please give the best answer you can.

1. In general, would you say your health is: (Please tick **one** box)

Excellent

Very good

Good

Fair

Poor

2. Compared to one year ago, how would you rate your health in general now? (Please tick **one** box)

Much better than a year ago

Somewhat better now than one year ago

About the same as one year ago

Somewhat worse now than one year ago

Much worse now than one year ago

3. The following questions are about activities you might do during a typical day. Does your health now limit you in these activities? If so, how much? (Please circle one number on each line.)

Activities	Yes, limited a lot	Yes, Limited a little	Not limited at all
------------	--------------------------	-----------------------------	--------------------------

Vigorous activities, such as running, lifting heavy objects, participating in strenuous sports	1	2	3
Moderate activities, such as moving a table, pushing a vacuum cleaner, bowling, or playing golf	1	2	3
Lifting or carrying groceries	1	2	3
Climbing several flights of stairs	1	2	3
Climbing one flight of stairs	1	2	3
Bending, Kneeling, or stooping	1	2	3
Walking more than a mile	1	2	3
Walking several blocks	1	2	3
Walking one block	1	2	3
Bathing or dressing yourself	1	2	3

4. During the past four weeks, have you had any of the following problems with your work or other regular activities as a result of your physical health? (Please circle one number on each line?)

Activities	Yes	No
Cut down on the amount of time you spent on work or other activities	1	2
Accomplished less than you would like	1	2
Were limited in the kind of work or other activities	1	2
Had difficulty performing the work or other activities (for example, it took extra effort)	1	2

5. During the past four weeks, have you had any of the following problems with your work or other regular daily activities as a result of any emotional problems (e.g. feeling depressed or anxious)? (please circle one number on each line.)

Activities	Yes	No
Cut down on the amount of time you spent on work or other activities	1	2
Accomplished less than you would like	1	2
Didn't do work or other activities as carefully as usual	1	2

6. During the past 4 weeks to what extent has your physical health or emotional problems interfered with your normal social activities with family, friends, neighbours, or groups? (please tick one box)

Not at all

Slightly

Moderately

Quite a bit

Extremely

7. How much physical pain have you had during the past four weeks? (please tick one box.)

None

Very mild

Mild

Moderate

Severe

Very Severe

8. During the past four weeks, how much did pain interfere with your normal work (including both work outside the home and housework)? (Please tick one box.)

Not at all

A little bit

Moderately

Quite a bit

Extremely

9. These questions are about how you fell and how things have been with you during the past 4 weeks. Please give the one answer that is closest to the way you have been feeling for each item. (Please circle on number on each line)

	All of the time	Most of the time	A good bit of the time	Some of the time	A little of the time	None of the time
Did you feel full of life?	1	2	3	4	5	6
Have you been a very nervous person?	1	2	3	4	5	6

Have you felt so down in the dumps that nothing could cheer you up?	1	2	3	4	5	6
Have you felt calm and peaceful ?	1	2	3	4	5	6
Did you have a lot of energy?	1	2	3	4	5	6
Have you felt downhearted and blue?	1	2	3	4	5	6
Did you feel worn out?	1	2	3	4	5	6
Have you been a happy person?	1	2	3	4	5	6
Did you feel tired?	1	2	3	4	5	6

10. During the past four weeks, how much of the time has your physical health or emotional problems interfered with your social activities (like visiting with friends, relatives etc.)  
(Please tick one box.)

- All of the time
- Most of the time
- Some of the time
- A little of the time
- None of the time

11. How TRUE or FALSE is each of the following statements for you? (Please circle on number on each line.)

	Definitely true	Mostly true	Don't know	Mostly False	Definitely False
I seem to get sick a little easier than other people	1	2	3	4	5
I am as healthy as anybody I know	1	2	3	4	5
I expect my health to get worse	1	2	3	4	5
My health is excellent	1	2	3	4	5

**This is the end of the questionnaire, thank you for participating.**



# Bone-Specific Physical Activity Questionnaire (BPAQ)

SUBJECT ID:	DATE:
-------------	-------

2. Please list the sports or other physical activities (be as specific as possible) you participated in regularly during the last 12 months and indicate the average frequency (sessions per week)?

Activity: \_\_\_\_\_ Frequency (per week): \_\_\_\_\_

**This is the end of the questionnaire, thank you for participating**

# Appendix G- International Physical Activity Questionnaire

## International Physical Activity Questionnaire

ID#: \_\_\_\_\_

Date : \_\_\_\_\_

Visit no : \_\_\_\_\_

The following will be used to determine how physically active you are. Please answer each question even if you do not consider yourself to be an active person. Please think about all the activities you do including those you do at work, home, to get from place to place and in your spare time for recreation, exercise or sport.

Think about all the **vigorous** activities you did in the last 7 days. **Vigorous** activities refer to those that take hard physical effort and make you breathe much harder than normal. Think only about those activities which you did for at least 10 minutes at a time.

1. During the last 7 days, on how many days did you do vigorous physical activities.  
E.g. heavy lifting, running, fast bicycling?

\_\_\_\_\_ Days per week

No vigorous activity **skip to question 3**

2. How much time did you usually spend doing vigorous activities per day?

\_\_\_\_\_ Hours per day

\_\_\_\_\_ Minutes per day

Don't Know

Think about all the moderate activities that you did in the last 7 days. Moderate activities refer to

those that take moderate physical effort and make you breathe somewhat harder than normal. Think only about those activities which you did for at least 10 minutes at a time.

3. During the last 7 days, on how many days did you do moderate exercise? E.g. carrying light loads, bicycling at a normal pace. Do not include walking.

\_\_\_\_\_ Days per week

No moderate activity **skip to question 5**

4. How much time did you usually spend doing moderate activities per day?

\_\_\_\_\_ Hours per day

\_\_\_\_\_ Minutes per day

Don't know

Think about how much time you spent **walking** in the last seven days. This includes around the home, to and from work, or as recreation, sport or leisure.

5.

6. During the last 7 days, on how many days did you walk for at least 10 minutes?

\_\_\_\_\_ Days per week

No walking **skip to question 7**

7. How much time did you usually spend walking per day?

\_\_\_\_\_ Hours per day

\_\_\_\_\_ Minutes per day

Don't know

This last question is about how much time you spent **sitting** during the weekdays of the last 7 days. Include time spent at work, at home and during leisure time. This includes time spent watching television.

8. How much time did you usually spend sitting on a week day?

\_\_\_\_\_ Hours per day

\_\_\_\_\_ Minutes per day

Don't know

**This is the end of the questionnaire, thank you for participating.**

# Appendix H- Participant Information Sheet-Study four

## Participant Information Sheet

### *Plasticity in human movement: Biomechanical adaptations in activities of daily living when using a prosthesis simulator.*

- Brief Introduction:

The incidence of lower limb amputation represents a significant, growing problem in western society. Amputees lose parts of their lower limbs vital for movement which reduces their ability to complete daily tasks. During rehabilitation, amputees' main aim is to regain and maintain a level of function. An understanding of how humans adapt to the mechanical constraints imposed by lower limb amputation must be established. Therefore, the current study will assess how healthy able-bodied individuals adapt to performing activities of daily living (ADL) such as level walking and standing when they have 'amputee like' mechanical constraints imposed upon them.

- Study Requirements:

You will be required to attend a maximum of five different data collection sessions where you will be required to perform a ~~number of~~ activities of daily living such as walking, ~~balancing and get up from and sitting into a chair~~. This will occur whilst reflective markers are placed upon you and your movement and the associated forces are recorded. It is estimated that you will be required to commit to a maximum of 12 hours of data collection over a maximum period of six weeks.

- Location:

The Lee Westwood Sports Centre and the Biomechanics Laboratory, Clifton Campus, Clifton Lane, Nottingham, NG11 8NS.

- Restrictions During Testing:

You will be asked to refrain from strenuous physical activity for a 48 hour period prior to data collection sessions

- Testing Protocol:

Typically, you will attend a data collection session wearing tight fitting clothing (e.g. lycra shorts and vest) and your everyday shoes. The use of high heeled shoes is forbidden. We will then record your height and weight. You will then be familiarised with the task of walking at a self-selected speed and making contact with a target on the floor. We will then attach 14mm passive reflective markers to specific anatomical locations on both your upper and lower limbs using double sided sticky tape, after which you will stand in the anatomical neutral position which will be recorded. ~~Skin preparation for the placement of electrodes will also be conducted which involves shaving the area of interest, lightly abrading the surface and then wiping clean with alcohol. This will be conducted at a maximum of 16 sites on the lower limbs.~~ Finally, we will collect five movement trials of you completing activities of daily living such as walking, ~~balancing and getting out of a chair.~~ In other data collection sessions, we will be fitting you with an ankle brace or a practice prosthetic limb and you will use these to complete the activities of daily living. As you will be partially clothed, you will be offered changing facilities in order to prepare for marker placement and data collection.

Potential Benefits to You:

You will gain some understanding of your movement and potential areas for improvement, should you wish to share this with a health professional.

- Potential Risks to You:

You may experience fatigue and/or tiredness associated with performing the activities of daily living. You are advised to bring along food and drink, and will be afforded generous rest periods in order to recuperate.

There is a small risk that you may trip and/or fall when performing activities of daily living. Although this is highly unlikely, first aid assistance will be on hand to provide care.

There is a small risk of a bad skin reaction to the double sided sticky tap and/or the EMG skin preparation. This will be tested on a small area and reviewed for a reaction. You will also be asked if

you are allergic to plasters and you must seek further clarification with regards to your participation with your GP if this is the case.

There is a risk of musculoskeletal soreness and abrasions from the orthosis and/or the prosthetic simulator. You will be afforded generous rest periods in order to recuperate and will be invited to stop the data collection sessions if abrasions occur and impact upon your ability to perform the tasks pain free.

- Contacts:

Miss Olivia Brown

Email: [Olivia.brown022015@my.ntu.ac.uk](mailto:Olivia.brown022015@my.ntu.ac.uk)

Dr. Cleveland T. Barnett

Email: [cleveland.barnett@ntu.ac.uk](mailto:cleveland.barnett@ntu.ac.uk)

Tel: 01158483824

Address: ERD244, Clifton Campus, Clifton Lane, Nottingham, NG11 8NS.

## Appendix I- Informed Consent form-Study four

Centre Number:

Study Number:

Patient Identification Number for this trial:

---

### CONSENT FORM

---

Title of Project: **Plasticity in human movement: Biomechanical adaptations in activities of daily living when using a prosthesis simulator**

Name of Researcher: **Miss Olivia Brown**

Please initial all boxes

1. I confirm that I have read and understand the information sheet dated \_\_\_\_/\_\_\_\_/\_\_\_\_ (version **PIS1.0**) for the above study. I have had the opportunity to consider the information, ask questions and have had these answered satisfactorily.
2. I understand that my participation is voluntary and that I am free to withdraw at any time without giving any reason, without my medical care or legal rights being affected.
3. I understand that relevant sections of my medical notes and data collected during the study, may be looked at by individuals from Nottingham Trent University and The Mobility Centre, Nottingham University Hospitals NHS Trust, from regulatory authorities or from the NHS Trust, where it is relevant to my taking part in this research. I give permission for these individuals to have access to my records.
4. I agree to take part in the above study.

\_\_\_\_\_  
Name of Participant

\_\_\_\_\_  
Date

\_\_\_\_\_  
Signature

\_\_\_\_\_  
Name of Person  
taking consent.

\_\_\_\_\_  
Date

\_\_\_\_\_  
Signature